AUTOMATED FLOW INJECTION INSTRUMENTATION FOR MONITORING NITROGEN SPECIES IN NATURAL WATERS

By

SIMON PHILIP COLES, CChem MRSC.

A thesis submitted to the University of Plymouth

in partial fulfilment for the degree of

DOCTOR OF PHILOSOPHY

Department of Environmental Sciences

Faculty of Science

In collaboration with

M Squared Technology Limited, Totnes.

September 1999

ABSTRACT

AUTOMATED FLOW INJECTION INSTRUMENTATION FOR MONITORING NITROGEN SPECIES IN NATURAL WATERS

SIMON PHILIP COLES

The provision of high quality analytical data is an essential prerequisite for understanding the biogeochemical cycling of nutrients in the aquatic environment. Due to the instability of samples collected for nutrient determinations however, in situ analysis is preferred. This approach also allows for high temporal and spatial resolution of the data and alteration of the sampling frequency to meet local environmental needs. Chapter One describes the role of nitrogen species, particularly ammonia and nitrate, in the aquatic environment, their sources, and possible environmental effects and summarises analytical techniques for their determination. Solid state miniaturised detectors and their suitability for in situ monitoring are also discussed.

The characterisation and evaluation of a miniature Ocean Optics PSD – 1000 spectrometer and its suitability for field deployment is described in Chapter Two. Parameters investigated were optical resolution, wavelength repeatability, photometric linearity and instrumental noise and drift. The incorporation of the Ocean Optics PSD – 1000 miniature spectrometer into a gas diffusion Flow Injection (FI) manifold for the determination of ammonia in natural waters is detailed in Chapter Three. Optimisation of the FI parameters and analytical performance are discussed in detail. The development of an immobilised pH indicator and adaptation to a laminar FI manifold is also considered. Chapter Four describes the use of the miniature spectrometer in a FI manifold for the determination of nitrate and nitrite, with analytical figures of merit detailed. The increased information potential of the spectrometer (i.e. full spectral acquisition) facilitated the removal of the refractive index problem using dual wavelength correction.

Miniaturisation and automation of the optimised nitrate manifold using micro-solenoid pumps and LabView™ graphical programming is described in Chapter Five. Field deployment of the automated system was assessed during a six week British Schools Exploring Society Expedition to Lesotho, S. Africa (in which an intensive biogeochemical survey of the Sehlabathebe National Park was conducted) and a three day campaign on the River Frome, Dorset, U.K. Chapter Six details the ion chromatographic analysis of major anions and cations (including ammonium and nitrate) in precipitation samples. Two sampling campaigns were conducted. One was at an urban site (Plymouth City Centre) from 27/01/98 – 11/05/98, and the influence of aerosol source on the chemical composition of Plymouth precipitation is discussed. The other involved the Austrian precipitation network and wet deposition trends for nitrate, ammonium and sulphate are discussed. The multivariate analysis technique of PCA was applied to both environmental datasets and the interpretation and merits of this statistical approach are considered.

ACKNOWLEDGEMENTS

For his help, relentless enthusiasm and support throughout my time in Plymouth and particularly for his efforts in bringing this thesis to life, I would first like to thank Professor Paul Worsfold (The Chief !), *"You the Man !"* My thanks also to Dr Malcolm Nimmo (Captain Nemo) for his contributions throughout my PhD.

I am grateful for the financial support provided by M Squared Technology Ltd, Totnes, and all the staff I have met over the years, in particular I would like to thank the old crew, Andy Sloper, Mark Ilewelyn, and Linda Lowry.

My partners in crime from Davy 113 / 106 / 102, past members being Hefty, Trevy Trev, Robby Rob, Matteaus with the immortal quote *"Hands are going to start flying in a minute"*, Spodder, Andy B and the replacement shift of, Rich, Phil, Toby, Orif and Tweedle Dee and Tweedle Dum (Paulo and Vinny). Also to the numerous visitors from pastures green, Tommy – Tom (my Viennese guide and Prague drinking partner), Cristina S., Manuel, the big Austrian Jo – Jo, and a big thankyou to Cristina Lausin whom I had the pleasure of working with for the duration of her stay and her help with the unenviable task of precipitation sampling and analysis. My thanks to everyone else in the Department of Environmental Sciences, especially the technical staff, Ian, Andy, Andrew ("The Wippet"), Roger E., Jesser, Jackie and Adrian. The departmental secretaries Kathryn, Debbie, Lee and the overworked and underpaid PERC secretaries Elaine and Jo (hard taskmasters I know !).

My close friends who have always managed to provide the best of times, the Rendall Boys (Steve & Kev), Gill, Justin (King of the large mission !), Roly (Billy – Ray), Lee (Get some ! Get some !), Manno (the best potato in the bag !) and also the loudest person I have met in my life, and last, but no means least " The Woodster" (There can be only one !), thanks Blue.

My thanks to my girlfriend Kay your friendship and support have made my "extra" year in Plymouth all the more enjoyable and for letting me fill your house with fish tanks ! Also thanks to Mike and my Dad for your support and belief in me.

Finally, the hardest person to thank, my Mum, your love, support, guidance, strength and courage have and will always continue to uplift and inspire me, Thanks !

AUTHORS DECLARATION

At no time during the registration for the degree of Doctor of Philosophy has the author been registered for any other university award.

The work was financed with the aid of a studentship from the Natural Environment Research Council, and with CASE support contributed by M Squared Technology Limited, Totnes, Devon. The work described in this thesis has entirely been carried out by the author. Relevant scientific seminars and conferences were regularly attended at which work was often presented; external institutions were visited for consultation purposes.

Signed.....

Date.....29/11/99.....

To Mum, Thanks !

TABLE OF CONTENTS

LIST OF TABLES

LIST OF FIGURES

LIST OF PLATES

Chapter One

Introduction

"All glory comes from daring to begin"

- William Shakespeare -

1 INTRODUCTION

1.1 THE NITROGEN CYCLE

Nitrogen (N) is essential for life. It is the cornerstone of amino acids, the building blocks for the synthesis of cell proteins. Nitrogen is a Group 5A element with atomic mass of 14.007 and it was first isolated by Rutherford in 1772. It is a colourless, odourless, tasteless gas and occurs in nature mainly as dinitrogen (N_2) (bp 77.3 K, -196°C) which comprises 78 % by volume of the earth's atmosphere. N_2 is considered a stable molecule due to the high triple bond energy (945.4 kJ mol^{-1}) between the two N atoms, it has five valence electrons and can take on oxidation states between + 5 and – 3. Table 1.1 shows the range of oxidation states of some of the most common nitrogen species found in the natural environments.

Table 1.1 Oxidation states of nitrogen in important nitrogen compounds.

OXIDATION STATE	COMPOUND
+ 5	N_2O_5 (g) HNO_3 (g) / (aq) $Ca(NO_3)_2$ (s)
+ 4	NO_2 (g) N_2O_4
+ 3	HNO_2 (g) / (aq)
+ 2	NO (g)
+ 1	N_2O (g)
0	N_2 (g)
- 3	NH_3 (g) NH_4^+ (aq) NH_4Cl (s) CH_3NH_2 (g)

The dynamic interaction between nitrogen species in the atmospheric, aquatic and terrestrial ecosystems is known as the global N cycle (Figure 1.1). The dominant combined N species in natural waters (excluding molecular N_2) are dissolved inorganic N as nitrate (NO_3^-), nitrite (NO_2^-) and ammonia (NH_3) / ammonium (NH_4^+), dissolved organic N and particulate N (Figure 1.2). Organic nitrogen[1] usually exists as naturally occurring compounds such as urea, peptides, proteins and nucleic acids or as partial breakdown products of these molecules.

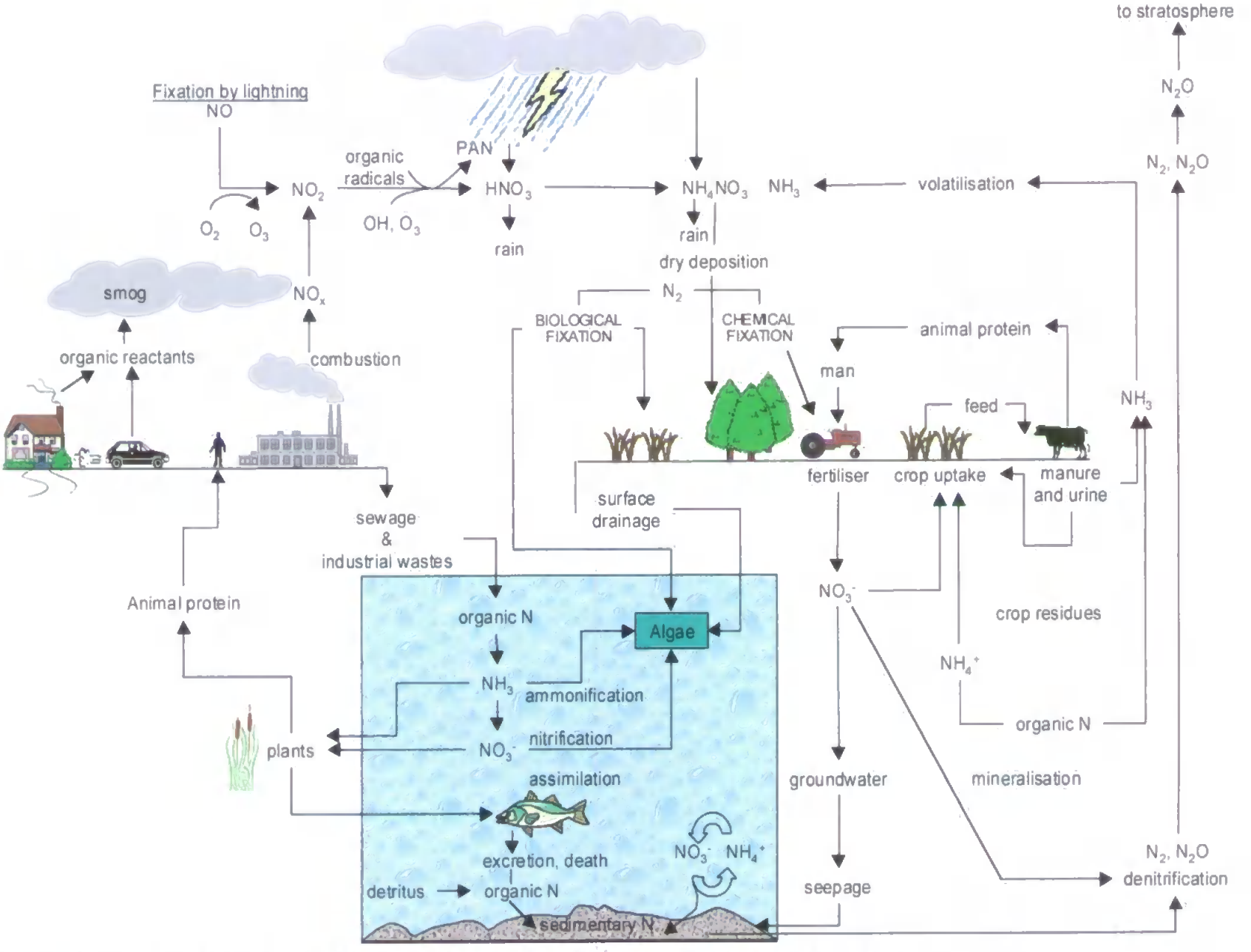

Figure 1.1 **The N cycle showing interactions between the atmospheric, terrestrial and aquatic ecosystems.**

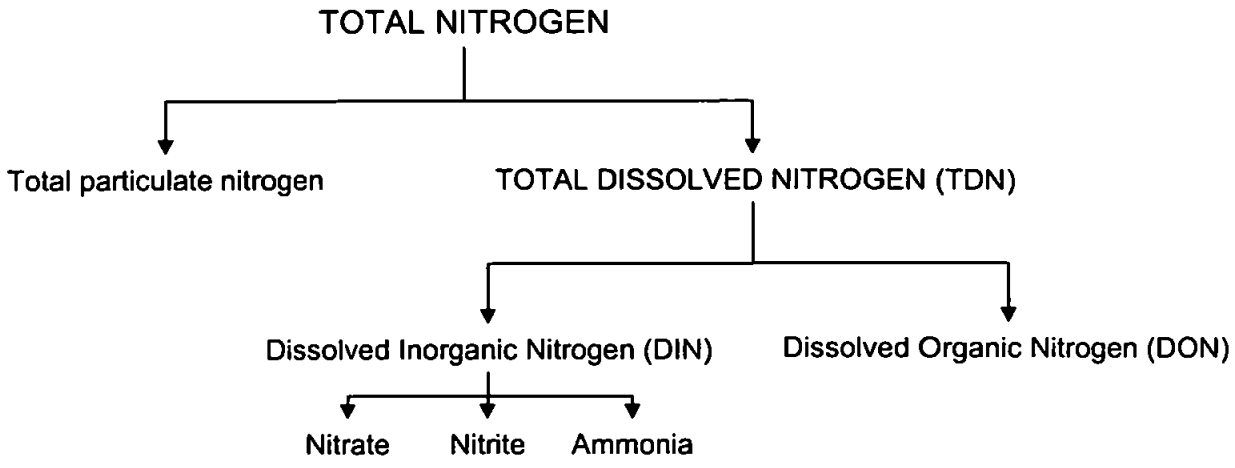

Groundwater	0-30+	<0.1	<0.1 (0.02 - 0.03)
Riverine waters	0-20+	<0.1	<0.1 (0.02 - 0.03)
Estuarine waters	(0.01-0.1)	<0.1	<0.1 (<0.005)
Coastal waters	(0.01-0.6)	<0.1	<0.1 (<0.005)

Figure 1.2 Nitrogen speciation in natural waters[2], showing typical concentrations expressed as mg l^{-1} N.

Surface waters and ground waters play an important role in the N cycle with up to 40 % of the total nitrogen flux occurring in these environmental compartments. Five possible nitrogen cycling reactions control the interaction and interconversion of nitrogen species in the aquatic environment; *fixation*, *assimilation*, *ammonification* (or mineralisation), *nitrification* and *denitrification*.

1.1.1 Nitrogen Fixation

Nitrogen fixation is the major process by which atmospheric molecular N (N_2) is converted to ammonia through the biological action of bacteria containing the enzyme nitrogenase. The reaction proceeds as shown below;

$$8\,H^+ + N_2 + 8\,e^- \longrightarrow 2\,NH_3 + H_2$$

Total nitrogen fixation in aquatic systems[3] rarely exceeds 20 kg N ha^{-1} annually, and although it is a primary terrestrial N transport mechanism, the importance of nitrogen fixation in the aquatic environment remains debated. However, there is evidence that N fixation is important in eutrophic lakes containing large populations of cyanobacteria, with up to 10 % of total nitrogen load accounted for by this mechanism[4].

1.1.2 Nitrogen Assimilation

Nitrogen is also required by phytoplankton for synthesis of their cellular amino acids. These organisms readily assimilate nitrate, ammonia and urea, with standing crops and production rates of phytoplankton[5], aquatic macrophytes[5] and macroscopic green algae[6] all known to increase with an increase in eutrophication of the water. Plankton assimilation of nitrate was demonstrated using a ^{15}N –tracer study[7]; after 14 days of adding ^{15}N enriched sodium nitrate, 90 % of it was located in the cyanobacterium *Microcystis aeruginosa*. Lake sediments can store large authigenic nitrogen fractions[8] due to sedimentation of dead organisms[9], with stored N available for possible re-release.

1.1.3 Ammonification

Production of ammonium can occur in the water column[7] and sediments[10] of rivers and lakes through microbial decomposition of organic N. The aerobic process is an important route for the regeneration of available N from decomposing matter for reassimilation by primary producers such as phytoplankton. The process can result in rapid turnover of N between the sediment / water interface (Figure 1.1). The rate of N release can be important in determining nutrient limitation in freshwaters[11] (although phosphorus is usually limiting).

1.1.4 Nitrification

Nitrification is a two-stage oxidation process in which; 1) ammonia is converted to nitrite, 2) nitrite is converted to nitrate, through the action of nitrifying bacteria. Chemoautrophic bacteria such as species of *Nitrosomonas* and *Nitrobacter* are more abundant than chemoheterotrophic forms in freshwaters and highest biological activity usually occurs at the sediment / water interface where ammonium – N generated from sediments is available[7]. The reaction is exothermic, producing energy available for biosynthetic processes.

$$NH_4^+ + OH^- + 1\tfrac{1}{2}\,O_2 \xrightarrow{\text{Action of } \textit{Nitrosomonas} \text{ bacteria}} H^+ + NO_2^- + 2\,H_2O \quad (\Delta H = -84 \text{ kcal mol}^{-1})$$

Subsequent oxidation to nitrate

$$NO_2^- + \tfrac{1}{2}\,O_2 \xrightarrow{\text{Action of } \textit{Nitrobacter} \text{ bacteria}} NO_3^- \quad (\Delta H = -18 \text{ kcal mol}^{-1})$$

The net reaction is

$$NH_4^+ + O_2 \longrightarrow NO_3^- + H_2O + 2\,H^+$$

The conversion of ammonia to nitrite by *Nitrosomonas* is usually rate limiting, so nitrite is rarely present in appreciable concentrations. The end product, nitrate, is highly oxidised, soluble and biologically available. The process of nitrification is oxygen demanding due to the *Nitrosomonas* and *Nitrobacter* requiring a minimum oxygen concentration of approximately 2 mg l^{-1} to function and this can create anoxic conditions. The nitrifying bacteria are also pH and temperature susceptible[12], with optimum pH range of 8.4 – 8.6 and an optimum temperature above 15°C. This temperature limitation has led to the suggestion that optimum rates of nitrification in British rivers and lakes are rarely reached[13]. However nitrification can not be ignored due to its influence during summer months when temperatures are higher and retention times are longer due to lower flows. In addition the discharge of nitrifying wastewater effluents to rivers and lakes will favour nitrification. A high rate of nitrification is essential for efficient N cycling in freshwaters, particularly as nitrate is an important substrate for denitrification.

1.1.5 Denitrification

Nitrate resulting from either the process of nitrification or drainage from the land can be lost from river or lake systems through the major mechanism of denitrification. Micro-organisms such as *Pseudomonas* species are able to reduce nitrate to molecular (N_2) or nitrous oxide. These bacteria function anaerobically and require a supply of carbon for growth and metabolism. Therefore the rate and extent of denitrification is controlled by the oxygen supply and available energy provided by organic matter. Denitrification was found to account for up to 54 % of nitrate removal from Lake Grasmere in the Lake District, U.K[14].

1.2 SOURCES OF NITROGEN IN FRESHWATERS

Nitrogen in freshwaters is derived from three key sources;

1. Domestic sewage and industrial effluents (point sources)
2. Agricultural land (diffuse sources)
3. Rainfall and dry deposition.

Whilst local catchment factors such as geochemistry and topography will establish the potential for nitrogen content of a receiving water body, it is human (anthropogenic) activities which result in far greater nutrient fluxes than natural factors.

1.2.1 POINT SOURCES OF NITROGEN

Point sources of nitrogen largely arise from domestic sewage and industrial wastes, but agricultural point sources such as manure and silage wastes also exist. Approximately 70 % of sewage effluent with its N load is discharged to inland freshwaters, with the remaining 30 % discharged to estuaries and to the sea. Similar volumes of industrial wastewater and effluent are also privately discharged but the N content is generally much lower than that of domestic sewage[15]. Nitrogen loads from human wastes has been estimated at 10.8 g N per person per day[11] and nitrogen in wastewaters can be up to 50 – 60 % NH_4-N, up to 5 % NO_3-N, up to 5 % NO-N and 40 – 60 % organic N. If sewage enters a water body untreated it contains approximately 55 mg l^{-1} of total nitrogen and 25 mg l^{-1} of NH_3-N, secondary sewage treatment reduces this load to approximately 20 – 50 mg l^{-1} total nitrogen[16]. The variable degree of nitrification during treatment of sewage results in wide concentrations of nitrate which were found to fluctuate between 40 – 50 mg l^{-1} NO_3-N[16].

1.2.2 DIFFUSE (NON – POINT) SOURCES OF NITROGEN IN FRESHWATERS

Although point sources can be considered important on a local catchment scale, it is diffuse sources of nitrogen that dominate nitrogen transport pathways from the terrestrial to the aquatic environment[3] (Figure 1.1). Inputs of nitrogenous matter from agricultural activities to the aquatic environment include; nitrogen wastes from livestock, organic manures / slurry applications, inorganic fertilisers, and the subsequent discharges or diffuse runoffs associated with these factors. Cattle manures / slurries contain 1.5 % N and poultry manure can contain up to 10 % N[3]. In England and Wales, the total nitrogen load arising from livestock faeces and urine has been calculated as 739 kt (1978 figures), almost approaching that of inorganic fertilisers at 924 kt. Between 50 – 100 % of this is voided onto the land and it has been calculated that up to 75 % of this nitrogen can be lost to the aquatic environment in 3 – 4 months[17].

1.2.3 PRECIPITATION

Nitrogen compounds from natural and anthropogenic (e.g. combustion and fertiliser application) sources play an important role in the nitrogen cycle (Figure 1.1). The most important compounds are nitrogen oxide (NO) and nitrogen dioxide (NO_2) which are precursors of nitrous (HNO_2) and nitric

(HNO_3) acids, nitrous oxide (N_2O), ammonia (NH_3), peroxyacetyl nitrate (PAN – $CH_3CO.O_2NO_2$) and the nitrate radical ($NO_3^{\cdot}$). The transfer of atmospheric nitrogen compounds from the atomsphere to the Earth's surface occurs through various wet and dry deposition processes. Water soluble species such as acids, acid anhydrides, peroxides and ammonia are particularly susceptible to wet removal mechanisms. Due to the vast variation in the processes that influence deposition a typical composition of precipitation is an impractical concept. However, Table 1.2 lists the mean annual concentrations of a range of major ions including ammonium and nitrate in Leeds, U.K. wet precipitation[18].

Table 1.2 Mean annual concentration of wet deposition in Leeds, U.K. (1986-1987)

Analyte	Cl^-	NO_3^-	SO_4^{2-}	NH_4^+	Na^+	K^+	Ca^{2+}	Mg^{2+}
Conc. ($\mu eqv\ l^{-1}$)	126	46	121	30	94	9	62	29

It has been estimated that land in the U.K., whether used for agricultural practices or not, may receive up to 40 kg ha^{-1} N from atmospheric sources[19] (rain & dry deposition). This is roughly equivalent to 20 % of the mean annual application of N fertilisers. It is known that as a result of human activities, atmospheric inputs of N to the terrestrial and aquatic environments have been increasing and may continue to increase unless legislative controls are applied[20-22].

1.2.4 INORGANIC FERTILISERS

Use of nitrogen-based fertilisers (mainly ammonium, nitrate and urea) has increased over tenfold in the U.K. in the last 50 years[23] and has been predicted to continue to increase by 4 – 5 % annually[3]. Applications of fertiliser to arable land typically occur in large quantities thus avoiding damage to crops if re-application is required. The excess nutrients not required by crop demand in uptake are potentially a major diffuse source of nitrogen supply to the aquatic environment. Surface runoff, mainly derived from precipitation, leads to nitrogen leaching of fertilisers from agricultural land and up to one third of the annual application of fertilisers is lost through leaching[24;25].

1.3 ENVIRONMENTAL & HEALTH EFFECTS

1.3.1 Environmental Effects of Ammonia

Ammonia (NH_3) is an important pollutants in the aquatic environment due to its relatively high toxicity to aquatic species and its ubiquity in surface water systems. It is closely interrelated with nitrite (NO_2^-) and nitrate (NO_3^-) through the biological oxidation of ammonia to nitrate, the process of *nitrification*. Ammonia in water can exist in two forms, the equation below shows the equilibrium of the two forms, the gaseous free form (ammonia, NH_3) and the ionic (ammonium, NH_4^+) form.

$$NH_{3(g)} + nH_2O(l) \rightleftharpoons NH_3.nH_2O(aq) \rightleftharpoons NH_4^+ + OH^- + (n-1)H_2O(l)$$

The relative concentrations of the two ammonia species in a given solution are principally dependent on the physiochemical properties of the solution, in particular pH, temperature and ionic strength. Of these, pH is by far and the most important factor, the toxicity of NH_3 increases as the pH of the solution increases, with an increase of just one pH unit giving a ten fold increase in the NH_3 concentration[26]. In an aqueous ammonia solution at 25°C with a pH of 7.0 the ionic species NH_4^+ accounts for virtually all of the dissolved ammonia, however at pH 11.0 the ionic form is almost completely converted to the toxic free form, NH_3. Temperature also affects the speciation of ammonia but to a lesser extent than pH. A temperature increase of 5°C between the range 0-30°C at a pH of 7.0 gives an increase in the NH_3 concentration of 40-50%. Physico-chemical parameters however are not the only factors controlling ammonia toxicity.

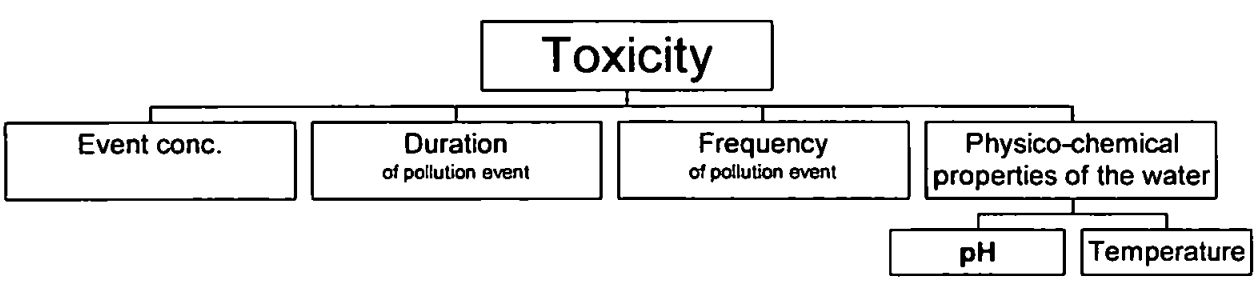

Figure 1.3 Factors affecting the toxicity of ammonia in natural waters.

Besides pH and temperature, it follows that the nature of a pollution event is also critical in determining its severity on the environment, e.g. concentration, the duration of the event, how frequently the event occurs, and the location (type of ecosystem) and timing (seasonal) are also important factors.

The most important species in terms of environmental impact is the un-ionised gaseous form, ammonia, NH_3. It is widely accepted that of all the aquatic species, the fish group are the most susceptible to high ammonia concentrations. There are a number of theories about the mode of toxic action to fish and these have been reviewed in the literature[27]. It is known that ammonia has a direct effect of on the central nervous system but the mechanisms of ammonia toxicity have not been firmly established[28]. Ammonia toxicity manifests itself by hyperactivity, convulsions, loss of equilibrium, lethargy, coma and death. Long term exposure of aquatic species to ammonia affects metabolic processes, retarding health, growth and reproduction[29;30]. Additionally ammonia toxicity is species dependant, ammonia toxicity to salmonids and freshwater species under different environmental conditions has been extensively reviewed[31;32]. According to Ruffier et al.[33], 96-h LC_{50}s (lethal concentration of 50 % of the population for a 96-h exposure) averaged 3.1 mg l^{-1} NH_3-N in catfish (*Ictalurus punctatus*) to 0.32 mg l^{-1} NH_3-N in rainbow trout (*Oncorhynchus mykiss*). In sensitive species such as salmonids, the maximum ammonia concentration that fish can tolerate may be as low as 0.02 mg l^{-1} NH_3-N[34]. In marine fish, little information exists for acute or chronic ammonia toxicity[35;36].

1.3.2 Health Effects of Nitrate in Drinking Water

Present concern about high nitrate and nitrite in drinking water arises from evidence that sustained ingestion of high concentrations of these compounds can lead to methaemoglobinaemia and stomach cancer. Methaemoglobinaemia is a condition that affects babies less than six months old and is also known as "Blue Baby Syndrome". It is caused by the reaction of nitrite in the blood stream with haemoglobin to form methaemoglobin. The link with nitrate levels in water centres on the combination of infants' low gastric acidity, which favours bacterial growth that encourages the reduction of nitrate to nitrite, and their high fluid intake (three times that of an adult). Infants also have a reduced activity of an enzyme (NADPH – dependant methaemoglobin reductase) which reduces the concentration of methaemoglobin in the blood[37;38].

Potentially much more serious is the reputed risk of stomach cancer. Bacteria in the human gastro-intestinal tract are capable of reducing nitrate to nitrite and this can react with digestion products to form N–nitroso compounds. These compounds are potent carcinogens that may be capable of initiating stomach cancer in humans[39] and results of early epidemiological studies supported the possibility of a link between stomach cancer and nitrate exposure[40;41]. However subsequent investigations have mostly failed to confirm this association[42;43]. With the conflicting evidence present, the long latency of the disease, combined with the fact that nitrate concentrations in surface and groundwaters are continuing to rise there remains a need for careful monitoring of the situation.

1.3.3 Eutrophication

Nutrient enrichment (particularly nitrogen and phosphorus) of lakes, reservoirs and rivers is known to be a causal effect in the production of excess algal growth[44], which can result in undesirable changes in the freshwater ecosystem[45] and affect drinking water supplies[46;47]. In May 1990 in the U.K., the National Rivers Authority (NRA), now the Environment Agency, detected blue-green algal blooms in 90 % of their water regions, with at least 70 % of these blooms being toxic to humans[48]. Although it is acknowledged that phosphorus is the limiting nutrient in many freshwater ecosystems, in some cases nitrogen availability can be the growth limiting factor[11;49]. Figure 1.4 summarises the potential sources of nutrient inputs, the causes of blue-green (cyanobacteria) algal growth and their potential impact on the environment and human health.

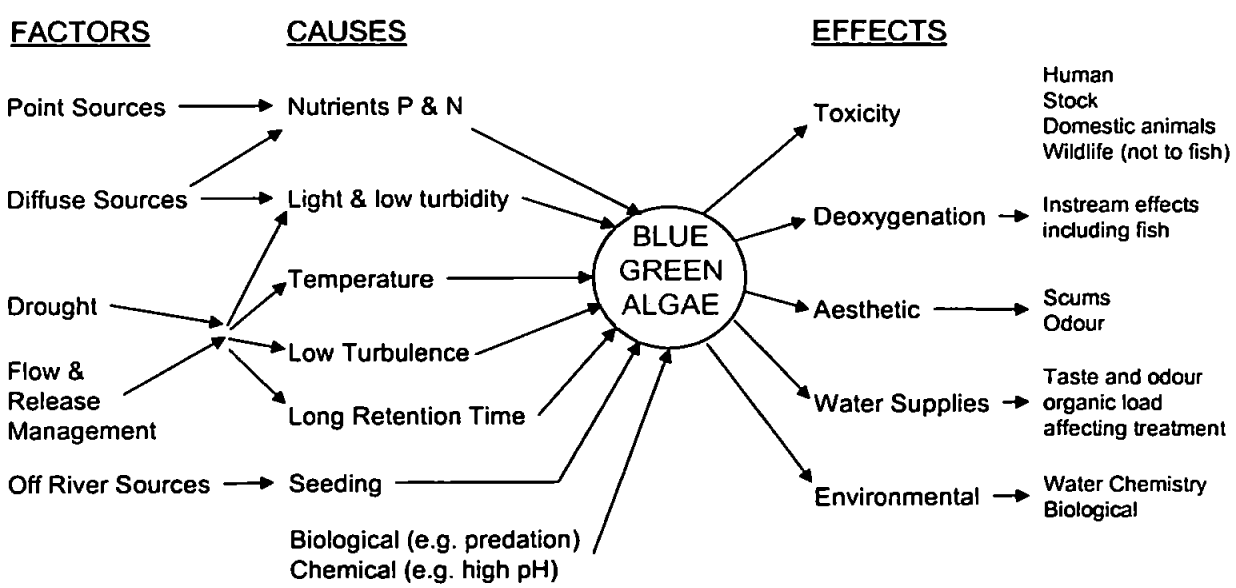

Figure 1.4 A conceptual model of algal dynamics showing major causes and effects of blue-green algal blooms[2].

1.4 ENVIRONMENTAL LEGISLATION

The previous 20 – 30 years have seen an increasing concern over the quality of the natural environment, with increasingly stringent legislation being introduced to preserve or improve the quality of aquatic ecosystems. Mean average concentrations of nitrogen species for the world rivers in a "pristine state" have been reported as 0.015 mg l^{-1} NH_4-N, 0.001 mg l^{-1} NO_2-N and 0.1 mg l^{-1} NO_3-N by Meybeck et al.[50]. However a joint report[51] published by the World Health Organisation (WHO) and the United Nations Environment Programme (UNEP) found that less than 10 % of European rivers could be classified as pristine. The median nitrate concentration in European rivers was 4.5 mg l^{-1} NO_3-N compared to 0.25 mg l^{-1} NO_3-N outside Europe. Over 10 % of European rivers had a nitrate concentration ranging from 9 – 25 mg l^{-1} NO_3-N, exceeding the EC maximum admissible concentration (MAC) for nitrate in drinking water of 11.3 mg l^{-1} NO_3-N (Table 1.3), (EC Directive on Drinking Water, COM 80/788/EEC)[52]. Ammonia concentrations in river waters rarely exceed 0.5 mg l^{-1} (NH_3-N), with higher concentrations normally resulting from pollution events[2]. In an attempt to control the rise of nitrogen species in freshwaters EC agricultural policy has shifted emphasis from the Common Agricultural Policy (CAP) towards wider environmental concerns. Policies such as the EC Directive on Nitrate (91/676/EEC)[52] concerns the protection of waters against pollution by nitrates from agricultural sources and allows the designation of Nitrate Vulnerable Zones (NVZ) with compensation to farmers adopting practices compatible with environmental protection (EC Directive COM 90/366/EEC).

Table 1.3 Maximum admissible concentrations and guide levels for various nutrient species in water to be used for human consumption

Species	MAC (mg l^{-1} N)	Guide Level (mg l^{-1} N)
Nitrate (NO_3-N)	11.3	5.65
Ammonia (total)	0.38	0.038
Nitrite	0.03	-
Kjeldahl nitrogen	1.0	1
Phosphorus (PO_4-P)	1.09	0.087

In the U.K. under section 107 of the Code of Good Agricultural Practice Act (Ministry of Agriculture, Fisheries and Food, MAFF 1991)[53] it is an offense to knowingly discharge pollutants into receiving waters. In a similar manner to the EC Directive (91/676/EEC), the Code of Good Agricultural

Practices allows the identification of Nitrate Sensitive Areas (order S1 1990/1013) and includes compensation measures for loss of agricultural products.

Due to its adverse effect on the oxygen balance in the aquatic environment, ammonia is included in the EC Water Directive (74/464/EEC)[52], more commonly known as the Dangerous Substances in Water Directive and is applicable to:

".....The discharge by man, directly or indirectly, of substances or energy into the aquatic environment, the results of which are such to cause hazards to human health, harm living resources and to aquatic ecosystems, damage to amenities or interference with other legitimate uses of water"

The directive aims to eliminate the pollution of the Community's surface, territorial, coastal and ground waters by substances mentioned in Lists I and II of the Annexe and intends to reduce or eliminate the consequences of its present pollution. Ammonia and nitrite are contained in List II of the directive which is concerned with substances having a deleterious effect on the aquatic environment. A number of criteria documents[54;55] specify a limit of 20 – 30 $\mu g\ l^{-1}$ NH_3-N based on the toxicity of ammonia to sensitive cold-water fish. The EC Freshwater Fish Directive (78/659/EEC)[52] stipulates the quality objectives for fresh water pertaining to the protection of fish populations, it quotes mandatory values of 0.025 mg l^{-1} NH_3-N and $\leq$ 1.0 mg l^{-1} N for total ammonia[56]. Perhaps a more accurate model is the US Environmental Protection Act (EPA 1985) which includes pH and temperature data and exposure time criteria in the model. Values for salmonid fish species are quoted for 1 hour and 4-day equivalent exposure times as 0.076mgl^{-1} & 0.048 mgl^{-1} for free ammonia at 20°C and pH 7.0.

It is generally accepted that the concentration of nitrogen species, particularly nitrate in surface waters, has increased in recent decades[51;57], with a Royal Society study[3] reporting a 50 – 400 % increase over the past 20 years. However, due to the primarily diffuse nature by which nitrogen reaches surface waters it is difficult to clearly identify the links between land use, human activities (e.g. fertiliser use) and water quality. Therefore the need to study, monitor and understand the processes of nitrogen transfer between atmospheric, terrestrial and aquatic environments remains crucial.

1.5 DETERMINATION OF AMMONIA

A variety of analytical techniques have been reported for the determination of ammonia in natural waters, including ion chromatography, potentiometry, optical sensors and spectrophotometric methods. The analytical figures of merit (linear range and detection limit) for a selection of recent publications using these key techniques are shown in Table 1.4.

1.5.1 ION CHROMATOGRAPHY

Cation chromatographic methods are a popular choice as a means of ammonia analysis in natural waters. One of the main advantages of ion chromatographic methods is their ability to simultaneously determine a range of analytes of interest. Mizobuchi et al.[68] describe a method based on the reaction with fluorescamine for the analysis of river, effluent and rain waters achieving a limit of detection of 6 $\mu g\ l^{-1}$. A recent application combined ion chromatographic separation with potentiometric detection using ion-selective electrodes[68]. Cation ion selection electrode membranes consisting of a dibenzo (18–crown-6) polymer were used to determine potassium, rubidium, caesium and ammonium in river, sea and tap waters with detection limits in the range 10 – 100 $\mu g\ l^{-1}$. A potentiometric ion-selective electrode sensor array was also used by Shen et al.[69] for the determination of ammonium, sodium, potassium, magnesium and calcium after a gradient ion chromatographic elution.

1.5.2 POTENTIOMETRY

Electrochemical sensors have several advantages over other methods of analysis; they are relatively inexpensive, convenient, simple to use, applicable to in-situ analysis and have a wide dynamic range. Recent applications have seen their use in conjunction with other techniques e.g. ion chromatography, and the development of miniaturised systems for the in-situ measurement of a range of nutrients (ammonia, nitrate, phosphate) in surface waters[70]. Hara et al.[71] have ultilised an ammonia gas sensing membrane in conjunction with gas diffusion for the FI analysis of lake waters in the range 0.1 – 5 μM. A stream of ultrapure water was mixed with 0.21 M NaOH and the solution passed through a microporous gas-permeable PTFE tube immersed in 0.5 M H_2SO_4 to remove traces of ammonia in the reagent. Standard or sample was then added to the solution and passed to a mixing chamber for detection by the gas-sensing membrane electrode.

Table 1.4 Analytical techniques for the determination of ammonia / ammonium in natural waters.

TECHNIQUE	SAMPLE	CONDITIONS	LINEAR RANGE	LOD	REF.
Conductimetry	Aqueous samples	"reagentless", solid phase basification with gas diffusion into pure water stream	N/A	10 $\mu g\ l^{-1}$	58
Conductimetry	Natural waters	Sample mixed with NaOH-EDTA soln, gas diffusion to conductance cell	30 – 500 $ng\ ml^{-1}$	5 $ng\ ml^{-1}$	59
Potentiometry	Waste/river waters	Nonactin based ammonium selective sensor	$10^{-4} – 10^{-2}$ mol l^{-1}	10^{-6} mol l^{-1}	60
Gas – phase absorption spectrometry	River waters	Addition of NaOH in reaction vessel, signal measured at 201 nm	0 – 0.8 $\mu g\ ml^{-1}$	10 $ng\ ml^{-1}$	61
Fluorometry	Sea/ estuarine Waters	Reagents of phthalaldehyde, sulphite and sodium tetraborate, detection at 425 nm (ex. 365 nm)	12 – 250 μM	1.5 nM	62
Amperometry	Lake/rain waters	Gas diffusion, glassy carbon electrode electrodeposited with cupric hexacyanoferrate	2 – 40 μM	N/A	63
Chromatography	Seawater	Gas diffusion with collection on IonPac Ion exchange column with conductivity detection	0 – 2000 nM	20 nM	64
Chemiluminescence	Waste waters	HPLC detection system	160 ng N	5 ng N	65
Chromatography	River/sea/tap waters	Ion chromatographic separation with potentiometric detection using anion and cation ion selective electrodes	N/A	100 $\mu g\ l^{-1}$	66
Optical Sensors	Natural waters	pH-sensitive dye, cetyltrimethylammonium salt of bromothymol blue in silicone polymer	0.59 μM – 1 mM	10 $\mu g\ l^{-1}$	67

1.5.3 OPTICAL SENSORS

Optical fibre sensor development has been a growing technology during the past decade, with an increasing number of publications describing this technology. A number of critical reviews have discussed their potential and application in environmental analysis[72;73] and FI analysis[74]. Typical ammonia sensors are based on the reaction of ammonia with an encapsulated reagent to produce a detectable colour change which can be measured spectrophotometrically. Ammonia analysis in natural waters has been performed using immobilised pH indicators, such as bromocresol green in a PTFE membrane[75] or the cetyltrimethylammonium salt of bromothymol blue in a silicone polymer[67]. Response times were 1 – 10 min depending on ammonia concentration and detection limits were 0.02 mg l^{-1} and 0.01 mg l^{-1} respectively. The results obtained showed good agreement with ion chromatography, ion-selective electrodes and conventional spectrophotometry. A recent application[76] used an ammonia sensitive sol-gel based on aminofluorescein with fluorescence measurement at 510 nm for the determination of ammonia in the range 1 – 20 mg l^{-1} NH_3-N.

1.5.4 SPECTROPHOTOMETRIC METHODS

The large majority of published methods for ammonia determination are based on spectrophotometric methods. Historically, the most popular methods for manual and automated use, was the *Berthelot* reaction, more commonly referred to as the *Indophenol Blue* method. This involves the sample (containing dissolved ammonia) reacting with a phenolic compound and a chlorine-donating agent in an alkaline solution in the presence of a catalyst. This produces an intensely coloured blue indophenol dye, the intensity of which is proportional to the concentration of ammonia in the sample. The indophenol blue method is the standard method recommended by the Environment Protection Agency and in quoted in 'Blue Book' 'Methods for the Examination of Waters and Associated Materials'[77]. Workers at the Water Research Centre U.K. have reported detailed studies[78] carried out on the application of automated indophenol blue procedures to the determination of ammonia in river waters. The indophenol blue reaction is often used as the reference method by which the accuracy of potential new approaches is validated.

Table 1.5 FI methods with spectrophotometric detection for the determination of ammonia in natural and polluted waters.

SAMPLE	CONDITIONS	LINEAR RANGE	LOD	REF.
Effluents	Automated monitor, gas diffusion manifold, bromothymol blue indicator, LED photometer detection at 635 nm	1 – 100 mg l^{-1}	0.6 mg l^{-1}	80
Natural waters / effluents	Sequential injection analysis, indophenol blue method	0 – 50 mg l^{-1}	0.36 mg l^{-1}	81
Lake waters	NH_3 oxidation to nitrite by hypochlorite, azo dye formation with sulphanilamide + N1NED, detection at 540 nm	0.2 – 12 µM	0.072 µM	82
Natural waters	Gas diffusion, mixed indicator of bromocresol violet, bromothymol blue and cresol red	10 – 1000 µg l^{-1}	5 ug l^{-1}	83
Natural waters	Sequential injection analysis, gas diffusion with bromothymol blue indicator	0 – 60 mg l^{-1}	0.5 mg l^{-1}	84
River waters	Automated monitor, gas diffusion manifold with bromothymol blue indicator, LED photometer detection at 635 nm	0 – 5000 µg l^{-1}	17 µg l^{-1}	85
Natural waters	Preconcentration on cation exchange BioRad AG 5OW-X8 resin, detection with Nessler at 410 nm	50 – 500 µg l^{-1}	3 µg l^{-1}	86
Landfill leachate	Automated monitor, gas diffusion manifold with bromothymol blue indicator, LED photometer detection at 635 nm	0 – 300 mg l^{-1}	2.5 mg l^{-1}	87
Waste waters	Berthelot[a] and bromothymol blue[b] gas diffusion, methods	[a]0.1 – 10 mg l^{-1} [b]2 – 60 mg l^{-1}	[a]0.03 mg l^{-1} [b]1 mg l^{-1}	88
Seawater	Gas diffusion manifold, phenol red indicator, green LED photometer	0.1 – 10 µM	0.05 µM	89

An attractive alternative is the use of a flow injection procedure incorporating a gas diffusion unit, originally described by Ruzicka and Hansen[79]. Due to the pH control of its speciation ammonia can be liberated in an alkaline donor stream and diffuse across a hydrophobic microporous membrane into an acid – base indicator stream, with the resultant colour change being measured spectrophotometrically. Gas-diffusion flow injection is further discussed in section 3.3.1. Table 1.5 summarises the analytical performance of reported methods for the FI determination of ammonia using spectrophotometric detection.

1.6 DETERMINATION OF NITRATE

Determination of nitrate in natural waters has been performed by a myriad of analytical techniques, the most important of which are described below.

1.6.1 CHROMATOGRAPHIC TECHNIQUES

There are various chromatographic techniques for the determination of nitrate / nitrite in natural waters, including gas chromatography[90-93], capillary electrophoresis[94;95] and ion chromatography[96-99]. A novel gas chromatographic method[91] utilised the bacterium *Pseudomonas chlorographis* to convert nitrate to nitrous oxide as the basis of analysis for nitrate in natural waters. Many other gas chromatographic methods are based on derivitisation, e.g. of nitrite to volatile organic compounds (e.g. nitrobenzene[90;92] and 2 – phenylphenol[93]) in an acidic medium. Detection limits of 0.5μg l^{-1} NO_2-N have been reported using electron capture[90] and flame ionisation[93] detection. Although good sensitivity can be achieved using these methods, the disadvantages are the expense of the instrumentation, the need for derivitisation prior to analysis and the lack of portability.

Ion chromatographic techniques are also popular for the determination of nitrate and nitrite in a wide range of environmental matrices including natural waters. Method of detection include UV spectrophotometry[96;100], conductivity[97;99;101;102] and chemiluminescence[98]. Ion chromatographic techniques have the major advantage of being able to perform simultaneous determination of several anions of interest, including nitrate, nitrite, chloride, sulphate and phosphate[103], with typical limits of detection being 1 μg l^{-1} for NO_3-N and 10 μg l^{-1} for NO_2-N.

Comparisons between ion chromatographic and flow analysis techniques for the determination of nitrate in natural waters have been conducted[104;105] and it was concluded that ion chromatographic techniques achieved lower detection limits but the sampling rate was limited (10 samples h^{-1}) in comparison with flow injection analysis (30 – 60 samples h^{-1}).

1.6.2 CHEMILUMINESCENCE

Chemiluminescence (CL) techniques have been successfully applied to the determination of nitrate and nitrite in natural waters. A large proportion of reported methods use the selective reduction of nitrate to nitric oxide, which is then reacted with ozone to form an energetically excited form of nitrogen dioxide. The measurement involves the subsequent relaxation of the nitrogen dioxide to the ground state in which a photon is emitted and detected. The sequence of reactions involved in the CL determination of nitrate are as follows:

$$NO_3^- + H^+ \longleftrightarrow NO_2^-$$

$$NO_2^- + H^+ \longleftrightarrow HONO \longrightarrow NO$$

$$NO + O_3 \longrightarrow NO_2^* \longrightarrow NO_2 + h\nu$$

Reagents for the reduction step include vanadium (III)[106] and titanium (III)[107;108] and the methods have been utilised for the analysis of river[107;108] and lake waters[108]. Another chemiluminescence method for the analysis of nitrate in river waters uses photochemical activation and subsequent reaction with an alkaline solution of luminol[109;110].

1.6.3 ION SELECTIVE ELECTRODES

The general principles of ion selective electrodes and the application of a nitrate electrode to the analysis of natural waters has been reported by Koschay[111]. The attractions are low cost, ease of operation and portability and the typical linear range is 0.14 - 1400 mg l^{-1} NO_3-N[111], which is not sensitive enough for the analysis of some natural waters (e.g. seawaters). Other disadvantages include major interference from chloride and bicarbonate ions and the need for constant pH and ionic strength. Recent work has focussed on the development of new electrode coatings and improved design to enhance sensitivity and minimise interferences.

Design improvements such double membrane systems[112] have been reported, with a limit of detection of 0.01 mM, extended pH range (2 – 9) and operational lifetimes of up to six months. New electrode coatings such as polypyrrole films[113], prepared by electropolymerisation of an acetonitrile solution containing 50 mM pyrrole, 0.1 M $LiNO_3$, 15 % dibutylphthalate (plasticiser) and 1 % H_2O, have achieved a limit of detection of 47 μM. Another approach is the oxidative detection of nitrite at an electrocatalytic [$Ru(bipy)_2$ poly-(4-vinylpyridine)$_{10}$ Cl]Cl modified electrode[114] in a flow injection manifold incorporating a Cu / Cd reductor column.

1.6.4 DIRECT SPECTROPHOTOMETRIC METHODS

There have been several methods proposed for the direct UV detection of the nitrate ion at 210 nm for use in natural waters. Nitrite, which absorbs in a similar part of the ultraviolet region, is a potential source of interference but can be removed by the addition of sulphamic acid[115]. Although reliable results can be obtained for natural waters low in organic matter (e.g. humic acids), waters containing higher levels of organic matter and / or iron give a positive bias and a correction has to be applied. The correction factor is usually determined by measuring the absorbance of the solution at 275 nm, a region where the nitrate ion has negligible absorbance. This absorbance is then multiplied by a pre-determined empirical factor which is related to the expected organic content of the water. Nitrate concentration is determined from the difference between the two absorbances but the main problem is that the correction factor is dependent on the nature of the water. Various manual correction methods have been reported to overcome interference from organic matter such as coagulation with aluminium hydroxide followed by filtration[116]. Interfering species have also been removed by the addition of sodium hydroxide solution to raise sample pH to 12.6, prior to an activated charcoal filtration step[117]. Correction for absorbance from organic matter has been made using second – derivative spectrophotometry or multilinear regression in the determination of nitrate in potable water[118], and comparison with ion selective electrode and ion chromatographic methods showed good agreement. Second derivative spectrophotometry was also used for the determination of total nitrogen in lake waters using a persulphate oxidation. The detection limit was 0.07 mg l^{-1} N and there was excellent agreement with standard USEPA (United States Environmental Protection Act) methods.[119] Zheng[120] determined nitrate in tap, river, well, stream and reservoir waters after interference was removed by treatment of the samples with $ZnSO_4$, NaOH, HCl and 1 % ammonium sulphamate, with absorbance

measurements at 220 nm and 275 nm for correction. The main disadvantages of all of these manual correction techniques is that they involve significant chemical manipulation of the sample, are often based on difference measurements and are not easily automated.

1.6.5 INDIRECT SPECTROPHOTOMETRIC METHODS

Indirect spectrophotometric methods for the determination of nitrate involve reacting the sample with selective reagents to produce a colour change that can be measured. Typical reagents include brucine[121] (10, 11-dimethoxystrychine), chromotropic acid[122], methylene blue[123] and 2,4-xylenol[122]. Spectrofluorimetric methods have also been used and a recent review[124] details various methods, limits of detection and fluorescence wavelengths. However the majority of methods for nitrate are based on its reduction to nitrite via a homogeneous reduction or, more commonly, a heterogeneous reduction. Homogeneous reduction methods have utilised hydrazine in the presence of copper ions as a catalyst[125], however the reduction step takes up to 24 h and poisoning of the catalyst can take place. More recent work has decreased the reduction time to 2 h[125;126]. Heterogeneous reduction methods use a variety of powered or granular metals such as zinc[127;128] or amalgamated zinc[129]. The most widely reported heterogeneous reduction step uses cadmium in various forms, e.g. cadmium filings[130], amalgamated cadmium[131] and copperised cadmium[132-134]. Of these, copperised cadmium is the most commonly used and widely reported method for the reduction of nitrate to nitrite. A comprehensive study of the reaction conditions using cadmium reduction, i.e. effect of pH, temperature, chloride concentration and contact time (flow rate) through a packed reduction column has been conducted by Nydahl[135].

Maximum yield of nitrite approached 100 % at pH 9.5 and temperature was found to have little effect between 20 – 30°C, but reduction was reported as significantly slower at 10°C. The use of copperised cadmium is now well established for the determination of nitrate. The reduction conditions are adjusted so that the nitrate is quantitatively reduced to nitrite and no further.

The principle reaction is:

$$NO_3^- + Me_{(s)} + 2H^+ \longrightarrow NO_2^- + Me^{2+} + H_2O$$

The reduction yield is dependent upon the metal used in the reductor, the pH of the solution, and the activity of the metal surface. Reaction solutions which are too alkaline, or inactive metal surfaces, result in only partial reduction. Conversely, if the reaction solution is too acidic or the metal used too electronegative, then the reduction step proceeds further than nitrite. In weak alkaline or neutral conditions, such as those often found in natural waters, the cadmium ions formed during the reduction of nitrate react with hydroxyl ions to form a precipitate.

In a neutral or weak alkaline solution:

$$NO_3^- + H_2O + 2e^- \longrightarrow NO_2^- + 2OH^-$$

Additionally the reduction potential required for the reduction of nitrate to nitrite is dependent on the hydrogen ion activity within the solution. This infers that solution pH is changed if the solution is not buffered, particularly in the vicinity of the metal reductor surfaces, therefore ammonium chloride is added to act as a buffer and as a complexant:

$$2\,NH_4^+ \longrightarrow 2NH_3 + 2H^+$$

$$Cd^{2+} + 2NH_3 \longrightarrow [Cd(NH_3)_2]^{2+}$$

The two hydroxyl ions formed are neutralised and the ammonia is bound in the diammine complex. Under controlled conditions, the nitrite originally present in the water sample passes through the reduction stage without further reduction. This nitrite therefore contributes to the total concentration, known as Total Oxidised Nitrogen (TON), and should therefore be subtracted to give the nitrate concentration.

The most commonly used detection principle is spectrophotometry, based on the two stage Greiss-Ilosvay reaction, which involves:

1) Formation of an intermediate diazonium ion from the diazotisation reaction between nitrite and an aromatic amine in an acidic solution.
2) Formation of a coloured azo dye from the reaction of the diazonium ion intermediate with an aromatic compound containing amino or hydroxy substituents.

Compounds used in this reaction for the spectrophotometric determination of nitrate and / or nitrite in natural waters include, 4-aminoacetophenone and 1,3-phenylenediamine[136], 4-nitroaniline and 1-napthol[137] and mercaptoacetic acid and N-(1-napthyl) ethylenediamine[138], and more recently, sulphanilic acid and 1-naphthol-4-sulphonate[139] and procaine hydrochloride and 1-naphthol-4-sulphonate[140]. The standard method however uses sulphanilamide as the diazotisation compound and N-(1-naphthyl)ethylenediamine as the coupling reagent. Figure 1.5 shows the reaction sequence for the diazotisation and coupling steps using these two compounds.

Diazotisation

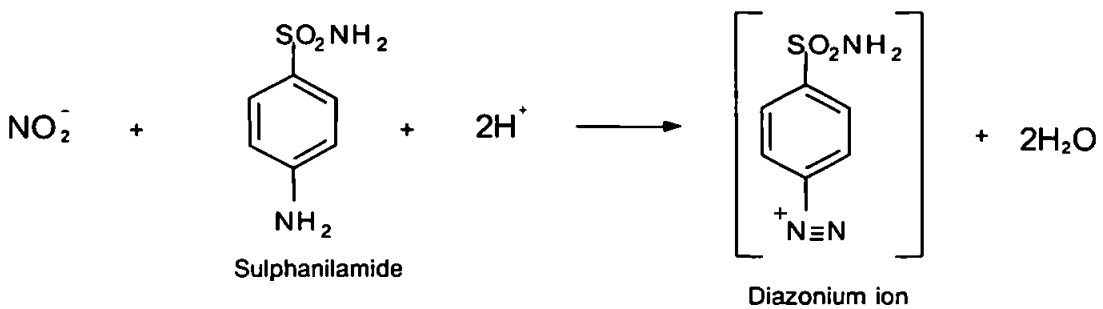

Sulphanilamide

Diazonium ion

Coupling

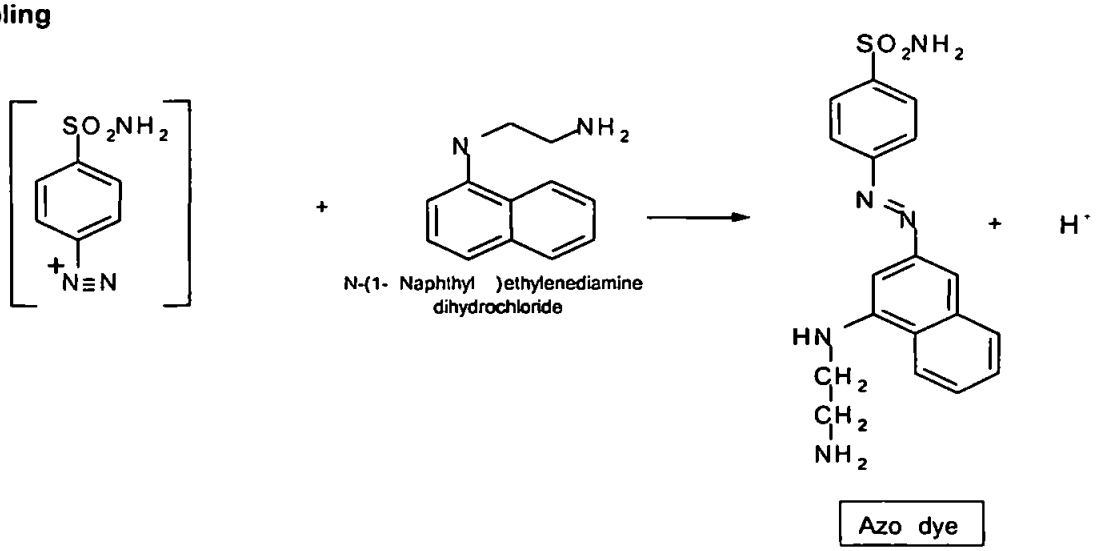

N-(1- Naphthyl)ethylenediamine dihydrochloride

Azo dye

Figure 1.5 Reaction sequence of the diazotisation and coupling reactions.

1.6.6 FLOW INJECTION DETERMINATION OF NITRATE

The need for high sample throughput in water laboratories and the desire to continuously monitor nitrate in situ require the use of automated methods. As discussed above, the most widely used detection principle is derivitisation based on the Griess Ilosvay reaction and spectrophotometric detection. One of the best approaches to the automation of this reaction (in the lab and the field) is the technique of flow injection (FI)[2;141] (see section 1.7). The characteristic features of FI are well suited to in-situ or on-line analysis and a number of publications have discussed its potential for monitoring process streams[142;143] and natural waters[144;145]. Automated nitrate monitors have been developed and deployed in a range of natural waters[146], including estuarine and coastal waters[147] and river waters[145;148]. Recent developments of nitrate analysis include the use of micro flow injection systems[149], new reagents[150-152], catalytic methods[153;154], azo dye preconcentration columns[139;140] and photo-induced reduction methods[155;156;157-159]. Table 1.6 summarises recently reported FI procedures for the determination of nitrate / nitrite in natural waters, with an emphasis on spectrophotometric detection.

1.7 PRINCIPLES OF FLOW INJECTION ANALYSIS

Flow injection analysis was first described by Ruzicka and Hansen[79] in 1975. It is based on the injection of a liquid sample (typically 10 – 200 μl) into a continuously flowing liquid carrier stream. Following injection, the sample zone is transported through narrow-bore tubing (typically PTFE, 0.5-0.8 mm i.d.) at typical flows rate between 0.1-5.0 ml min^{-1} via the action of a peristaltic pump, towards a flow-through detector for measurement of a specific physico-chemical parameter (e.g. absorbance). If the carrier stream also contains a reagent, then a zone of dispersed reaction product is formed. The detected response is in the form of a transient peak, the height of which is usually directly related to analyte concentration. A schematic representation of a simple, single-channel FI manifold is given in Figure 1.6. The basic components typically comprise a propulsion unit (e.g. a peristaltic pump), a six-port rotary injection valve, a reaction column or coil and a flow-through detector (e.g. spectrophotometer).

Table 1.6 FI methods for the determination of nitrate / nitrite in natural waters.

TECHNIQUE	SAMPLE	CONDITIONS	LINEAR RANGE	LOD (limit of detection)	REF.
Fluorescence	Natural waters	Cu/Cd column, nitrite reaction with 3-amino-1,5-napthalenedisulphonic acid	0 – 2 x 10 M (NO_3^-)	1 x 10^{-8} M NO_3	160
Fluorescence	River / waste waters	Cu/Cd column, kinetic spectrofluorometric method	0 – 460 ng ml^{-1} (NO_2^-)	27 ng ml^{-1} NO_2^-	161
Fluorescence	Rain water	Devarda Alloy reduction to NH_3, optical sensor reaction with o-phthalaldehyde	1 – 5 mg l^{-1} NO_3-N	N/A	162
Amperometric	River / well waters	Glassy carbon working electrode with crosslinked redox polymer	0.1 – 190 mg l^{-1} NO_3-N	50 µg l^{-1} NO_3-N	163
Biamperometric	Natural / waste Waters	UV photoreduction of nitrate, 2 platinum electrodes	N/A	25 µg l^{-1} NO_2-N 50 µg l^{-1} NO_3-N	164
Voltammetric	River / drinking Waters	Cyclic voltammetry, mercury drop electrode	N/A	21 µg l^{-1} NO_3-N	165
Voltammetric	River / drinking waters	Differential pulse voltammetry, mercury drop electrode	N/A	20 µg l^{-1} NO_3-N	166
Voltammetric	Mineral / lake waters	Linear sweep voltammetry, gold ultramicroelectrodes	N/A	2.6 µM NO_2^-	167
Conductivity	Natural / tap waters	Zinc reduction to NH_3, gas diffusion to conductance flow cell	0.2 – 1.5 µg ml^{-1}	20 ng ml^{-1} NO_3^-	168
Conductivity	Natural / tap waters	Zinc reduction to NH_3, gas diffusion monitored by bulk acoustic wave impedance sensor	2.5 µM – 100 mM	1.7 µM NO_3^- 1.8 µM NO_2^-	128
Chemiluminescence	Natural waters	Luminol reaction with peroxynitrite	0 – 1 x 10^{-5} M (NO_2^-)	1 x 10^{-9} mol l^{-1} NO_2^-	169
Chemiluminescence	River waters	Ti (III) reduction, chemiluminescence of NO with O_3	5 µg l^{-1} – 1 mg l^{-1} NO_3-N 3 µg l^{-1} – 1 mg l^{-1} NO_2-N	0.7 µg l^{-1} NO_3-N 0.35 µg l^{-1} NO_2-N	170
Chemiluminescence	Natural waters	On-line UV photoreduction of nitrate	7 x 10^{-8} – 1 x 10^{-4} M		171
Visible Spectrophotometry	Natural waters	Reverse FI, 4-nitroaniline in acidic medium, nitrite addition results in a decrease in signal	5 µg – 5 mg l^{-1} NO_2-N	2 µg l^{-1} NO_2-N	172
	Natural waters	Nitrite reaction with 4-iodo-N,N-dimethylaniline	0 – 1000 µg l^{-1} NO_2-N	2 ug l^{-1} NO_2-N	173

Conversion factors :- 1 mg l^{-1} NO_3-N = 71.43 µM; 1 mg l^{-1} NO_3^- = 16.1 µM.

Table 1.6 Contd. **FI methods for the determination of nitrate / nitrite in natural waters.**

TECHNIQUE	SAMPLE	CONDITIONS	LINEAR RANGE	LOD (limit of detection)	REF.
Visible Spectrophotometry	Natural waters	Cu/Cd reduction column, procaine hydrochloride and 1-napthol-4-sulphonic acid, azo dye preconcentration column	6 – 120 ng ml^{-1} NO_2-N 4.5 – 90 ng ml^{-1} NO_3-N	5 ng ml^{-1} NO_2-N 3.7 ng ml^{-1} NO_3-N	140
	Natural waters + soil extract	Cu/Cd reduction column, sulphanilamide and 1-napthol-4-sulphonic acid, azo dye preconcentration column	2 – 40 ng ml^{-1} NO_2-N 1.5 ng ml^{-1} NO_3-N	1 ng ml^{-1} NO_2-N 0.75 ng ml^{-1} NO_3-N	174
	Estuarine/ coastal waters	Cu/Cd reduction column, sulphanilamide and N1NED	0.0014 – 0.77 mg l^{-1} NO_3-N	0.0014 mg l^{-1} NO_3-N	147
	River / well/ lake Waters	Cu/Cd reduction column, catalytic reaction with napthol green B (NGB)	10 – 1000 ng ml^{-1} NO_3^-	0.25 µg l^{-1} NO_2-N 2.5 µg l^{-1} NO_3-N	175
	Waste/ coastal waters	Cu/Cd reduction column, reaction with proflavin in acidic medium	0.1 – 25 µg l^{-1} NO_3^-	0.1 µg l^{-1} NO_3^-	176
	Waste waters	Peroxodisulphate microwave digestion, nitrate reduction with hydrazine, sulphanilamide and N1NED	0 – 20 mg l^{-1} N	0.21 mg l^{-1} N	177
	Sea water	Cu/Cd reduction column, sulpanilamide and N1NED	0 – 100 µM NO_3-N	0.45 µM NO_3-N	178
	River / tap waters	Photo-induced reduction, sulphanilamide and N1NED	1 x 10^{-7} – 1 x 10^{-4} M NO_3^-	3 x 10^{-8} M	155
	River / sea waters	Photo-induced reduction, sulphanilamide and N1NED	1 x 10^{-7} – 1 x 10^{-4} M NO_3^-	0.05 µM NO_3^-	157
	Tap / sea Mineral waters	Sequential injection, Cu/Cd reduction column, sulphanilamide and N1NED	.5 – 40 µmol l^{-1} NO_2-N 2 – 100 µmol l^{-1} NO_3-N	0.1 µmol l^{-1} NO_2-N 0.45 µmol l^{-1} NO_3-N	179

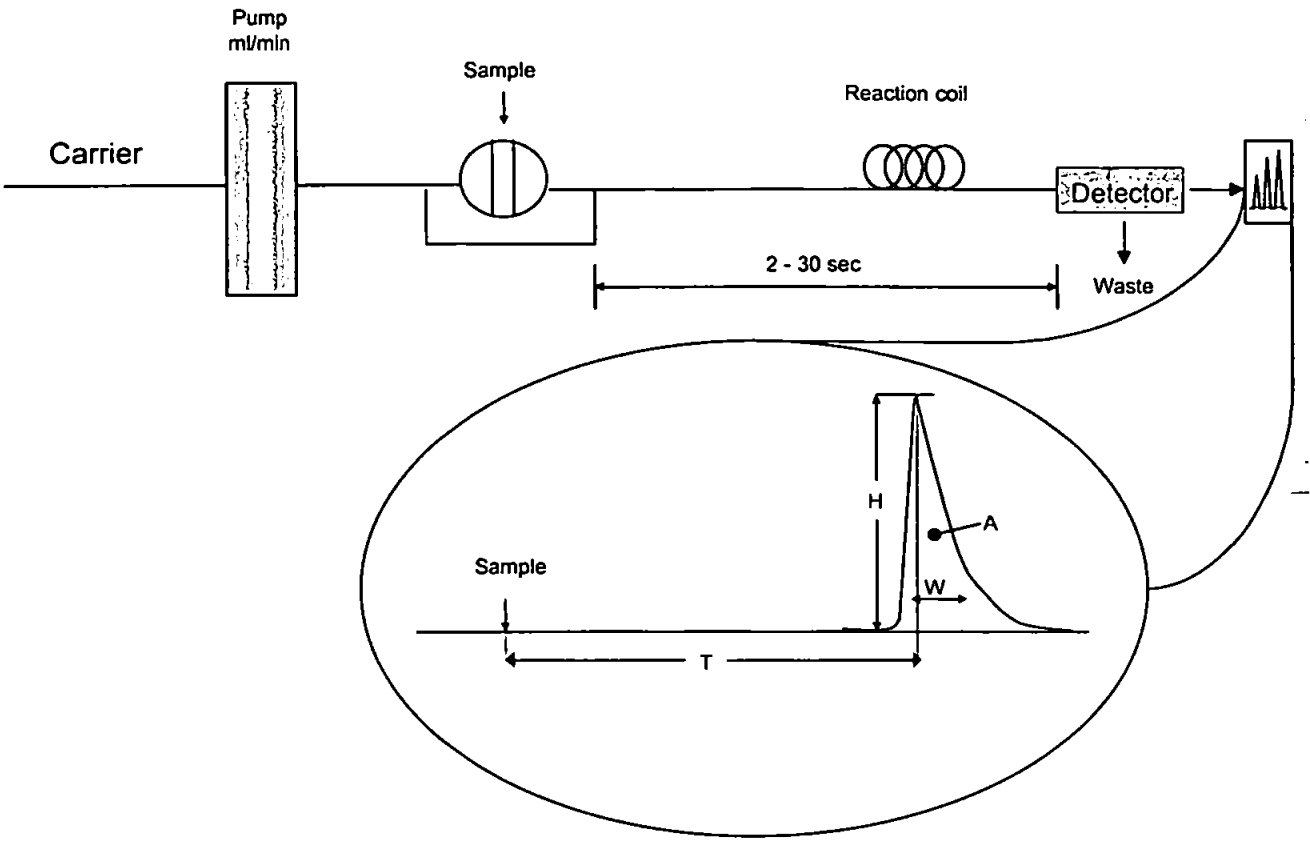

Figure 1.6 **FI manifold with chart recorder output; (T) is the residence time corresponding to the peak maximum, (H) is the peak height, (W) is the peak width and (A) is the peak area.**

A typical recorder output has the form of a peak as shown in Figure 1.6. The height (H), and area (A) are related to the concentration of the analyte. The time span between the sample injection and the peak maximum is the residence time (T), during which the chemical reaction between sample and reagents takes place. FI is characterised by rapid response times, typically in the range 5 – 30 s which facilitate high sampling frequencies. Sample volumes are typically 10 – 200 µl which require as little as 0.5-2.0 ml of reagent per sampling cycle. Other attractions of FI include good reproducibility (typically < 2 % RSD), low capital and operating costs, versatility and simplicity of the instrumentation, portability and ease of automation.

FI is based on the combination of three principles: Sample injection, controlled dispersion of the injected sample zone, and reproducible timing. In a conventional single channel sample injection manifold the chemical reaction takes place whilst the sample material is dispersing within the reagent. The concentration gradient of the sample zone in the reagent is formed by the physical dispersion

processes where the sample zone broadens as it moves downstream and changes from the original asymmetrical shape to a more symmetrical and eventially Gaussian form[180]. This shape is governed by axial dispersion (resulting from frictional forces at the tube walls) and radial diffusion (driven by the flow profile and reaction concentration gradient). For standard conditions, the procedure is highly reproducible in that one injected sample behaves the same way as all other subsequently injected samples.

A sample contained in the sample loop of the injection valve is homogenous and has an original concentration C^0. When the sample is injected, it follows the movement of the carrier stream, forming a dispersed zone, the form of which depends on the geometry of the channel and the flow velocity[181]. This continuum (Figure 1.7) of concentrations can be viewed as being composed of individual elements of fluid, each having a certain concentration, C.

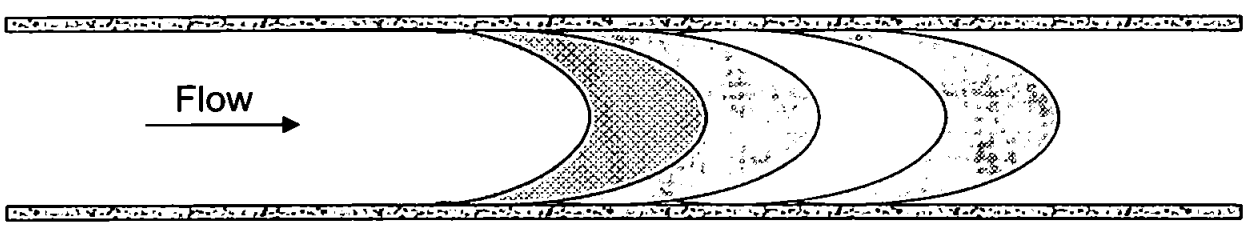

Figure 1.7 Dispersion in a Flow Injection System.

Therefore the response curve has the shape of a peak reflecting this continuum of concentrations (concentration gradient). The degree of dispersion is quantified in terms of the *Dispersion Coefficient* (D).

$$D = C^0 / C$$

For example if D = 2, then the sample has been diluted 1:1 with the carrier stream. Dispersion is generally defined[182] as limited for D = 1 – 3, medium for D = 3 – 10 and high for D > 10. The degree of dispersion can manipulated to optimise analytical performance (e.g. to reduce detection limits), with limited dispersion generally used to increase sensitivity, while high dispersion is employed when on-line sample dilution is required prior to measurement. Higher dispersion coefficients are produced by more rapid flow rates, which increase axial dispersion owing to the increased frictional forces generated between the flowing stream and the tubing. The incorporation of coiled or knitted lengths of tubing increase the degree of radial mixing between the sample and the carrier / reagent, but minimises axial dispersion[183;184].

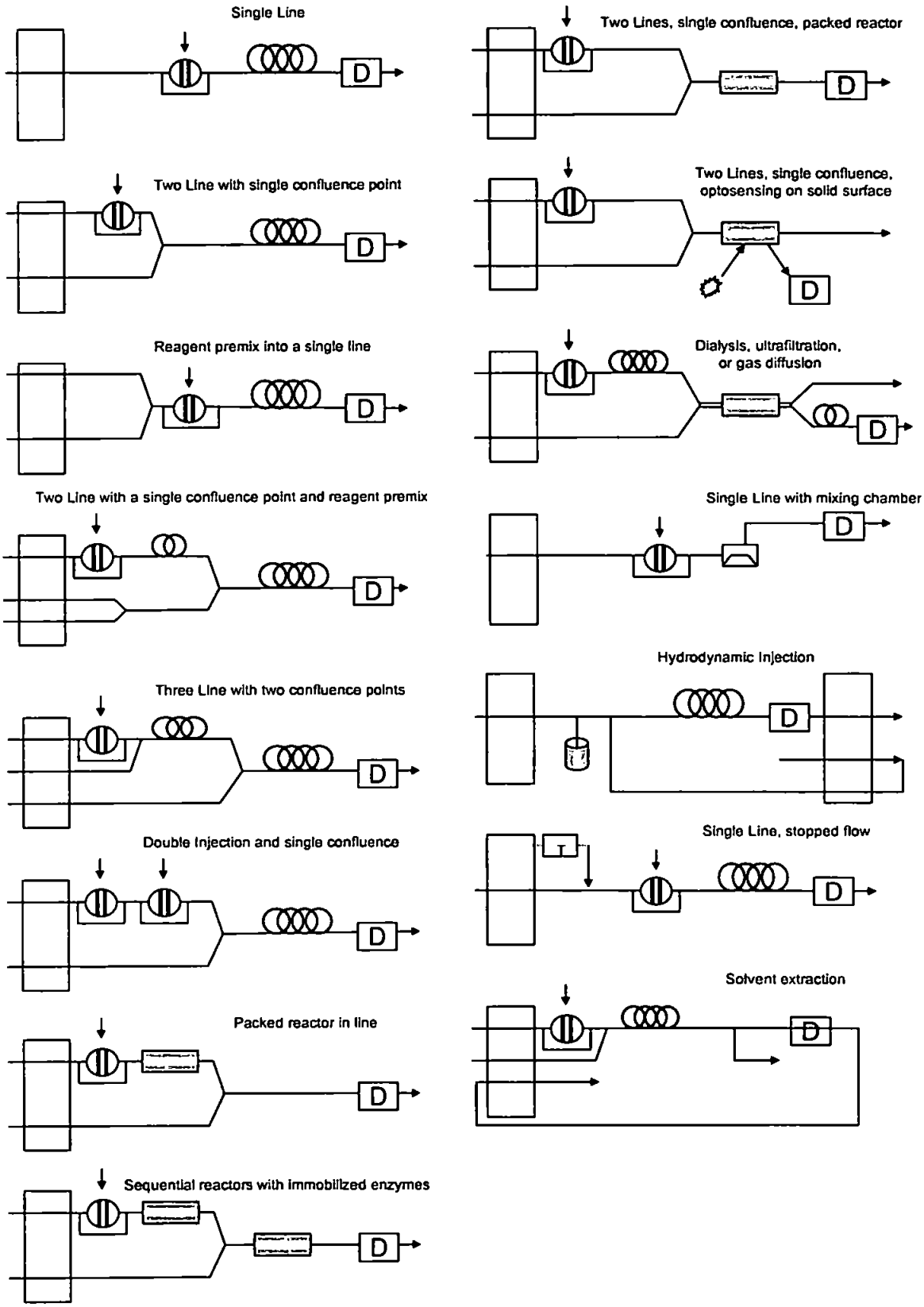

Figure 1.8 Examples of the flexibility of FI manifold design.

In addition to the many attractions of FI described above for the automation of wet chemical methods, the ability to perform both physical and chemical pre-treatment in-line in a major advantage. Figure 1.8 shows schematically a selection of manifold designs that have been used in reported FI methods. Within the context of natural water analysis, key features include the possibility of performing in-line filtration, photochemical oxidation, dialysis and addition of biocide (to minimise biofouling). With respect to the determination of ammonia, key advantages are the use of gas diffusion principles, on-line pH control (control of ammonia / ammonium speciation) and incorporation of immobilised reagent systems. With specific reference to the determination of nitrate, attractions include the incorporation of solid phase reactors (cadmium reduction column) and switching valves (for simultaneous or sequential nitrate / nitrite determination and the ability to adjust the linear range (to suit different environmental situations) by changing the dispersion.

1.8 SOLID STATE UV-VISIBLE SPECTROPHOTOMETRY

For laboratory based FI methods commercial spectrophotometers are most commonly used but for field deployment the light emitting diode (LED) / photodiode combination is preferred[185-188]. Recent advances in miniaturisation however allow the possibility of deploying array detectors in the field to provide full spectral information. This section provides an overview of spectrophotometric detection, with emphasis in field deployable devices.

Ultraviolet-visible (UV-Vis) spectrophotometry is a branch of molecular spectroscopy and involves absorption of near ultraviolet (180 – 390 nm) or visible (390 – 780 nm) electromagnetic radiation by molecules. It is primarily a quantitative analytical technique and is the most widely used analytical technique in chemical and clinical laboratories.

Absorption of UV-Vis radiation, involves transfer of energy to the analyte molecules through the process of excitation. Excitation involves the promotion of electrons residing in ground state molecular orbitals to higher-energy orbitals. For absorption to occur the energy ($h\nu$) of a photon must exactly match the energy of the difference between the two orbital energies. Electronic energy levels consist of the σ and π bonding levels plus the σ^* and π^* antibonding levels, and non-bonding levels (n). Organic compounds generally absorb energy in the UV-Vis region due to $\sigma \rightarrow \sigma^*$, $n \rightarrow \sigma^*$, $n \rightarrow \pi^*$ and

$\pi \rightarrow \pi^*$ transitions. Figure 1.9 shows a partial energy level diagram that depicts a range of energy changes that occur during absorption, non-radiative relaxation and fluorescence.

In conjunction with electronic transitions, molecules also exhibit vibrational and rotational transitions. Vibrations states are associated with each of the electronic states of a molecule (Figure 1.9) but have much smaller quantised energy levels. Additionally even smaller quantised rotational energy levels (not shown in Figure 1.9) are associated with each vibrational level. Electronic transitions can occur between many of these levels, consequently the spectra incorporates a series of closely spaced absorption lines (band of transitions). In the condensed state, solid, liquid and in the presence of solvent molecules the 'band' becomes blurred and give rise the characteristic continuous absorption spectra of UV-Vis spectrophotometry.

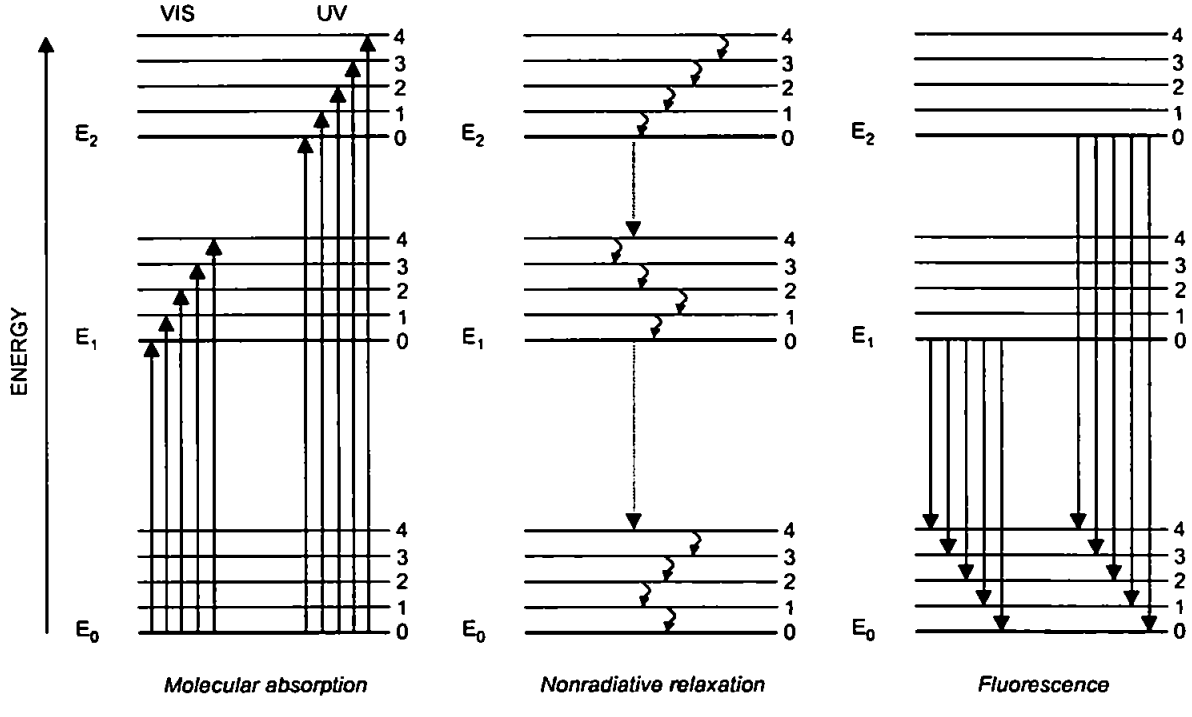

Figure 1.9 **Partial-energy level diagram, highlighting some of the energy changes that occur during absorption, nonradiative relaxation, and fluorescence by a molecular species**

1.8.1 LED PHOTOMETRY

Light emitting diode and photodiode components offer several distinct advantages over conventional spectrophotometers, particularly in the design and application of systems intended for in-situ or on-line deployment. These include small size, high power efficiency and minimal cost. The potential of

utilising LEDs and photodiodes in an optical visible photometer was first discussed in 1973[189]. Since that time the application of LED photometers in FI analysis have been reported in several publications[190-192].

A wide range of LEDs are now commercially available which span the visible and near infrared regions. Detection of emitted light can be performed by phototransistors or photodiodes[190;192]. Although phototransistors have greater sensitivity at lower wavelengths they exhibit a slower response than photodiodes which offer a wider range of linear response to transmitted light. FI flow cell designs commonly include single LED / photodiode configurations, however incorporation of a number of LEDs with different emission wavelengths enables the production of multi-wavelength photometers[193;194] with fibre optic transmission of the emitted light.

LED photometers have been used in the on-line automated FI determination of nitrate in the outflow water of a hydroponic water cress bed[188], and the in-situ FI determination of ammonia during a 3-day automated field trial on the River Avon, Wiltshire[187]. Similar systems have been used for the on-line analysis of aluminium[185] and iron[186] in drinking waters.

1.8.2 DIODE-ARRAY SPECTROPHOTOMETRY

Hewlett Packard introduced the first commercial diode-array (HP 8450A) in 1979. The use of diode-array instruments has steadily increased since that time and has found wide use as a stand alone spectrophotometer and as a detector for liquid chromatography and simultaneous multicomponent determinations in flow injection[195;196]. The optical bench of a diode-array spectrometer differs from conventional single and double beam instruments due to its use of reverse optics (dispersion after sample) as shown in Figure 1.10. Polychromatic light from the source (typically deuterium or tungsten) is focussed onto the sample, and the transmitted light passes into a polychromator and impinges on the surface of a fixed holographic reflection grating. The angular nature of the grating produces spectral dispersion of the incident light and the dispersed radiation then impinges across the photodiode array. Typically photodiode arrays consist of 1024 photodiode elements (individual width 15 – 50 μm) fabricated along the length of a silicon chip.

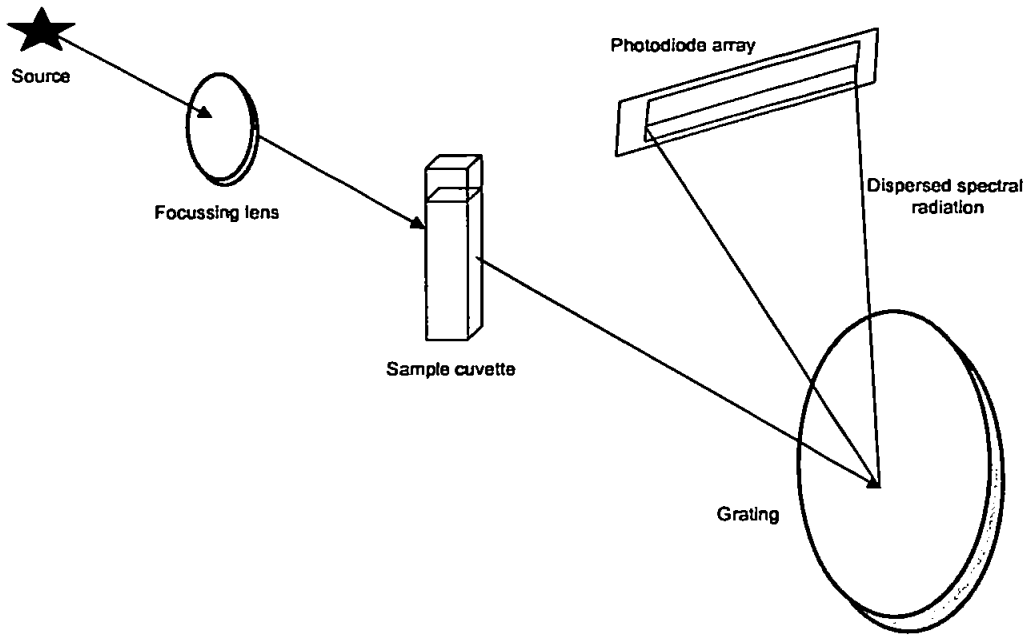

Figure 1.10 Schematic diagram of a diode-array spectrophotometer.

Each detector element in the photodiode array is dedicated to a particular waveband in the spectrum, dictated by the dispersion produced by the grating. Incorporated into the design of the microchip are a capacitor and electronic switch for each detector element. A spectrum is obtained by electronic sequential scanning of a shift register through all the elements of the array. This shift register momentarily closes the solid-state switch connected to each diode which causes each capacitor to be charged to – 5 V. Radiation impinging on any diode surface results in a partial discharge of its dedicated capacitor, the loss of charge is restored during the next sequential scan. The degree of current required to re-charge the capacitor is directly proportional to the intensity of incident light reaching the diode surface. These currents are amplified, digitised and recorded. The entire cycle is very rapid and an entire spectrum can be obtained in as little as 100ms (0.1 s).

1.8.3 ADVANTAGES OF DIODE ARRAY SPECTROPHOTOMETRY

Advantages of diode-array techniques over conventional scanning spectrophotometry are discussed in a range of analytical texts[197;198] and are summarised below.

Fast Spectral Acquisition: The parallel acquisition of spectral data can be obtained in milliseconds and as a consequence several spectra can be acquired and averaged together, enhancing the signal-to-noise ratio. The benefit of fast acquisition has facilitated the use of diode arrays in the

measurement of dynamic flowing systems e.g. in flow injection analysis, process control, enzymatic processes and kinetic measurements.

Simultaneous Multiwavelength Acquisition: A diode array spectrophotometer measures at all points in the spectrum simultaneously which enables a number of useful techniques for improvements in data quality. Two important uses of this advantage are internal referencing and wavelength averaging. Internal referencing utilises the absorbance(s) at a single or range of wavelengths (usually baseline) which can be subtracted from the absorbance at the analytical wavelength. This allows compensation for wavelength – dependent errors that can cause erroneous readings e.g. lamp fluctuations and imprecise cuvette positioning. Wavelength averaging of response across a number of diodes can improve the signal-to-noise ratios. As data points on either side of an absorbance maximum are averaged together, the average absorbance declines slowly at first (due to the broad band nature of most absorbance profiles), then more quickly as lower absorbances on the side of the band are included. At the same time, as data points are averaged, noise decreases by the square root of the number of data points. The signal-to-noise ratio improves as more data points are averaged but an optimum value is reached and signal-to-noise ratio eventually declines again as lower absorbance values are included.

Wavelength Repeatability: Conventional scanning spectrophotometers rely on moving mechanical optical components which have an inherent wavelength repeatability error which increases with time as mechanical parts wear. Diode array spectrophotometers have no moving parts and consequently have very good short and long term reproducibility.

High Sensitivity: Due to the fast simultaneous acquisition of a spectrum the sensitivity can be improved by utilising wavelength averaging (discussed above) and time averaging techniques. By averaging measurements over time (providing the sample remains constant) noise can theoretically be reduced by the square root of the number of measurements (*Felgett's Advantage*) and the signal-to-noise ratio is correspondingly improved. Acquiring several spectral measurements and averaging also has the advantage of providing measurement statistics for each point in the spectrum, effectively

measuring the precision of each data point, which is a useful tool for monitoring analytical performance.

From the perspective of in-situ or on-line monitoring the most significant advantage of diode array instruments is their lack of moving parts. The fixed optical bench ensures they have a high degree of reliability and robustness and are therefore suitable for applications in harsh environments e.g. on-line process control monitors or in-situ environmental monitors.

1.8.4 CHARGE-COUPLED DEVICES (CCD)

Charge-coupled devices (CCD) are part of a group of solid state multichannel detectors known as charge transfer devices (CTD). CCDs are ultra-sensitive photon detectors that have found application in low-level light determinations, particularly in imaging and astronomy, their use in spectroscopy is increasing[199-201].

A CCD consists of an array of detector elements (pixels) fabricated onto a silicon chip. The elements consist of several conductive electrodes that overlie an insulating layer which forms a series of metal oxide semi-conductor (MOS) capacitors. Photo generated electrons are collected in the pixels as charge packets which are then transferred to a serial register, and thereupon to a charge sensing amplifier (i.e. intra-cell transfer). The electrodes, which are held at different potentials, control the intra-cell transfer. Photons impinging on the surface of the CCD cause electrons to be generated in a doped depletion layer of the silicon substrate. Generated electrons are retained in position by the potential applied to the electrodes and stored in potential wells, accumulated charge is then transferred (coupled) to adjacent electrodes by altering their relative potentials. In this way the charge pattern, corresponding to incident light intensity, can be moved along the CCD and into the output register and amplifier for digitisation. CCD and diode array detectors share the advantages of fast spectral acquisition, reliability and mechanical simplicity but in addition, CCDs are capable of higher sensitivity and resolution.

1.8.5 MINIATURE SPECTROMETERS & FIELD APLICATIONS

Miniaturisation has been a key area of research in all fields of science and engineering. Constant advances are being made, not only in electronics, but also in mechanics (microstructure technology)

and optics[202-205]. Using well known process sequences from microelectronics (e.g. batch processing), it is possible to dramatically reduce the fabrication costs of mechanical and optical components. Consequently such processing techniques facilitate the construction of microsystems which combine electronic, optical and mechanical elements and open up new fields of application for such devices.

In April 1992, the Ocean Optics S1000 miniature spectrometer became commercially available and dramatically reduced the size (approx. 150 x 140 x 60 mm) and cost (approx. £ 1500) of optical sensing systems. It was originally developed for an open ocean optical pH-sensing system. Since that time the Ocean Optics spectrometer has seen applications industrial process, control, medical diagnostics and environmental monitoring[206].

Several other manufacturers have since released miniature spectrometers, including a monolithic miniature spectrometer MMS 1 (Carl Zeiss GmbH, Jena) and a truly microspectrometer manufactured by the LIGA process[207] (LIGA is the abbreviation of the German words Lithographie, Galvanoformung and Abformung). The LIGA process was developed at the Karlsruhe Nuclear Research Centre and has been commercialised by MicroParts (Dortmund). The process enables microscale structures which can be fabricated with arbitrary lateral shapes, structural heights of several hundred microns (μm), lateral detail dimensions down to a tenth of a micron and sub-micron accuracy over the total height of the structure[208]. Figure 1.11 shows a schematic layout of a LIGA spectrophotometer.

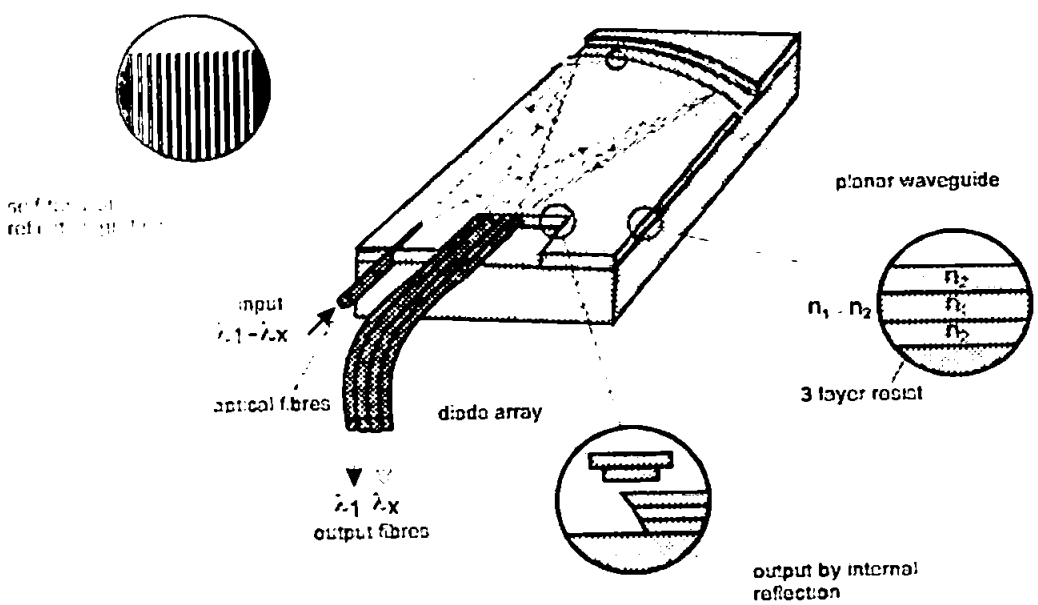

Figure 1.11 Schematic layout of a LIGA miniature spectrometer.

The unit is approximately 20mm x 6mm x 1mm and can be used with diode array technology or photo ASIC (Application Specific Intergrated Circuit) devices. It can be combined with fluid handling components, optochemical sensors and micro-computer systems to provide a integrated analysis system.

Although miniaturised spectrometers are becoming increasingly popular, relatively few applications have been reported to date. Several recent publications discuss new fabrication techniques utilising micromachining technologies and their application to the production of miniature spectrometers[209;210]. Advances have led to new miniaturised solid-state X-ray spectrometers[211] for deployment on spacecraft, currently (early 1999) deployed in the study of the near-Earth asteroid, 433 Eros. Other workers[212] have reported the construction and application of a miniaturised mass spectrometer with dimensions only a few cubic centimeters. Yee et al.[213] discuss the potential and application of miniature spectrometers in biochemical analysis. Environmental applications of miniaturised spectrometers also exist and these include the determination of cadmium in stream waters using a portable, battery-powered tungsten coil atomic absorption spectrometer[214]. The detection system was based on a miniature charge-coupled device (CCD) spectrometer controlled by a laptop computer, detection limit was reported as 3 $\mu g\ l^{-1}$ for a 20 μl sample. Recently Osterloh[215] applied a LIGA spectrometer for measurement of the colour of process and waste water, the spectrophotometric determination of nitrate, ammonia and phosphate in natural waters, and the determination of Ni, Co and Cu in plating solutions.

An Ocean Optics miniature spectrometer (PSD-1000) was recently used in the detection of nitrogen and phosphorus status in Bermuda grass (*Cynadon dactylon L.*) using spectral radiance[216]. NASA have incorporated a S-1000 Ocean Optics spectrometer into a robotic microrover (Rocky 7) for reflectance measurements[217]. Reflectance measurement using a S-1000 Ocean Optics spectrometer also form the basis of a novel self-contained diver-operated underwater instrument for the in-situ measurement of spectral fluorescence and reflectance of benthic marine organisms and substrates[218]. In fluorescence mode, the unit provides manual user-selectable excitation wavelength and measures fluorescence via fibre optic cable over the full visible spectrum. The instrument has been used at several field locations (Bahamas, Florida Keys and S. California) for the investigation of optical properties of coral reef organisms.

1.9 RESEARCH AIMS AND OBJECTIVES

The overall objective of this research was to incorporate a miniature array detector into a fully automated FI instrument for the field determination of nitrogen species in natural waters.

The individual aims were:

1. To fully characterise the analytical performance of a miniature array detector.
2. To optimise a FI manifold incorporating an array detector for the determination of ammonia in natural waters.
3. To optimise a FI manifold incorporating an array detector for the determination of nitrate in natural waters.
4. To fully automate the operation of the FI manifold and data acquisition and processing using graphical programming.
5. To evaluate the performance of the automated instrumentation in contrasting environments.

Chapter Two

Characterisation of the PSD-1000 Miniature Spectrometer

"Those who follow the crowd are quickly lost in it"

- Anonymous -

2.1 INTRODUCTION

With the recent advances in miniaturised detection technology[215;218;219] it is possible to take traditional laboratory based instrumentation e.g. spectrometers, to remote sites for in situ monitoring. When coupled with the flexibility of flow injection analysis, which has been proven to meet in situ monitoring needs[80;85] miniaturised detection technology provides the basis for a potentially powerful analysis tool. However prior to deployment and in order to obtain reliable field measurements, it is necessary to fully characterise the instrumentation in terms of performance, limitations and possible sources of error. This chapter describes work conducted in the evaluation of a PSD-1000 Ocean Optics spectrometer in terms of its wavelength repeatability, photometric linearity and instrumental noise and drift.

2.2 EXPERIMENTAL

2.2.1 REAGENTS & STANDARDS

Solid potassium permanganate ($KMnO_4$) (SpectrasoL grade,Merck Ltd., Poole, Dorset, U.K) was dried for 1 h at 105°C. A stock solution with an absorbance value of 3 A.U.* was prepared by dissolving 0.2034 g of potassium permanganate in 1 l of Milli-Q water. A set of absorbance standards (0.5, 1.0, 1.5, 2.0, 2.5 A.U.) was prepared by serial dilution of the 3 A.U. stock solution. These standards were analysed as soon as possible after preparation to avoid degradation due to the absence of a stabilising agent such as acid.

2.2.2 INSTRUMENTATION

The spectrometer used in this work was an Ocean Optics PSD-1000 miniature fibre optic spectrometer (Anglia Instruments Ltd, Cambridge, U.K.). The PSD-1000 spectrometer consists of two 1024 element linear CCD arrays (NEC μPD3575D) and two detector channels, designated Master (covers UV – VIS) and Slave (covers VIS – NIR). Figure 2.1 shows the OEM component of the spectrometer (single not dual channel spectrometer shown). The picture shows a cut-away view of the optical bench (schematic diagram Figure 2.2) with the linear CCD mounted at the top of the picture. The master channel was fitted with a collimating lens (cylindrical quartz collection lens made of Suprasil 2) to improve sensitivity. The slave channel was fitted with both a

* Absorbance is a dimensionless parameter but for clarity the term A.U. will be used throughout the thesis to represent absorbance measurements.

collimating lens and a 2 mm optical glass (Schott OG 515) cut-off filter to remove all radiation of wavelength less than 515 nm.

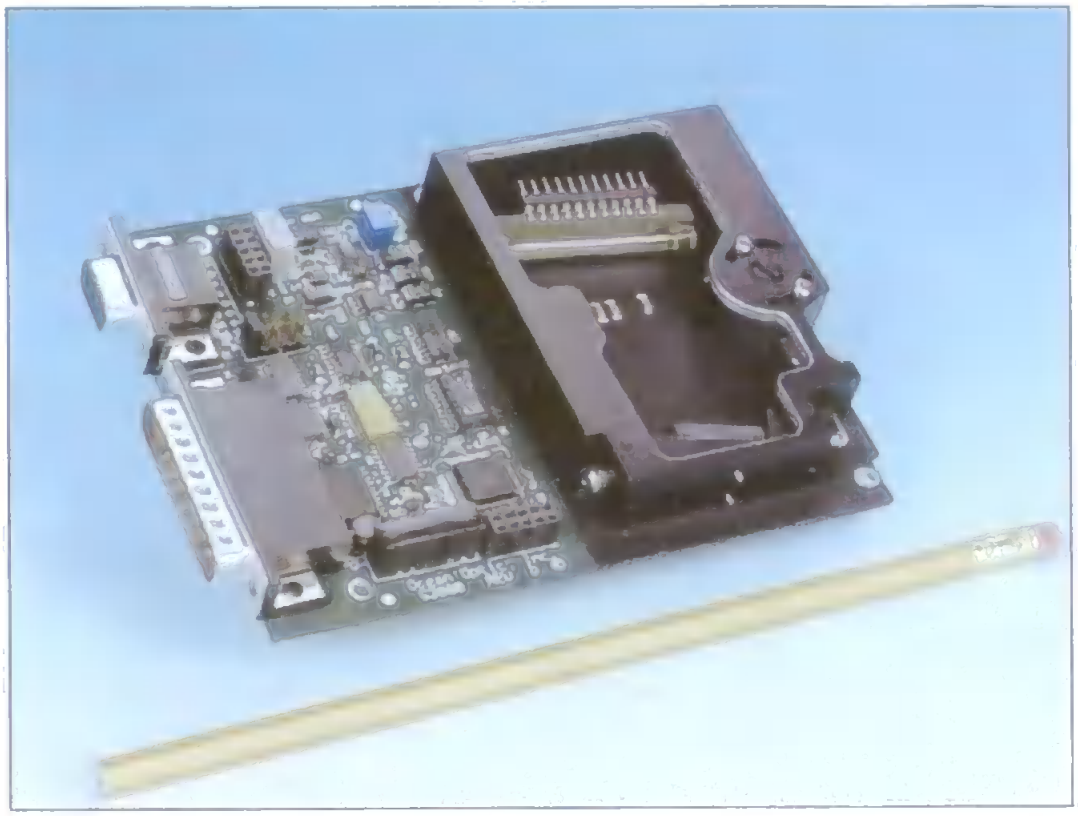

Figure 2.1 **OEM component of Ocean Optics spectrometer (single channel unit shown, not dual as used).**

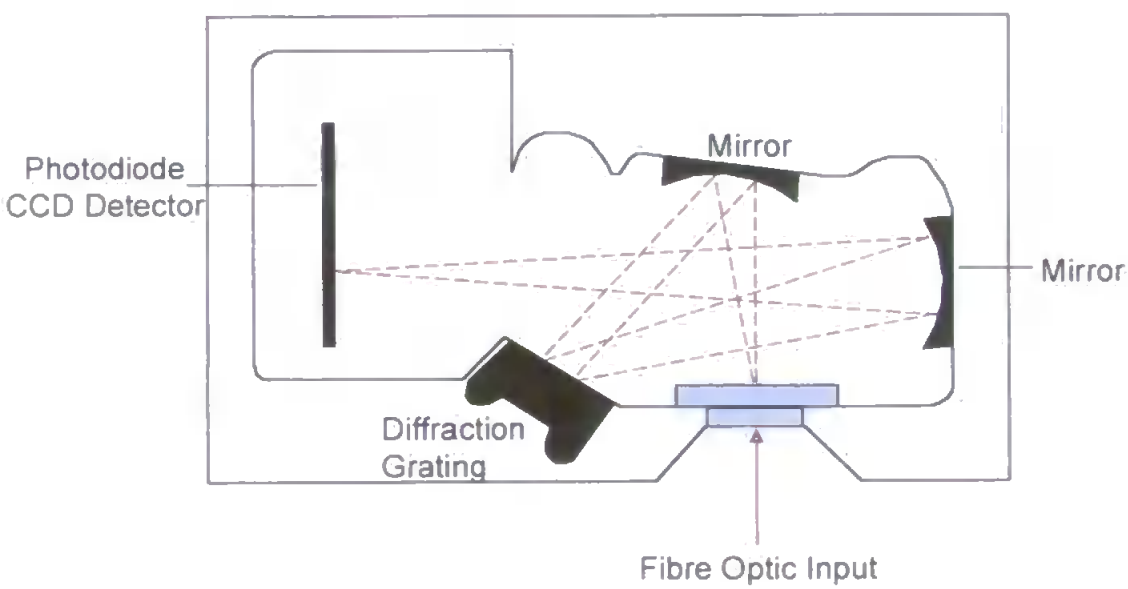

Figure 2.2 **Schematic of PSD - 1000 Ocean Optics spectrometer.**

The master grating had 600 lines mm^{-1} blazed at 300 nm and enabled a spectral range of 200-700 nm. The slave grating had 600 lines mm^{-1} blazed at 750 nm giving a spectral range of 500-1000 nm. The optical assembly was arranged in a cross Czerny-Turner configuration with two spherical mirrors and a flat holographic grating working with first order refracted light. Physical specifications of the PSD – 1000 spectrometer are given in Table 2.3. All-silica core, fluorine doped silica cladding, 200 μm single core UV-VIS fibres (Anglia Instruments Ltd) were used in all applications, unless otherwise stated. A miniature tungsten halogen light source (LS-1 Ocean Optics Inc.), was used as the light source (specifications given in Table 2.1) for all experiments using the PSD-1000 spectrometer, unless otherwise stated. The LS-1 source was fitted with a 10 000 hour long life bulb which has a 2800 K colour temperature (Figure 2.3).

Table 2.1 Specifications of the LS-1 light source.

Parameter	Specification
Spectral range	360-1000 nm
Size	9.0 x 5.0 x 3.2 cm (LWH)
Weight	185 g
Power Input	12 V, 750 mA
Power Output	6.5 watts
Bulb Life	900 hour (standard) 10 000 (long life)
Bulb Colour Temperature	900 hour bulb = 3100 K 10 000 hour bulb = 2800 K
Bulb Output	7400 foot candles
Output Regulation	0.2 % voltage
Thermal Stabilisation	30 – 40 min for 100%
Filter Slot	3 mm
Focal Distance	Approx. 12.5 mm, adjustable
Connector	SMA 905

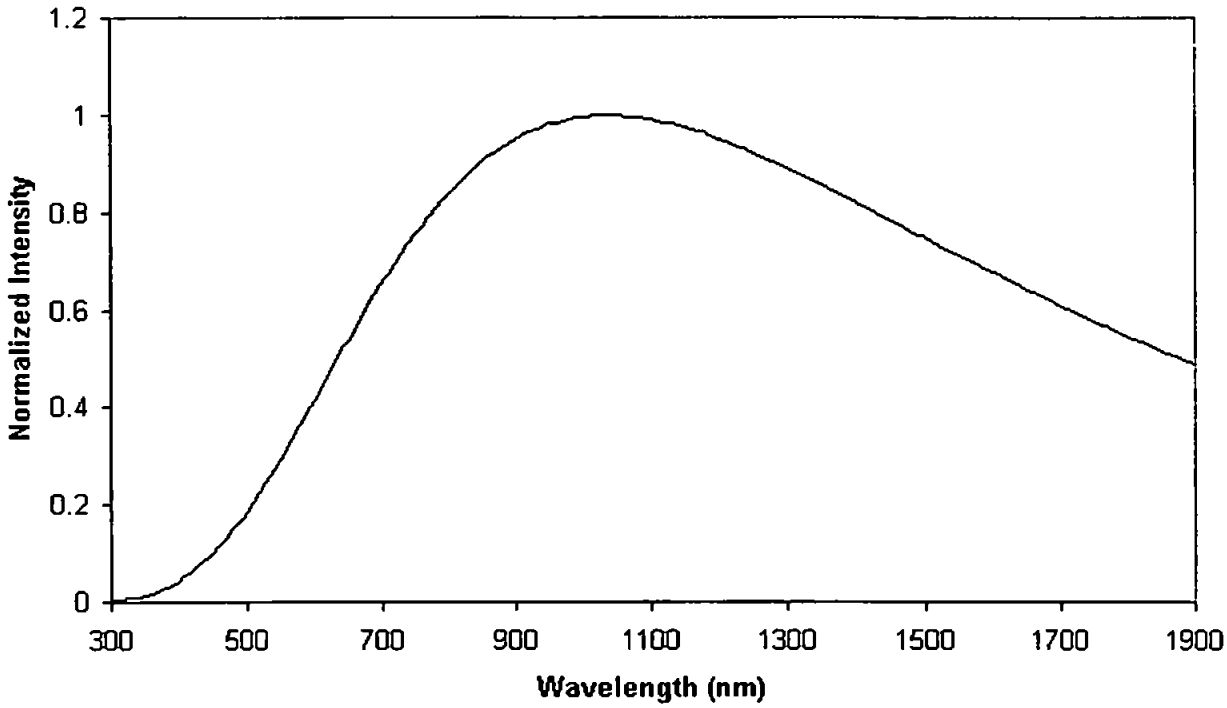

Figure 2.3 **LS-1 Tungsten Halogen light source spectral response of 10 000-hour bulb (2800 K)[206].**

This graph represents a blackbody curve for a tungsten halogen light source with 2800 K colour temperature. The actual spectral output of the LS-1 varies according to spectrometer configuration and sampling optics used, as well as inherent fluctuations in LS-1 output.

Data communication to and from the spectrometer was performed using a type II PCMCIA DAQ-700 data acquisition card (National Instruments, Newbury, Berks, U.K) and a 486-75 T2130CS notebook PC (Toshiba Information Systems Ltd, Weybridge, Surrey, U.K). All data acquisition was performed in Spectrascope version 2.3 (Ocean Optics Inc.) with the later exporting to Excel 5.0 (Microsoft Corporation) and Origin v.2.78 (Microcal Software Inc) for processing. Wavelength calibration was performed using a HG-1 low pressure mercury / argon calibration lamp (Anglia Instruments Ltd), the specifications of which are given in Table 2.2.

Table 2.2 **Specifications of the HG-1 calibrating lamp.**

Parameter	Specifications
Size	94 x 60 x 25 mm
Weight	84 g : excl. battery
Output	40 $\mu W/cm^2$ irradiance
Spectral Range	200 – 1200 nm
Amplitude Stabilisation	1 min
Internal Voltage	600 V @ 30 KHz
Power Requirement	9 V battery or 12 V DC

A liquid nitrogen cooled (140 K) two dimensional Charge-Coupled Device (CCD) array (256 x 1024 pixels, 27.6 x 7 mm grid of 27 micron square pixels) with 270 M imaging spectrograph (Instruments S.A.) and Spectramax Version 1.1d software (Jobin Yvon Optics and Spectroscopy) was used to provide reference information about the HG-1 mercury / argon calibrating lamp.

A Hewlett-Packard 8453 UV-visible spectrometer running under Hewlett-Packard UV-Visible Chemstation (Rev. A. 02. 04, 1995) software was used as a reference spectrometer. The optical system of the spectrophotometer is shown in Figure 2.4 and physical specifications are given in Table 2.3. Its radiation source is a combination of a deuterium-discharge lamp for the ultraviolet (UV), which emits over the 190 nm to 800 nm wavelength range. The other lamp is a low-noise tungsten lamp for the visible (VIS) and short wave near-infrared (SWNIR) and emits over the 370 nm to 1100 nm wavelength range. The image of the filament of the tungsten lamp is focussed on the discharge aperture of the deuterium lamp by means of a special rear-access lamp design, which allows both light sources to be optically combined and share a common axis to the source lens.

The source lens forms a single, collimated beam of light. The beam passes through the shutter/stray-light correction filter area then through the sample to the spectrograph lens and slit. In the spectrograph light is dispersed onto the diode array by a concave holographic grating. This allows simultaneous access to all wavelength information.

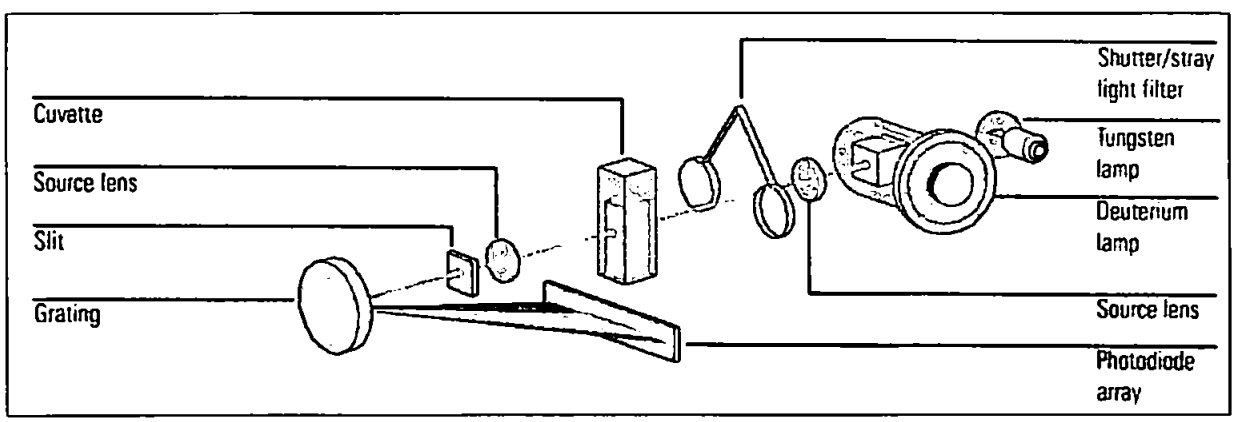

Figure 2.4 Optical system of Hewlett Packard 8453 spectrometer[220].

Table 2.3 Physical specifications of Hewlett Packard and Ocean Optics spectrometers.

Type	Hewlett Packard 8453 Specifications	Ocean Optics PSD-1000 Specifications
Dimensions	34.4 cm (length) 56.0 cm (width) 18.5 cm (height)	17.7 cm (length) 13.2 cm (width) 3.8 cm (height)
Weight	14 kg	0.48 kg
Power consumption	220 VA	
Ambient operating temperature	0 – 55 °C	N / A
Humidity	< 95 %, at 25 - 40°C	N / A
Operating Altitude	Up to 2000 m	N / A

2.2.3 PROCEDURES

2.2.3 (a) WAVELENGTH REPEATABILITY

Figure 2.5 shows the line spectrum of the HG-1 mercury / argon calibrating lamp with corresponding wavelength values. The HG-1 lamp was allowed to warm up for 10 min before use and connected to the appropriate spectrometer channel using a 50 μm UV-VIS optical fibre for the Master channel or a 50 μm VIS-NIR optical fibre for the slave channel.

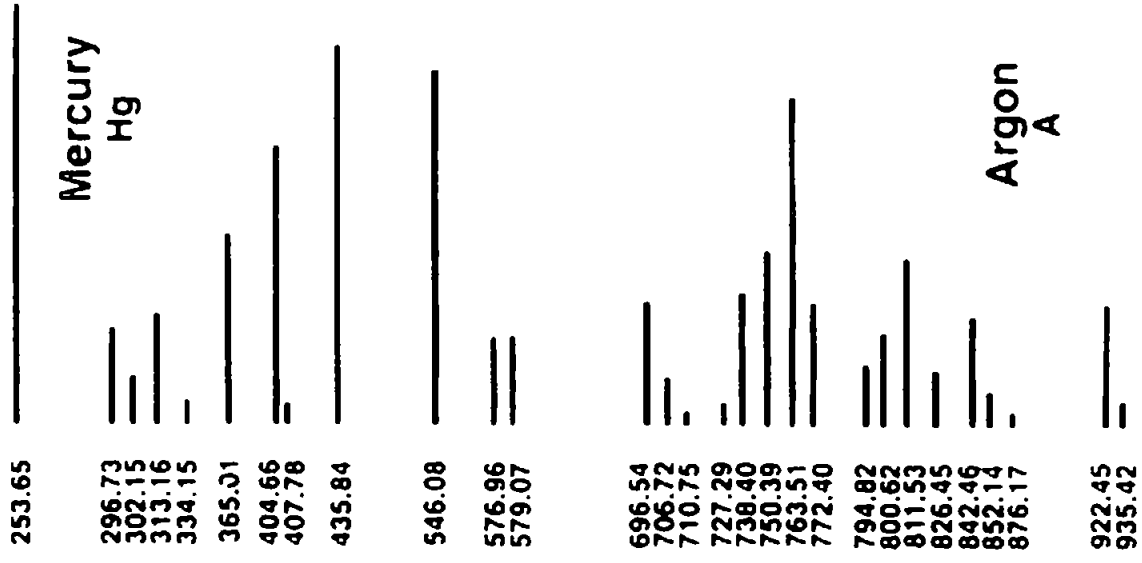

Figure 2.5 Line spectrum of HG-1 mercury / argon calibrating lamp.

Using a data cursor function within the Spectrascope software, individual spectral lines were highlighted at their point of maximum intensity and their reported wavelengths and pixel number recorded. Each peak was then manually identified by its reported wavelength and comparison of its peak height with neighbouring peak heights from the mercury / argon reference line spectrum (Figure 2.5).

Using the " Auto Calibration" facility within the Spectrascope software, each peak was assigned its true wavelength value. The software then performed a subpixel calibration routine[221] in order to determine the wavelength calibration coefficients for the spectrometer.

The relationship between pixel number of the detector elements and wavelength is given by a second-order polynomial.

$$\lambda_p = I + C_1 p + C_2 p^2$$

Where λ is the wavelength of pixel p, I is the intercept corresponding to the wavelength at detector pixel 0, C_1 is the first coefficient and corresponds to the dispersion (nm / pixels), C_2 is the second coefficient (nm / pixel^2) and corrects for non-linearity of response across the wavelength range.

The calibration coefficients were used to report the true wavelengths associated with each pixel and for labelling graphs and the data cursor readout within the software. These values are then entered into the "Unit cal data" option of the software, which allows the setting of wavelength calibration coefficients to re-calibrate the spectrometer. Calibrations of both Master (UV-VIS) and Slave (VIS-NIR) channels of the spectrometer were performed using the calibration facility within the Spectrascope software described above. After calibration the wavelength values of the line spectra of the mercury / argon lamp were noted and recorded on a spreadsheet.

In order to assess how often re-calibration of the spectrometer would be required, wavelength repeatability was checked daily for a duration of five weeks and the individual deviations of the recorded lines from the true mercury / argon wavelengths (Figure 2.5) were recorded. These individual line deviations were averaged to give an overall deviation of the whole line spectrum from the initial calibration.

2.2.3 (b) PHOTOMETRIC LINEARITY

Five spectra of the $KMnO_4$ (1 per second) standards were acquired on the Ocean Optics spectrometer. These readings were then averaged to give a mean absorbance value. All standards were also analysed using a Hewlett Packard 8453 diode array spectrometer with a 1cm path length quartz cuvette, with five replicate analyses per standard as a comparison.

2.2.3 (c) INSTRUMENTAL NOISE

Spectra of the $KMnO_4$ standards were acquired on the Ocean Optics spectrometer as a pseudo-continuous 15 min scan at the wavelength maximum*(523nm) using the "History Channel". The history channel is a function within the software that allows user defined operations e.g. single diode monitoring, mathematical functions on single diodes or a number of diodes. Up to four user defined history channels can run simultaneously and in effect the history channel can be described as a digital chart recorder.

Due to the need for computer processing time (dependent on the mathematical operations required by the user) the minimum acquisition time between data points was 0.25 s, which meant that 3600 data points were acquired and averaged during the 15 min scan and exported to a spreadsheet. Instrumental noise was recorded as the peak-to-peak variation defined as (max signal - min signal) over the 15 min scan for the absorbance standards specified in section 2.2.1.

2.2.3 (d) INSTRUMENTAL DRIFT

Using the history channel instrumental drift was assessed by monitoring a 1.0 A.U. permanganate standard at λ_{max} over a period of six hours. As a reference the permanganate standard was also monitored using a Hewlett Packard 8453 diode array spectrometer for six hours (21600 s) with individual spectra recorded every 2 min (120 s) resulting in the acquisition of 181 spectra.

2.3 RESULTS & DISCUSSION

2.3.1 SPECTROMETER CALIBRATION

Figure 2.6 shows the line spectrum of the mercury / argon calibration lamp taken by the 2D Spex CCD spectrometer. The spectrum showed excellent agreement in terms of wavelength accuracy and relative peak heights to neighbouring lines with the line spectrum quoted by the manufacturer Figure 2.5.

Figures 2.7 & 2.8 show both the Master and Slave line spectra before and after the initial calibration described in section 2.2.3 (a). The recalibrated Master channel had a +10 nm shift to higher wavelengths from the uncalibrated spectrum.

---

* For clarity the abbreviation $\lambda_{max.}$ will be used throughout this thesis.

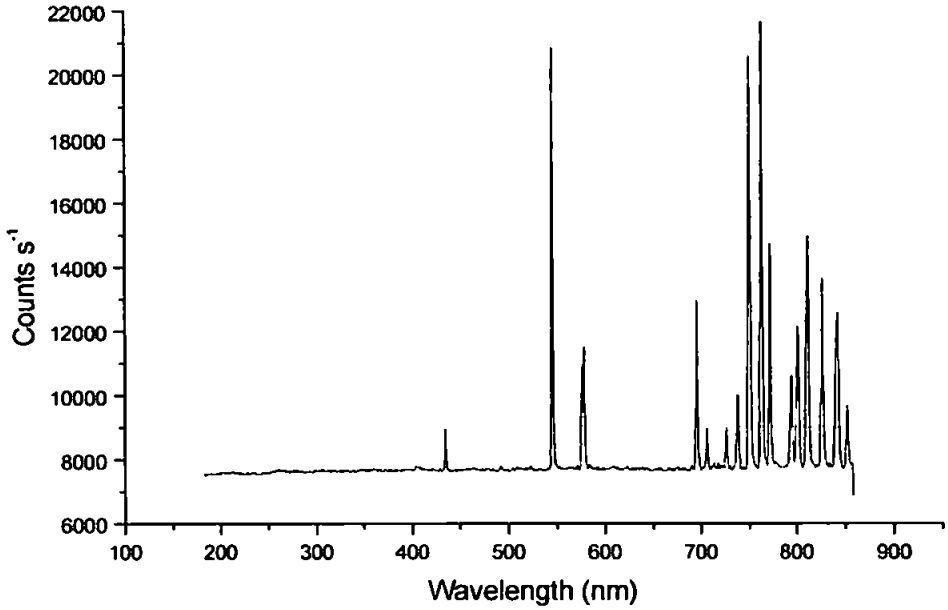

Figure 2.6 Two-dimensional CCD spectrum of Hg/Ar calibration lamp.

Recalibration of the Slave channel showed a +6 nm shift from the uncalibrated spectrum. These shifts from the factory shipped settings were considerable but should be viewed as a one-off large deviation. The increased sensitivity of the recalibrated spectra was due to the incorporation of collimating lenses into the spectrometer housing to focus light from the fibres onto the CCD. Section 2.3.3 discusses the evaluation of the spectrometer in terms of long term wavelength drift and repeatability.

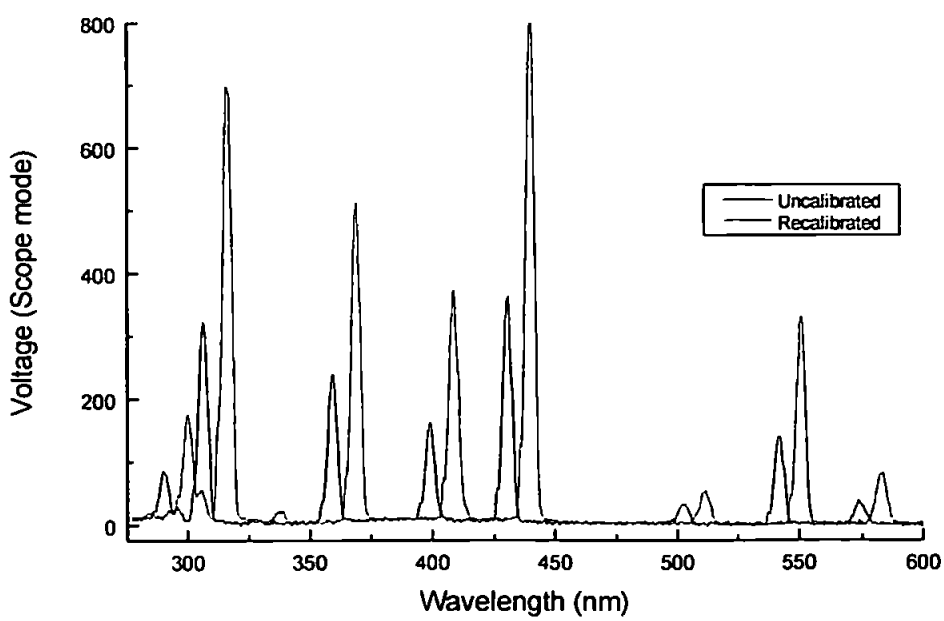

Figure 2.7 Ocean Optics Master channel spectrum of Hg / Ar calibration lamp.

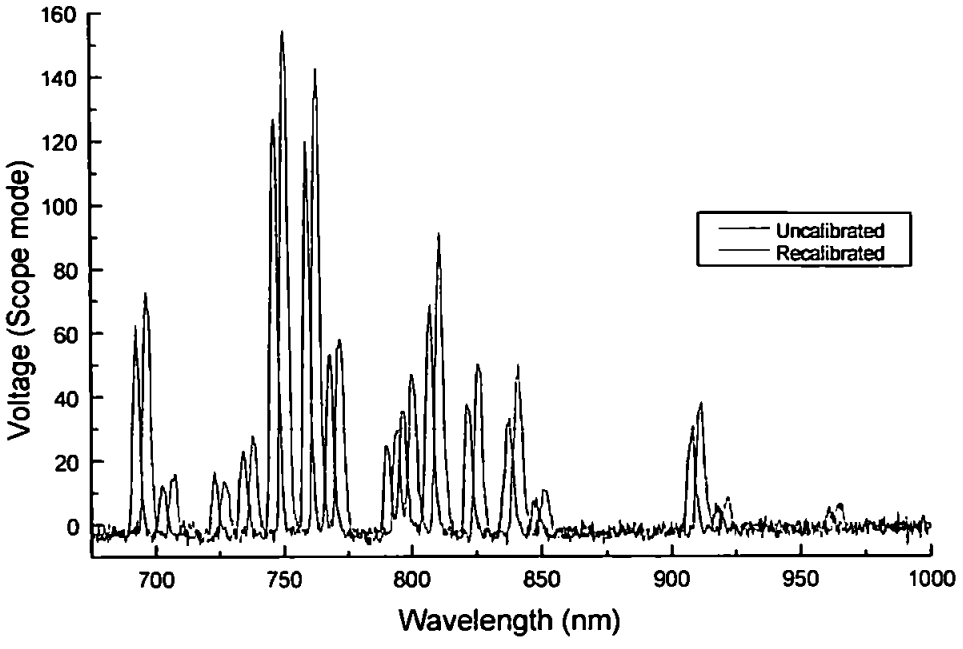

Figure 2.8 Ocean Optics Slave channel spectrum of Hg / Ar calibration lamp.

Figure 2.9 shows the 510 nm – 585 nm region of the Mercury / Argon lamp viewed by the 2D CCD spectrometer. The Ocean Optics spectrometer however was unable to resolve the pair of Hg lines at (576.960 and 579.066 nm)[222] that occurs at approximately 578 nm (Figure 2.7), in comparison to the 2D CCD spectrum Figure 2.9, which clearly shows the pair of lines occurring at 576.85 nm and 587.97 nm. These values are only + 0.1 nm deviation from the true values of 576.96 nm and 579.07 nm as shown in Figure 2.5.

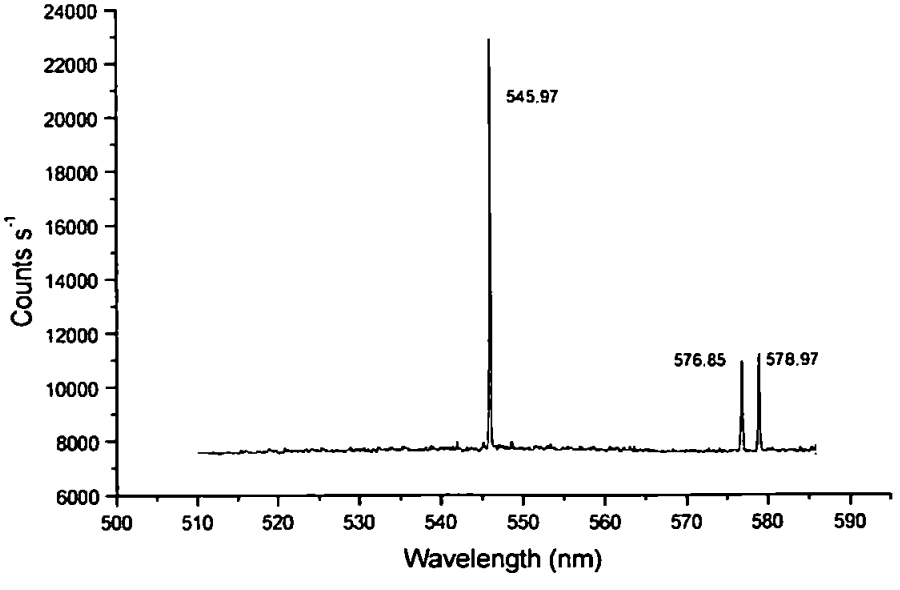

Figure 2.9 2D CCD spectrum of Hg 576.960 and 579.066 nm lines.

2.3.2 OPTICAL RESOLUTION

Optical resolution can be defined as a measure of the instruments' capability to distinguish between two closely adjacent wavelengths. Two wavelengths are considered resolved, if the minimum between the two peaks of the detector signal is lower than 80 % of the maxima, known as the Rayleigh Criterion[197], as shown in Figure 2.10.

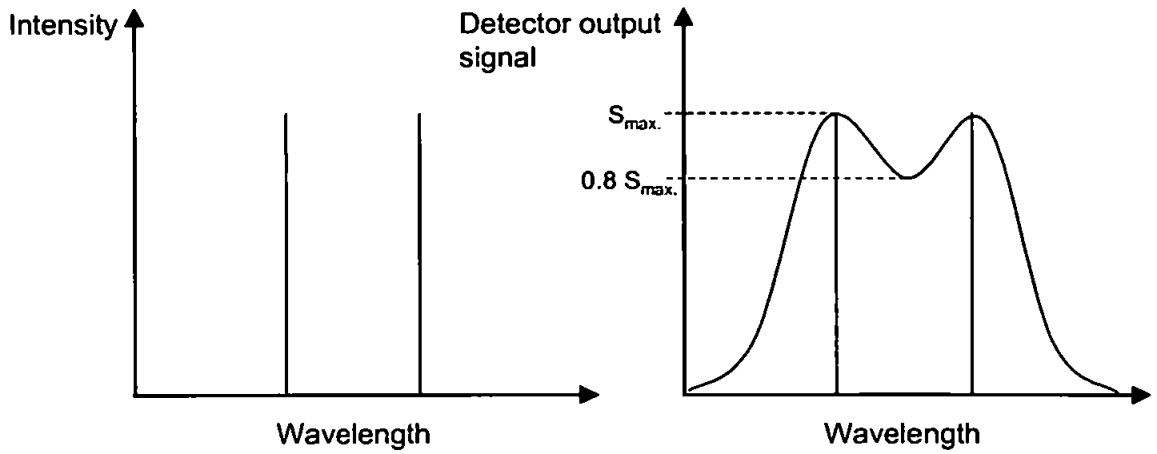

Figure 2.10 Schematic diagram of resolution as defined by the Rayleigh Criterion.

Resolution is dependent upon two factors;

The first is "instrumental spectral bandwidth" (SBW), measured as the Full Width Half Maximum (FWHM) of a monochromatic source. For scanning instruments SBW is primarily a function of the entrance and exit slits of the monochromator and the dispersion of the grating. For a diode array instrument it depends primarily on the groove density (lines / mm) of the grating and the diameter of the entrance optics (optical fibre or slit).

The second factor affecting resolution is known as the "sampling interval". For a conventional scanning spectrophotometer the resolution is usually the same as the SBW because the sampling interval is variable, usually dependent upon the scan speed and therefore resolution is not affected. However diode array instruments, in which the signal is digitised, the sampling interval is fixed due to array parameters and this can affect resolution (see Figure 2.11). As a result diode array spectral resolution also depends on the number of detector elements per spectral range.

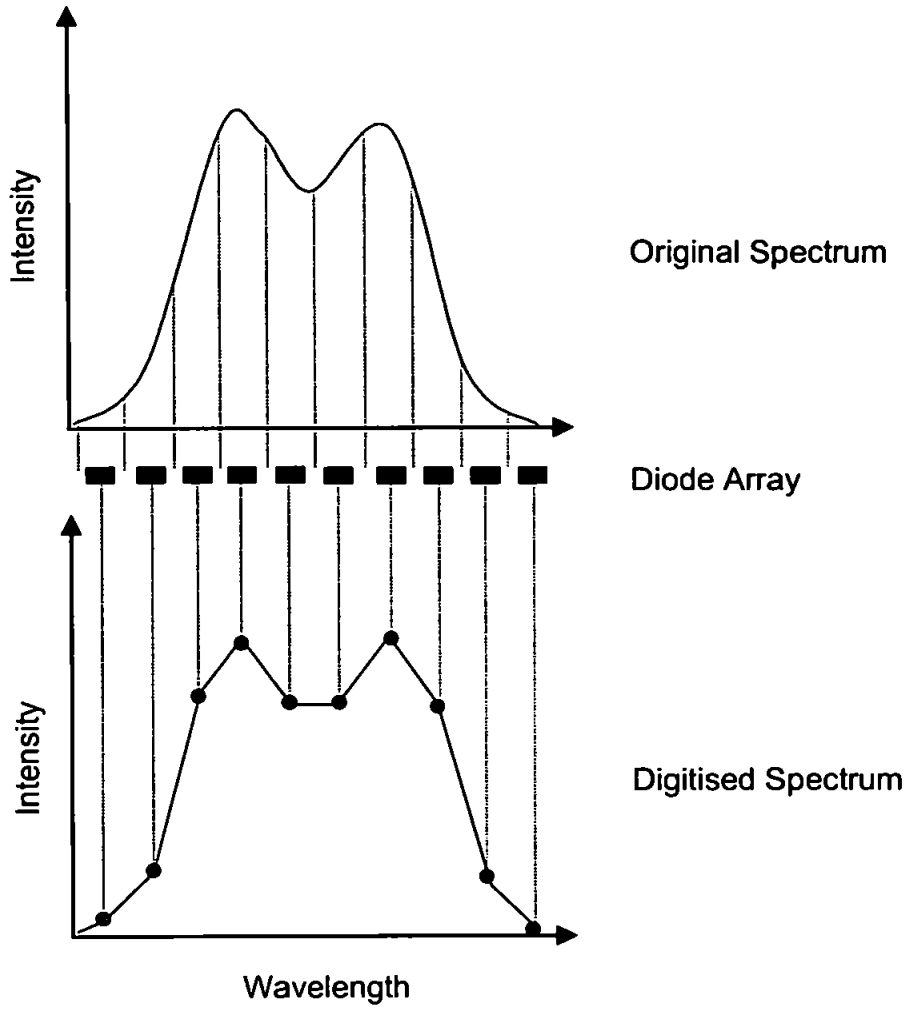

Figure 2.11 The effect of digital sampling on spectral data.

Spectra obtained are "digitised" and the distance between the centre of two diodes is the sampling interval. If the sampling interval is small relative to the natural bandwidth of the measured sample, it will have little effect on the resolution.). Accuracy of a measured sample depends on the ratio of the SBW to the natural bandwidth (NBW) of the absorbing sample. NBW is defined as the width of the absorption band at half the absorption maximum. Typically the ratio between instrumental bandwidth and natural band width should be around 0.1 or less[197]. If this ratio is larger then resolution can be degraded (Figure 2.11).

The optical resolution for the Ocean Optics system[222] in nm (FWHM) was calculated as shown below :

Optical Resolution (nm) = Dispersion (nm / pixels) x Resolution (pixels)

Where :-

Dispersion (nm / pixel) = spectral range of the grating ÷ number of detector elements.

Master Channel :

$$\text{Dispersion (nm / pixel)} = \frac{700 - 200}{1024} = \textbf{0.49 nm / pixel}$$

Slave Channel :

$$\text{Dispersion (nm / pixel)} = \frac{1000 - 500}{1024} = \textbf{0.49 nm / pixel}$$

Typical pixel resolution by fibre diameter

- 10 micron fibre = 3.2 pixels
- 25 micron fibre = 4.2 pixels
- 50 micron fibre = 6.5 pixels
- 100 micron fibre = 12.0 pixels
- 200 micron fibre = 24.0 pixels

Therefore resolution for the PSD-1000 Ocean Optics spectrometer can be defined as:

Optical Resolution (nm) = Dispersion (nm / pixels) x Resolution (pixels)

200 micron fibre

0.49 nm / pixel x 24.0 pixels = 11.8 nm ≈ **12 nm**

100 micron fibre

0.49 nm / pixel x 12.0 pixels = 5.9 nm ≈ **6 nm**

50 micron fibre

0.49 nm / pixel x 6.5 pixels = 3.2 nm ≈ **3 nm**

Resolution can be increased by increasing in groove density of the grating, decreasing the slit or optical fibre diameter, or decreasing the size of the diodes within an array. This is achieved at the expense of spectral range and signal strength respectively. However in practice, the majority of UV/Visible spectroscopy applications involve broad band spectra, particularly in solution where NBWs' are usually greater than 20 nm[197]. Sensitivity of the field-deployed system was given a higher priority than a high resolution system. This was because broad band spectra (e.g. Greiss azo dye, Figure 2.18) were typically involved in the field deployed system and therefore high resolution was not required.

Therefore gratings were chosen to facilitate a wide spectral range (500 nm) and relatively large diameter 200 μm optical fibres were used for increased sensitivity, both at the expense of resolution.

2.3.3 WAVELENGTH REPEATABILITY

Wavelength repeatability can be defined as the ability of an instrument to correctly return to the set wavelength repeatedly. It is different to wavelength accuracy, which is only of importance if measurements made on different instruments are to be compared. The difference can be considered analogous to the difference between accuracy and precision. The importance of wavelength repeatability is demonstrated in Figure 2.12. If a wavelength at the absorption maximum, λ_{max}, is selected as the analytical wavelength for quantitative measurements, then small wavelength errors in resetting to that wavelength will have a minimal effect on the measured absorbance A1 and consequently will give the most reproducible quantitative results. If a wavelength on the side of the absorption band, λ_{side}, is selected, the resulting errors in measured absorbance A2, with the same wavelength resetting error, will be more significant and the quantitative results will therefore be less reliable.

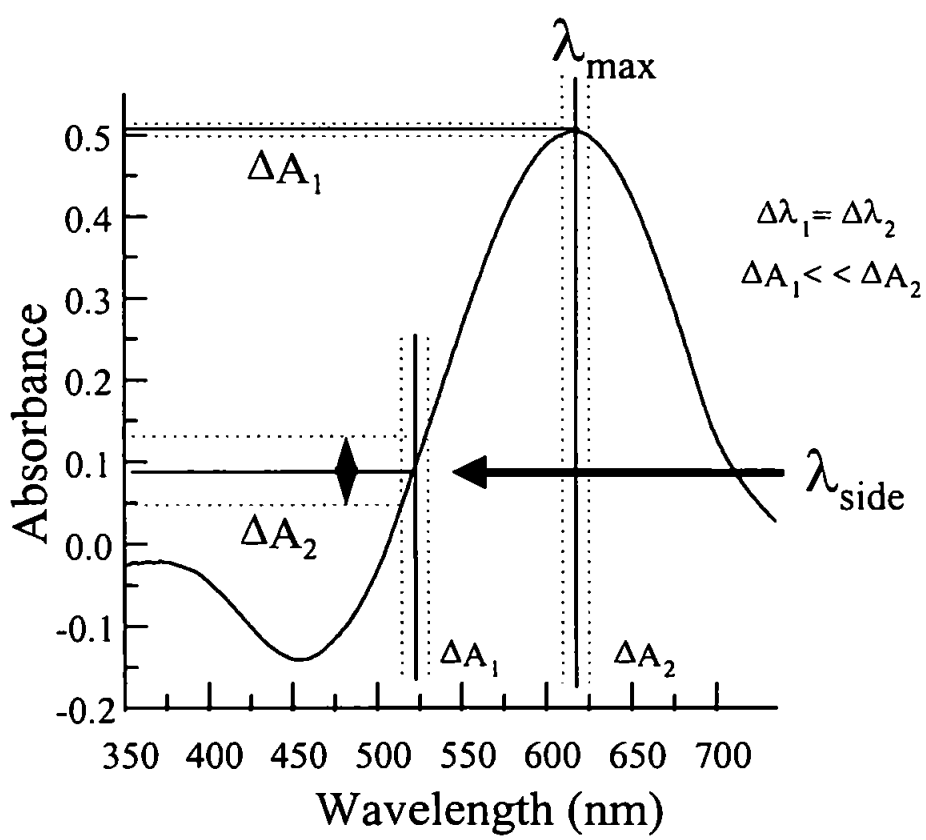

Figure 2.12 Error in wavelength repeatability.

Conventional mechanical scanning spectrophotometers have an inherent wavelength repeatability error due to their mechanical working parts and this error increases with time as parts wear. Diode array instruments have no mechanical parts (except a shutter in some cases) and therefore there is no mechanical error. The availability of data from all parts of the spectrum, unaffected by wavelength repeatability errors, permits the freedom to chose optimum wavelengths for improved dynamic range, sensitivity and selectivity and the increased information available can also provide the basis for the use of other advantages such as wavelength averaging. In addition, increased confidence can be placed on previously measured spectra of standards which have been stored in computer memory and then recalled for later use, aiding productivity and negating problems associated with expensive or unstable standards.

Figure 2.13 shows the deviation in nm of the Master (UV-VIS) channel from the initial calibration over a period of five weeks (refer to section 2.2.3 (a)). There was net negative drift from the original calibration of - 0.6 nm with a maximum deviation of -1.3 nm.

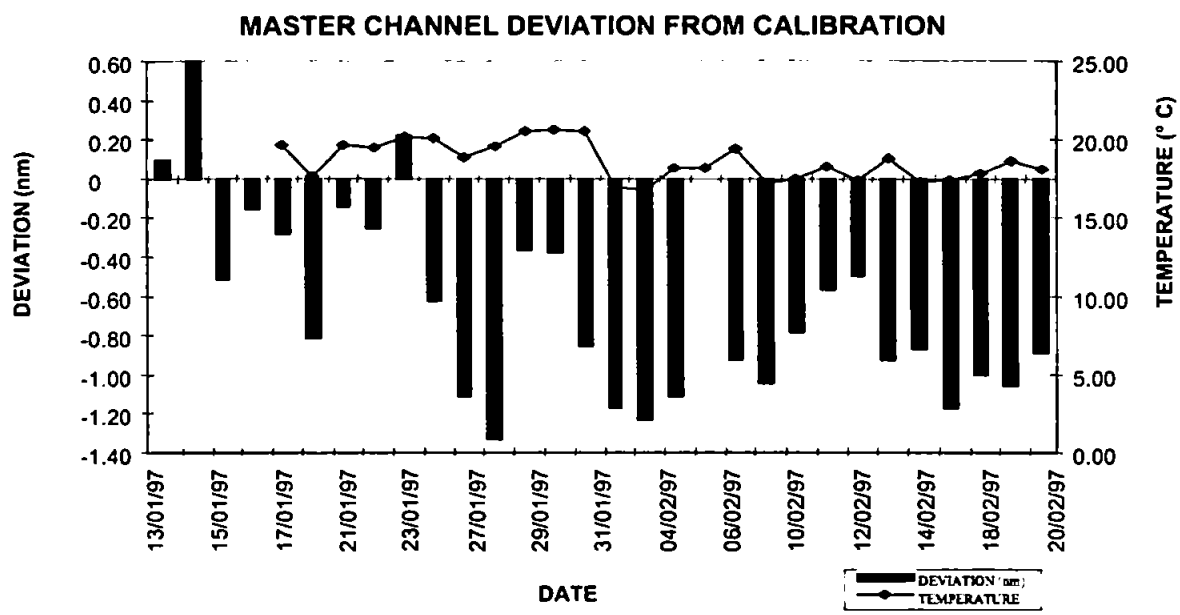

Figure 2.13 Wavelength repeatability of the Master channel.

Figure 2.14 shows the deviation in nm of the Slave (VIS-NIR) channel from the original calibration. There was a net positive drift of 0.7 nm with a maximum deviation of 1.2nm.

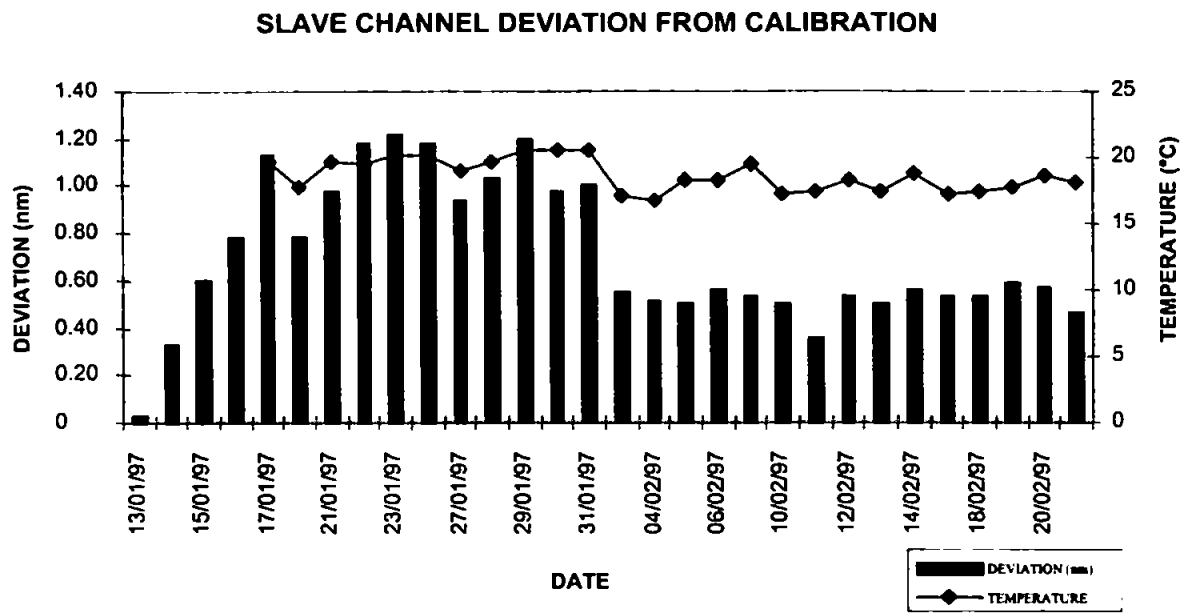

Figure 2.14 Wavelength repeatability of the Slave channel.

Figures 2.15 and 2.16 show scatter plots of mean daily wavelength deviation against air temperature for the Master and Slave channels respectively. There was a poor correlation and other factors, such as the relatively poor quality of the individual optical components and optical bench will also contribute to this deviation.

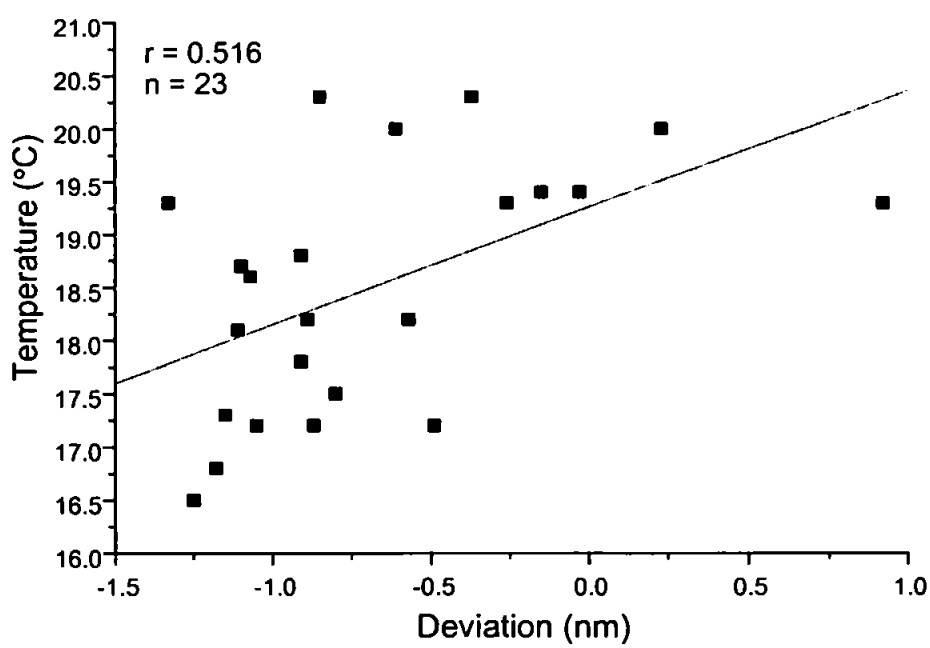

Figure 2.15 Scatter plot of mean daily deviation versus laboratory temperature (Master channel).

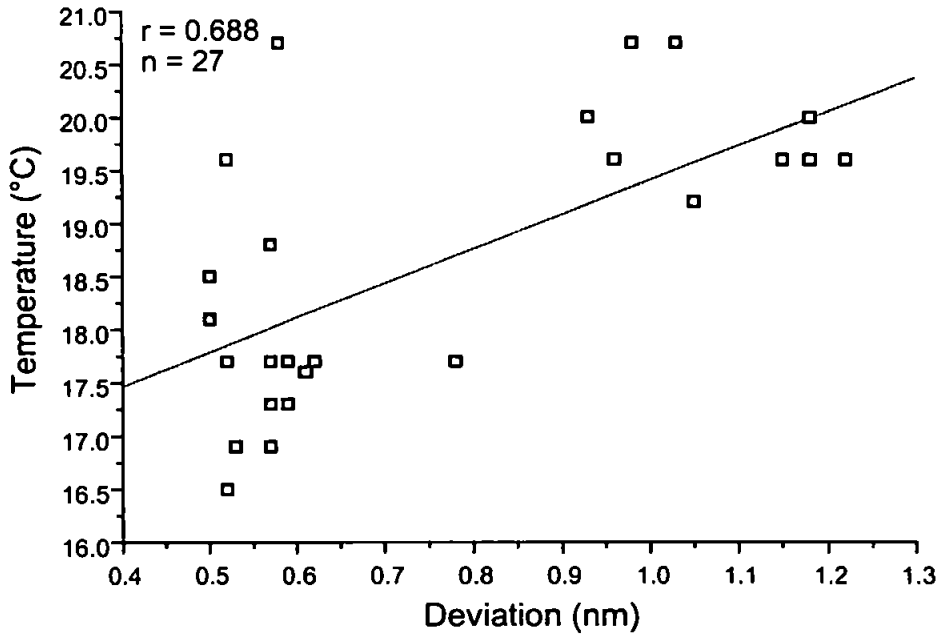

Figure 2.16 Scatter plot of mean daily deviation versus laboratory temperature (Slave channel).

It should also be noted that the fluctuations in air temperature were relatively small and a wider temperature variation (such as would be encountered in a process or field deployment) will cause expansion or contraction of the mirror within the spectrometer and consequently affect wavelength repeatability.

Figures 2.17 and 2.18 show spectra of a 1.0 A.U. permanganate standard and an azo dye peak formed by the Greiss reaction between nitrite, sulphanilamide and N-(1-naphthyl) ethylenediamine dihydrochloride. Table 2.4 gives the absorbance values at $\lambda_{max.}$, $\lambda_{max.} \pm 4$ nm and $\lambda_{max.} \pm 8$ nm for both compounds. Differences in absorbance from $\lambda_{max.}$ at the other wavelengths are given in terms of A.U. and %.

Table 2.4 Effect of wavelength drift on absorbance measurements.

Wavelength drift From $\lambda_{max.}$ (nm)	Absorbance $KmnO_4$ (1A.U std.) $\lambda_{max.}$ @ 523 nm	Difference from $\lambda_{max.}$	% Diff.	Absorbance Greiss azo dye $\lambda_{max.}$ @ 540 nm	Difference from $\lambda_{max.}$	% Diff.
-8	0.928	-0.102	**-9.9**	0.460	-0.010	**-2.1**
-4	0.992	-0.038	**-3.7**	0.468	-0.002	**-0.4**
0	**1.030**	**0.000**	**0.0**	**0.470**	**0.000**	**0.0**
4	0.979	+0.051	**+5.0**	0.467	+0.003	**+0.6**
8	0.939	+0.091	**+8.8**	0.465	+0.005	**+1.1**

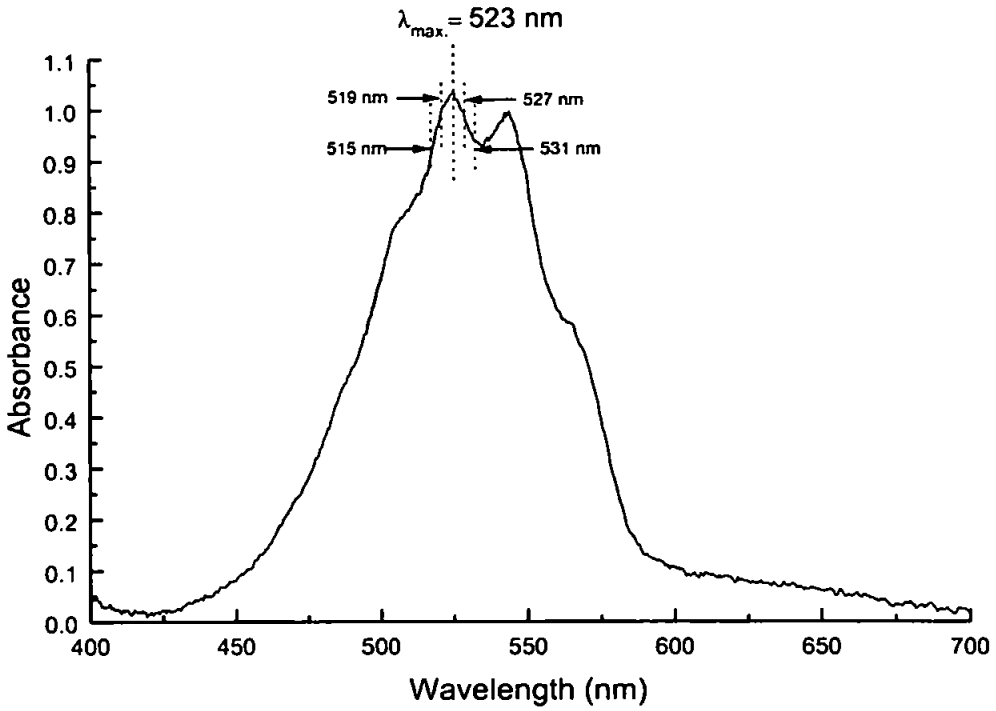

Figure 2.17 Spectrum of 1.0 A.U. permanganate standard.

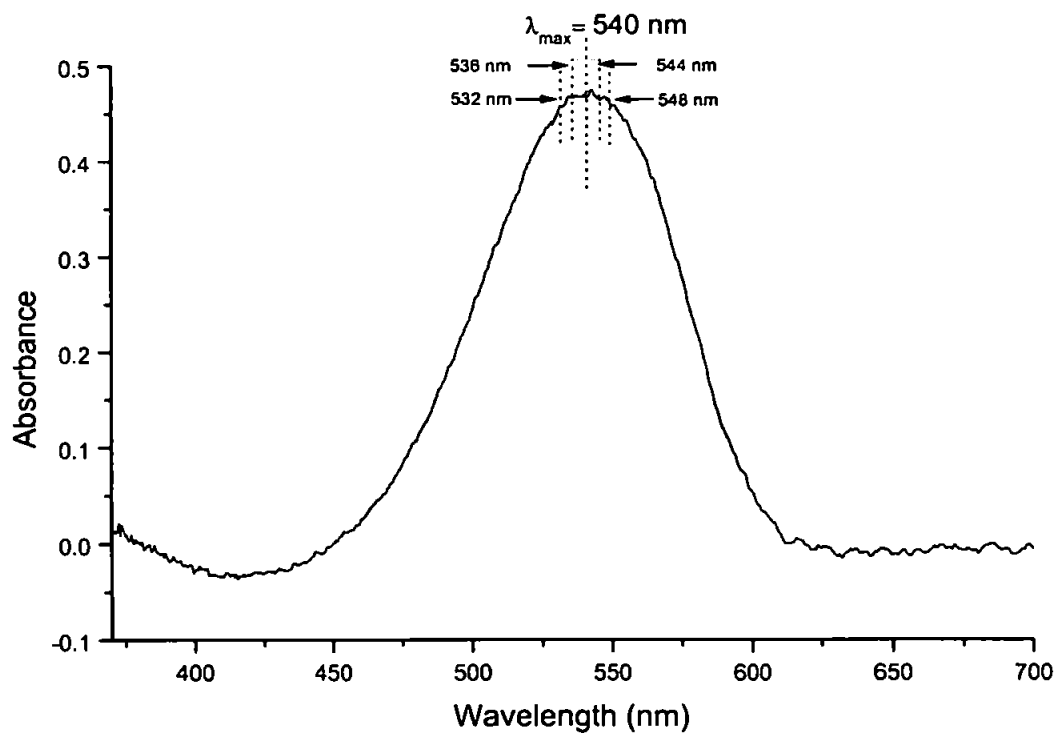

Figure 2.18 Spectrum of Greiss azo dye.

For the intended application and proposed environmental deployment, the change in absorbance resulting from a wavelength drift of 4 nm was deemed acceptable, i.e.< 5%. The maximum wavelength drifts recorded over a 5-week period are typically less than ±1.5 nm and therefore the effect on absorbance measurements would be well within this ±5 % tolerance. With this information, and consideration of field conditions compared to laboratory conditions, a field deployment of up to 5 weeks without recalibration would therefore be feasible in terms of wavelength drift. In a field environment however there will be significant diurnal and seasonal temperature fluctuations that will not only affect wavelength drift but other system parameters, including reaction rate. Therefore thermostatting of the detector (and other components and reagents) would be advantageous.

2.3.4 PHOTOMETRIC LINEARITY

Photometric linearity can be defined as how accurately an instrument measures absorbance with increasing concentration. The most accurate method is to measure the additive absorbance of a series of calibrated neutral density glass filters[224] but a more cost effective and widely used method is to use liquid absorbance standards. The use of solution standards combine operator errors and cell errors (optical defects) in one set of measurements and, providing that Beer's Law is obeyed for the standard concerned, can be used at any absorbance level in the range of the instrument. The advantage of using a solution as an absorbance standard is that the procedure for its measurement closely resembles that for a normal sample. The disadvantages of solution standards are that they do not posses the high degree of optical neutrality found with solid filters, they require careful preparation and they usually have larger temperature coefficients than solid standards.

Potassium dichromate in 0.005 M sulphuric acid is a commonly used solution standard for the routine calibration of spectrophotometers[224] and is readily available from commercial suppliers as a calibration set. However potassium dichromate standards are used in the 200-400 nm region of the spectrum, requiring a UV source, which at present is not available for the Ocean Optics system. Therefore a standard that absorbs in the visible region was required. Potassium permanganate was therefore chosen as the standard for the visible region due to its well defined absorption spectrum and abundance of literature information concerning its absorption characteristics[225].

Figure 2.19 shows the overlaid spectra for permanganate standards in the range 0-2 A.U. recorded by the Ocean Optics spectrometer. Figure 2.20 shows the overlaid spectra for the same permanganate standards in the range 0-3 A.U. recorded using the Hewlett Packard 8453 instrument.

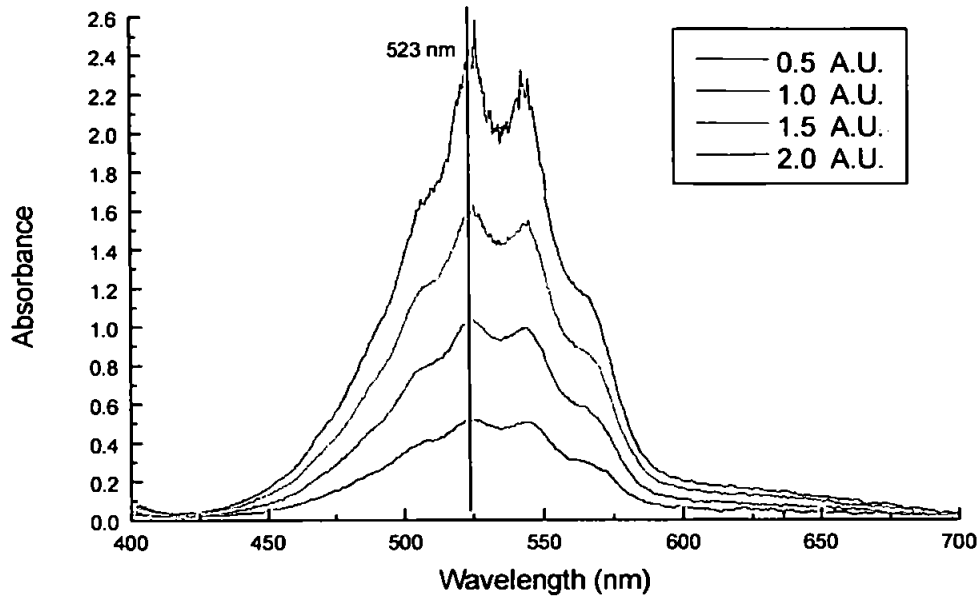

Figure 2.19 **Spectra of permanganate absorbance standards (PSD-1000 Ocean Optics spectrometer).**

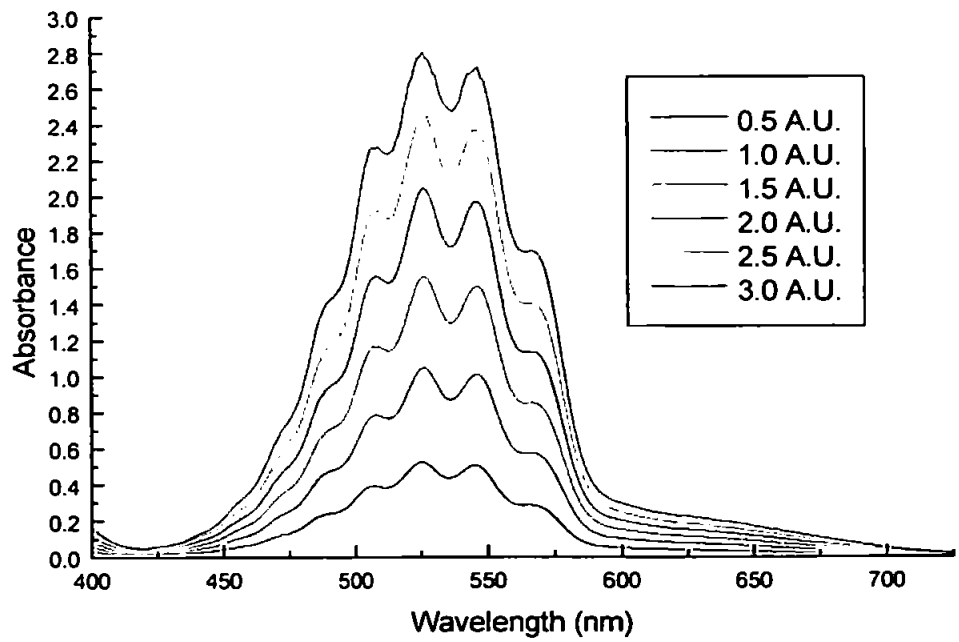

Figure 2.20 **Spectra of permanganate absorbance standards Hewlett Packard 8453 spectrometer.**

The spectra taken by the Ocean Optics spectrometer (Figure 2.19) show the characteristic absorbance profile of permanganate. However in comparison with the spectra recorded by the Hewlett Packard 8453 (Figure 2.20) the absorbance profiles lack the resolution of the high performance laboratory instrument, which is quoted as 2 nm. This is dependent on the type and quality of the optical and electronic components used, particularly the grating and the diode array and the ~£15 k bench top laboratory instrument has higher grade components than the ~£ 1.5 k portable instrument.

In addition the absorbance profiles from the Ocean Optics contain a higher degree of noise than the Hewlett Packard spectrometer, particularly at the higher absorbances. This again is due to the poorer design of the Ocean Optics particularly with regard to light scatter and stability of the optical and electronic components. Table 2.5 shows a comparison of the results obtained using the two spectrometers.

Table 2.5 Comparison of results between PSD-1000 Ocean Optics spectrometer and Hewlett Packard 8453 spectrometer.

Abs. Standard (A.U.)	Ocean Optics Mean Abs. (A.U.)	Error ±	R.S.D (%) (n=5)	HP 8453 Mean Abs. (A.U.)	Error ±	R.S.D (%) (n=5)
0.5	0.512	+0.012	0.23	0.513	+0.013	0.02
1.0	1.019	+0.019	0.56	1.024	+0.024	0.03
1.5	1.570	+0.070	0.61	1.521	+0.021	0.04
2.0	2.265	+0.265	3.2	2.001	+0.001	0.05
2.5	N/A	N/A	N/A	2.418	-0.082	0.14

The Hewlett Packard 8453 out performed the PSD-1000 spectrometer in terms of photometric accuracy with mean absorbance values obtained being in excellent agreement with the theoretical values for the standards at absorbances less than 2.5 A.U. The Ocean Optics spectrometer does show good agreement absorbance with the true values at lower absorbances (0 – 1.0 A.U.) but loss of linearity starts to occur at 1.5 A.U. The spectrum for 2.0 A.U. shows a noisy profile and an elevated absorbance value (≈ 2.3 A.U.), which is indicative of the poor performance of the Ocean Optics CCD detector at low light levels. At even higher absorbances (2.5 A.U.), the Ocean Optics spectrometer was unable to detect enough incident radiation to perform an integration (Figure 2.21) and any sample absorbing at this level clearly exceeds the photometric range of this instrument.

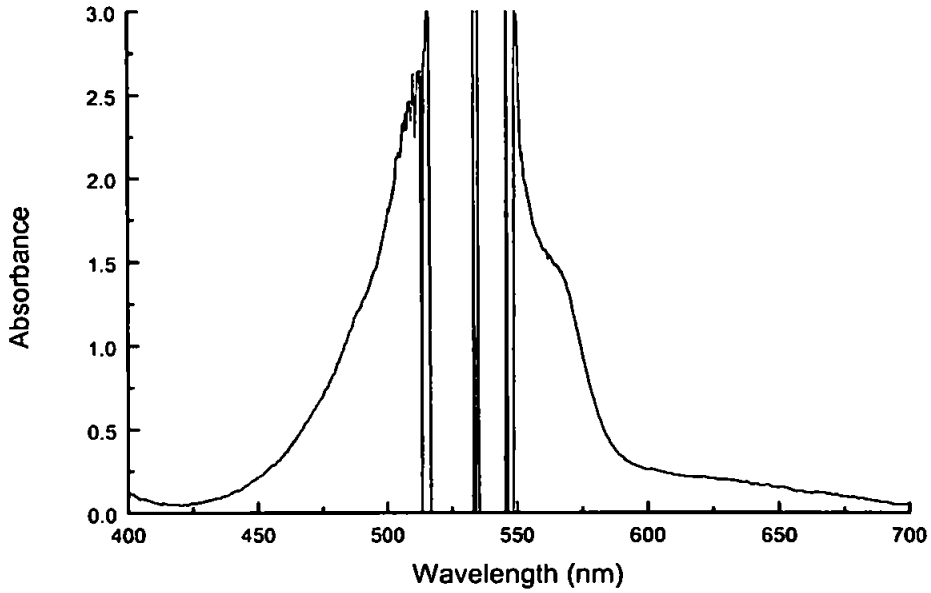

Figure 2.21 Spectrum of 2.5 A.U. permanganate standard (PSD-1000 Ocean Optics Spectrometer).

With reference to the relative standard deviations (R.S.D.s) for both instruments, first observations show that the Ocean Optics spectrometer R.S.Ds are typically an order of magnitude higher than those of the Hewlett Packard 8453 instrument. Again it is reasonable to expect the Hewlett Packard spectrometer to have a higher performance than the Ocean Optics spectrometer in terms of precision due to the higher quality optics involved.

Figures 2.22 and 2.23 show the linear plots for the measured absorbance versus the theoretical absorbance values for the standards for both instruments. Error bars represent three standard deviations (n = 5) for each standard. Good linearity was found with both instruments; the Ocean Optics spectrometer was linear up to 1.5 A.U. (r = 0.9996, n = 4), the Hewlett Packard 8453 spectrometer was linear up to 2.5 A.U. (r = 0.9994, n = 6). With respect to the regression coefficient of 0.9927 the linear range of the Ocean Optics spectrometer could be quoted up to an absorbance of 2 A.U. However considering the higher measured value of 2.3 A.U. compared to the theoretical value of 2.0 A.U. and the effect of instrumental noise, which increases the uncertainty of the measurement (see error bars), it would be prudent to quote the linear range of the Ocean Optics spectrometer lower than this at 1.5 A.U.

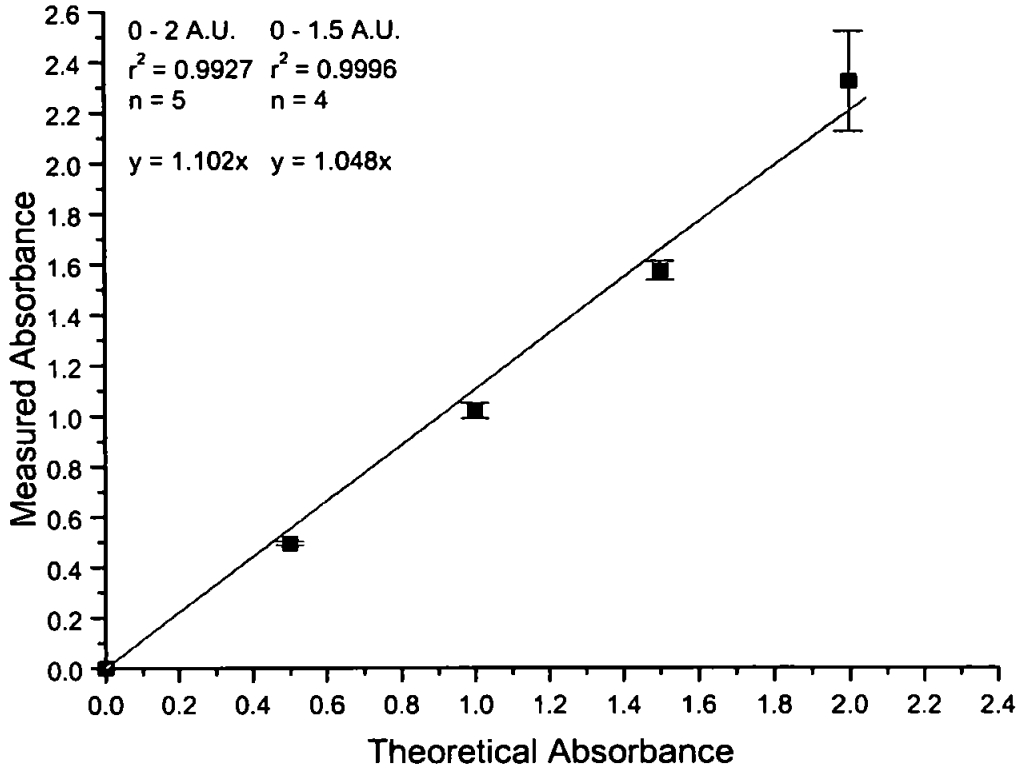

Figure 2.22 Photometric linearity of the PSD 1000 Ocean Optics spectrometer.

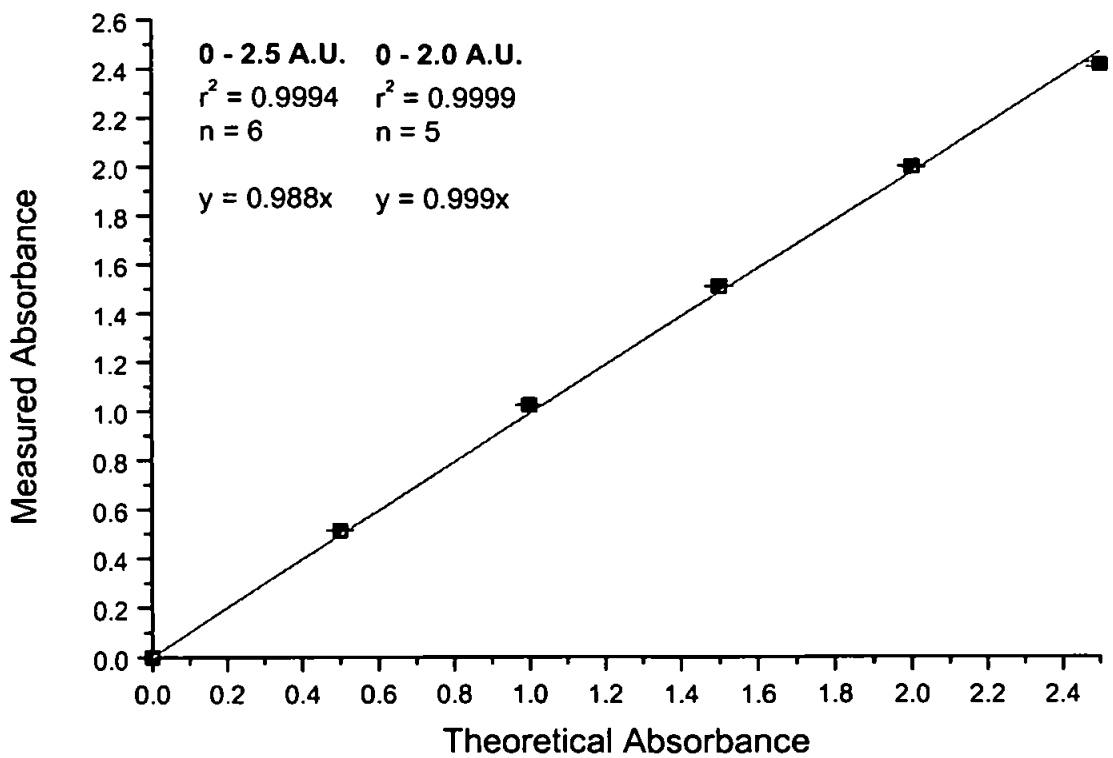

Figure 2.23 Photometric linearity of the HP 8453 spectrometer.

2.3.5 INSTRUMENTAL NOISE (Photometric Precision)

Noise is short-term (seconds) variation in the measured absorbance. It is associated with each component of an instrument, that is, with fluctuation in source intensity, all signal processing elements, and the detector itself. The noise from each of these elements may consist of several types which arise from several sources. Thus, the noise that is finally observed is a complex composite that usually cannot be fully characterised. The precision of spectrophotometric analyses are often limited by the uncertainties or noise associated with the instrument[226]. In order to make a spectrophotometric measurement three steps must be taken; a 0% T adjustment, a 100% T adjustment and a measurement of % T with the sample in the radiation path. The noise associated with each of these individual steps combine, resulting in a net uncertainty for the final value obtained for T. Through a detailed theoretical and experimental study[227] the equation below has been derived:

$$\frac{\sigma_c}{c} = \frac{\sigma_t}{T \ln T} = \frac{0.434\sigma_t}{T \log T}$$

For a limited number of measurements, population standard deviations σ_C and σ_T are replaced with sample standard deviations s_C and s_T to give :

$$\frac{s_c}{c} = \frac{0.434 s_t}{T \log T}$$

This equation relates the relative standard deviations c (s_C/c) to the absolute standard deviation of the transmittance s_T. Clearly this illustrates that the uncertainty in a photometric concentration measurement varies in a complex way with the magnitude of the transmittance. However in many circumstances the situation is more complicated because the uncertainty s_T is also dependent upon T. Several sources of instrumental uncertainties have been shown to have a net effect on the precision of transmittance measurements. These uncertainties in transmittance measurement fall into three categories depending on how they are affected by the magnitude of the transmittance T. Case I uncertainties, where the precision s_T is independent of T and equal to a constant k_1. Case II uncertainties, where s_T is proportional to $\sqrt{(T^2 + T)}$ and case III uncertainties, where s_T is directly proportional to T. Table 2.6 summarises information regarding the sources of these three types of uncertainties and the kind of instruments where each is likely to be encountered.

Table 2.6 **Types and sources of uncertainties in transmittance measurements. (where k_1, k_2 and $k_3$are constants for a given system)[198].**

Category	Characterised by	Typical Sources	Likely to be important in
Case I	$s_T = k_1$	Limited readout resolution	Inexpensive spectrophotometers
		Heat detector Johnson noise	IR and NIR spectrophotometers
		Dark current and amplifier noise	Regions where source intensity and detector sensitivity are low
Case II	$s_T = k_2 \sqrt{(T^2 + T)}$	Photon detector shot noise	High quality UV/visible spectrophotometers
Case III	$S_T = k_3T$	Cell positioning uncertainties	High quality UV/visible and IR spectrophotometers
		Source flicker	Inexpensive spectrophotometers

Figure 2.24 shows peak-to-peak noise at absorbances of 0.5, 1.0, 1.5 and 2.0 A.U. for a 15 min continuous sampling period. This information is summarised in Table 2.7.

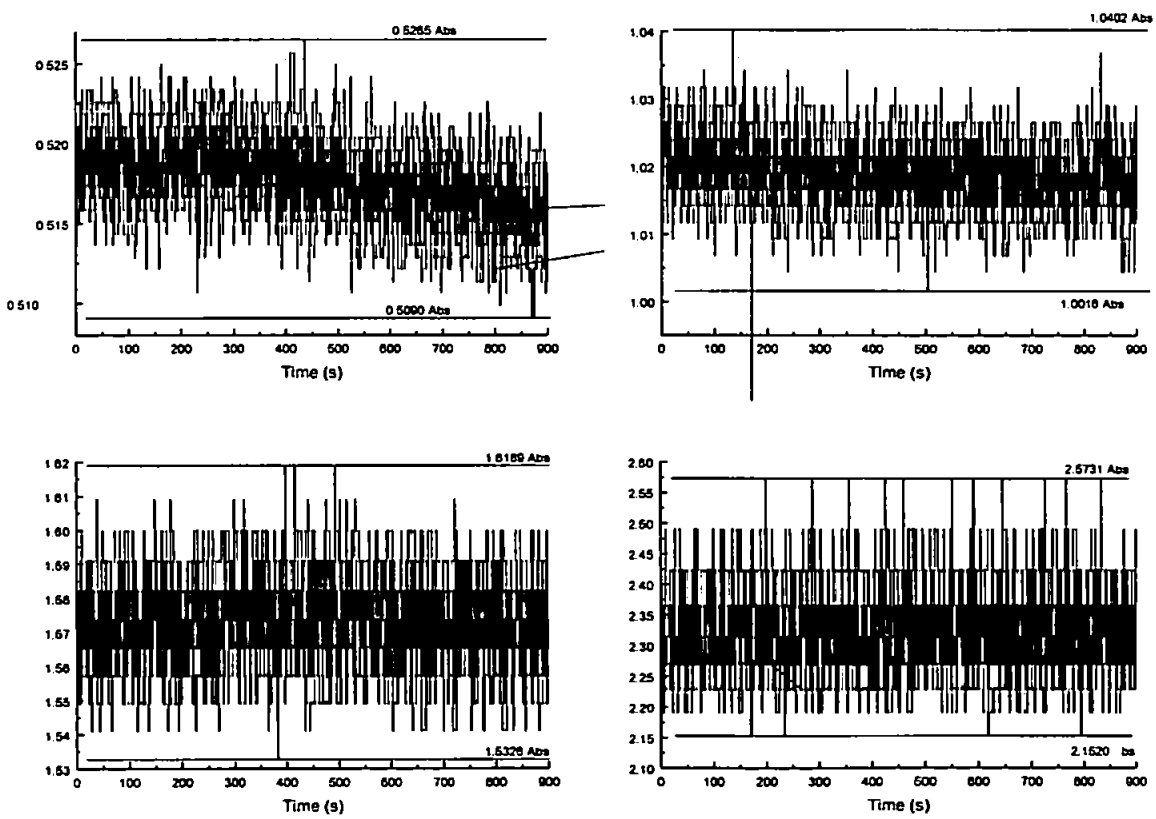

Figure 2.24 **Peak-to-peak noise at various absorbance levels.**

Table 2.7 Peak-to-peak noise of the Ocean Optics PSD-1000 spectrometer.

Abs Standard (A.U.)	Ocean Optics Mean Abs. (15min)	Noise (peak-to-peak) (A.U.)
0.5	0.493	0.018
1.0	1.019	0.038
1.5	1.572	0.086
2.0	2.322	0.421
2.5	N/A	N/A

A graphical plot of this information, shown in Figure 2.25, illustrates the relationship between absorbance and instrumental noise for the Ocean Optics spectrometer.

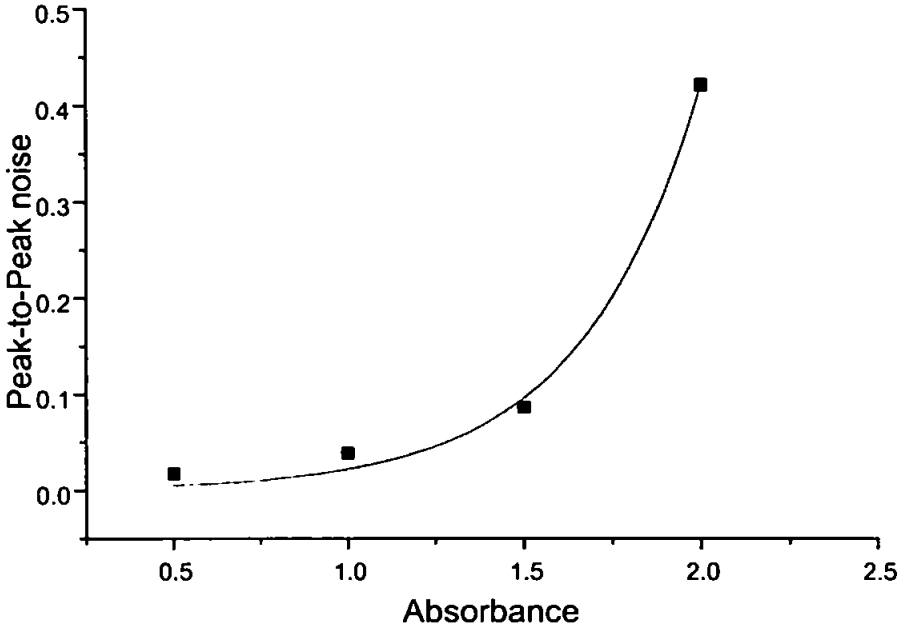

Figure 2.25 Absorbance versus peak-to-peak noise (PSD-1000 spectrometer).

At absorbances below 1.0 A.U the noise present was less than 0.05 A.U and therefore provided a good level of precision for analytical measurements. At higher absorbances up to 1.5 A.U the noise level, although twice that of the 1.0 A.U standard was still considered acceptable for the intended application of a field deployed instrument. However the noise level rose exponentially thoughout the data (Figure 2.25) and at absorbances of 2.0 A.U, the precision of analytical measurements would be adversely affected by the noise level of ± 0.4 A.U.

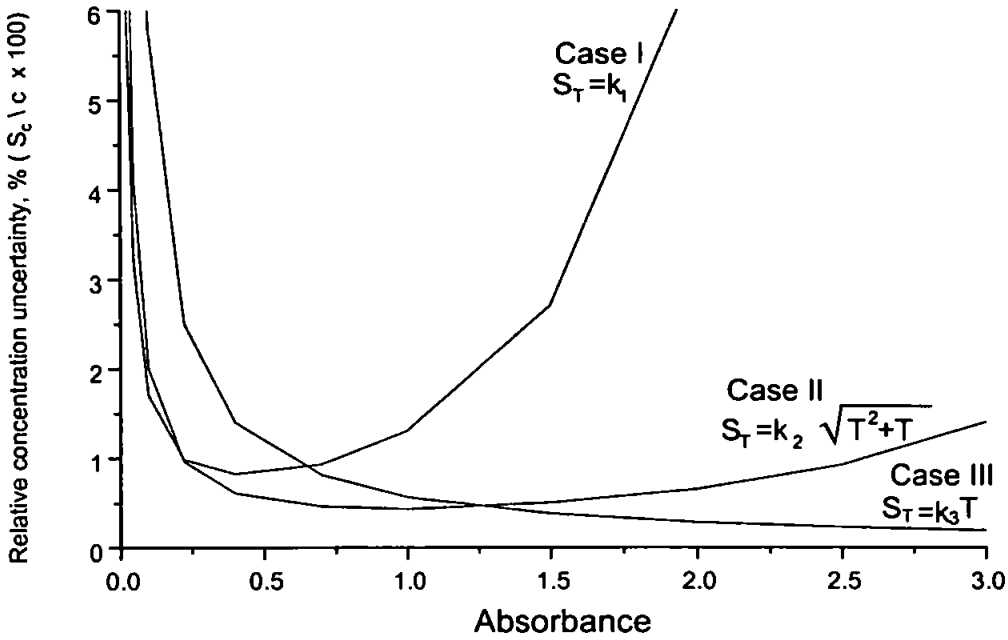

Figure 2.26 Relative concentration uncertainties versus absorbance Case I, Case II and Case III.

This high noise level at higher absorbance was due to the low analytical signal detected by the spectrometer relative to the signal arising from noise. As has been mentioned above this was due to the quality of both optical and electronic components of the diode array assembly.

Figure 2.26 shows a plot from experimentally derived data[198], and comparison with Figure 2.25 indicated that the instrumental noise of the Ocean Optics spectrometer arose from CASE 1 noise. CASE 1 uncertainties are often encountered with less expensive spectrophotometers such as the Ocean Optics system. CASE 1 is characterised by $S_T = k_1$, where S_T is the absolute standard deviation of the transmittance measurement. Due to CASE 1 noise the precision of a particular concentration determination depends upon the magnitude of T even though the instrumental precision is independent of T. An instrument limited by CASE 1 noise can be expected to give rise to concentration errors of 1-2% relative, but this level of precision can only be realised if the absorbance of a sample lies in the range 0.1 - 1 A.U.

This reinforces the discussion on photometric linearity (section 2.3.4) in which it was suggested that samples absorbing above 1.5 A.U. should be diluted (Ocean Optics system only). This protocol will also ensure good precision in concentration determinations.

2.3.6 INSTRUMENTAL DRIFT

Drift is long term (hours) variation in the measured absorbance. Drift should be very low with double or split-beam spectrophotometers because they inherently correct for this problem. However for single beam instruments such as the Ocean Optics spectrometer the drift is important because it is an indicator of how frequently a blank measurement must be made to ensure a desired accuracy. Table 2.8 shows the results obtained with the Ocean Optics spectrometer using a permanganate standard of 1.0 A.U monitored at $\lambda_{max.}$ over a period of six hours.

Table 2.8 Instrumental drift of the Ocean Optics spectrometer.

Time slices (min)	Mean abs	Std Dev	Max	Min	+ ve from mean	- ve from mean
0-13.5	1.022	0.005	1.038	1.009	0.015	0.013
13.5-27	1.018	0.005	1.035	1.005	0.017	0.014
27-40.5	1.014	0.018	1.033	0.998	0.019	0.016
40.5-49.5	1.010	0.005	1.026	0.996	0.015	0.015
49.5-63	1.006	0.005	1.026	0.991	0.019	0.015
63-76.5	1.001	0.005	1.016	0.987	0.015	0.014
76.5-90	0.995	0.005	1.014	0.980	0.018	0.015
90-103.5	0.990	0.005	1.009	0.974	0.020	0.016
103.5-117	0.984	0.005	1.000	0.970	0.016	0.015
117-130.5	0.979	0.004	0.996	0.963	0.016	0.016
130.5-144	0.975	0.004	0.991	0.961	0.017	0.013
144-157.5	0.969	0.005	0.987	0.953	0.018	0.016
157.5-171	0.964	0.004	0.978	0.947	0.014	0.017
171-184.5	0.960	0.012	1.570	0.945	0.609	0.015
198-211.5	0.955	0.004	0.970	0.939	0.014	0.016
211.5-225	0.951	0.004	0.965	0.937	0.015	0.013
225-238.5	0.947	0.004	0.961	0.933	0.015	0.013
238.5-252	0.945	0.004	0.959	0.931	0.014	0.013
252-265.5	0.940	0.004	0.953	0.926	0.013	0.014
265.5-279	0.935	0.017	0.949	0.922	0.014	0.013
279-292.5	0.931	0.011	1.530	0.918	0.599	0.013
292.5-306	0.926	0.004	0.941	0.911	0.015	0.015
306-319.5	0.922	0.004	0.935	0.909	0.014	0.013
319.5-333	0.918	0.004	0.933	0.902	0.016	0.016
333-346.5	0.914	0.004	0.926	0.900	0.012	0.014
346.5-360	0.909	0.016	0.922	0.895	0.013	0.014

The six hour sampling period was divided into 26 time slices and a mean absorbance was calculated for each time slice. The maximum and minimum absorbance during a time slice was also recorded and the positive (+ve) and negative (-ve) deviation from the mean absorbance was calculated from these results.

Figure 2.27 shows the plot of the six hour experiment, where negative error bars correspond to the negative deviation from the mean and positive error bars correspond to the positive deviation from the mean. The large positive deviations at time slices (171-184.5 min) and (279-292.5 min) shown in Table 2.8 are due to transient noise spikes that occurred during that time slice; the positive error bars corresponding to these erroneous results have been omitted from Figure 2.27 for clarity.

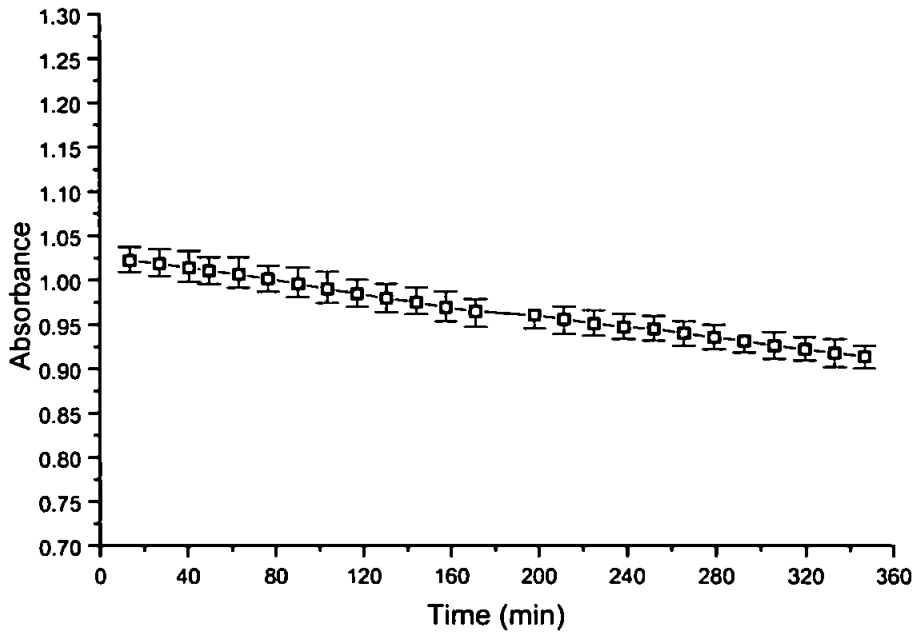

Figure 2.27 Instrumental drift of the PSD-1000 Ocean Optics spectrometer.

Figure 2.27 clearly shows a slight drift of - 0.019 A.U. / h for the Ocean Optics spectrometer, which is an order of magnitude higher than the quoted specification for the Hewlett Packard 8453 instrument of 0.001 A.U/h. However the photometric precision (noise) shown by the error bars remains relatively constant throughout the six hour period. Figure 2.28 shows the plot of a 1.0 A.U. permanganate standard monitored at $\lambda_{max.}$ over a period of six hours using the Hewlett Packard instrument.

The measured absorbance of the standard remained constant throughout the six-hour period and shows that the standard does not degrade over this period. A drift of ± 0.001 A.U. is quoted by the manufacturer but no drift was observed for this experiment; therefore the drift observed with the Ocean Optics system was purely an instrumental drift and not due to standard degradation.

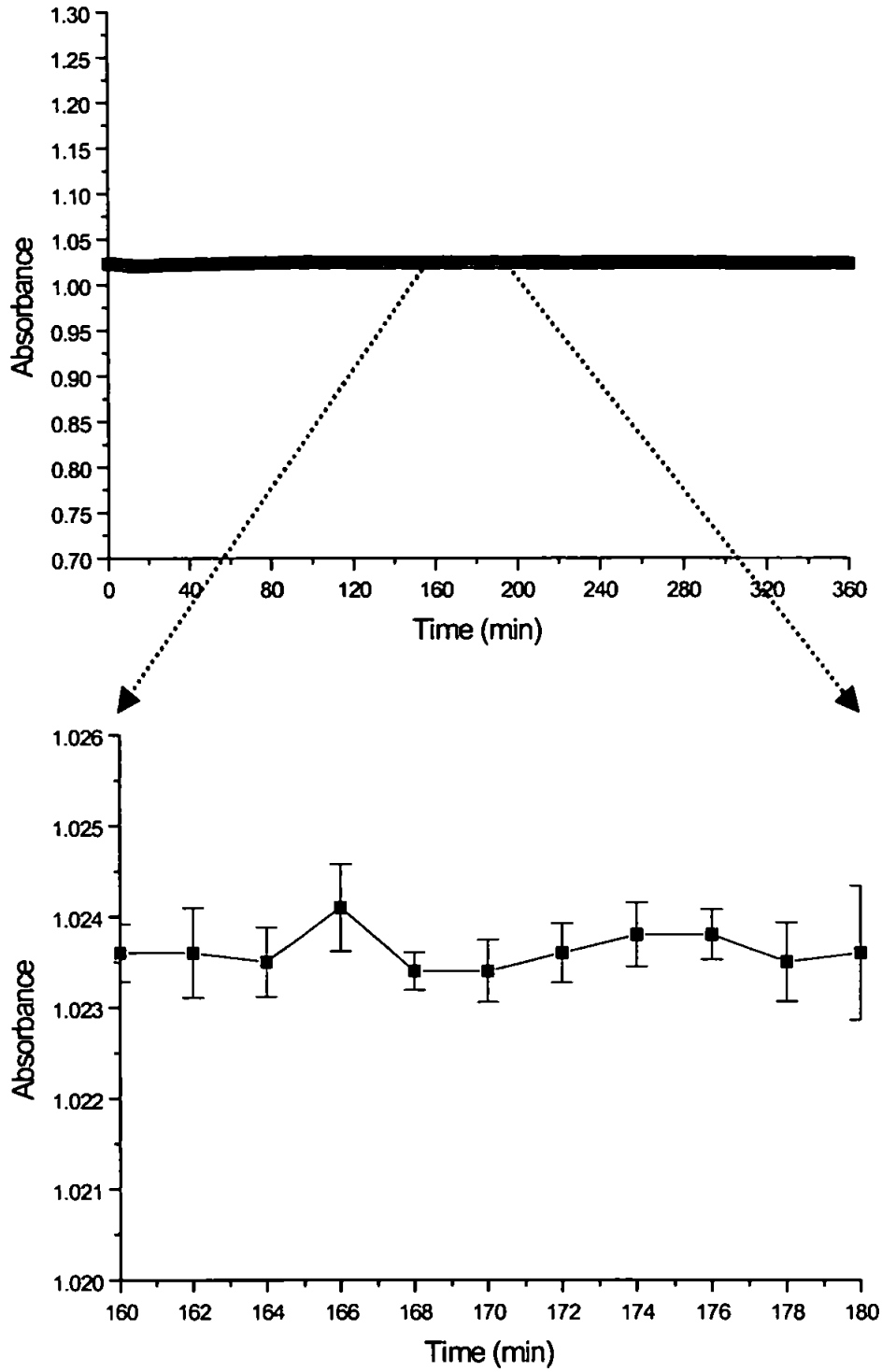

Figure 2.28 Instrumental drift of the HP 8453 spectrometer.

Table 2.9 summarises the performance characteristics of the Ocean Optics PSD-1000 spectrometer as identified in this chapter and compares them with the manufacturers quoted values for the Hewlett Packard 8453 instrument.

Table 2.9 **Performance specifications of PSD-1000 Ocean Optics and Hewlett Packard 8453 spectrometers.**

Type	Specifications PSD-1000 Ocean Optics spectrometer	Comments	Specifications Hewlett Packard 8453 spectrometer[220]	Comments
Wavelength range	200 – 700 nm (Master) 500 – 1000 nm (Slave)	UV-Vis Vis / Near IR	190 – 1100 nm	UV-Vis / Near IR
Slit width	N / A	No slit used in optical assembly	1 nm	
Resolution	12 nm 6 nm 3 nm	200 micron fibre 100 micron fibre 50 micron fibre	2 nm	
Stray light	(Master) (Slave) < 0.1 % N/A < 0.01 % < 0.01 % N/A N/A	Yellow Dye Blue Dye Molybdate	< 1.0 % < 0.07 % < 0.05 %	@ 200 nm, solution. of 1.2 % KCl (EP method) @ 220 nm, solution of 10 gl^{-1} NaI (ASTM method) @ 340 nm, solution of 50 gl^{-1} $NaNO_2$ (ASTM method
Wavelength accuracy	< ± 1.5 nm	Measured as daily deviation from Hg/Ar line source over 5 weeks	< ± 0.5 nm	NIST 2034, Holmium Oxide standard
Wavelength reproducibility	< ± 1.5 nm	Measured as daily deviation from Hg/Ar line source over 5 weeks	< ± 0.04 nm	10 consecutive scans with NIST 2034 standard
Photometric accuracy	+ 0.019 A.U.	5 averaged scans of $KMnO_4$ standard @ 1 A.U.	± 0.005 A.U.	NIST 930e standard @ 1 A.U.
Photometric noise	0.018 A.U. peak-to-peak 0.086 A.U. peak-to-peak	15 min scan @ 0.5 A.U.$KMnO_4$ Standard 15 min scan @ 1.5 A.U. $KMnO_4$ Standard	< 0.0002 A.U. rms	60 consecutive scans on air, 0.5s integration @ 0 A.U. 11 point moving average
Photometric stability	0.019 A.U. / h	Scan @ 1 A.U. $KMnO_4$ standard	< 0.001 A.U./ h	Scan on air @ 0 A.U., 340 nm, 0.5s integration

2.4 CONCLUSIONS

The following specific conclusions can be drawn from the research reported in this chapter:

1. The Ocean Optics PSD – 1000 spectrometer performance was stable enough to meet the ± 5% absorbance tolerance required for environmental monitoring in the field.

2. Wavelength repeatability of the instrument was measured daily over a 5 week period, and mean repeatability was ± 1.5 nm, with daily deviations typically less than 1.5 nm.

3. Photometric linearity of the instrument was measured using five averaged spectra of a $KMnO_4$ standard at 1 A.U. and found to be + 0.019 A.U. at 1.A.U. The instrumental photometric linear range was linear up to 1.5 A.U. (r^2 = 0.9996, n = 4), and therefore samples with higher absorbances require dilution.

4. Instrumental noise (peak-to-peak) of the instrument was 0.018 A.U. at an absorbance of 0.5 A.U. and 0.086 A.U. at an absorbance of 1.5 A.U.

5. Instrumental drift of the instrument was measured by pseudo-continuous scanning at 1 A.U. ($KMnO_4$ standard) for six hours, and the mean drift was 0.019 A.U. h^{-1}.

6. The performance characteristics of the PSD – 1000 spectrometer (given in Table 2.9, compared with the HP 8453 spectrometer), coupled with its near-continuous scanning capabilities, simplicity of use, high versatility, compactness and robustness make it ideally suitable for incorporation into an automated monitor for environmental field deployment.

Chapter Three

Determination of Ammonia by Flow Injection with Gas Diffusion & Spectrophotometric Detection

"Nothing in life is to be feared. It is only to be understood"

- Marie Curie -

3.1 INTRODUCTION

This chapter describes the integration of the Ocean Optics PSD – 1000 spectrometer into a gas diffusion manifold for the determination of ammonia. The system has been optimised and utilising the multi-wavelength capabilities of the array detector is linear over the range 0 – 10 mg l^{-1} NH_3-N achieving a detection limit of 17 μg l^{-1} NH_3-N. In order to reduce the volume of wet reagents used, a flow cell incorporating a bromocresol green immobilised indicator was designed, constructed and evaluated.

3.2 EXPERIMENTAL

3.2.1 REAGENTS AND STANDARDS

All solutions were prepared using deionised water purified by a Milli-Q analytical reagent grade water purification system (18.2 MΩ cm^{-1} at 25°C) (Millipore Waters, Bedford, Massachusetts 01730, U.S.A.) or an Elgastat UHQ II (Elga Ltd, High Wycombe, Bucks, U.K.) water purification system. All reagents were of AnalaR grade (Merck Ltd, Poole, Dorset, UK) unless otherwise stated. A stock ammonia solution (100mg l^{-1} NH_3-N) was prepared by dissolving 0.3819g of ammonium chloride (previously dried at 105°C) in 1 l of water. Ammonia calibration standards were prepared by serial dilution of the stock solution. A 1 mol l^{-1} sodium hydroxide stock solution was prepared by dissolving 40 g of sodium hydroxide pellets (Aristar grade - Merck Ltd) in 1 l of water, with serial dilution used to produce 0.1 and 0.01 mol l^{-1} working solutions. A stock bromothymol blue solution was prepared by dissolving solid bromothymol blue (0.4 g ; Merck indicator grade) in 64 ml of 0.01 mol l^{-1} sodium hydroxide and diluting to 1 l with water. All glassware and plastic storage ware used was soaked in Decon solution (Merck Ltd) for at least 24 hours and then rinsed with Milli-Q prior to use.

3.2.2 INSTRUMENTATION

The spectrometer used in this work was an Ocean Optics PSD - 1000 miniature fibre optic spectrometer (Anglia Instruments Ltd, Cambridge, U.K). Full technical specifications have been given in section 2.2.2. All-silica core, fluorine doped silica cladding, 200 μm single core UV-VIS fibres (Anglia Instruments Ltd) were used in all applications, unless otherwise stated. Data communication to and from the spectrometer was performed using a type II PCMCIA DAQ-700 data acquisition card (National Instruments, Newbury, Berks, U.K). The controlling notebook PC was a Toshiba 486-75 T2130CS (Toshiba Information Systems Ltd, Weybridge, Surrey, U.K).

All data acquisition was performed in Spectrascope version 2.3 (Ocean Optics Inc., Dunedin, FL, U.S.A.) and later exported to Excel 5.0 (Microsoft Corporation) and Origin v.2.78 (Microcal Software Inc) for processing.

The flow injection manifold (Figure 3.1) used for the initial method development was adapted from a manifold reported by Clinch et al.[85]. Poly(tetrafluoroethylene) (PTFE) tubing of 0.8 mm i.d. (Anachem, Luton, Beds., UK) was used in the construction of the manifold. A peristaltic pump (Ismatec Mini-S 820, Ismatec, Carshalton, Surrey, UK) with poly(vinyl chloride) (PVC) pump tubing (Elkay, Basingstoke, Hants., UK) was used to propel the sample and sodium hydroxide streams through a mixing coil to a pneumatic six-port rotary valve unit (PS Analytical, Sevenoaks, Kent, UK). A second peristaltic pump was used to propel the water carrier (i.e donor) and the indicator (i.e acceptor) streams through an in-house Perspex® gas diffusion cell.

The gas diffusion cell used for this work comprised two blocks with identical, but mirror image, flow channels on the surface, which formed the donor and acceptor halves of the cell (see Figures 3.2 and 3.3). The two blocks screw-fastened together so that the flow channels faced each other and a microporous membrane was placed between the channels to form a barrier between the donor and acceptor streams. The direction of flow is usually parallel (concurrent) for both the donor and acceptor streams to maximise the period of diffusion and increase sensitivity, although countercurrent flow can also be used. A diffusion path of 240 mm length x 1.5 mm depth (volume = 72µl on either side of the membrane) was used. General-purpose PTFE tape (width = 22mm, thickness = 8-9µm; RS Components, Corby, Northants, UK) was used as the gas diffusion membrane. In all experiments concurrent flow was used for the carrier and indicator streams when passing through the diffusion cell.

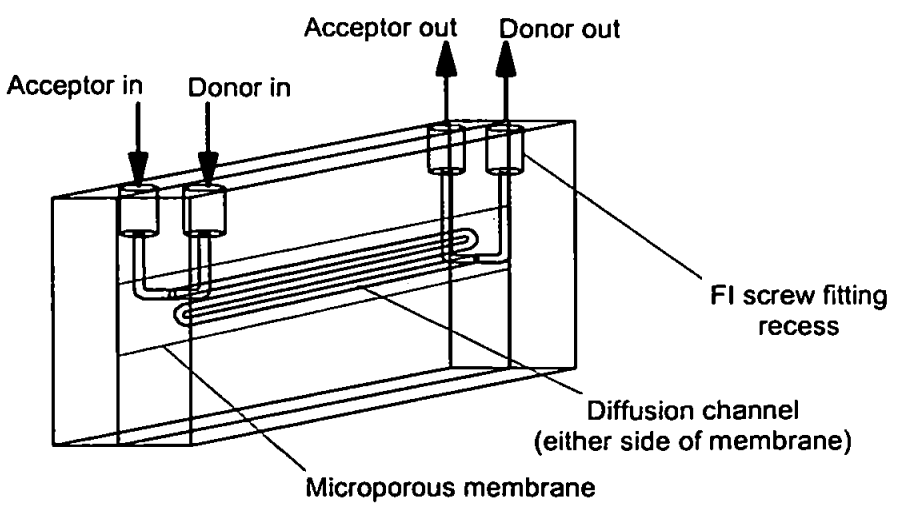

Figure 3.2 Diagram of the FI gas diffusion cell.

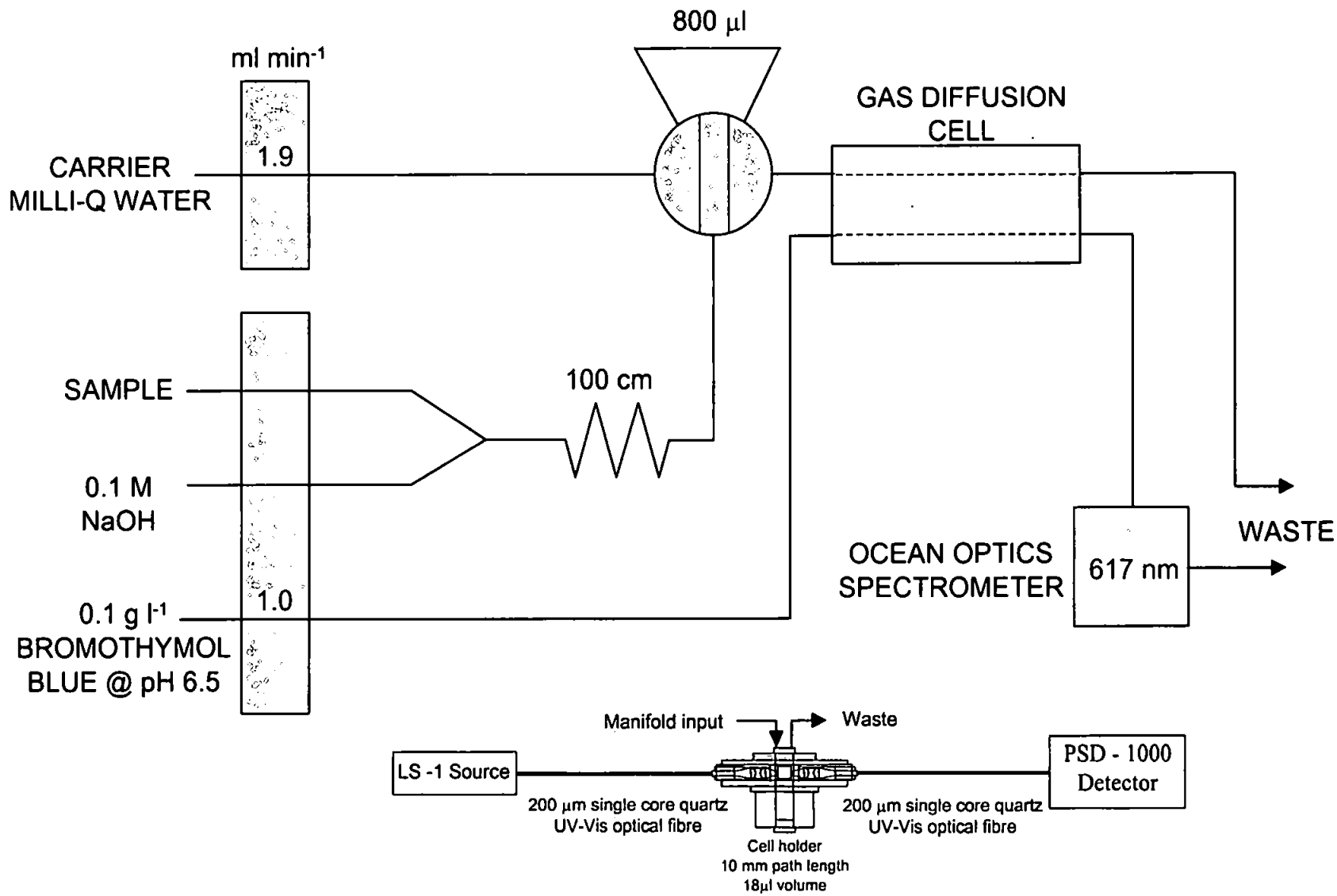

Figure 3.1 **Flow Injection manifold for the determination of ammonia.**

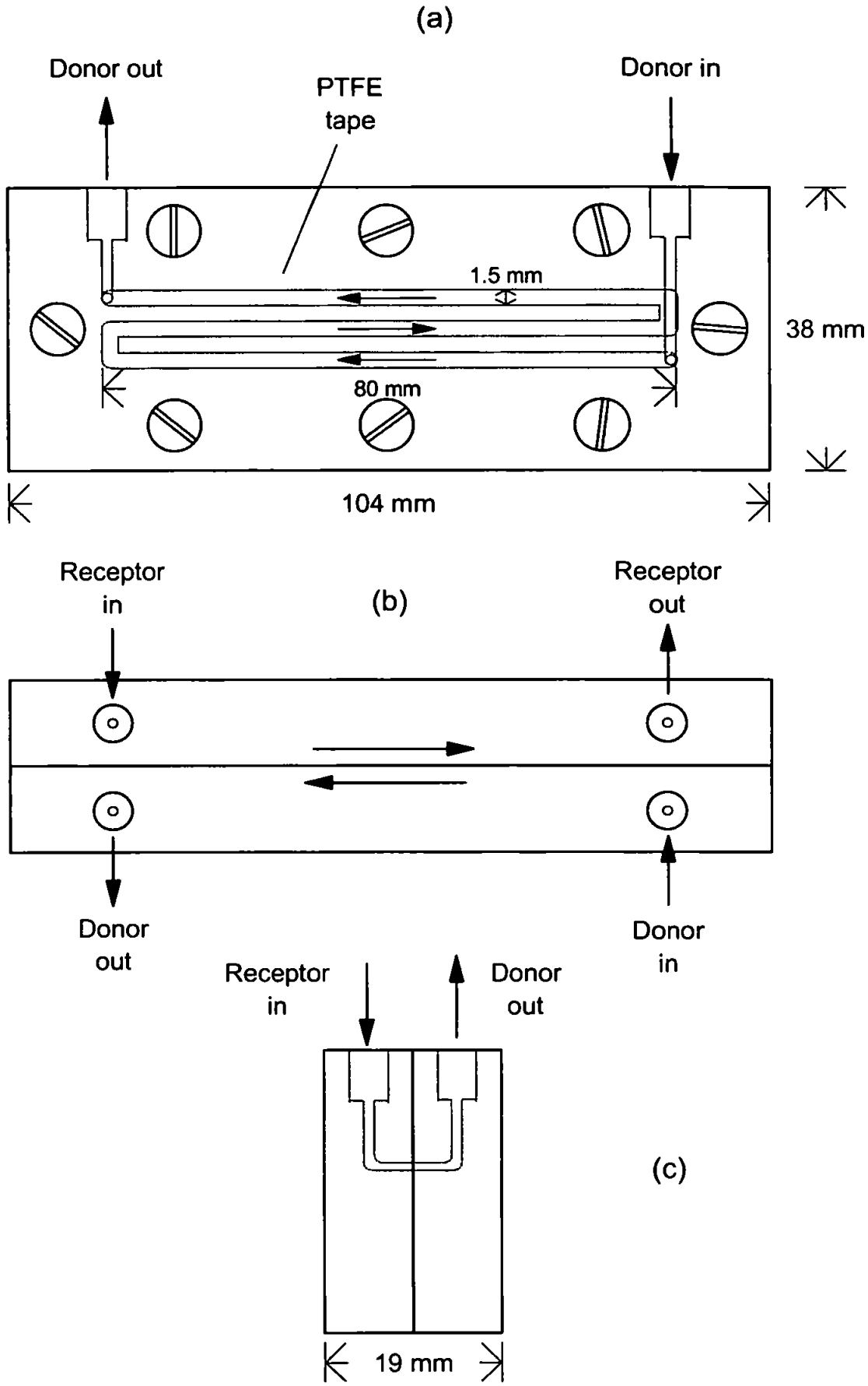

Figure 3.3 **Diagram of the gas diffusion cell (a) side view ; (b) plan view ; (c) end view.**

The indicator stream was passed into an 18 µl flow cell of 10 mm pathlength (Hellma, Westcliff-on Sea, Surrey, UK) housed in a fibre optic cuvette cell holder (Instruments S.A., New Eddison, New Jersey, USA). The cell holder was connected to a LS-1 miniature tungsten / halogen light source (Anglia Instruments Ltd, Cambridge,U.K.) (full specifications given in section 2.2.2) and to the Ocean Optics PSD - 1000 miniature fibre optic spectrometer via 200 µm UV-Vis optical fibres with SMA connectors (Figure 3.1). Carrier and indicator stream flow rate optimisations were performed using two Minpuls 2 (Gilson, Villiers-le-Bel, France) variable speed peristaltic pumps.

3.2.3 FI PROCEDURES

The FI manifold was optimised with respect to manifold variables in order to produce the lowest detection limit for ammonia in aqueous samples. A 1.0 mg l^{-1} ammonia standard was used to assess the performance of the manifold shown in Figure 3.1. History channel functions (see section 2.2.3 (c) for full description of history channel) on the spectrometer were set to monitor at 617nm ($\lambda_{max.}$) with a 50 kHz acquisition and set to average every 5 scans. Following initial investigation into manifold performance a calibration was performed using 0.1, 0.5, 1.0, 3.0, 5.0 mg l^{-1} NH_3-N standards. Further optimisation of manifold conditions utilised a full simplex optimisation (full details of simplex optimisation are given in section 3.3.3 (a)) for four manifold parameters, namely the carrier and indicator stream flow rates, the volume of injected sample and the concentration of the indicator. Starting conditions, based on the work of Clinch et al.[85] where indicator pH was set at pH 6.5 with sodium hydroxide concentration set at 0.1 mol l^{-1}. The simplex procedure was conducted using a 0.2mg l^{-1} NH_3-N standard to enable maximum sensitivity at the concentration range of interest in natural waters. Optimised parameters were calculated from the blank corrected responses of the 0.2mg l^{-1} standard.

3.2.4 LAMINAR FLOW CELL

(a) MEMBRANE PREPARATION

Membrane "staining" solution was prepared by dissolving 1.317 g of Bromocresol Green (BCG) indicator (Merck Ltd) in 1 l of analytical grade tetrahydrofuran (THF) (Merck Ltd) with the use of a magnetic stirrer. The PTFE tape used for the preparation of the membranes was standard "thread-sealing" tape (width 22mm, thickness 8-9µm) obtained from (RS Components Ltd, Corby, Northants, U.K). Using clean (grease free) glassware, the PTFE tape was wrapped around a glass U-frame to produce a series of horizontal bands.

The tape was then immersed in the THF solution for 10 min before being removed and allowed to dry in a fume cabinet. Following drying, the tape was washed with Milli-Q water to remove any excess dye on the outer surface of the tape. The tape was then dried again in air yielding a golden yellow colour. The versatile nature of the tape enabled it to be cut into various shapes to suit the intended application. The initial laminar flow cell used was constructed out of white PTFE and the dye impregnated membrane tape was held in place by a glass cover slide and the flow cell housing. The viewing optics consisted of two 1000 μm plastic clad, slica core quartz optical fibres terminated by SMA connectors and encased in a stainless steel tube held in place by a potting mixture.

The final laminar flow cell used was designed and machined in house, in conjunction with Mr Steve Rendall (Sales Engineer, Hepco Slide Systems Ltd., Tiverton, Devon) and Mechanical Technical Services at the University of Plymouth. Figures 3.4 and 3.5 show technical drawings of the top and bottom sections of the laminar flow cell respectively. To ensure a clearance fit between the two components the crucial dimensions were ϕ 50.0 and ϕ 60.0. Faces A & B had to be parallel to ensure that they sealed against each other. The construction material chosen for the laminar flow cell was 316 Stainless Steel due to its high corrosion resistant properties (low carbon content); full chemical specifications are given in Table 3.1 below and the degree of corrosion strength given in Appendix I. The 316 stainless steel has a high rating of corrosion resistance to a large variety of chemical agents and shows good resistance to 10 % sodium hydroxide at 100°C.

Table 3.1 Chemical specifications of 316 stainless steel.

Chemical Element	% Composition
C	0.12
Si	0.20
Mn	2.0
Ni	8.0 - 12.0
Cr	17.0 - 20.0
Mo	1.50 - 2.50
S	0.045
P	0.045

Ammonia calibration standards for the immobilised reagent determination of ammonia were 50, 100, 200, 500, 4000 and 10000 μg l^{-1}. The standards were dosed with 1 ml of sodium hydroxide just prior to analysis and spectra were acquired 1 min after standard introduction to the flow cell. The membrane was then allowed to reverse for 3 min by passing Milli-Q water through the system. This complete process was repeated in triplicate for each standard.

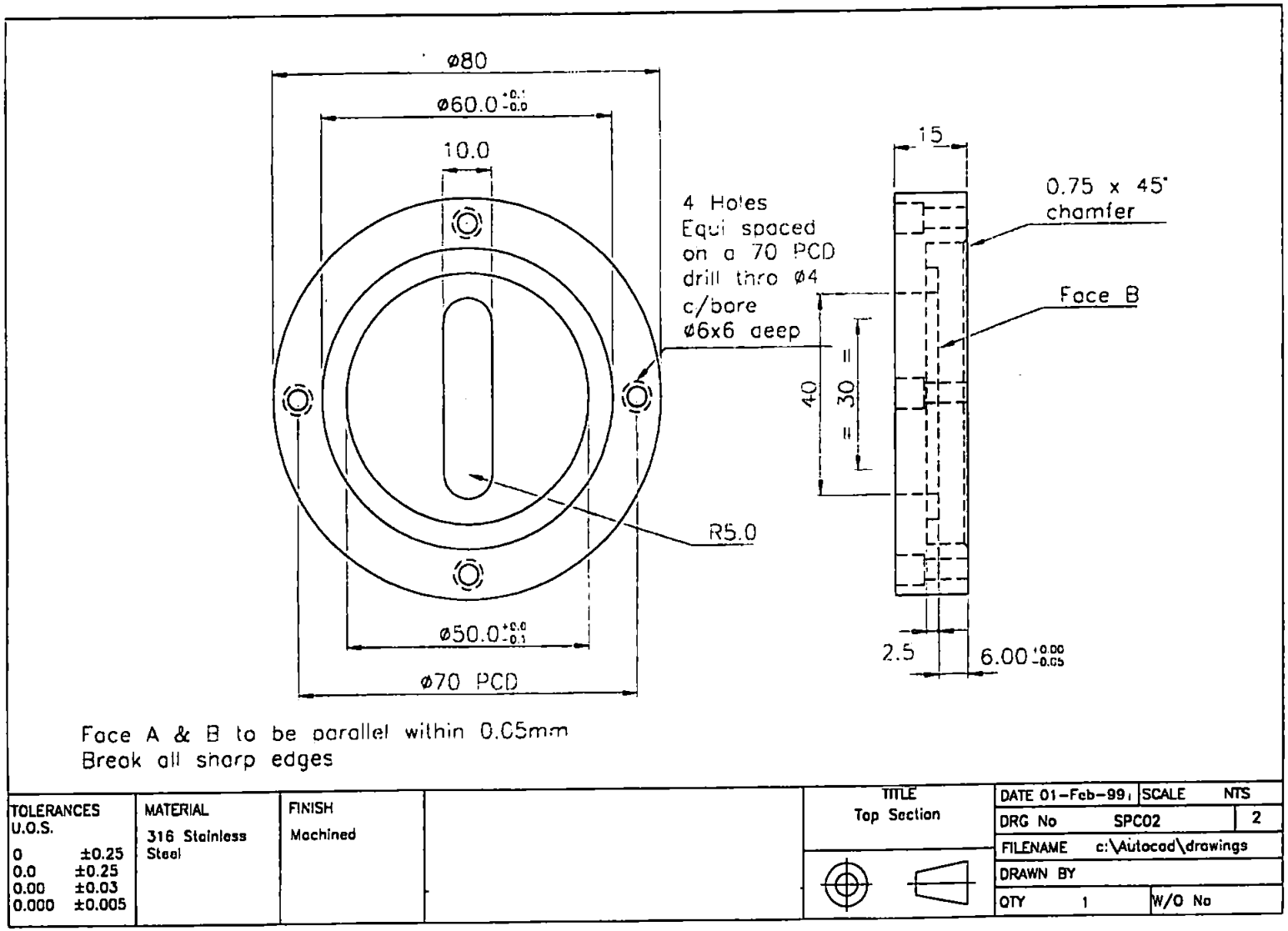

Figure 3.4 **Technical drawing of final laminar flow cell, top section.**

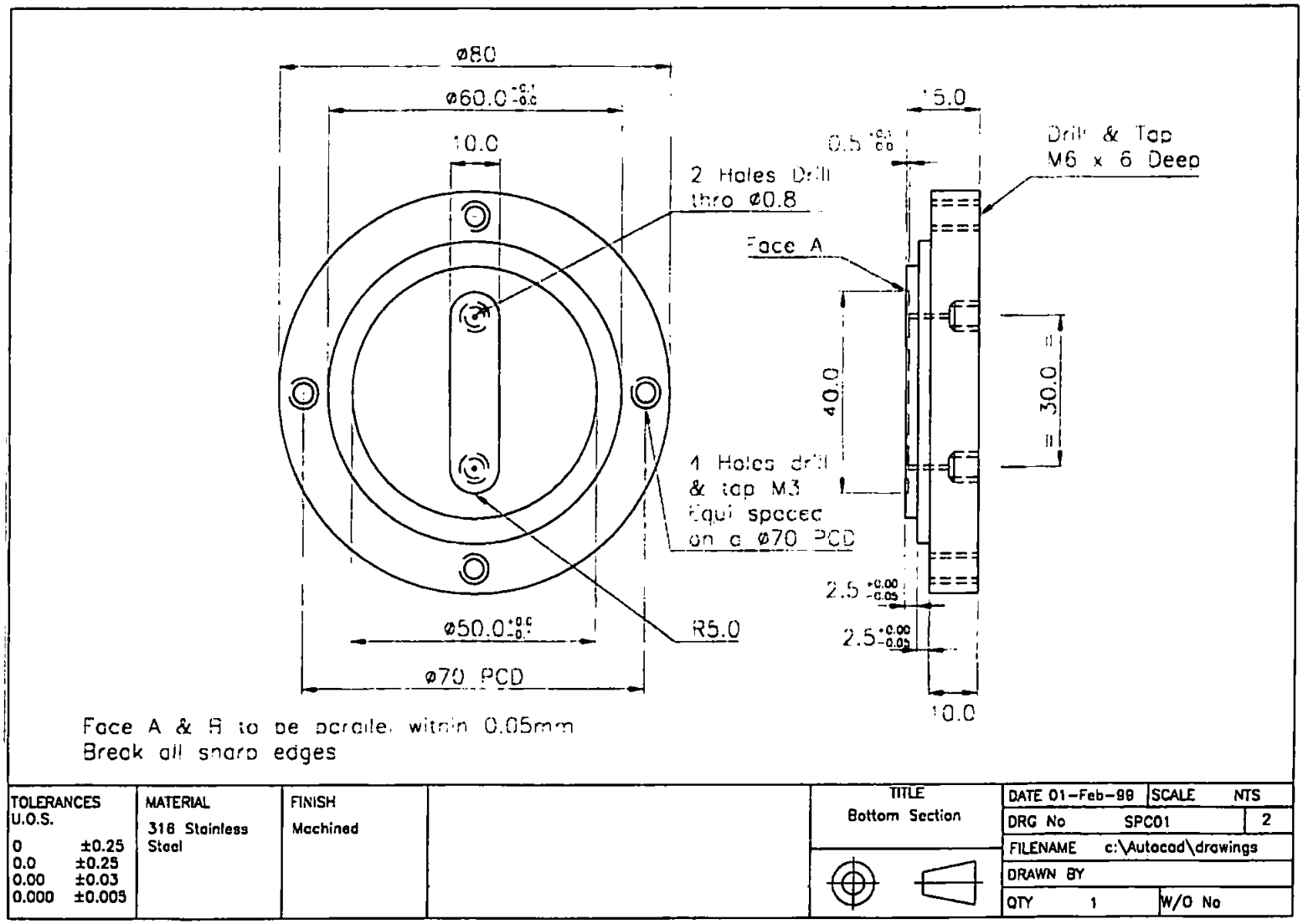

Figure 3.5 **Technical drawing of final laminar flow cell, bottom section.**

To enable better modelling of the calibration the number of calibration standards was increased to eleven. Standards of 0.05, 0.1, 0.2, 0.4, 0.6, 1.0, 2.0, 4.0, 10.0 and 30.0 mg l^{-1} NH_3-N were prepared by serial dilution from a 100 mg l^{-1} stock solution. All other procedures were as stated above.

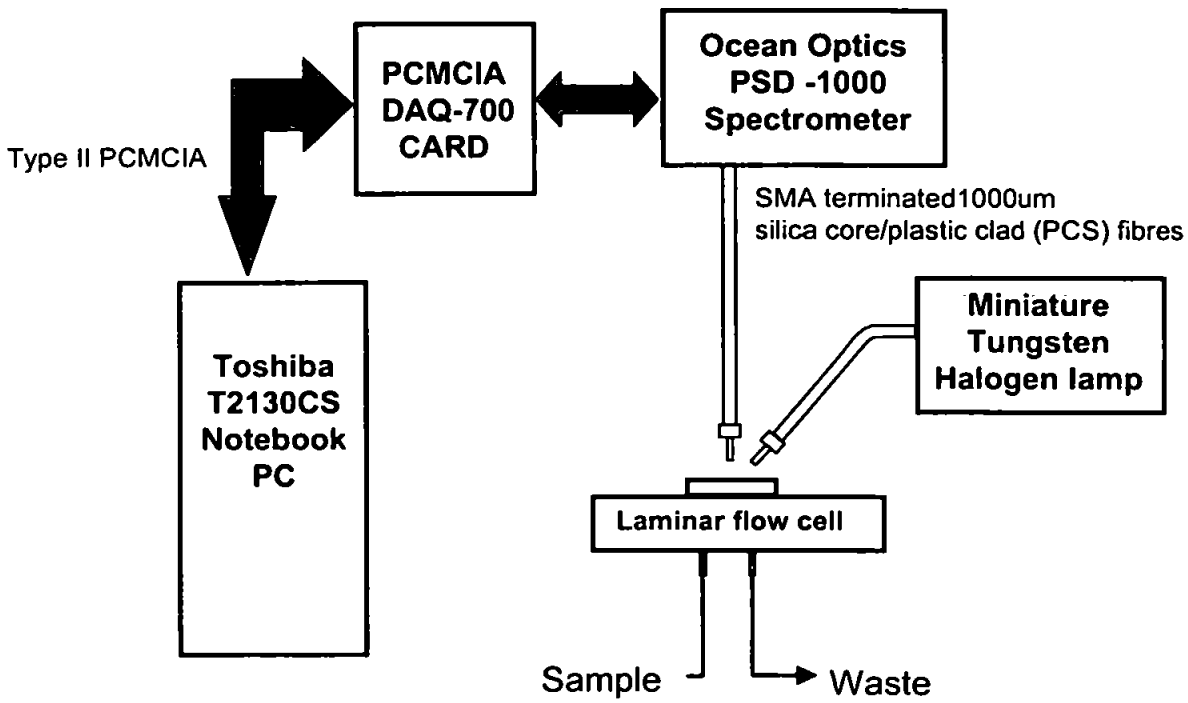

Figure 3.6 Schematic diagram of overall system configuration.

The dye impregnated tape was illuminated by a miniature tungsten halogen lamp (spectral range 360nm-1000nm) via 1000μm fibre optics. Illumination was conducted at 45° to the normal with light collection at 90° to the normal (Figure 3.6). This configuration minimised the amount of reflected light reaching the spectrometer and maximised the scattered light originating from the tape. The illuminated area of the tape measured approximately 3mm in diameter.

3.3 RESULTS AND DISCUSSION

3.3.1 PRINCIPLES OF GAS-DIFFUSION FLOW INJECTION

Gas diffusion represents an important technique for separation and preconcentration of volatile analytes in flow injection analysis. It can be used to remove potential matrix interferences and to enhance both selectivity and the sensitivity of analyses. Gas diffusion involves the reproducible transport of gaseous analytes from a sample or "donor" stream through a hydrophobic, microporous membrane into a detector or "acceptor" stream. This diffusive transport produces a change in the physico-chemical nature of the acceptor stream, which is proportional to the

concentration of the gaseous analyte. The efficiency of diffusion is also influenced by the residence time of the sample in the diffusion cell (dependent on flow rate and diffusion channel length), the surface area of the sample at the membrane in relation to the volume of the diffusion channel, and the porosity of the membrane. The hydrophobic nature of the membrane permits only the exchange of gaseous molecules, and prevents the transfer of liquids, dissolved ionic species and particulates. Volatile analytes determined by gas diffusion flow injection (GD-FI) methods have included ammonia (see Table 1.5), carbon dioxide[228] and sulphite[229].

The pH of the sample stream is a fundamental factor in gas diffusion separations, since pH conditions determine whether the solution equilibrium favours the gaseous or ionic species of a particular analyte. Maximum diffusion efficiency is achieved when the sample pH is such that the dissolved analyte is fully converted to its gaseous form. In the case of ammonia in aqueous solution at 25°C, the ionic species ammonium, NH_4^+, accounts for virtually all of the dissolved ammonia at pH 7.0, but is almost completely converted to the gaseous NH_3 species at pH 11.0 (Figure 3.7).

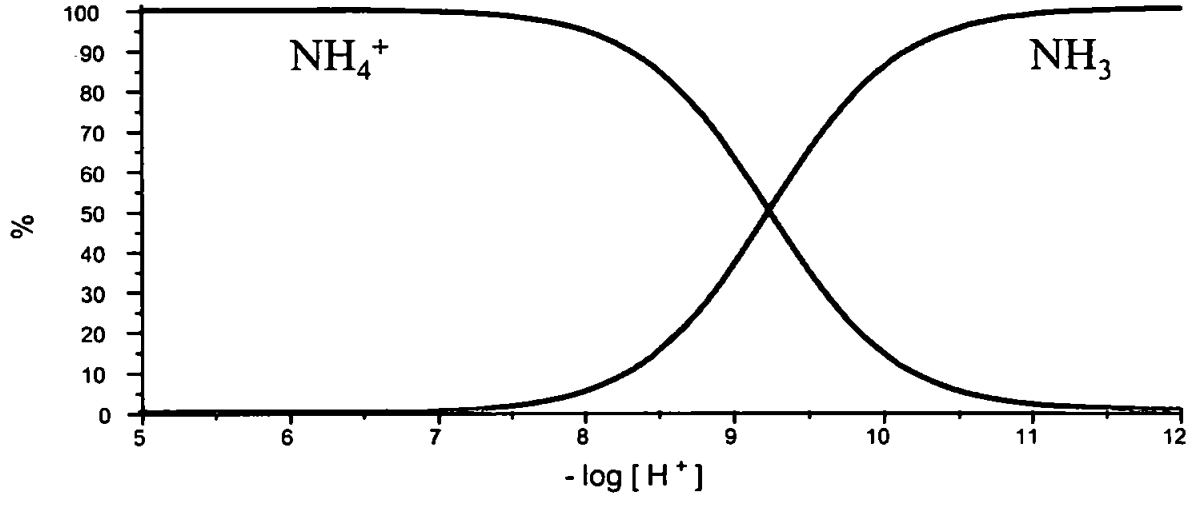

Figure 3.7 Effect of pH on dissolved ammonia speciation at 25°C.

Acid-base indicator solutions are frequently used as the acceptor streams in GD-FI analyses. In the case of ammonia determinations, the acidic form of the indicator (HI^-) is used as the initial acceptor stream. As ammonia diffuses across the membrane, a proportion of the indicator is converted to its basic form (I^{2-}), as shown below.

$$NH_3 + HI^- \longrightarrow NH_4^+ + I^{2-}$$

The formation of I^{2-} in the acceptor stream is then measured spectrophotometrically, with the height or area of the I^{2-} absorbance peak proportional to the concentration of ammonia originally present in the sample stream. Figure 3.8 illustrates the structural formulae for the acidic and basic forms of the bromothymol blue (3', 3''-dibromothymolsulponphthalein) indicator used in this work.

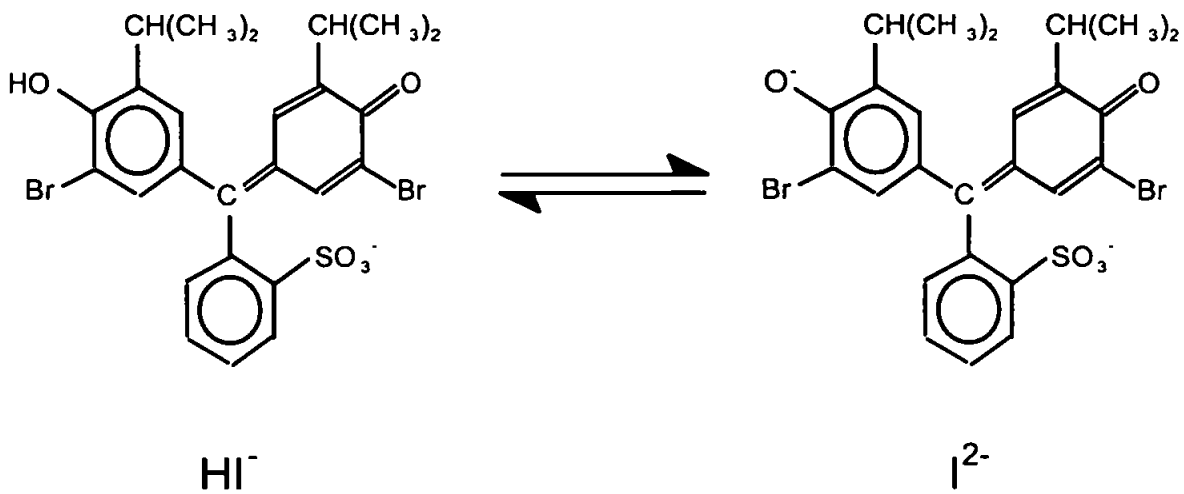

HI^- I^{2-}

Figure 3.8 Structural formulae of the acidic (HI^-) and basic (I^{2-}) forms of bromothymol blue indicator, $pK_a = 7.30$, transition pH range 6.2 – 7.6.

The relationship between ammonia concentration and the absorbance change produced is linear over a certain range, depending on the pK_a, concentration and initial pH of the indicator. This relationship is known as the *Henderson – Hasselbalch* equation and is shown below.

$$HI^- \longleftrightarrow I^{2-} + H^+ \qquad (1)$$

$$K_1 = \frac{[I^{2-}][H^+]}{[HI^-]} \qquad (2)$$

$$\log K_1 = \log \frac{[I^{2-}]}{[HI^-]} + \log [H^+] \qquad (3)$$

$$pH = pK_1 + \log \frac{[I^{2-}]}{[HI^-]} \qquad (4)$$

Changing the indicator to one with a lower pK_a, e.g. bromocresol green with a pK_a of 4.90 (transition range 4.0 – 5.6 pH units) would require less ammonia in the indicator stream to shift the acidic form to the basic form, thereby increasing sensitivity and lowering the linear range.

3.3.2 CONVENTIONAL FLOW INJECTION

Figure 3.9 shows the initial evaluation of the GD manifold shown in Figure 3.1 for replicate injections of a 1 mg l^{-1} NH_3-N standard. Baseline stability of the system was excellent, typically less than ± 0.002 A.U. and peak shapes were well defined and reproducible with an R.S.D. of 1.3 % (n = 5). This demonstrates that the Ocean Optics PSD – 1000 spectrometer can be integrated into a FI manifold and that the on board software can be used to process transient FI peaks.

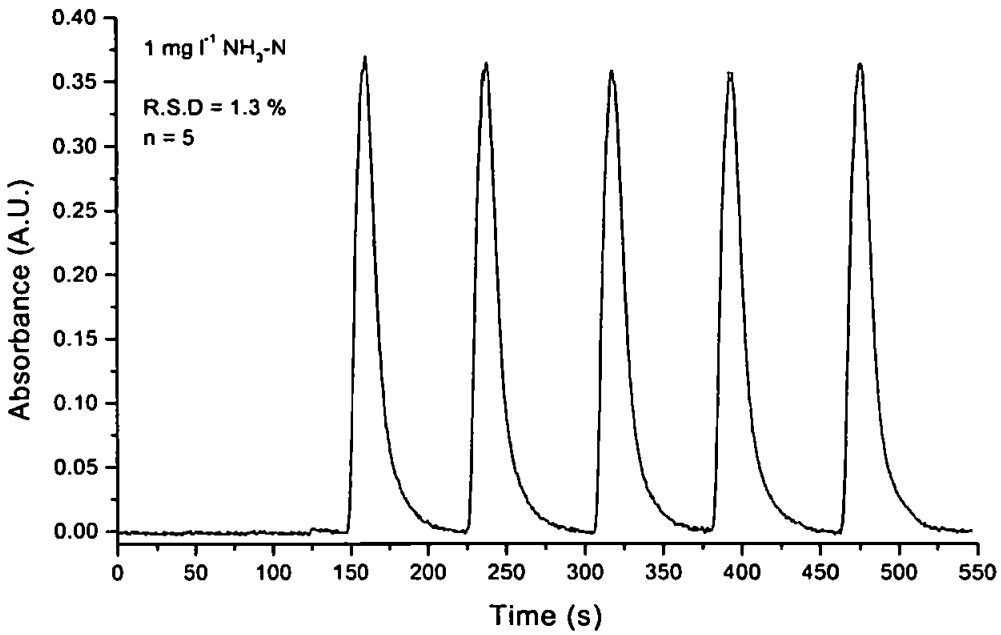

Figure 3.9 Replicate injections of a 1mgl^{-1} NH_3-N standard detected at λ_{max} (617 nm).

(a) INITIAL CALIBRATION

Figure 3.10 shows calibration data obtained using the initial manifold and the associated statistical data are given in Table 3.2. The response given by the 5 mg l^{-1} NH_3-N standard (2.670 A.U.) exceeded the linear range of the PSD – 1000 spectrometer specified at 1.5 A.U. (discussed in section 2.3.4), reproducibility was also impaired with an R.S.D. (n=5) of 12.5 % compared to typical calibration R.S.D.s which were less than 2.6 % R.S.D. (n = 5).

However the Milli-Q blank had a relatively high absorbance at 0.036 A.U. (RSD 2.6 %, n = 5) and this indicates the difficulty of performing low level (< 100 µg l^{-1} NH_3-N) ammonia measurements, i.e. those typically found in unpolluted natural waters (see section 1.1). The high blank was due to contamination from atmospheric ammonia and other laboratory operations (see section 3.3.2 (b)).

Table 3.2 Statistical data for initial GD-FI NH_3-N calibration.

Standard ($mg\ l^{-1}$)	Mean (A.U.)	S.D. (A.U.)	R.S.D.% (n=5)
BLANK	0.036	0.001	2.6
0.1	0.056	0.001	2.1
0.5	0.137	0.003	2.5
1.0	0.256	0.002	0.9
3.0	0.781	0.016	1.9
5.0	2.670	0.334	12.5

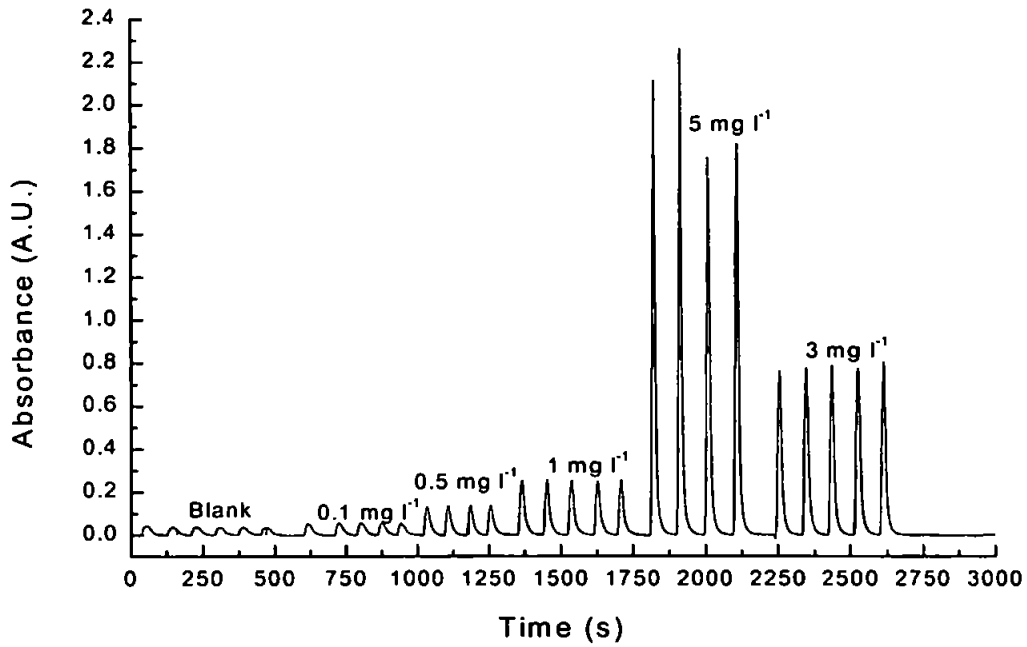

Figure 3.10 Calibration data for 0 – 5 mg l^{-1} NH_3-N, monitored at λ_{max} (617 nm).

Analytical figures of merit obtained from the calibration plot (Figure 3.11) were a limit of detection of 0.063 mg l^{-1} NH_3-N (calculated from the mean plus three standard deviations of the blank) and a linear response (r^2 = 0.999, n = 5) in the concentration range 0 – 3 mg l^{-1} NH_3-N.

(b) AMMONIA BLANK LEVELS

The low-level determination of ammonia is highly susceptible to contamination of reagents and samples during storage, handling and the preparation stages of analysis. The main sources are the general background of atmospheric ammonia and amines (particularly in urban laboratories), the analyst (skin contamination and exhaled breath, particularly smokers), and the presence of other ammonia based volatile chemicals. Fingerprints and air have been shown to be sources of serious ammonia contamination[62]. The background level of ammonium ions in aqueous solutions, even those prepared from high grade purification systems is very difficult to keep below 10^{-8} mol l^{-1} and this is attributed mainly to contamination from atmospheric sources[230].

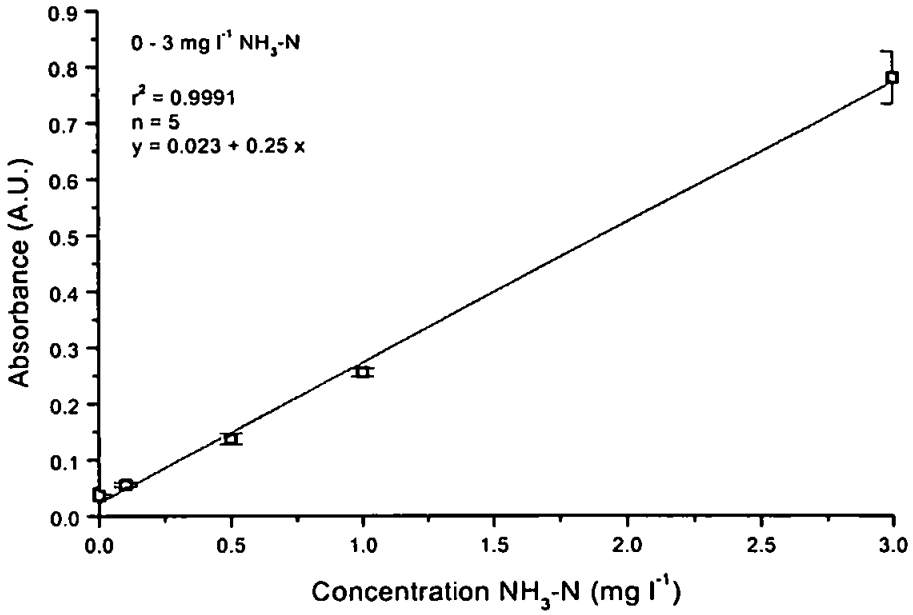

Figure 3.11 Calibration graph for 0 – 3 mg l^{-1} NH_3-N, monitored at λ_{max} (617 nm).

Figure 3.12 shows the results obtained from an international laboratory inter-comparison study[231;232] (ICES-International Council for the Exploration of the Sea) for the determination of nutrients (ammonia, nitrate, nitrite and phosphate) in sea water. A total of 132 laboratories participated in the study, 106 of which determined ammonia. The spread of the ammonia results (Figure 3.12 (a)) contrasted with those for nitrate (Figure 3.12 (b)) and showed the particular difficulty encountered by analytical chemists in the accurate determination of this nutrient, with relative standard deviations greater than 20 %. Other inter-comparison studies[233] have also reported large standard deviations for the determination of ammonia in natural waters.

In a communal laboratory (e.g. university research laboratory), potential sources of ammonia contamination are numerous and difficult to control. The use of nitrogenous compounds, many of which are volatile and vapour from adjacent laboratories and ventilation ducts can contribute significantly to background levels. Proximity of other analyte determinations such as nitrate, silicate, phosphate and trace metals (use of ammonium salt solutions), waste water analyses, floor cleaning products, general laboratory handling (reagent transfer steps e.g. pouring and pipetting), the use of polyethylene bottles for storage / preparation (known to slowly release ammonia[234]), even the presence of individuals who smoke can all contribute to the background concentration, making low level ammonia analysis extremely difficult. Recent research efforts have centred on identifying and quantifying sources of ammonia contamination[235;238], methods of contamination control[231;236;237] and stability and storage effects[238;239].

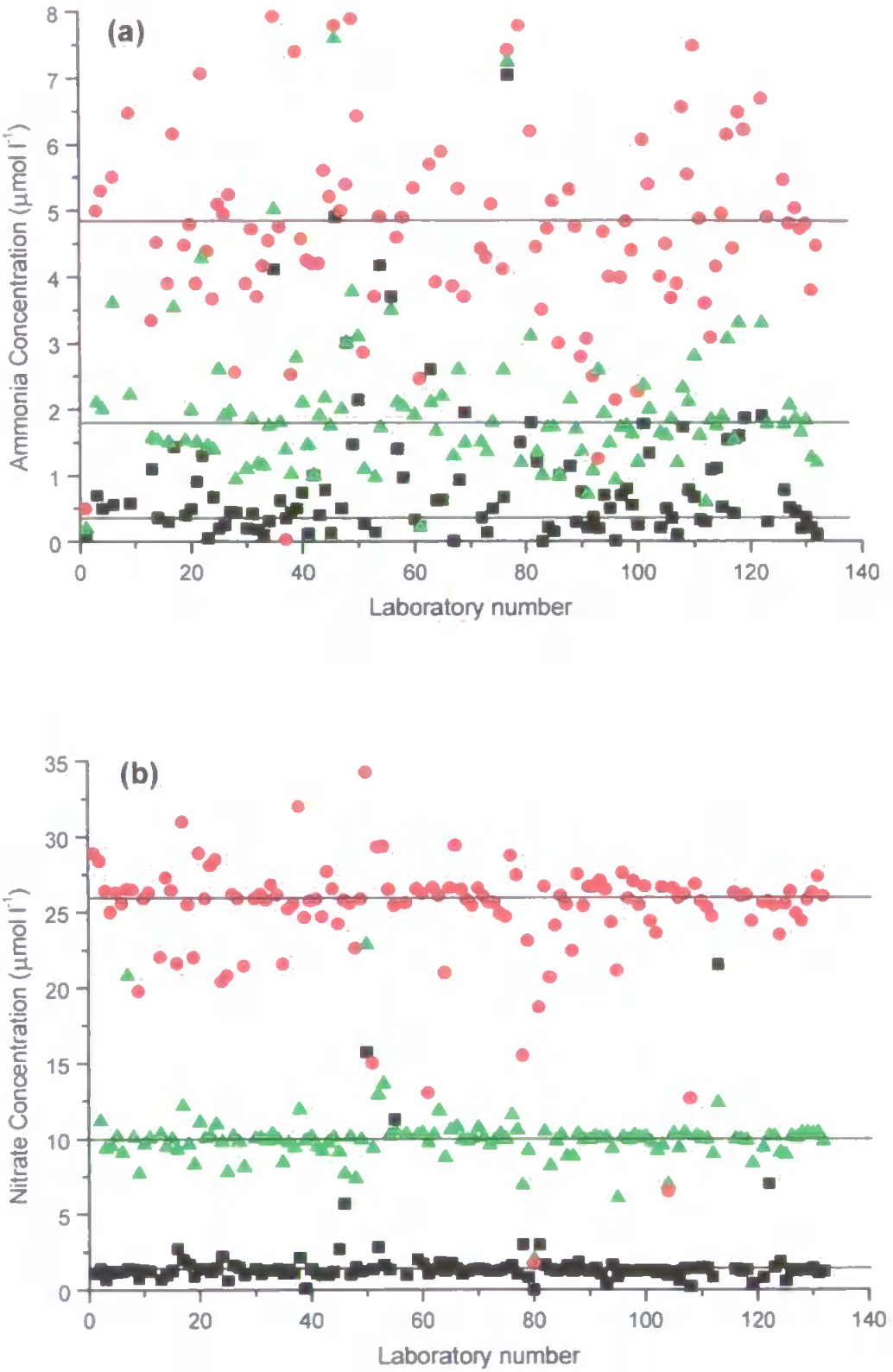

Figure 3.12 (a) ICES intercomparison study – Ammonia results;concentrations (µmol l^{-1}) versus laboratory number[232],assigned concs.; ■ = 0.34, ▲ = 1.83, ● = 4.86. (b) ICES intercomparison study – Nitrate results; concentrations (µmol l^{-1}) versus laboratory number[232], assigned concs.; ■ = 1.33, ▲ = 9.98, ● = 26.03.

Numerous methods have been described that limit ammonia contamination, examples being the use of modified Kjeldahl's apparatus[238] and the use of the gas-diffusion principle in a continuous-flow, constant dilution system[71] to remove ammonia prior to a gas sensing electrode. However these methods and those that employ complex off-line clean-up procedures are difficult to implement, add to the complexity and operational / running costs and are often unsuitable for adaptation to a field deployed FI system.

Simpler methods suggested for the preparation of "ammonia free water" involve passing distilled / deionised water through a strongly acidic cation exchange resin (hydrogen form)[240] or re-distillation of distilled / deionised water with 0.1 ml l^{-1} of sulphuric acid[240]. Distillation with alkaline potassium permanganate (3 ml to every 1 l of distilled / deionised water) has also been suggested[241]. Investigation of blank levels of ammonia in this work included the use of various water sources (different high grade water purification systems), possible sources of contamination and methods to minimise these sources. Different clean up procedures such as the use of cation-exchange (Amberlite IR – 120 (H), analytical grade resin) and the distillation procedures mentioned above were also attempted but these yielded little reduction in the response given by a blank Milli-Q injection. Therefore the simplest methods recommended for the minimisation of ammonia contamination are;

- Cleaning of HDPE storage bottles in 50 % HCl for a minimum of 24 h, ten rinses with Milli-Q water, dried and stored in two zip lock bags in a cool dark place.
- Storage / sample bottles cleaned and opened only when necessary.
- Use of gloves at all times (skin contamination).
- Freshly prepared high quality demineralised water, used as soon as drawn from the equipment.
- Blanks and standards used immediately after preparation (within minutes if possible) and discarded afterwards.
- Aliquot / reagent / standard transfer volumes as large as possible.
- Minimisation of transfer steps ◄⟶ bottle ◄⟶ volumetric flask ◄⟶ reaction cells
- Reduction / control of other external and laboratory factors.

3.3.3 SIMPLEX OPTIMISATION

The need to optimise the parameters that characterise FI systems in order to improve their analytical response (usually sensitivity) is now commonly accepted. One of the most commonly used optimisation methods is known as simplex optimisation. This is a multivariate optimisation technique, which was first proposed by Spendly et al.[242] to assist in the efficient running of an industrial process. It works by locating the summit of the response surface defined by the system variables. The summit is assumed to be the optimum system conditions (e.g. conditions which give the highest signal to noise ratio). Simplex optimisation may be applied when all the factors are continuous variables. A simplex is a geometric figure which has $n + 1$ vertices when a response is being optimised with respect to n factors. For example, for two factors (V_1 and V_2) the simplex will be a triangle. The method of optimisation is illustrated in Figure 3.13. The points labelled 1, 2 and 3 define the initial simplex. In the first experiment the response is measured at each of the combinations of factor levels given by the vertices of the simplex. The worst response would be found at point 1 and it would be logical to conclude that a better response would be obtained at a point which is the reflection of 1 with respect to the line joining 2 and 3 i.e. 4. The points 2, 3 and 4 form a new simplex and the response for the points 2, 3 and 4 will shows that 2 gives the worst response. The reflection procedure is repeated to give the simplex defined by 3, 4 and 5. It can be seen that no further progress beyond the stage shown, since points 9 and 13 both give a worse response than 11[243].

In order to improve the performance of the simplex method various modifications have been proposed, incorporating extra rules to allow the simplex to change size and shape, increasing the efficiency of the procedure[244-247]. If the initial simplex is taken as a regular figure in n dimensions, then positions taken by the vertices in order to produce such a figure will depend upon the scales used for the axes. The scales should be chosen so that unit change in each factor gives roughly the same change in response. The choice of the size of the initial simplex is not critical if it can be expanded or contracted as the method proceeds. When using a simplex for an optimisation of experimental systems, each vertex corresponds to a set of experimental conditions. The purpose of the simplex is to move rapidly into the region of the optimum. The simplex can be very effective and efficient for this purpose. But when the simplex has located the region of the optimum it becomes relatively inefficient for finding the exact location of the optimum. To find the exact maximum a simplex that contracts near the maximum can be used.

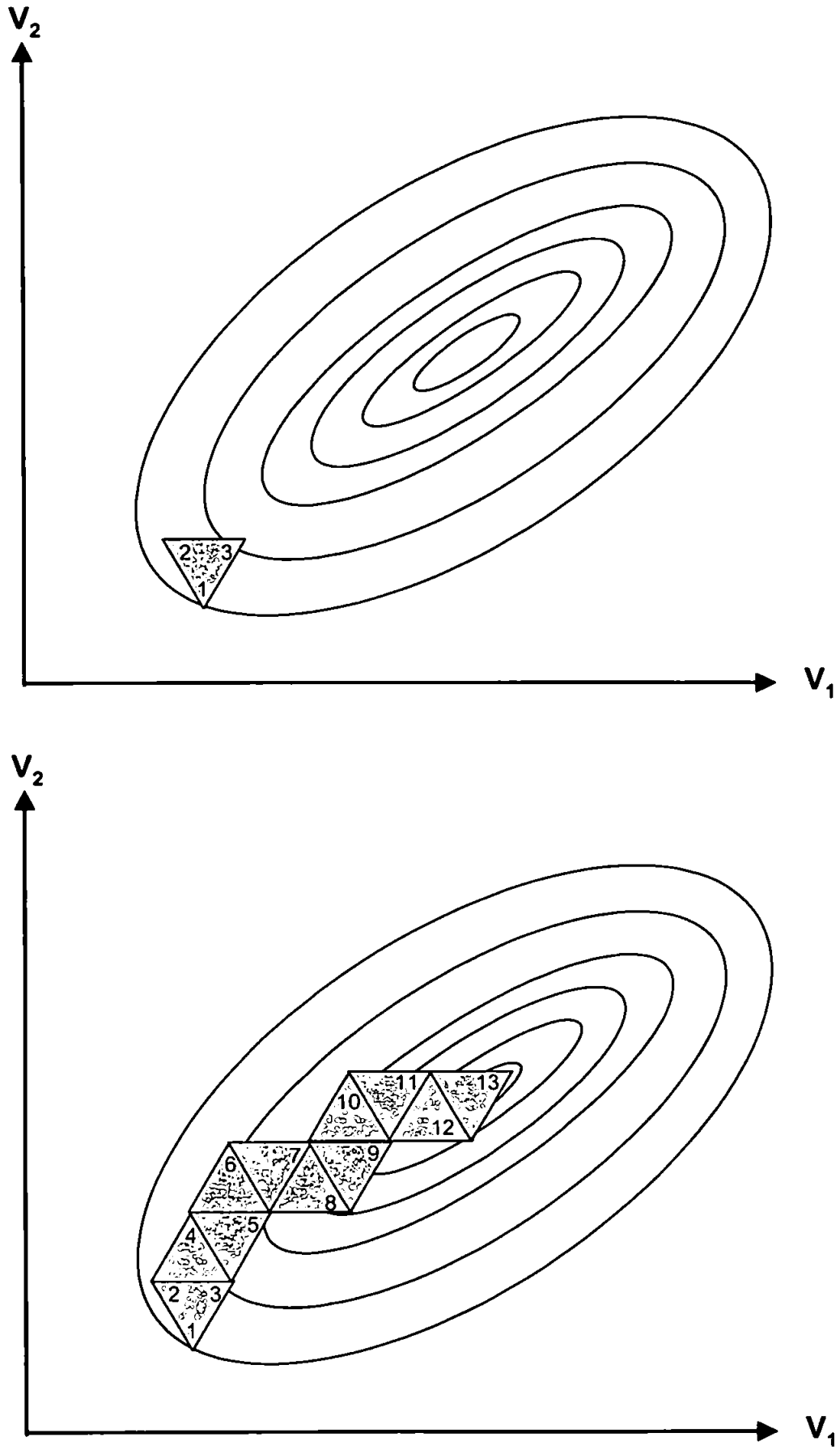

Figure 3.13 **Simplex optimisation for a two variable system, (a) initial vertex ; (b) complete fixed step size simplex optimisation for a two variable system.**

FI techniques are well suited to optimisation using simplex procedures because performance (e.g. sensitivity) is usually controlled by a limited number of interacting experimental variables (sample volume, carrier flow rate, pH of reaction, concentrations of reagents) that can easily be changed. In addition results can be obtained rapidly and therefore a complete simplex optimisation can usually be performed in a day with typically 20 – 30 iterations.

Simplex optimisation has been used in many areas of FI analysis including atomic absorption spectrometry[248], potentiometry[249;250], fluorimetry[251] and spectrophotometry[252;253]. Alteration of the original simplex algorithm has led to other improved versions such as the super modified simplex[252;254], with computer controlled FI systems now being optimised by simplex algorithms[254].

(a) SIMPLEX OPTIMISATION OF THE AMMONIA GD-FI MANIFOLD

A simplex algorithm[255] written in Basic was used to optimise the ammonia GD-FI manifold. The key variables for maximising the absorbance signal were considered to be the sample loop volume, the flow rates of the Milli-Q carrier and the Bromothymol blue indicator stream and the concentrations of the indicator and sodium hydroxide solutions. The starting conditions for each of the variables are given in Table 3.3. The range, step size and precision are also stated. The range defines the minimum and maximum limits of each variable that the algorithm can use, step size defines the maximum increment by which any variable can be increased or decreased between successive simplex experiments and precision is the minimum increment of a variable that can be measured.

Table 3.3 Conditions used for initial simplex optimisation.

FI VARIABLE	UNITS	RANGE	STEP SIZE	PRECISION	STARTING CONDITIONS
Sample Loop Volume	µl	200 – 1000	200	10	600
Carrier Flow Rate	N/A*	50 – 1000	50	1	500
Indicator Flow Rate	N/A*	50 – 1000	50	1	500
Indicator Concentration	g l^{-1}	0.05 - 0.5	0.05	0.05	0.1
Sodium Hydroxide Concentration	mol l^{-1}	0.1 - 0.5	0.1	0.01	0.1

* Pump rates are given in arbitary pump units.

For the simplex optimisation of the GD-FI ammonia manifold a 0.2 mg l^{-1} standard was used throughout. The absorbance at $\lambda_{max.}$ (basic form of bromothymol blue - 617 nm) was used as the response surface for the simplex optimisation. Table 3.4 shows the variable conditions for each simplex experiment and Figure 3.14 plots the simplex history in terms of response for the 0.2 mg l^{-1} standard and Milli –Q blank and the blank corrected response.

Table 3.4 Simplex history for each variable.

EXPERIMENT NUMBER	SAMPLE LOOP VOLUME (µl)	CARRIER FLOW RATE	INDICATOR FLOW RATE	INDICATOR CONC. (g l^{-1})	SODIUM HYDROXIDE CONC.(mol l^{-1})	RESPONSE
1	600	500	500	0.1	0.1	0.023
2	800	500	500	0.1	0.1	0.029
3	800	800	500	0.1	0.1	0.029
4	800	600	800	0.1	0.1	0.026
5	800	600	550	0.2	0.1	0.030
6	800	600	550	0.1	0.2	0.021
7	800	600	600	0.1	0.1	0.021
8	800	600	550	0.1	0.1	0.024
9	800	600	250	0.1	0.1	0.034
10	600	600	50	0.2	0.1	0.123
11	800	700	50	0.2 (0.3)	0.1	0.128
12	600	450	150	0.2 (0.3)	0.1	0.056
13	600	700	150	0.2 (0.3)	0.1	0.071
14	600	650	150	0.2	0.1	0.069
15	600	850	150	0.2	0.1	0.066

The simplex optimisation was able to determine the FI conditions that produced the optimal response but knowledge of FI and analysis conditions were needed to decide on the most practical experimental conditions. After 15 experiments of the initial simplex the blank corrected absorbance signal was increased to 0.066 A.U., almost a three-fold increase from the initial starting point. In all experiments the blank response increased with increased standard response (Figure 3.14); latter experiments showed an increase in the blank corrected response with optimal values given by the FI conditions at experiments 10 & 11, due to lower flow rates and therefore more efficient gas diffusion. However these experimental conditions gave rise to long analysis times (6 min per injection) counteracting one of the fundamental advantages of FI analysis (high sample throughput).

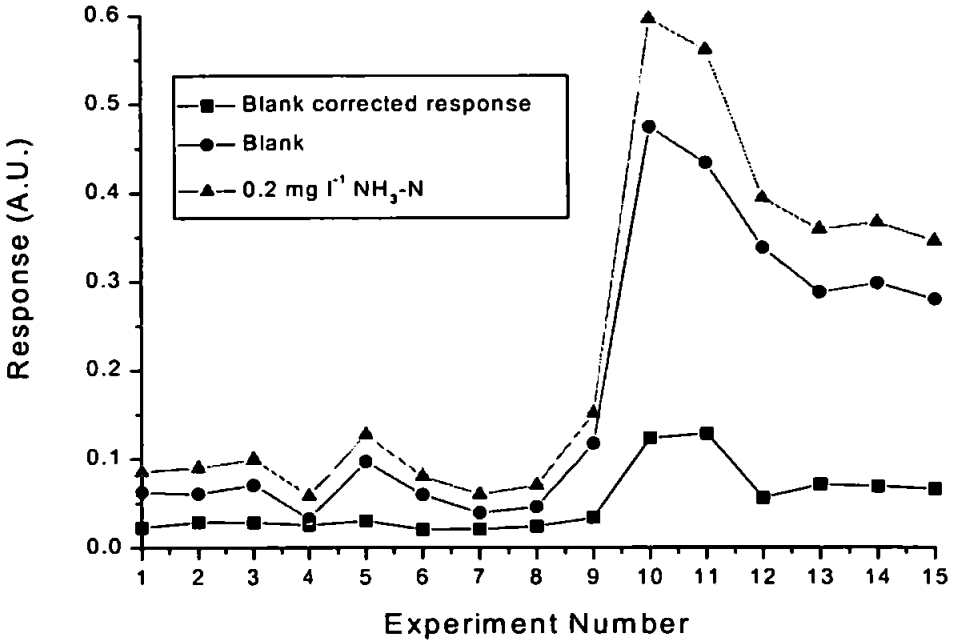

Figure 3.14 Simplex optimisation response profile.

Where the simplex algorithm detailed an indicator concentration of 0.3 g l^{-1} to be used it was found that the absorbance values for the 0.2 mg l^{-1} NH_3-N standard were greater than 1.5 A.U., i.e., beyond the linear range of the spectrometer (identified in section 2.3.4). Therefore 0.2 g l^{-1} bromothymol blue solution was used when required instead of 0.3 g l^{-1} solution. In addition, the use of high indicator concentrations (> 0.2 g l^{-1}) gave rise to a dramatic increase in baseline noise (± 0.01 A.U.) due to the low light transmittance. Therefore use of indicator concentrations of 0.3 g l^{-1} and above were considered unacceptable for the intended application of a field deployed FI monitor. In general, response increased with increasing indicator concentration, but poorer linear range and noise considerations limited the use of high indicator concentrations. Slow indicator flow rates and large injection volumes increased response, but change in carrier flow rate gave no significant change in response, indicating that the diffusion process was very rapid. It was noted however that very high carrier flow rates led to a decrease in the signal, due to the reduction in the period during which ammonia could diffuse across the membrane.

The simplex algorithm did not vary the initial sodium hydroxide concentration of 0.1 mol l^{-1} and therefore it was decided that a concentration of 0.1 mol l^{-1} sodium hydroxide would be used for all further GD-FI experiments. Although experiments 10 and 11 gave optimum responses, the manifold parameters were not appropriate for an FI system (due to long analysis times (6 min) and

noisy response). Therefore a compromise between sensitivity and suitable analysis time was required. Experimental conditions for runs 13 – 15 gave good sensitivity and reasonable analysis times. A further simplex optimisation (21 experiments) with boundary conditions, centring around the results obtained from runs 13 – 15, was then performed. Table 3.5 shows the final boundary conditions used for the second simplex optimisation.

Table 3.5 Conditions used for final simplex optimisation.

FI VARIABLE	UNITS	RANGE	STEP SIZE	PRECISION	STARTING CONDITIONS
Sample Loop Volume	µl	200 – 1000	200	10	600
Carrier Flow Rate	N/A	500 – 1000	50	1	600
Indicator Flow Rate	N/A	500 – 1000	50	1	600
Indicator Concentration	g l^{-1}	0.05 – 0.25	0.05	0.05	0.1

Sodium hydroxide concentration was fixed at 0.1 mol l^{-1}. As for the previous simplex, knowledge of analysis conditions was required and a compromise between sensitivity and practical parameters was required. Final manifold conditions are given in Table 3.6. Optimum conditions chosen for the final simplex gave a two-fold increase in response from the optimum of the initial simplex.

Table 3.6 Optimum gas diffusion manifold parameters.

Injection Volume	800µl
Carrier Flow Rate	1.9 ml min^{-1} (700 units)
Indicator Flow Rate	1.0 ml min^{-1} (400 units)
Indicator conc.@ pH 6.5	0.1 g l^{-1}

3.3.4 MULTI-WAVELENGTH CALIBRATION

Calibrations were performed using the optimum manifold conditions identified in section 3.3.3. History channel functions were used to extend the linear range of the manifold by simultaneously monitoring different wavelengths on the absorption spectrum of bromothymol blue (Figure 3.15). Three wavelengths were selected; $\lambda_{max.}$ at 617 nm, 550 nm (50 % of the absorbance maximum) and 510 nm (5 % of the absorbance maximum). The negative dip occurring at approximately 460 nm was a function of the reference measurement made on the indicator (acceptor) stream prior to measurement.

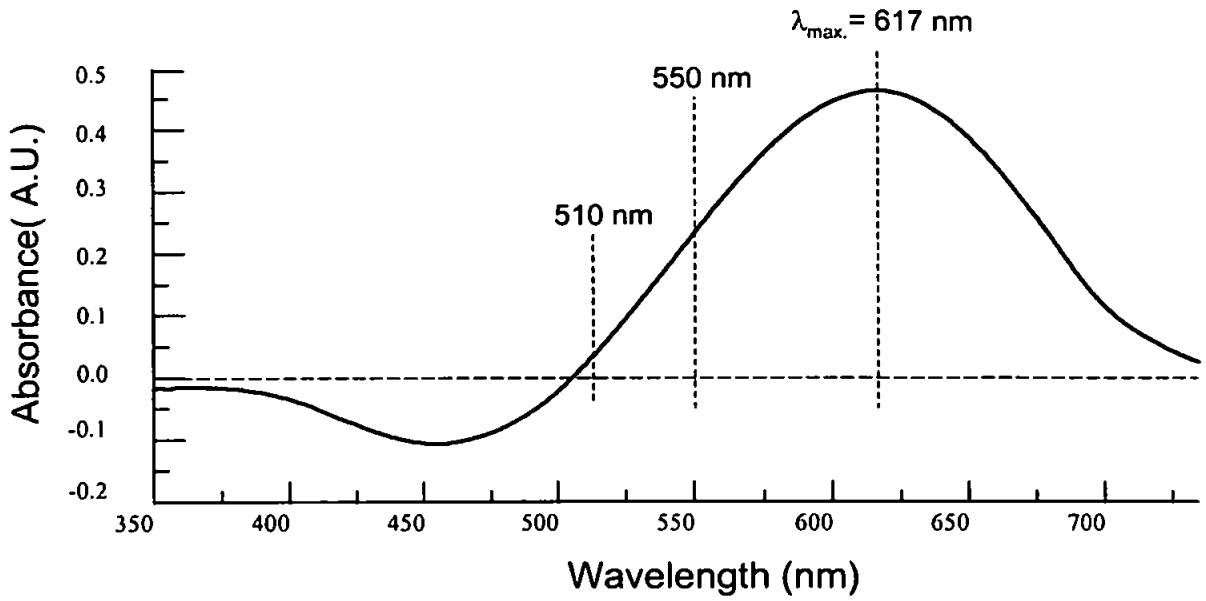

Figure 3.15 Extension of linear range using multi-wavelength monitoring.

Figure 3.16 shows the results obtained from the multi-wavelength calibration (concentrations in mg l^{-1}). Calibration data obtained at 617 nm are shown in Figure 3.17 and Table 3.7. Results are linear over the concentration range 0 - 2 mg l^{-1} NH_3-N with a regression coefficient of 0.997 (n = 8). An increase in the linear range of the manifold can be achieved by utilising the increased information facilitated by using an array detector.

Table 3.7 Multi-wavelength calibration statistics.

Wavelength Monitored (nm)	Concentration Range (mg l^{-1})	r^2	n	Gradient	Intercept
617	0 – 1	0.9995	7	0.393	0.077
550	0 – 10	0.9994	10	0.122	0.039
510	0 – 30 polynomial regression*	0.9996	8	A1 - 0.03 A2 – 0.0005	0.0009

Calibration data extracted from Figure 3.16 shows simultaneous calibration data can be obtained using the PSD – 1000 spectrometer. Extension of the linear range was achieved by monitoring at 550 nm, with excellent linearity (r^2 = 0.9994, n = 10) for the concentration range 0 – 10 mg l^{-1} NH_3-N. High reproducibility was also observed throughout with RSDs typically less than 2 % (n = 5). The dynamic range can be further extended by monitoring at 510 nm but the low absorbances measured lead to increased noise and deviation from linearity.

* Polynomial regression $y = A0 + A1\,x + A2\,x^2 + \ldots$.

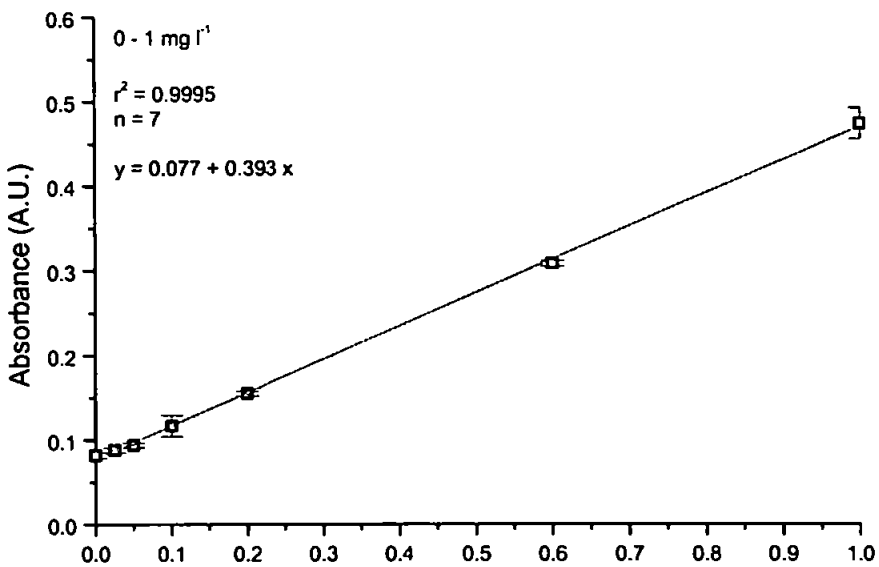

Figure 3.17 Calibration for final GD - FI manifold monitored at 617 nm.

Table 3.8 shows analytical figures of merit for the GD-FI manifold. Sample throughput (36 h^{-1}) was typical of FI manifolds[182] (10 - 100 h^{-1}) and sufficient for the intended temporal resolution of the portable system. Limit of detection, calculated from the mean of the blank signal plus three standard deviations of the blank signal[243], was 0.017 mg l^{-1} and this compares excellently with that of Clinch et al.[85] (0.017 mg l^{-1}). An advantage of this method was the extended linear range of 0 – 10 mg l^{-1} (compared with 0 –2 mg l^{-1}) achieved using the multi-wavelength capabilities of the miniature spectrometer. Good reproducibility was observed throughout the calibration with excellent R.S.Ds, typically less than 1.5 % (n = 5).

Table 3.8 Analytical figures of merit of optimised GD-FI manifold using multi-wavelength acquisition.

PARAMETER	RESULT
Sample throughput	36 h^{-1}
Linear Range @ 617 nm r^2 = 0.9995	0 - 1 mg l^{-1}
Linear Range @ 550 nm r^2 = 0.9994	0 - 10 mg l^{-1}
Limit of Detection (617 nm)	0.017 mg l^{-1}
R.S.D (0.05 mg l^{-1}) (617 nm)	0.9 % (n=5)
R.S.D (1.0 mg l^{-1}) (617 nm)	1.3 % (n=5)
R.S.D (1.0 mg l^{-1}) (550 nm)	1.1 % (n=5)
R.S.D (10 mg l^{-1}) (550 nm)	0.5 % (n=5)

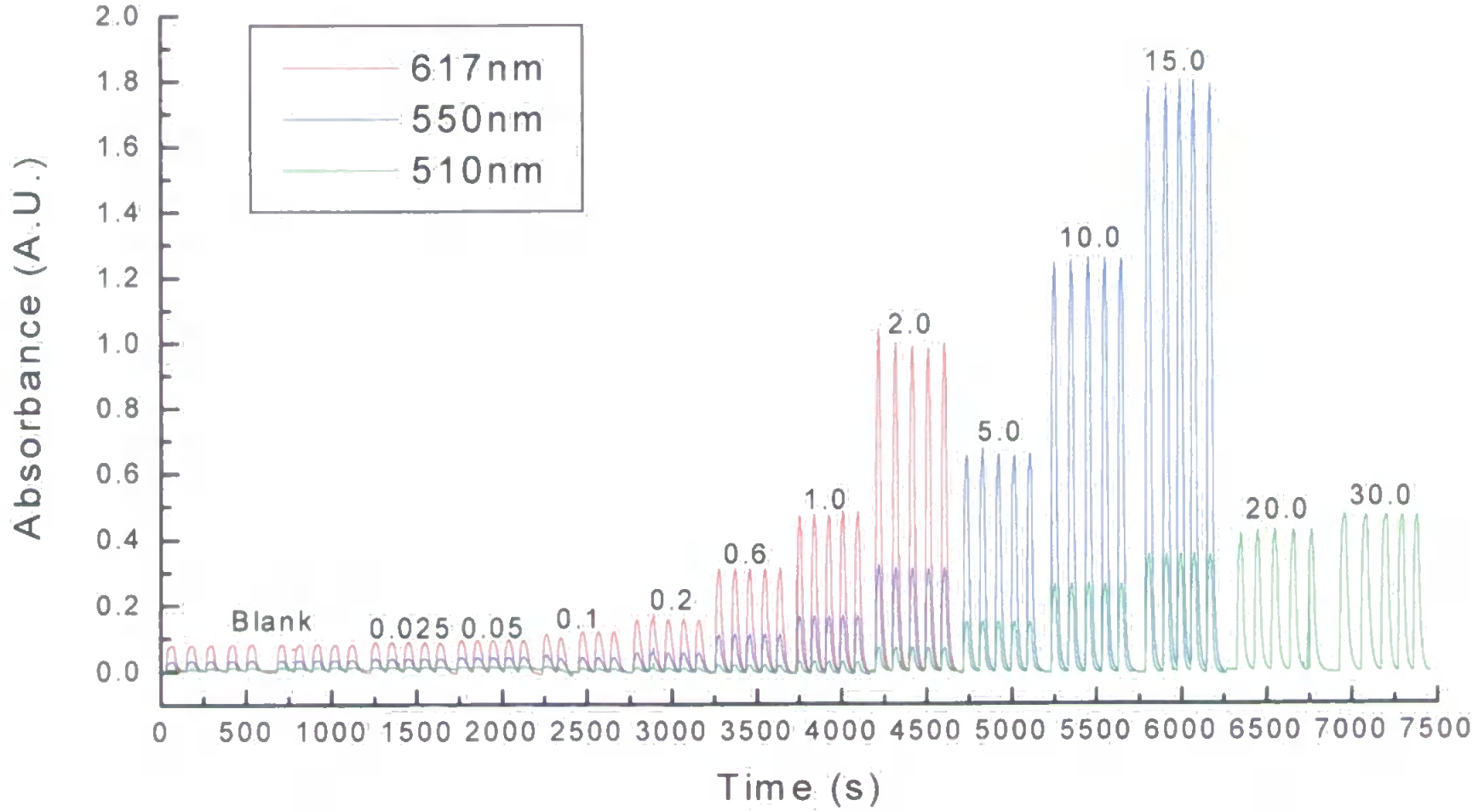

Figure 3.16 Multi - wavelength calibration data for ammonia (0 – 30 mg l^{-1} NH_3-N), monitored at λ_{max} (617 nm), 550 nm and 510 nm

3.3.5 IMMOBILISED REAGENTS

FI has traditionally been "wet chemistry" based, with the use of a series of reagent solutions that bring about a selective reaction that produces a detectable product e.g. spectrophotometrically. However the application of wet reagents to field-deployed systems can have several disadvantages, e.g. wet reagents are bulky and add to the overall weight of a field monitor, some reagents are expensive, there are possible stability problems and they generate waste (possibly toxic) that must be correctly disposed of. Therefore there is a considerable interest in the use of "dry" or immobilised reagent systems. Optical fibre sensor technology has seen considerable growth over the past decade[67;74;75] and offer an attractive alternative to more conventional FI approaches. Based on the simple concept of coupling a reagent sensing phase to an optical fibre, the measurement is based on a change in the optical properties of the reagent brought about by contact with the desired analyte. The advantages of optical fibre sensors include; the fibre optic light guides are capable of transmission of light over large distances with low attenuation of optical power, they can measure concentrations without significantly perturbing the sample, they are not subject to electrical interference due to the optical nature of the signal, they are geometrically flexible, corrosion resistant, capable of being miniaturised and compatible with telemetry systems. They can also be of low cost, of rugged construction and provide intrinsically safe, efficient and capable of operation in remote and hostile environments.

Sensors used for ammonia determination have been based on IR absorption of gaseous ammonia and the selective reaction of a reagent with ammonia to give a detectable colour. A typical example is reported by Sellien et al.[256] who based their sensor on an immobilised pH indicator. The indicator was entrapped / immobilised into the structure of a gas permeable membrane. As ammonia diffused through this membrane, the indicator was deprotonated and the resultant colour change measured spectrophotometrically. Typical membranes consisted of PTFE and the indicator used was p-Xylenol Blue. Waste water samples were analysed with no pretreatment of the sample and results agreed well with conventional spectrophotometric methods of analysis and achieved a limit of detection of 1×10^{-6} mol l^{-1} NH_4^+. Utilising the same fundamental principle, Werner et al.[257] modified dyes by converting them into organic ion pairs which were homogeneously distributed inside a silicone membrane. Natural waters were analysed and the results proved the sensor stable over the concentration range 0.015 – 20 mg l^{-1}, relatively rapid response times (2 – 30 min), robust and highly sensitive, achieving a limit of detection of 15 μg l^{-1}.

Reichart[75] immobilised bromocresol green indicator in PTFE; the resulting membrane was incorporated into a battery operated, hand-held fibre optic photometer for the determination of ammonia in natural and waste waters. Response times were 1 – 10 min and the detection limit was 0.02 mg l^{-1}.

In this work a pH indicator was immobilised/ impregnated into the structure of standard "thread sealing" PTFE tape. The indicator found which gave the response was bromocresol green (BCG). Figure 3.18 shows the chemical structure of bromocresol green (tetrabromo-m-cresol sulphonphthalein). The indicator has a pK_a of 4.7 and a transition range of 3.8-5.4 pH units and undergoes a distinctive colour change from yellow to medium blue. The protonated acidic form of the indicator (yellow) when deprotonated gives the basic (blue) form of the indicator. The need for an indicator with a relatively low pK_a, compared to bromothymol blue (as used in the gas diffusion manifold), is due to the fact that the immobilised reagent system provides less efficient mass transfer of ammonia.

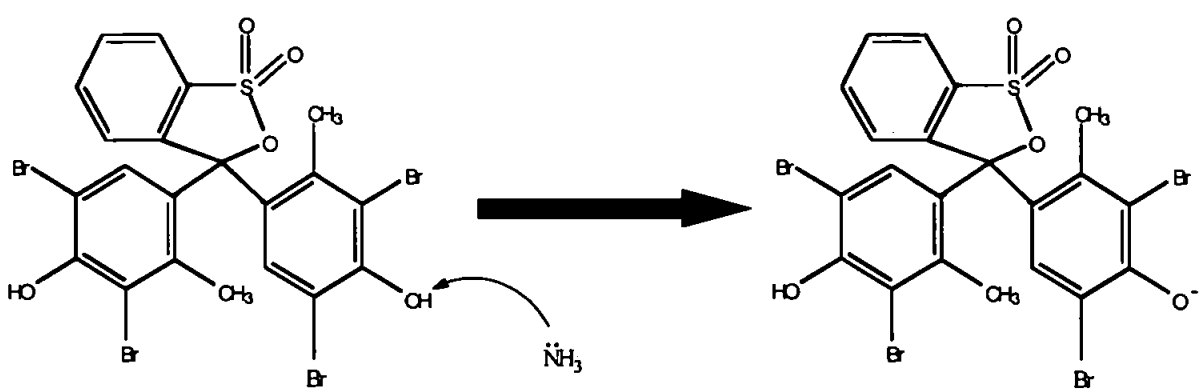

Figure 3.18 Schematic reaction showing the deprotonation of the BCG indicator.

Gaseous free ammonia in a solution is able to diffuse into the porous PTFE membrane structure, whereupon it comes into contact with the acidic form of the indicator. Subsequent deprotonation of the tetrabrom-m-cresol sulphonphthalein molecule occurs to give the resultant medium blue colour ($\lambda_{max.}$ 620 nm). This colour formation can be measured spectrophotometrically (Figure 3.19) with the maximum of the deprotonated absorbance peak being proportional to the concentration of ammonia present in the original sample.

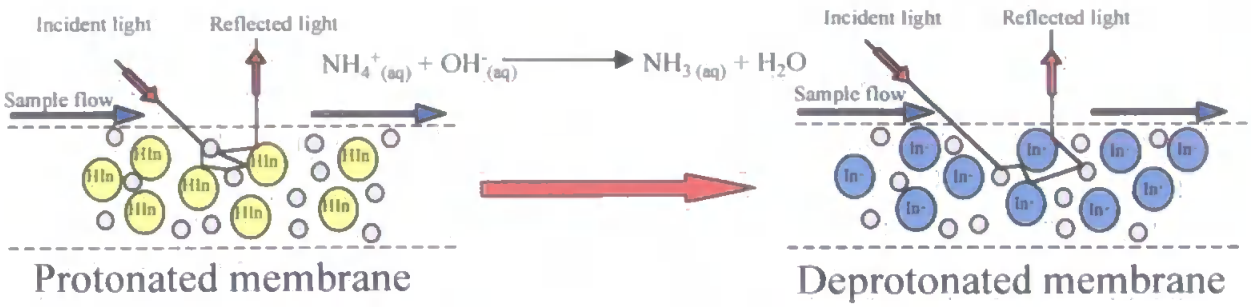

Figure 3.19 Diagram of membrane response in the presence of ammonia.

3.3.6 PERFORMANCE OF LAMINAR FLOW MANIFOLD

Aqueous ammonia standards were passed into the flow cell using a peristaltic pump and flowed in a laminar regime across the underside of the tape. Gaseous ammonia in the sample diffused into the membrane and produced a colour change in the immobilised pH indicator, which was viewed via reflectance optics connected to the PSD – 1000 spectrometer. The response of the uninhibited (not incorporated into flow cell) membrane was typically rapid, approximately 5 s for colour development and the tape was reversible by a simple flushing with Milli-Q water. The time to reverse the colour formation was dependent on the concentration of ammonia in the original sample. The higher the initial ammonia concentration the longer the reversing time, with a maximum time to reverse of 120 s.

Figure 3.20 shows the raw spectra obtained for the initial experiment (section 3.2.4), with both the acidic (λ_{max} = 450 nm) and basic (λ_{max} = 620 nm) forms of the indicator clearly visible. The isosbestic point of the indicator can be seen at 510 nm. The isosbestic point occurs when two species in chemical equilibrium have the same molar absorptivity (ε). The existence of the isosbestic point confirms the presence of only two coloured species in equilibrium that have overlapping absorption bands. The spectra shown in Figure 3.20 were inherently noisy and there are several reasons for this. There was no focusing of the illuminating or collection fibre optics, the flow cell was fabricated from white PTFE (causing high ambient reflected light) and the optical fibres were not permanently fixed in position.

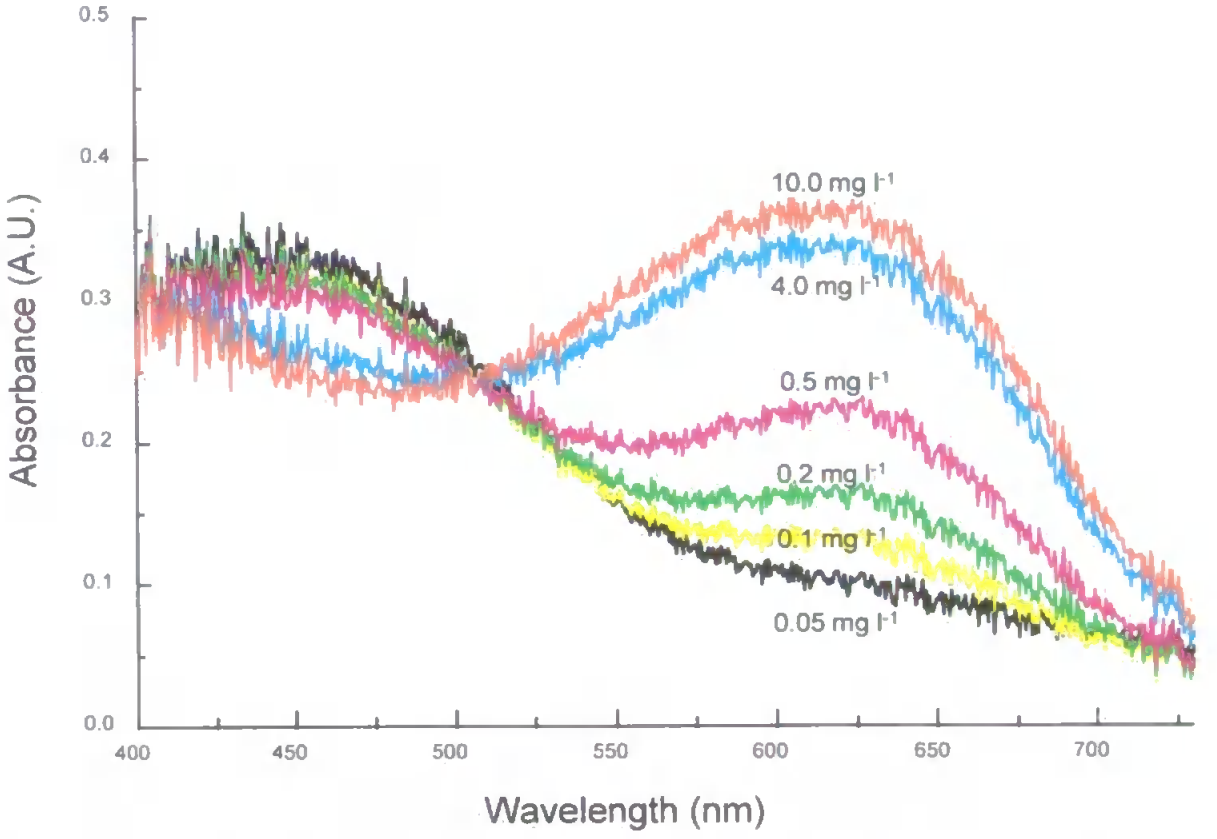

Figure 3.20 Initial laminar flow determination of ammonia (0.05 – 10.0 mg l^{-1} NH_3-N).

It is possible to perform post acquisition smoothing of the spectra, which is beneficial where response variables (e.g. absorbance at a particular wavelength) are subject to underlying noise as in this case. There are several smoothing algorithms available but a traditional smoothing function is the moving average or adjacent average. Each response variable value is replaced with a mean of *n* adjacent neighbours. *n* is an operator defined variable, determined from knowledge of the response variables. Figure 3.21 shows the effect of applying a 10 point moving average filter to Figure the data from 3.20.

In this case the noise in the spectra has been considerably reduced but the analytical information remains. However care must be taken when applying smoothing functions because if data is "oversmoothed", by including too many points in the averaging calculation analytical information can be lost with reduction in peak height, peak broadening and reduced sensitivity. By taking into account the response values for the determination at the maximum sensitivity of the tape (620nm) a sigmoidal calibration plot of the membrane tape was obtained as shown in Figure 3.22.

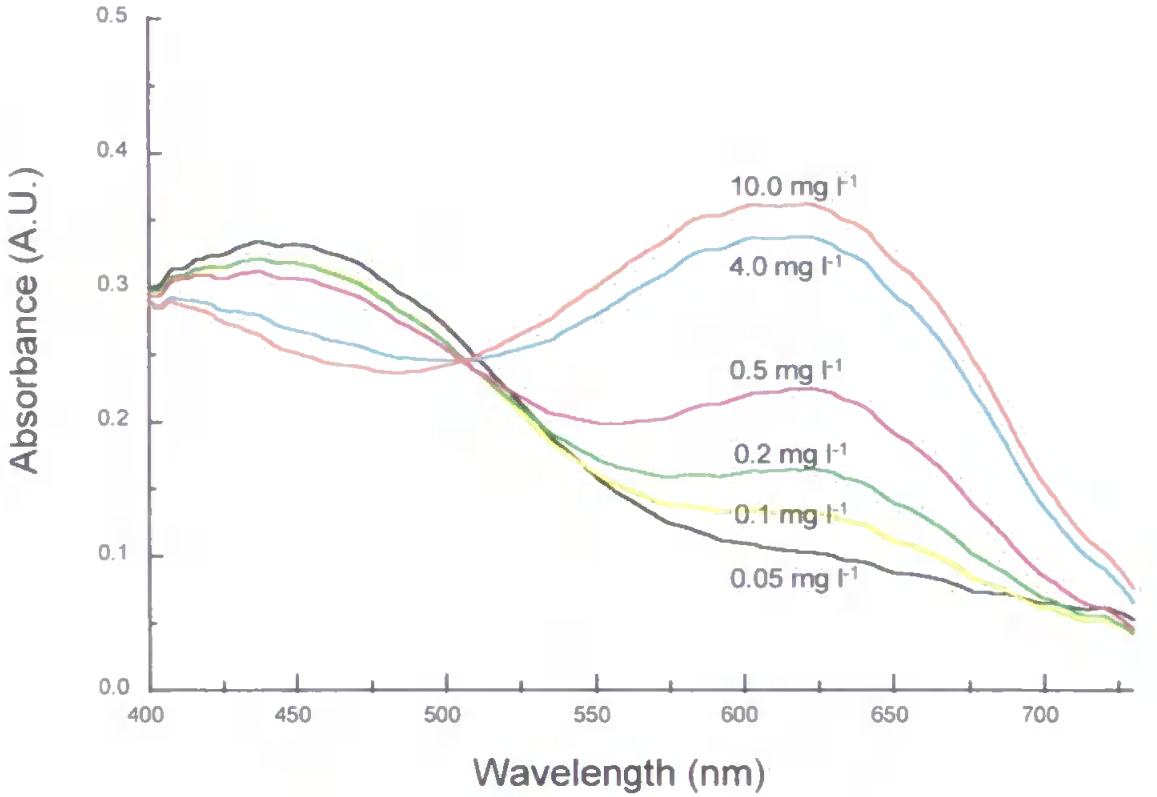

Figure 3.21 **Ten point moving average smoothed plot of the data shown in Figure 3.20.**

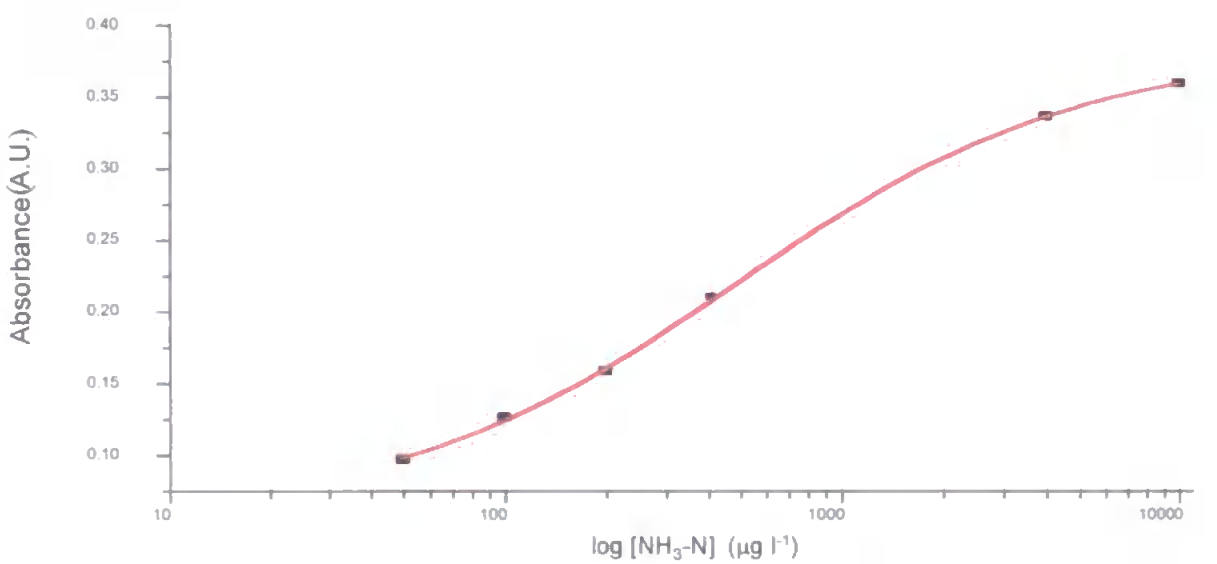

Figure 3.22 **Sigmoidal calibration graph for the determination of ammonia (0.05 – 10.0 mg l^{-1} NH_3-N) using the laminar flow cell.**

Through experimentation it was found that the response of the tape was temperature dependent, with the slope of the fit offsetting vertically depending on the temperature. The maximum operating temperature was 40°C; beyond this temperature expansion of the membrane caused water to enter and leach out the bromocresol green indicator.

Figure 3.23 shows a calibration performed using the final laminar flow cell design (Figures 3.4 and 3.5, section 3.2.4). Each spectrum is an average of 3 consecutive runs per standard and the spectra have also undergone a 10 point adjacent average smoothing algorithm. As can be seen, the spectra are considerably smoother in peak shape when compared with the data shown in Figures 3.20 and 3.21. This is due to an improvement in the arrangement of the viewing fibre optics (clamped in position, incident light angled at 45° to collected reflected light at the normal) and the reduction of ambient reflected light (due to improved optical configuration and shielding of the optics). As with the initial design, both the acidic and basic forms of the indicator were clearly seen,are visible with their absorption profiles intersecting at the isosbestic point (510 nm).

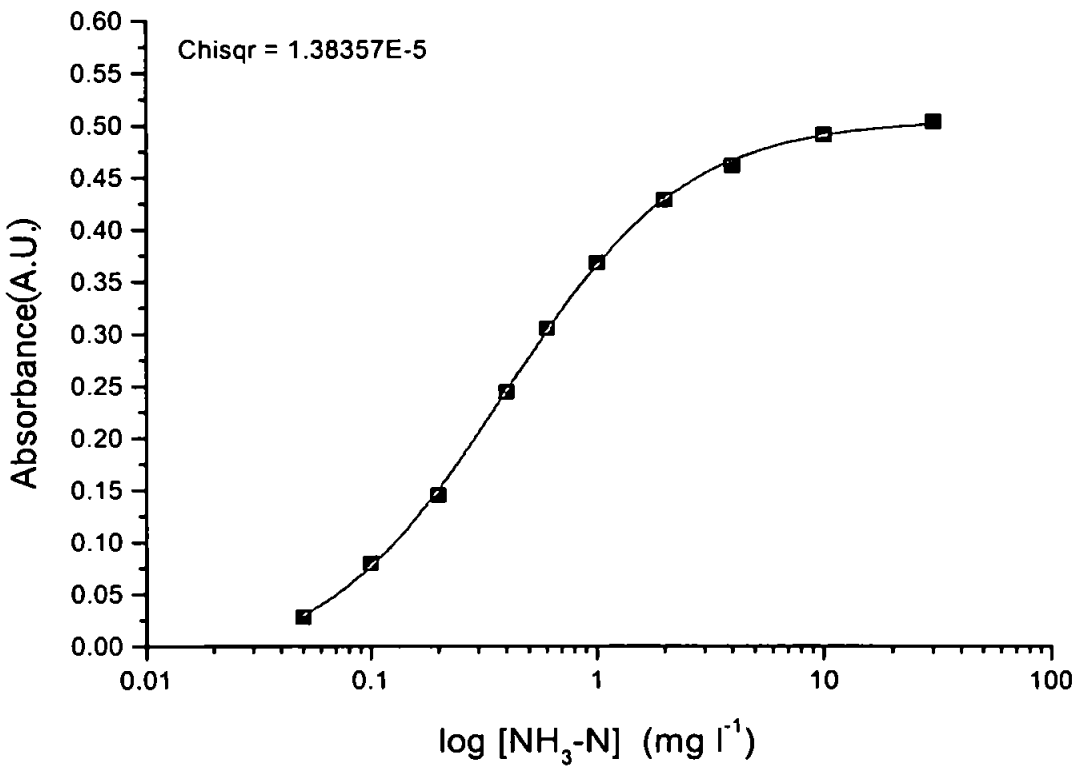

Figure 3.24 Sigmoidal calibration plot for the determination of ammonia (0.05 – 30.0 mg l^{-1} NH_3-N) using the redesigned laminar flow cell.

The calibration plot is shown in Figure 3.24 and the response of the tape was virtually linear between 0.2-1.0 mg l^{-1} and quantitative measurements can be made from 0.1-4.0 mg l^{-1}. The dynamic range of the membrane response was three orders of magnitude, however the system had limited sensitivity in the concentration range needed for low level ammonia measurements (< 0.1 mg l^{-1}) when compared with the conventional gas-diffusion FI manifold (Figure 3.17).

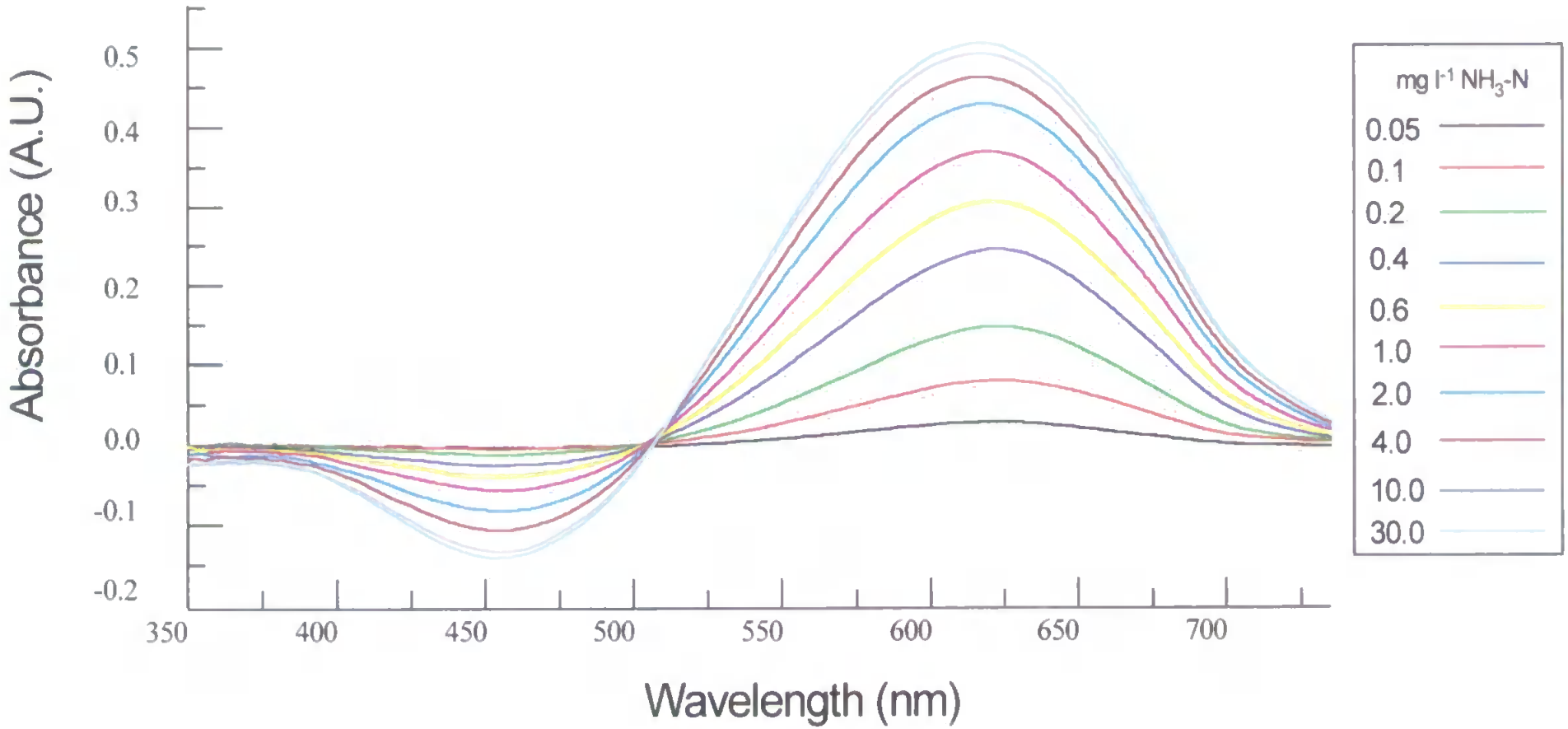

Figure 3.23 **Overlaid averaged calibration spectra for the FI determination of ammonia using the laminar flow cell (Figures 3.4 & 3.5) and immobilised bromocresol green acid-base indicator.**

Although noise was greatly reduced with the re-designed flow cell (Figures 3.4 and 3.5), a major problem encountered was the time taken for uniform colour development within the membrane. In addition, there was formation of "colour patches" with areas of protonated and deprotonated indicator. These problems were exacerbated by the relatively small illumination area (3 mm) of the tape. Another limitation was the time taken for the membrane to reverse from blue back to yellow after ammonia diffusion. Although diffusion was rapid in the uninhibited membrane, the constraints of the laminar flow cell gave rise to times of 3 –5 min dependent on concentration. This was longer than in the original design due to the increased pressure on the membrane. Therefore the implementation of the dye-impregnated membrane in a FI system for the determination of ammonia in natural waters was considered less suitable for field deployment than the conventional gas-diffusion FI system.

3.4 CONCLUSIONS

The following specific conclusions can be drawn from the research reported in this chapter:

1. The Ocean Optics PSD – 1000 spectrometer can be incorporated in an FI manifold and the on-board software used to acquire and process transient FI responses.
2. The GD-FI manifold with the Ocean Optics PSD – 1000 spectrometer can be used to determine ammonia in waters over the linear range of 0 – 10 mg l^{-1} (r^2 = 0.9994, n = 10) with a detection limit of 17 µg l^{-1} NH_3-N, a sample throughput of 36 h^{-1} and precision in the range < 2 % RSD (n = 5).
3. To determine ammonia at ambient levels in natural waters stringent cleaning protocols need to be adapted. It is recommended that all plastic and glassware be soaked for a minimum of 24 h in 50 % HCl, then thoroughly rinsed in Milli-Q water (ten times), dried and stored in two ziplock bags in a cool dark place.
4. The multi-wavelength capability of the Ocean Optics PSD – 1000 spectrometer allowed a significantly wider dynamic range than a single wavelength detector, 0 – 30 mg l^{-1} NH_3-N using λ_{max} (617 nm), 550 nm and 510 nm.
5. To minimise reagent (indicator) consumption, reagent can be physically immobilised in PTFE tape, incorporated in a laminar flow cell and coupled with a GD-FI manifold. The analytical performance (dynamic range 0.05 – 30 mg l^{-1} NH_3-N, detection limit 0.05 mg l^{-1} NH_3-N) was not as good as that of the conventional GD-FI manifold due to poorer mass transfer of the analyte into the membrane.

Chapter Four

Determination of Nitrate by Flow Injection With Spectrophotometric Detection

"The future belongs to those who believe in the beauty of their dreams"

- Eleanor Roosevelt -

4.1 INTRODUCTION

In the previous chapter a FI manifold incorporating an Ocean Optics PSD – 1000 spectrometer was optimised for the determination of NH_3 in natural waters. This chapter presents a similar approach to the optimisation of an FI manifold for total oxidised nitrogen (TON) which measures inorganic nitrate and nitrite combined. The refractive index problem associated with mixing a high ionic strength ammonium chloride stream (for the cadmium reductor column) with a low ionic strength sample has been systematically investigated. The multi-wavelength capability of the Ocean Optics detector has been shown to provide a better solution to this problem than physical approaches for the determination of TON in natural waters.

4.2 EXPERIMENTAL

4.2.1 REAGENTS

All solution were prepared from ultra-pure de-ionised water supplied by a Milli-Q system (Millipore Corp.), and all reagents were AnalaR® (Merck Ltd) unless otherwise stated. The carrier stream was prepared by dissolving ammonium chloride (10 g) in 1 l of water. The N-(1-naphthyl)ethylenediamine dihydrochloride (N1NED; Merck Ltd) and sulphanilamide (Merck Ltd) reagents were prepared by dissolving 0.5 and 25 g, respectively in 1 l of water containing 10% orthophosphoric acid (Merck Ltd). The colour reagent was prepared by mixing equal volumes of the N1NED and sulphanilamide reagents in a brown polypropylene container. The cadmium reductor was prepared by stirring 3 g cadmium metal powder (Merck Ltd, U.K.) in 50 ml of a 10 g l^{-1} copper (II) sulphate solution for 2 min. The copperised cadmium was then washed with 2 M hydrochloric acid and then a 10 g l^{-1} ammonium chloride solution. This was packed into an in-house designed acrylic column[258] (10 mm o.d. x 60 mm length). When not in use the cadmium column was stored in ammonium chloride solution (10g l^{-1}). A stock nitrate (NO_3-N)* solution (100 mg l^{-1}) was prepared by dissolving 0.7220 g of potassium nitrate (previously dried at 105°C for 1 h) in water. Working standards were prepared by serial dilution with water.

4.2.2 INSTRUMENTATION and PROCEDURES

The flow injection manifold (Figure 4.1) used for the initial method development was adapted from a manifold reported by David et al.[147], and the final FI manifold is given in Figure 4.15. Poly(tetrafluoroethylene) (PTFE) tubing of 0.8 mm i.d. (Anachem, Luton, Beds., UK) was used in

* All nitrate concentrations are expressed in mg l^{-1} nitrogen.

the construction of the manifold. A peristaltic pump (Ismatec Mini-S 820, Ismatec, Carshalton, Surrey, UK) with poly(vinyl chloride) (PVC) pump tubing (Elkay, Basingstoke, Hants., UK) was used to propel the sample and reagent streams. Investigations into refractive index correction used an in-house built glass bead mixing column (20 mm length, 3 mm i.d.), with 1.5 - 2 mm o.d. glass beads incorporated in the manifold upstream of the reductor column. A novel type of mixing device known as the *reed mixer* (Ionode Pty Ltd, Tennyson, QLD, Australia) was also evaluated. The mixer control circuit allowed reed vibrational frequencies between 2 and 150 Hz. All *reeds* were made from teflon-coated piano wire (Ionode Pty Ltd.) (see section 4.3.6).

Standards (260 µl) were injected into an ammonium chloride carrier stream, passed through the cadmium reductor column and then merged with the colour reagent in a 100 cm knitted reaction coil. The resultant pink-purple azo dye was detected using the Ocean Optics spectrometer (λ_{max} 540 nm) fitted with a 10 mm path length flow cell (18µl) (Helma U.K.). All optical fibre connections used all-silica core, fluorine doped silica cladding, 200 µm single core UV-VIS fibres (Anglia Instruments Ltd), unless otherwise stated. All spectrometer parameters were as described previously in section 2.2.2 unless otherwise stated.

4.3 RESULTS & DISCUSSION

4.3.1 PRELIMINARY EXPERIMENTS

The starting point for the optimisation used the manifold shown in Figure 4.1, a 10 g l^{-1} ammonium chloride carrier and a mixed colour reagent containing 25 g l^{-1} sulphanilamide, 0.5 g l^{-1} N1NED and 10% (v/v) orthophosphoric acid. All experiments were carried out using a 1 mg l^{-1} NO_3-N standard, unless otherwise stated. Figure 4.2 shows the baseline detector response for the nitrate manifold (Figure 4.1) monitored at the analytical wavelength (540 nm). There is clear evidence of a regular sinusoidal fluctuation of approximately 0.01 A.U. on the detector baseline. This short term oscillation is superimposed on a larger oscillation cycle with a period of approximately 100 s. Figure 4.2 highlights two problems within the FI system. Firstly the system is optically sensitive to the pulsing action of the pump. These short term sinusoidal variations have also been observed by Zagatto et al.[259] who reported oscillations as large as 0.05 A.U. when injecting 1.00 M sucrose solutions into a 0.01 M sodium tetraborate carrier stream. They concluded that the superimposed frequency was determined by the pulsation of the peristaltic pump and was caused by the intermittent presence of more concentrated and diluted portions of the sample zone in the spectrophotometer light path.

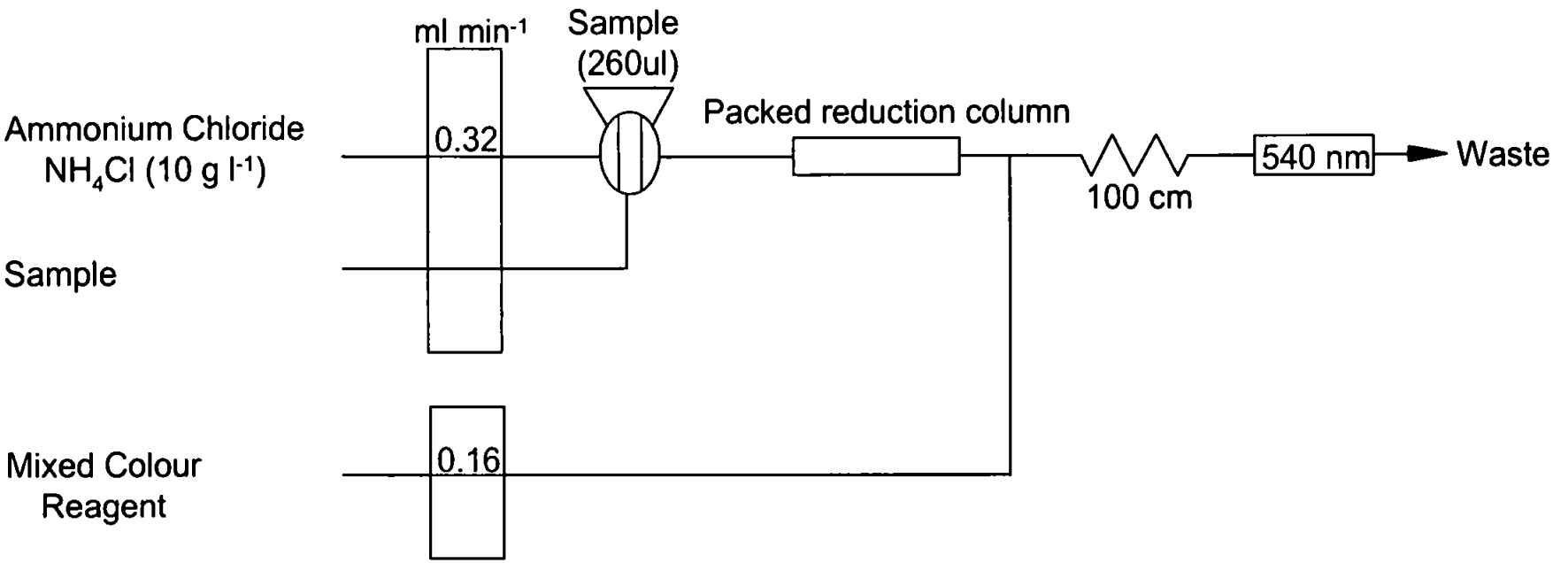

Figure 4.1 **Initial Flow Injection manifold for the determination of nitrate.**

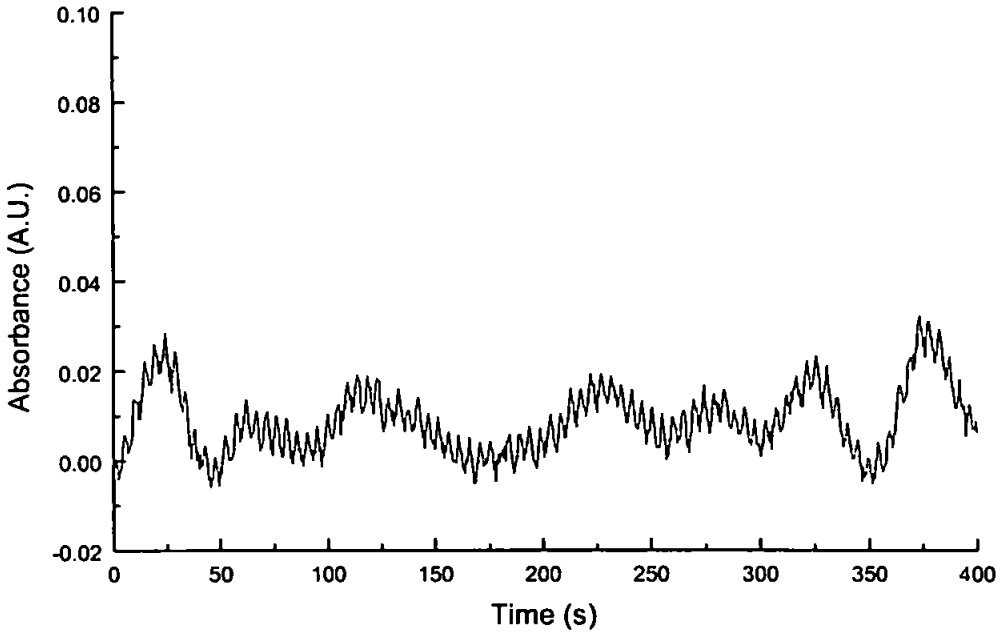

Figure 4.2 Pumping oscillations on the detector baseline monitored at 540 nm.

In an attempt to reduce the short term oscillation problem the Ismatec pumps were replaced with Gilson peristaltic pumps. Ismatec Mini-S 820 peristaltic pumps are fixed speed (20 rev min^{-1}) pumps with 8 rollers on a vertically mounted pump head. Varying flow rates are achieved by using different internal diameter pump tubing. Gilson Minipuls-3 pumps contain a gearbox mechanism that enables the user to "dial-up" a variable range of pump revolutions (given in arbitrary units). In addition 10 rollers are used in the horizontally mounted Gilson pump head.

The additional rollers and controllable speed of the Gilson pump combined to produce a more uniform flow within the FI manifold and the short-term fluctuations were reduced to ~ 0.005 A.U. Section 4.3.4 discusses the use of mixing devices such as coils and glass bead columns in a variety of different manifold configurations, in an attempt to further reduce the oscillation.

The second problem concerned the larger, lower frequency oscillation onto which the smaller pumping oscillations were superimposed. These longer term oscillations could arise from several sources, each of which is discussed below.

Fluctuations in the tungsten / halogen source intensity could cause oscillations such as those seen in Figure 4.2, especially due to the single beam configuration of the detection system. This, however, is unlikely with this system due to the electrical stability provided by the use of a surge / noise protector connected to the mains input to the lamp and also the output regulation voltage

provided by the lamp itself (Table 2.1, Chapter Two). Additionally the lamp achieved 100 % thermal stabilisation after 30 – 40 min, and all experimental work was carried out after a stabilisation period of 1 h. Experimental work reported in Chapter Two on the characterisation of the PSD – 1000 spectrometer also indicates that the long term oscillations are unlikely to arise from poor performance or stability of the detector itself. It is also unlikely that the longer-term oscillations are due to peristaltic pumps.

However the manifold has merging carrier (ammonium chloride) and reagent streams (N1NED and sulphanilamide) of different compositions, refractive indices and concentrations. It has been reported[259] that a "steady state" Schlieren signal or refractive index effect can be observed in FI systems in which two streams with large differences in concentration and refractive index merge. With incomplete mixing conditions, the baseline becomes noisy with a low frequency sinusoidal oscillation as shown in Figure 4.2. Under these conditions the liquid interfaces caused by the differences in refractive index cause disruptions to the amount of light reaching the detector and recorded traces can become noisy, with the sensitivity and reproducibility of quantitative analyses being degraded. This Schlieren or refractive index effect is discussed in detail in section 4.3.2.

Figure 4.3 shows a typical trace obtained when a water blank is injected into the manifold. The baseline undergoes a large negative shift in absorbance (- 0.13 A.U.) followed by a smaller positive shift (+ 0.03 A.U.).

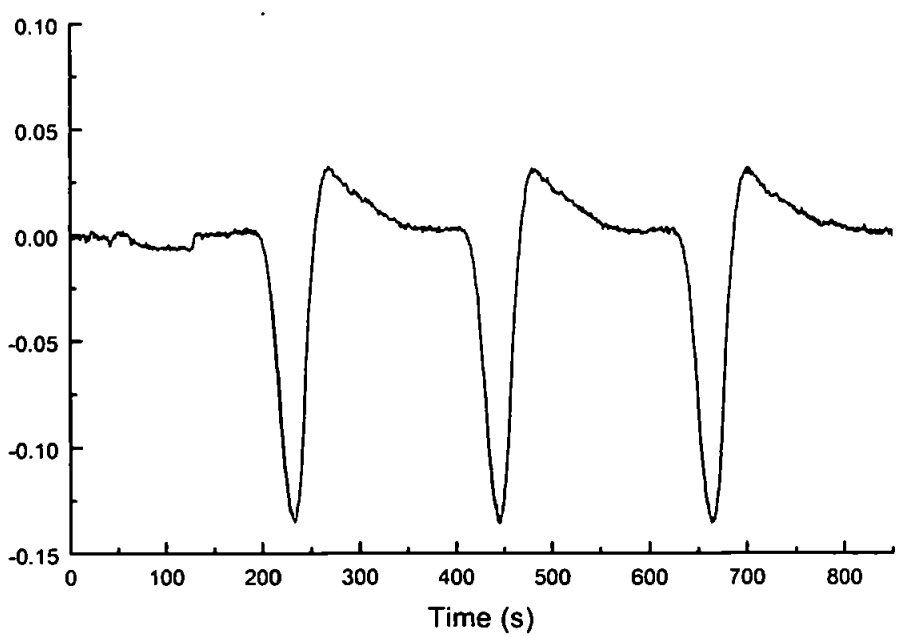

Figure 4.3 **Typical FI peak shape monitored at λ_{max} (540 nm) for blank injections showing the Schlieren effect.**

From Figure 4.3 it can be seen that the time base between the events that occurred during a water blank injection were regular. The time from injection for the baseline to drop to its minimum absorbance value of – 0.13 A.U. is reproducible (R.S.D 2.9 %, n=3) at 40 s. The time taken for the absorbance readings to rise from the minimum (- 0.013 A.U.) to the maximum (+ 0.03 A.U.) is also reproducible at 37 s (R.S.D 2.1 %, n=3). Figure 4.4 shows typical traces obtained at the analytical wavelength (540 nm) when a 1 mg l^{-1} NO_3-N standard in injected using the manifold shown in Figure 4.1.

The trace shows two unusual characteristics that are likely to be caused by the Schlieren effect. They are a slight negative dip in absorbance prior to the analyte peak, and a small shoulder region on the leading edge of the analyte peak at approximately half peak maximum. Comparison of the timings extracted from the blank injections (Figure 4.3) show good correlation with the timings of the regions of interest extracted from Figure 4.4 of the 1 mg l^{-1} NO_3-N standard injections. The time from the negative drop after standard injection to the shoulder region was 40 s and the peak maximum then occured 38 s after the shoulder region. These timings are directly comparable with those from Figure 4.3. The shoulder regions shown in Figure 4.4 corresponded to the peak minima of Figure 4.3 and consequently the peak maxima of both blank and standard injections have the same time base of 38 s. Figure 4.4 also shows evidence of low frequency sinusoidal oscillation in the baseline, particularly in the region ~1000 – 1300 s, which is indicative of the Schlieren or refractive index effect and has been discussed above.

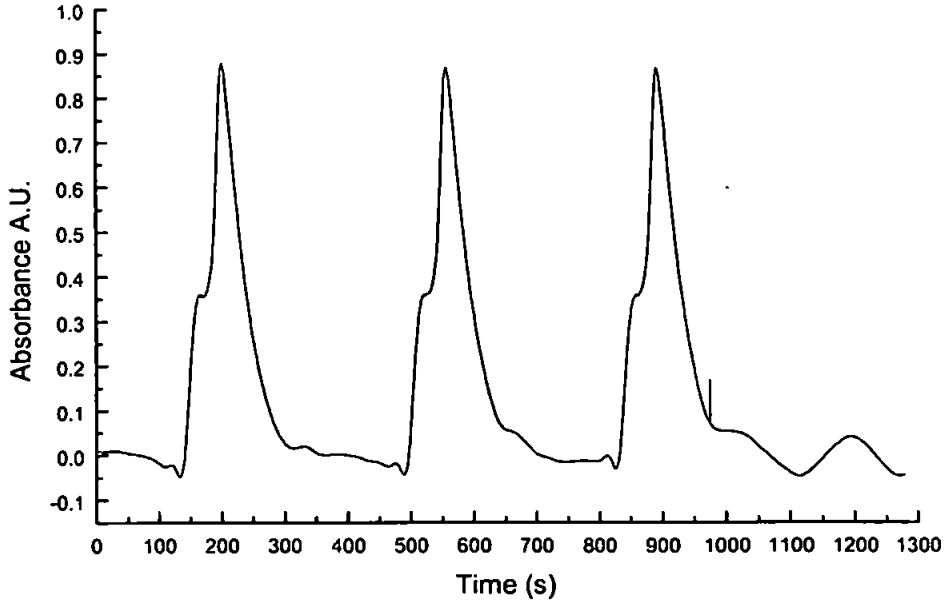

Figure 4.4 Replicate injections of a 1mg l^{-1} NO_3-N standard monitored at 540 nm.

4.3.2 SCHLIEREN EFFECT

A common problem encountered in FI spectrophotometry is the generation of peaks which result from the differences in refractive properties of the sample and carrier / reagent streams. Such a phenomenon is called the "refractive index" or Schlieren effect and can cause significant errors in quantification[261-263] when flow through detection is used. Zagatto et al.[259] have extensively studied the Schlieren effect and their methods to compensate for this effect are discussed below.

The Schlieren effect becomes more pronounced in single line systems when solutions of differing ionic strength are mixed, dispersion is limited and the sample reaches the detector without complete mixing with the carrier stream[182;264]. The Schlieren effect most commonly manifests itself as a negative frontal peak followed by a positive peak[265;266] using conventional FI but it can be additive or subtractive depending on sample composition (e.g. refractive index differences) and manifold design[266] (e.g. efficient mixing of streams). It occurs due to a lensing effect which arises from a combination of the parabolic geometry of the sample zone under laminar-flow conditions and the refractive index difference that exists between the sample and carrier or reagent stream(s). These liquid interfaces act as mirrors or lenses, either focussing light onto the detector or scattering it during the passage of the sample zone through the flow cell. The effect is also more pronounced at the front and tail portions of the sample zone where concentration gradients, and therefore refractive index gradients, are at their highest.

The first reported publication of the Schlieren effect in FIA involved the determination of sulphate by turbidimetry[267]. They reported *"a mixing boundary (Schlieren pattern) could be seen very clearly when the flow through cuvette was removed from the spectrophotometer and observed visually after injecting a blank or a sample"*, with the effect becoming less pronounced as the mixing conditions were improved.

Several approaches have been reported in the FI literature to overcome the problems associated with the Schlieren effect. According to Johnson et al.[268] one of the simplest methods is to match the refractive indices of the carrier stream and the injected sample. Their work involved the determination of nitrate in a sea water matrix by the Greiss reaction and the Schlieren effect was eliminated when 10 g l^{-1} NH_4Cl was added to each litre of N-(1-naphthyl) ethylenediamine dihydrochloride (N1NED).

However more recent work[269] attempted to utilise this approach for the in situ FI determination of nitrate and nitrite in seawater and reported a reduction of the Schlieren effect but not complete elimination.

It has been proposed that for higher sensitivity, sample injection into chemically inert solutions with similar matrix composition is preferred[261;182]. Although index matching of carrier and sample solutions is desirable, this approach can be limited when faced with samples with a wide range of concentrations such as the analysis of estuarine samples of variable salinity (0 – 35 $^{o}/_{oo}$). Index matching is further discussed with particular reference to the nitrate manifold in section 4.3.5.

In their studies on the Schlieren effect Zagatto et al.[259] suggested that FI parameters that affected dispersion also had a considerable effect on the Schlieren signal, particularly injection volume, reactor / mixer length, flow rates and confluent stream addition. The Schlieren effect can be offset by the use of large injection volumes[270]. Dispersion at the centre of a large sample zone is close to unity, and the Schlieren peaks interact only with the front and tailing portions of what is a very wide peak, leaving the central peak maximum essentially unaffected by light scattering. However the use of large sample injection volumes is not desirable in FI because of the adverse effect it has on sample throughput, which can be a key parameter for an automated, field-deployed monitor.

4.3.3 MULTI – WAVELENGTH SPECTROPHOTOMETRY

It has been reported that the magnitude of the Schlieren effect is independent of wavelength[259]. Therefore, real-time correction using the response at a non-absorbing wavelength can be applied for Schlieren effect compensation. Dual-wavelength spectrophotometry, currently exploited in liquid chromatography to suppress solvent peaks, can therefore be utilised to circumvent the Schlieren effect in FI[271]. A dual-wavelength beam passes through the flowing sample, the emergent light is dispersed and the resulting monochromatic beams are measured simultaneously by separate detectors. The difference in absorbance between the two constitutes the true absorbance of the sample. Therefore real-time subtraction of wavelength independent noise is also achieved. Dual wavelength spectrophotometry has been reported by several workers[259;269;272] as a powerful means of overcoming the Schlieren effect in FI.

Clearly this approach can be applied very effectively with array spectrophotometric detection. Simultaneously observing all wavelengths in the range 200 nm – 700 nm using the master channel of the Ocean Optics spectrometer enables dual wavelength ratioing and other multi-wavelength manipulations to be implemented.

Figure 4.5 shows a three-dimensional diode array spectrum of an injection of a 1mg l^{-1} NO_3-N standard versus time. Each spectrum consisted of 10 averaged spectra (1 per second). A qualitative analysis was performed in order to ascertain wavelengths either side of the Griess azo dye absorption spectrum that could be used as baseline reference wavelengths. It was found that wavelengths below 440 nm and above 625 nm were suitable to be used as baseline reference wavelengths to compensate for the Schlieren effect. Previous workers used wavelengths at 617 nm[259] and 630 nm[269] respectively. Although it was feasible to utilise wavelengths in this range, it was decided to use a baseline reference at 425 nm, to avoid problems that may be associated with the proximity of the end of the master channel wavelength range (200 nm – 700 nm), if wavelengths above 620 nm were used. As the sample zone approaches the flow cell there is a small drop in absorbance across the wavelength range as illustrated in Figure 4.5. Table 4.1 gives a comparison of absorbance values at the wavelengths of interest, $\lambda_{max.}$ (540 nm) and the non-absorbing baseline reference wavelength (425 nm). The decrease in absorbance corresponded to approximately - 0.02 A.U. for the 10 s time interval and increased to approximately - 0.03 A.U., 30 s after injection. Following the frontal edge of the sample zone, the overlap between the Schlieren and analytical signal occurred at approximately 50 – 60 s.

Normal Griess azo dye peak development occurred during the central part of the sample zone approximately 70 – 90 s after injection and this can be seen in Figure 4.5. At approximately 110 s after injection, the refractive effect of the tailing portion of the sample zone can be seen and the entire spectrum underwent a dramatic positive absorbance shift (Figure 4.5), reflected in the change in absorbance values given in Table 4.1. As the sample zone exited the flow cell the signal returned to the original baseline prior to the next injection.

Table 4.1 **Comparison of absorbance values at 425, 540 and (540 nm – 425 nm) for injection of a 1 mg l^{-1} NO_3-N standard into a 10 g l^{-1} NH_4Cl carrier stream.**

Time (s)	ABSORBANCE (A.U.)		
	@ 425 nm	@ 540 nm	@ 540 nm – 425 nm
10	-0.019	-0.017	0.002
20	-0.031	-0.026	0.005
30	-0.032	-0.026	0.006
40	-0.054	-0.014	0.040
50	-0.155	-0.035	0.120
60	-0.158	0.054	0.212
70	-0.051	0.271	0.322
80	-0.084	0.367	0.451
90	-0.135	0.384	0.519
100	-0.029	0.469	0.498
110	0.437	0.814	0.377
120	0.537	0.808	0.271
130	0.458	0.650	0.192
140	0.369	0.504	0.135
150	0.288	0.377	0.089

The response at the analytical wavelength (540 nm) exhibited Schlieren characteristics during the passage of a sample zone through the flow cell but the entire spectrum exhibited the same effects. Therefore a real-time baseline correction[259;269;272] can be performed to eliminate this problem by subtraction of the absorbance at a baseline reference point (425 nm) from the absorbance at the analytical wavelength (540 nm). Entering a mathematical calculation into the "history channel" function of the Ocean Optics software allowed this operation to be peformed easily and the result is shown in Figure 4.6 and Table 4.1.

The analytical wavelength (540 nm) shown by the red trace illustrates the negative drop in absorbance and enhanced positive signal characteristic of the Schlieren effect, as shown in Figure 4.3. The precision was variable but typically greater than 1 % R.S.D.(n = 3). Using dual wavelength correction (540 nm – 425 nm) compensation of the Schlieren effect can be performed (Figure 4.6 and Table 4.1) with an improvement in precision to 0.3 % R.S.D.(n = 3).

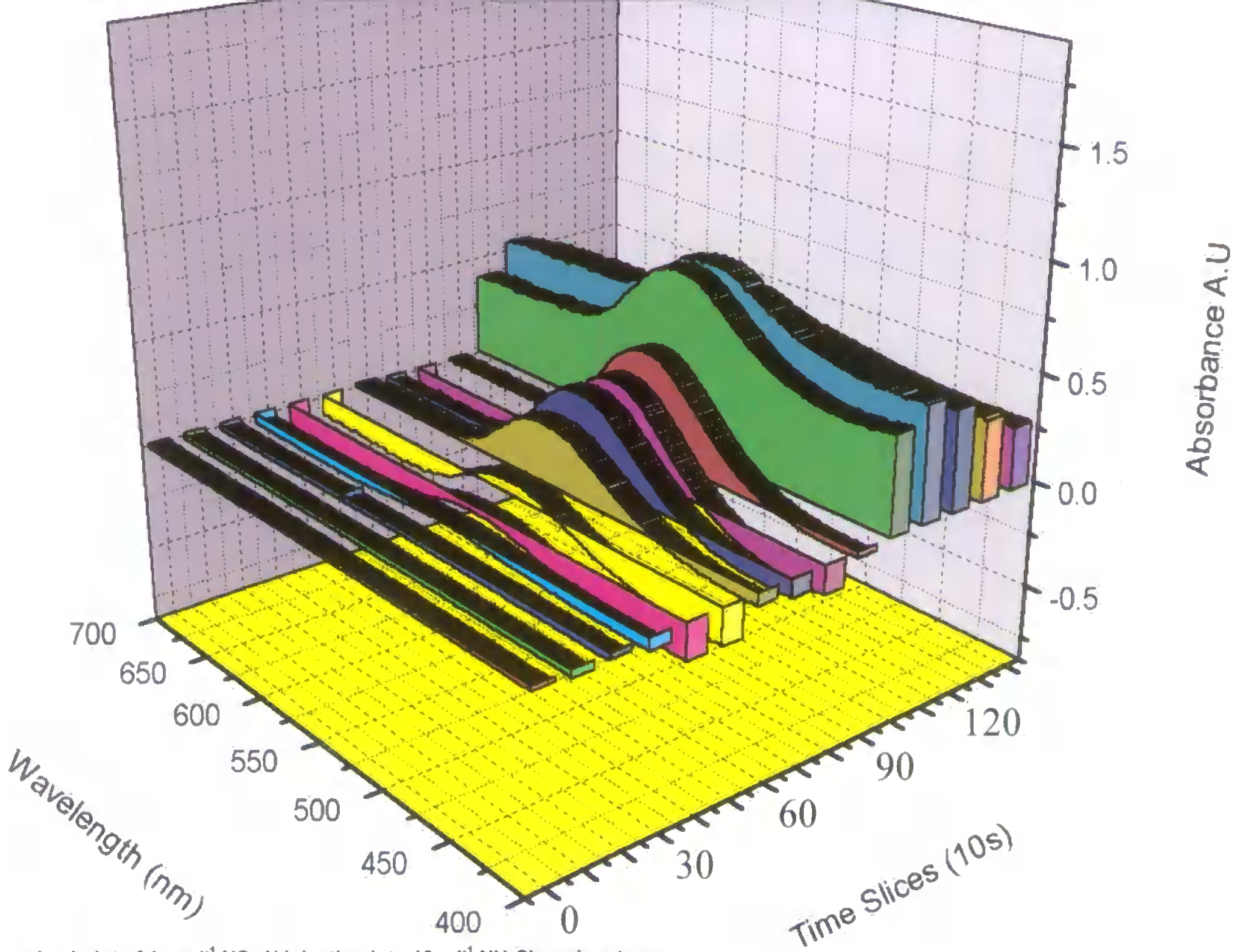

Figure 4.5 **Time resolved plot of 1 mg l^{-1} NO_3-N injection into 10 g l^{-1} NH_4Cl carrier stream.**

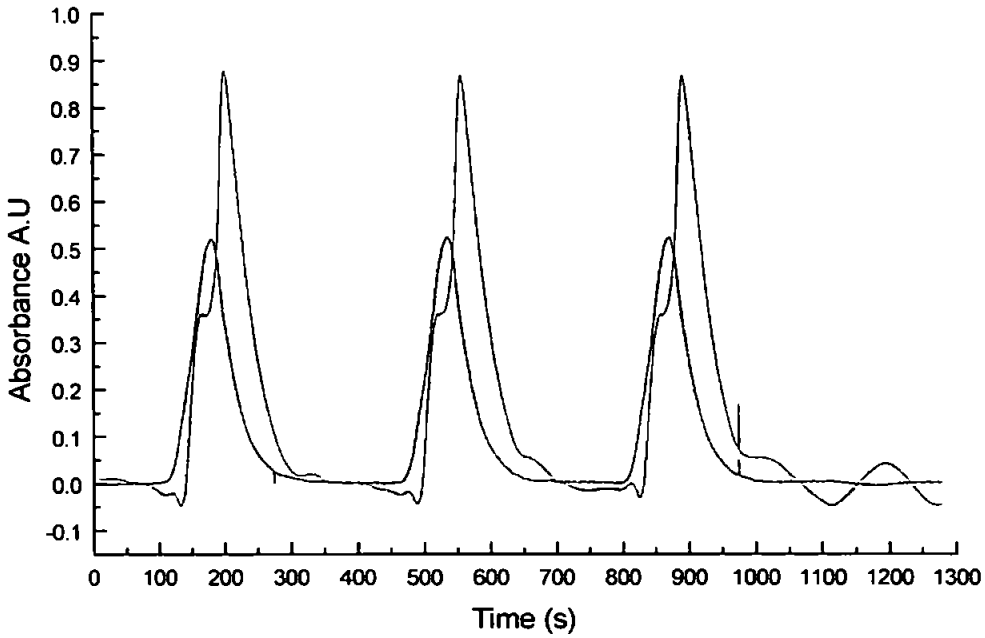

Figure 4.6 **Elimination of the Schlieren effect using dual wavelength correction, 1 mg l^{-1} NO_3-N (540 nm, red trace) (540 nm – 425 nm, black trace).**

4.3.4 MIXING CONDITIONS

The typical FI profile results from the action of frictional forces which give rise to both *axial* and *radial* dispersion. Axial dispersion is created by the interaction between horizontal concentration gradients at the leading and trailing edges of the sample zone and contributes significantly to the overall diffusion of the sample plug over time into the carrier stream, which in turn limits the sensitivity of the system. Radial dispersion promotes interaction between sample molecules at the centre of each imaginary cross-sectional portion of the sample zone and molecules at the tube walls. Concentration balancing occurs as molecules at the centre of the tube move towards the walls, while those molecules at the walls shift towards the centre of the tube. This process works against the convective forces at work in the stream, which in turn minimises sample dilution and increases sensitivity. Furthermore, radial diffusion results in the removal of sample molecules from the tube walls which ensures that contamination between successive samples is eliminated.

There are three effects which, separately or in combination, promote radial dispersion: *turbulent flow, molecular diffusion* and *secondary flow*. Turbulent flow involves totally random mixing of the streamlines in all directions, which results in rapidly averaged sample velocity profiles and minimal dispersion. Turbulent flow tends to exist only at high Reynolds number values, well outside the normal operating parameters of flow injection. In a standard FI system, radial dispersion is best

maximised through the combined effects of molecular diffusion and secondary flow processes. Helical alterations to the geometry of the flow path create a centrifugal force[182] upon the stream which gives rise to secondary flow circulation[273]. This has led to the use of such mixing devices as the coiled loop[273-275], 3-D knotted or knitted coils[183;184;276], and single-bead string reactors[277-279], all of which encourage geometrical disorientation of the stream and secondary flow, which in turn maximises radial dispersion.

The ideal FI mixing device would give perfect radial dispersion while not contributing to axial dispersion, producing enhanced sensitivity. With the extensive range of FI applications, different mixing devices have been developed to suit a variety of systems. The primary mixing devices used in FI, their mode of operation and degree of effectiveness are summarised below.

(a) COILED LOOPS

Coiled loop reactors are arguably the most widely used FI mixing device[273-275]. This can be attributed to their simple construction, negligible maintenance and effective control of radial dispersion. Considerable modelling of the forces at work in a coiled loop has been undertaken, and the existence of secondary flow forces[273] at work in coiled loop reactors has been proposed. The performance of a coiled loop is qualitatively defined by the relationship between the coil diameter and tube diameter, δ = coil diameter / tube diameter, where δ = dispersion function. It was reported that[280], for δ = 10, the dispersion caused by the coiled loop is one quarter that for an un-coiled loop; thus the smaller the coil diameter, the smaller the dispersion.

(b) KNOTTED AND KNITTED COILS

Knotted and knitted coils carry the principles of coiled loops to their logical conclusion: knots running the length of the tube act as dozens, if not hundreds, of micro-coils, each with a very small diameter. The effect of these micro-coils, each working to increase radial dispersion, produces a mixing device that is easy to construct (although reproducibility of construction is difficult) and yet provides excellent reductions in dispersional effects[183;184;276].

(c) SINGLE BEAD STRING REACTORS

Single bead string reactors (SBSR) are fabricated by packing small inert (normally glass) beads into standard PTFE tubing. The beads cause radical disruptions to the flowstream, but without the

hydrodynamic resistance characteristics of packed bed reactors, consequently bring about a dramatic reduction in the overall dispersion[277-279]. The importance of SBSRs is evident when one considers that the dispersion in the system is roughly 10 % of that of an equivalent system without the reactor, the sample throughput time is substantially reduced and parameters such as peak height or dispersion coefficients become nearly independent of flow rate with normal FI conditions. However the major disadvantages of SBSRs are the degree of difficulty involved in their construction and small air bubbles or particulates can be trapped within the SBSR, increasing carryover and flow resistance, a factor that has limited their acceptance within the flow injection community.

(d) MIXING CHAMBERS

Mixing or gradient chambers[182;280] have the common emphasis on complete sample-reagent mixing, usually at the expense of increased dispersion due to the increased mixer volume. Not only is a loss of sensitivity observed but also a reduction in the sample throughput, with the need for large sample and reagent volumes, thereby counteracting one of the primary advantages of FI. However, it should be noted that despite these disadvantages, mixing chambers are still widely used for concentration gradient work[281;282].

(e) TURBO MIXERS

The final mixer design worthy of note is the turbo (or Berger ball) mixer[283;284]. The turbo mixer has been shown to be a highly effective mixer in FI, giving 100 % mixing of sample and reagent a few microseconds after solutions merge, enhanced throughput (approx. +10 % compared with conventional mixers) and greater sensitivity over a wide detection range[285]. Its disadvantages lie in the difficulties and complexity of construction.

(f) COMPARISON OF MIXING CONDITIONS

Figure 4.7 shows four different FI manifold configurations that were used in an investigation into compensation of the Schlieren effect by various mixing configurations. Figure 4.7 (a) shows the initial manifold (Figure 4.1) described by McCormack et al.[258] and David et al.[147] in which the flow velocities of the NH_4Cl carrier and the mixed colour reagent were matched at 0.32 ml min^{-1}. Mixing of the two streams occurred through a "y-piece" and then a 100 cm 3D or knitted coil mixer. Figure 4.7 (b) shows the manifold in which the colour reagents N1NED and sulphanilamide are not

combined to one reagent but are merged together through a y-piece, prior to merging with the carrier as described above for Figure 4.7 (a).

To improve mixing conditions a glass bead mixing column (SBSR) (30 mm, 3 mm i.d., column filled with 1.5 to 2 mm o.d. glass balls) was introduced before the reduction column. Figures 4.7 (c & d) used this mixing column and additional 100 cm knitted mixing coils introduced to the manifolds. The FI trace shown in Figure 4.7 is a typical response for manifolds (c) and (d). A reduction in baseline noise and improvement to FI peak shape was observed when compared with manifolds (a) and (b). This demonstrates that reduction of Schlieren effects can be achieved by improving mixing conditions. However the analytical wavelength (540 nm) trace (shown in red) still exhibited clear double peak formation, an indication of both poor mixing and the Schlieren effect. In addition the increased complexity of the manifold design using various mixers lead to an increase in axial dispersion and consequently to a further decrease in sensitivity and an increase in the analysis time, both undesirable factors in FI. Using dual wavelength compensation (540 nm – 425 nm) (shown in black) as discussed in section 4.3.3, the problems caused by the Schlieren effect can be alleviated. Therefore, in conclusion, manifold design has been found to be less important in Schlieren effect compensation and dual / multi wavelength techniques facilitated by the PSD-1000 spectrometer provide the best and most convenient approach to Schlieren effect compensation.

4.3.5 INDEX MATCHING

Another recommended way to reduce the Schlieren effect is to match the refractive indices[178, 182, 261, 268] of the sample and the carrier solutions into which the sample is injected, (see section 4.3.2). However index matching of the nitrate manifold (Figure 4.1) does present two clear problems. If the sample stream is indexed matched to that of the carrier stream (10 g l^{-1} NH_4Cl), each sample would need to be individually matched.This would be time consuming and clearly impractical for field deployment. The alternative option is use an inert carrier solution e.g. Milli-Q water as opposed to the 10 g l^{-1} NH_4Cl stream, which effectively index matches both the sample and carrier streams. Although this is the simplest and most convenient way to eliminate the Schlieren effect, NH_4Cl is required in the carrier stream to act as complexant and buffer for the cadmium reduction column[135] as shown by the equations below.

$$2\,NH_4^+ \longrightarrow 2\,NH_3 + 2\,H^+$$

$$Cd^{2+} + 2\,NH_3 \longrightarrow [Cd(NH_3)_2]^{2+}$$

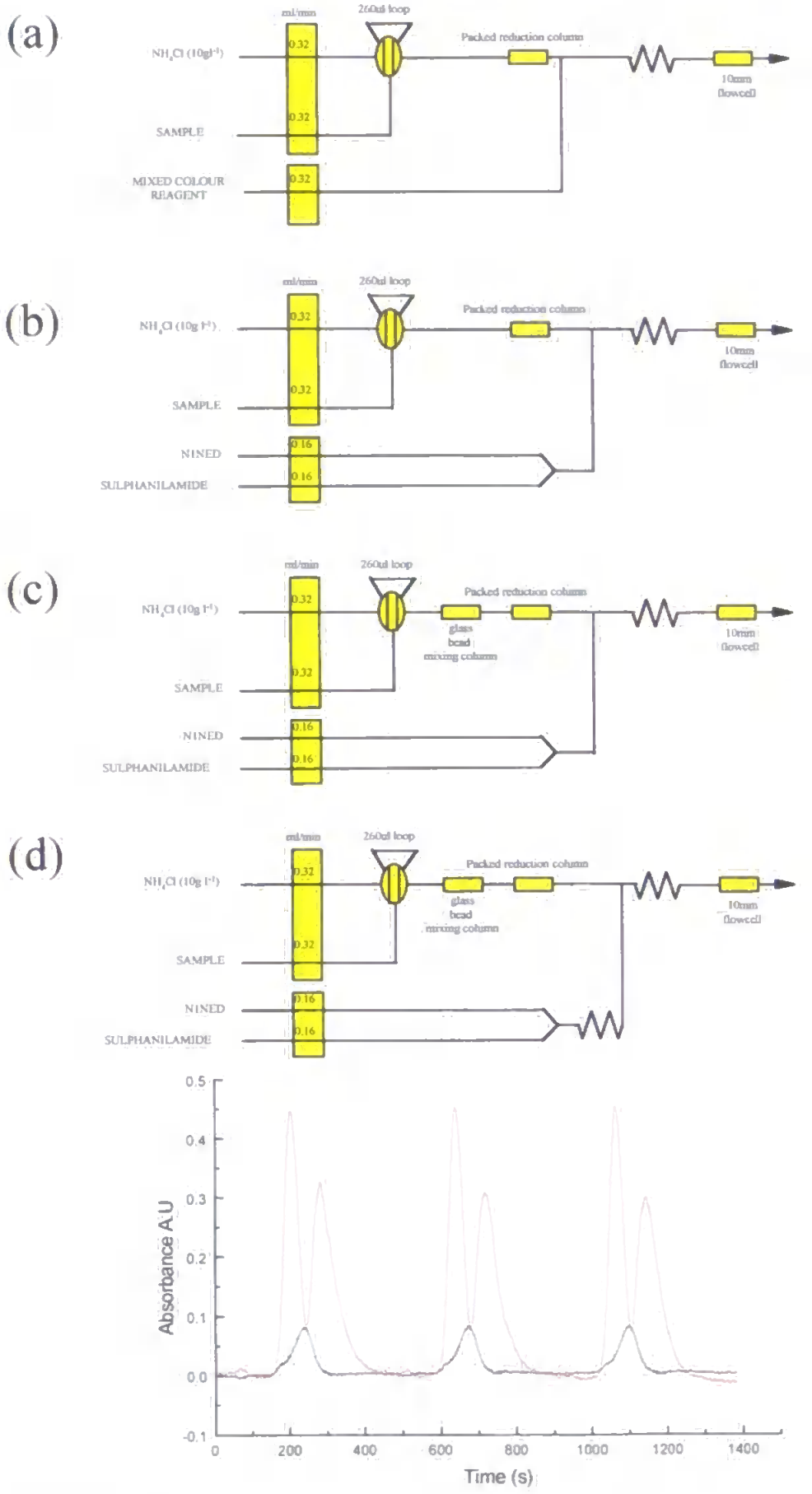

Figure 4.7 (a-d) **Investigation into mixing conditions using different manifold configurations, 0.5 mg l^{-1} NO_3-N standard injected into 10 g l^{-1} NH_4Cl, monitored at 540 nm (red) and (540 nm – 425 nm) (black).**

Therefore a compromise must be reached between providing sufficient buffering protection for the cadmium reduction column and reduction of the Schlieren effect. Strictly speaking, reducing the NH_4Cl concentration cannot be termed index matching, however Figures 4.8 and 4.9 show the effect of reducing the carrier concentration from 10 g l^{-1} to 5 g l^{-1} NH_4Cl.

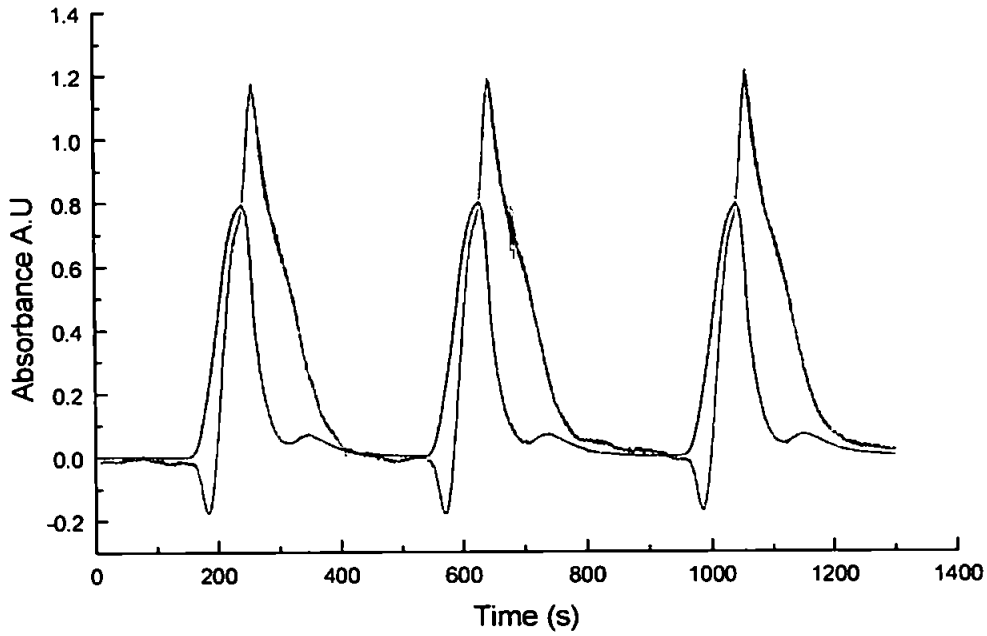

Figure 4.8 **Replicate injections of 1 mg l^{-1} NO_3-N using a 10 g l^{-1} NH_4Cl carrier $\lambda_{max.}$ (shown in red), baseline corrected (shown in black).**

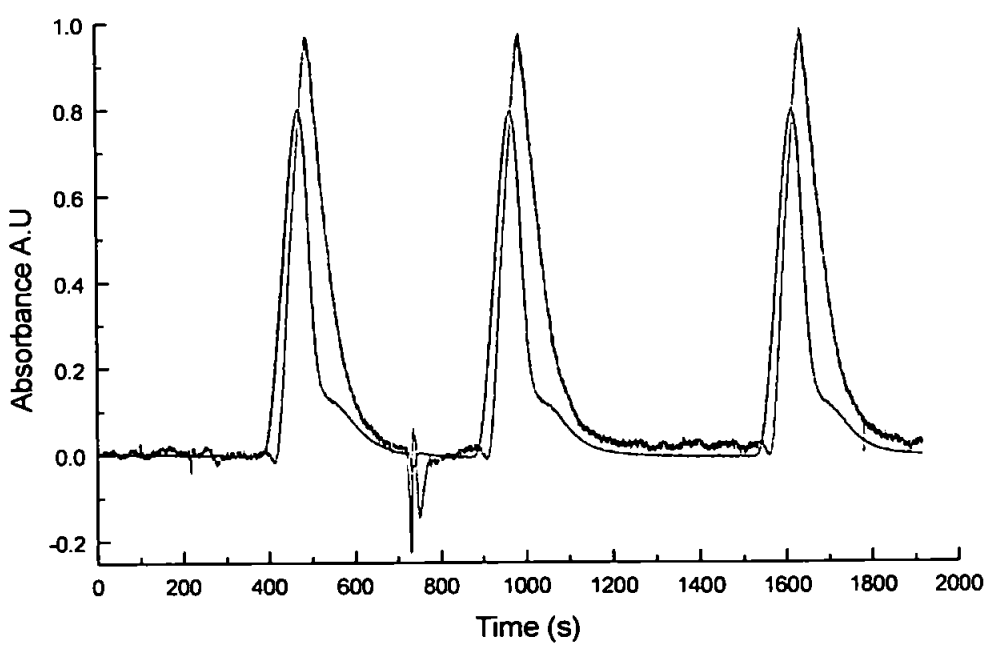

Figure 4.9 **Replicate injections of 1 mg l^{-1} using a 5 g l^{-1} NH_4Cl carrier $\lambda_{max.}$ (shown in red), baseline corrected (shown in black).**

Associated with the reduction in ammonium chloride concentration was a clear reduction in refractive index effects and an increase in the baseline stability. Table 4.2 compares the effect of reducing the ammonium chloride concentration.

Table 4.2 Comparison of effect of ammonium chloride carrier concentration.

	540 nm			540 nm - 425 nm		
	Concentration NH_4Cl (g l^{-1})					
	0	5	10	0	5	10
Mean	0.657	0.978	1.188	0.633	0.798	0.793
s.d.	0.055	0.005	0.007	0.063	0.001	0.003
R.S.D %	8.3	0.5	0.6	9.9	0.1	0.3

The use of a Milli-Q carrier (0 g l^{-1} NH_4Cl) resulted in a decrease in sensitivity due to degradation of the cadmium reduction column and unsatisfactory reproducibility (approximately 10 % R.S.D. n = 3). This degradation can be visibly observed over a relatively short time frame (minutes), with the appearance of void spaces as the packed density of the column is reduced and air bubbles start to form in the carrier stream. Reduction of the ammonium chloride concentration from 10 g l^{-1} to 5 g l^{-1} had almost a negligible effect on sensitivity and reproducibility but an increase in baseline stability with clear reduction in refractive index effects was seen. Therefore a concentration of 5 g l^{-1} ammonium chloride carrier stream was selected for all subsequent experiments.

4.3.6 REED MIXER

A reputedly highly efficient mixer has been developed by Ionode Pty. Ltd. (Tennyson, Qld, Australia), as a component of their Discontinuous Flow Analysis (DFA) instrumentation. DFA was first reported by Arnold et al.[286] in 1989 and was the subject of a provisional patent in 1985 in Australia by its inventors Petty et al.[287]. Subsequently a full United States patent was granted in 1992[288]. To date DFA has mostly been applied to titration measurements with various means of detection such as spectrophotmetry[289], potentiometry[290] and conductimetry[286]. In all of these systems efficient mixing of sample with reagents is paramount and, for this purpose, the reed mixer was developed. The reed mixer has been demonstrated to be a very efficient radial mixer without appreciable axial dispersion and has been investigated and compared with conventional mixers[291].

The principle of the reed mixer is relatively straightforward; the flow channel is situated between two electromagnets that are coupled to an oscillator. The electromagnets are alternately pulsed by the oscillator, with the frequency of the oscillation being determined by the operator. As shown in Figure 4.10, a length of ferrous material (the reed) is placed in the flow stream between the two electromagnets (Figure 4.10 A). When the oscillator is activated, the reed is correspondingly oscillated through the flow stream between one pole and the other (Figure 4.10 B and C).

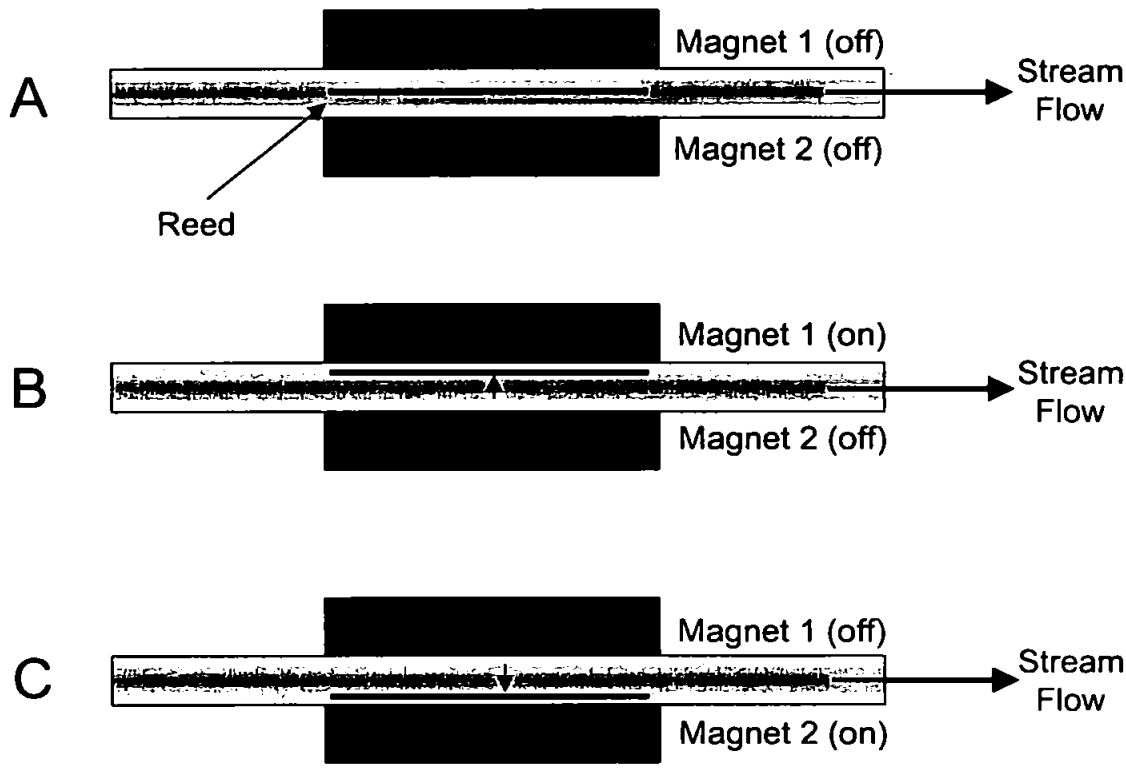

Figure 4.10 Schematic diagram of reed mixer operation.

The two most easily configured mixing parameters of the reed mixer are the oscillation frequency and the volume swept by the reed, which is controlled by the length of the reed. The mixer oscillator circuit supplied by Ionode allows the operator to select either a variable oscillation frequency, adjusted by a potentiometer between approximately 2 and 150 Hz, or a fixed frequency of approximately 70 Hz. A representation of the reed mixer is given in Figure 4.11 (b). Figures 4.12 and 4.13 show injections of 1 mgl^{-1} NO_3-N using the manifold configuration given in Figure 4.11 with different reed mixer oscillation frequencies of 0 and 150 Hz respectively. Absorbance data are given in Table 4.3.

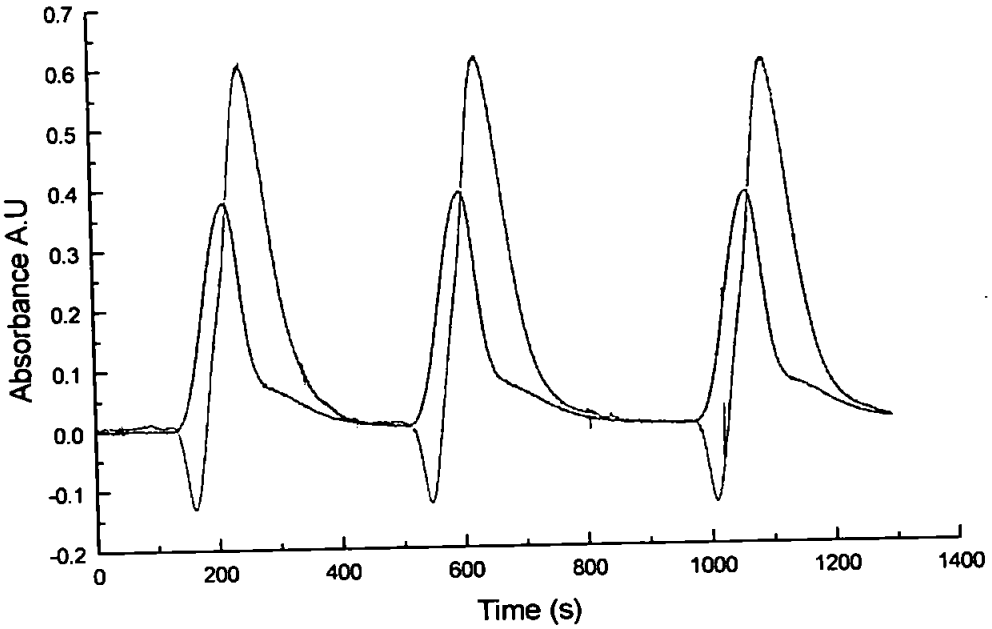

Figure 4.12 **Injection of 1 mg l^{-1} NO_3-N into 5 g l^{-1} NH_4Cl carrier with in-line reed mixer (zero oscillation), λ_{max} (red trace), baseline corrected (black trace).**

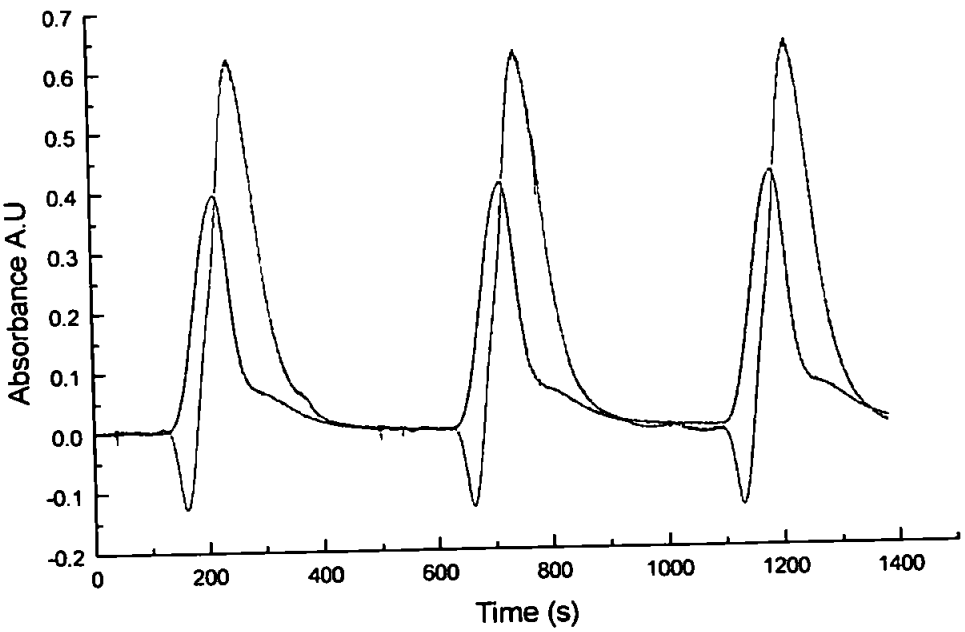

Figure 4.13 **Effect of reed mixer oscillation at 150 Hz on injection of 1 mg l^{-1} NO_3-N into 5 g l^{-1} NH_4Cl, λ_{max} (red trace), baseline corrected (black trace).**

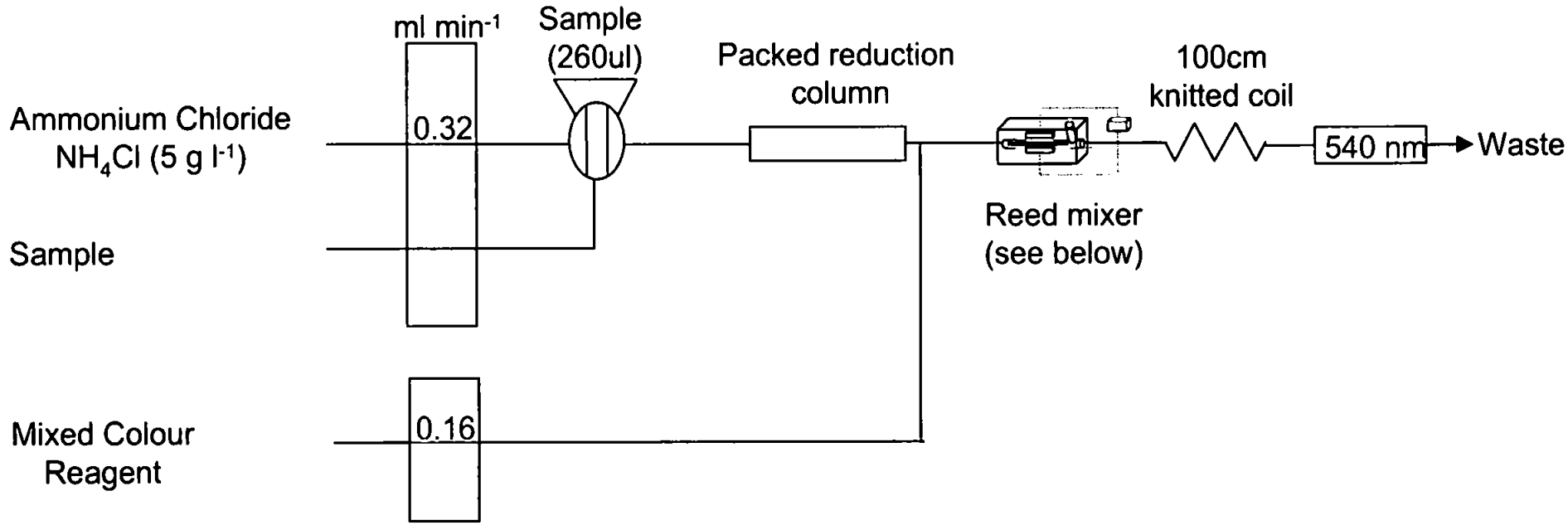

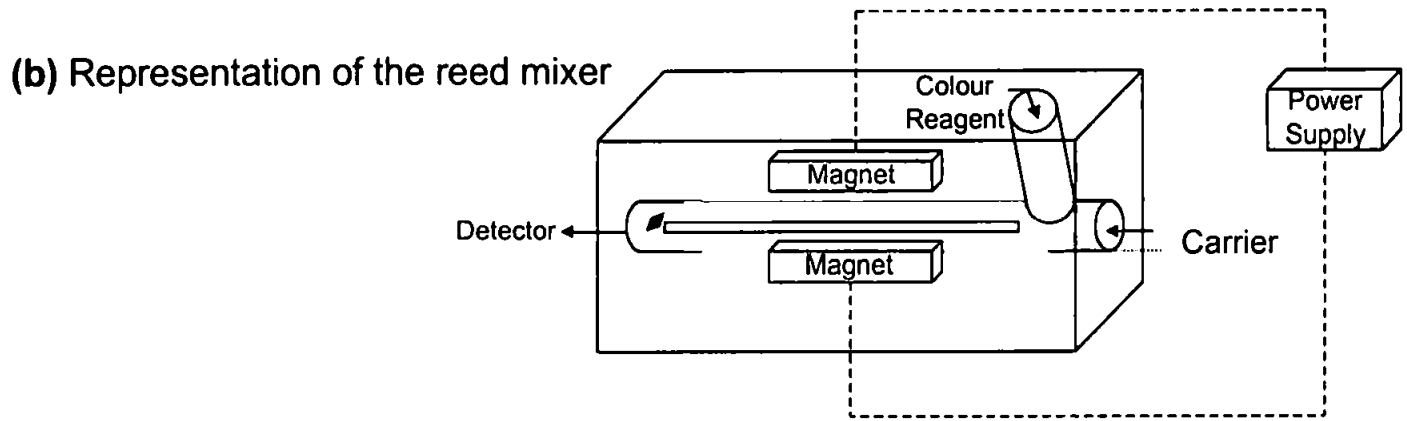

Figure 4.11 **Nitrate flow injection manifold (incorporating reed mixer).**

Table 4.3 Comparison of different reed mixer oscillation frequencies.

	540 nm			540 nm - 425 nm		
	Reed mixer speed (Hz)					
	0	75	150	0	75	150
Mean	0.610	0.690	0.628	0.382	0.454	0.408
s.d.	0.004	0.002	0.009	0.007	0.012	0.015
R.S.D %	0.7	0.3	1.4	1.7	2.6	3.7

The reed mixer had very little effect on the Schlieren effect using this manifold. Absorbance maximum data were unaffected by a maximum oscillation frequency 150 Hz (Figure 4.13) compared with 0 Hz (Figure 4.12). Both sets of data (Figures 4.12 and 4.13) show the Schlieren effect masking the analyte peak. Reproducibility also suffers when using the reed mixer, R.S.D.s for $\lambda_{max.}$ and baseline corrected data increased with reed mixer oscillation frequency. As previously discussed, dual-wavelength correction eliminated the Schlieren effect (Figures 4.12 and 4.13) and clearly is the most attractive option for a field based FI monitor. Whilst the reed mixer has been shown to offer advantages in some FI applications in terms of mixing[291] it was not applicable to this manifold and the intended field deployed system.

4.3.7 FLOW RATE OPTIMISATION

Univariate optimisations of both the carrier and mixed colour reagent flow rates were the final parameters investigated with respect to the nitrate manifold. Figure 4.14 shows the optimisation of the carrier flow rate in the range 0.31 – 0.88 ml min^{-1} and colour reagent flow rate from 0.08 – 0.88 ml min^{-1}. As flow rates increased the observed absorbance signal consequently decreased. Two factors explain this effect; as flow rate increases the contact time of a sample with the reduction column also decreases, therefore the nitrate within a given sample is less efficiently reduced to nitrite than at a lower flow rate and hence the signal decreases. In addition this nitrite then has less time to react with the sulphanilamide to form the diazonium ion which reacts with the N1NED to give the resultant pink azo dye, consequently the absorbance signal decreases. This would suggest the use of very low flow rates for the determination of nitrate / nitrite, however a compromise must be made between sensitivity and sample throughput, important parameters for an automated field deployed system. In addition baseline stability was also taken into consideration, therefore carrier and colour reagent flow rates of 0.43 and 0.31 ml min^{-1} respectively were used for all further work.

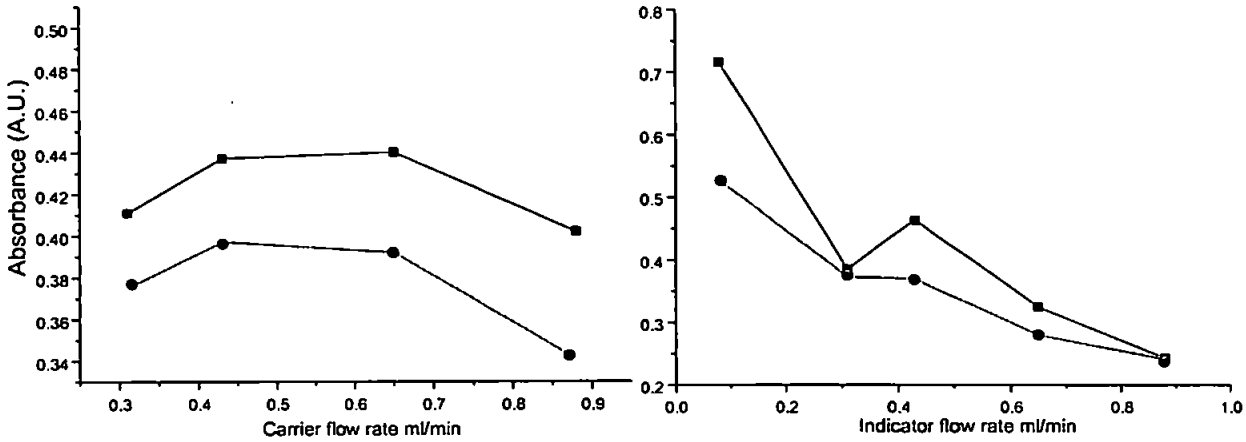

Figure 4.14 Carrier and indicator flow rate optimisations, ■ = 540 nm, ● = 540 – 425 nm.

4.3.8 DETERMINATION OF NITRATE USING THE MASTER CHANNEL

There are several contributory factors that affect the efficiency of the cadmium reduction column over time and these have been studied in detail by Nydahl[135]. Among other parameters it was noted that if the reductor column is fabricated using cadmium of different particle sizes (as is usually the case; a particle size range is given by manufacturers), then the smaller particles which are packed between the larger particles are used up first. This consequently reduces the available surface area of the column leading to a gradual decrease in column efficiency. However, the most dominant cause in the reduction of column efficiency is probably precipitation of hydroxides and other interfering substances onto the surface of the cadmium particles. As discussed previously (section 4.3.5) ammonium chloride is added to buffer the pH of the reaction and prevent the degradation of the cadmium column by binding the cadmium as a diammine complex.

$$NO_3^- + Cd + H_2O \longrightarrow NO_2^- + Cd^{2+} + 2\,OH^-$$

$$2\,NH_4^+ \rightleftharpoons 2\,NH_3 + 2\,H^+$$

$$Cd^{2+} + 2\,NH_3 \longrightarrow [Cd(NH_3)_2]^{2+}$$

In addition to the formation of cadmium ions resulting from the reduction of nitrate to nitrite, dissolved oxygen within a solution is also very rapidly and quantitatively reduced according to;

$$2\,Cd + O_2 + 4\,H^+ \longrightarrow 2\,Cd^{2+} + 2\,H_2O$$

Therefore without sufficient complexing agent the cadmium column can degrade rapidly. In the laboratory cadmium columns typically had an operating lifetime of 2 – 4 months, depending on the frequency of use. For field deployment however it is important to use a fresh column (and take a replacement column) because the natural water matrix (i.e. physical and chemical interferences) may reduce column lifetime, e.g. if the sample is unfiltered or saline. Therefore in the field it is recommended to replace the column every 28 days to ensure optimum performance.

Using the optimised manifold design shown in Figure 4.15 and data processing described above, the system was fitted with a new cadmium column and final analytical figures of merit obtained. Figure 4.16 shows the baseline corrected (540 – 425 nm) calibration data and Figure 4.17 gives the calibration graph for the data. Error bars are represented as three times the standard deviation of that standard. The performance of the manifold was linear up to 2.0 mg l^{-1} NO_3-N (r^2 = 0.9984, n= 9) however absorbance values for this standard exceeded the 1.5 A.U. limit recommended in section 2.3.4. Good linearity was obtained for the calibration standards 0 – 1 mg l^{-1} NO_3-N (r^2 = 0.9995, n = 8) and achieved a detection limit of 6 µg l^{-1} NO_3-N (calculated from the mean of the blank signal plus three times the standard deviation of the blank). Reproducibility was also good with R.S.D.s typically less than 2 % (n = 3).

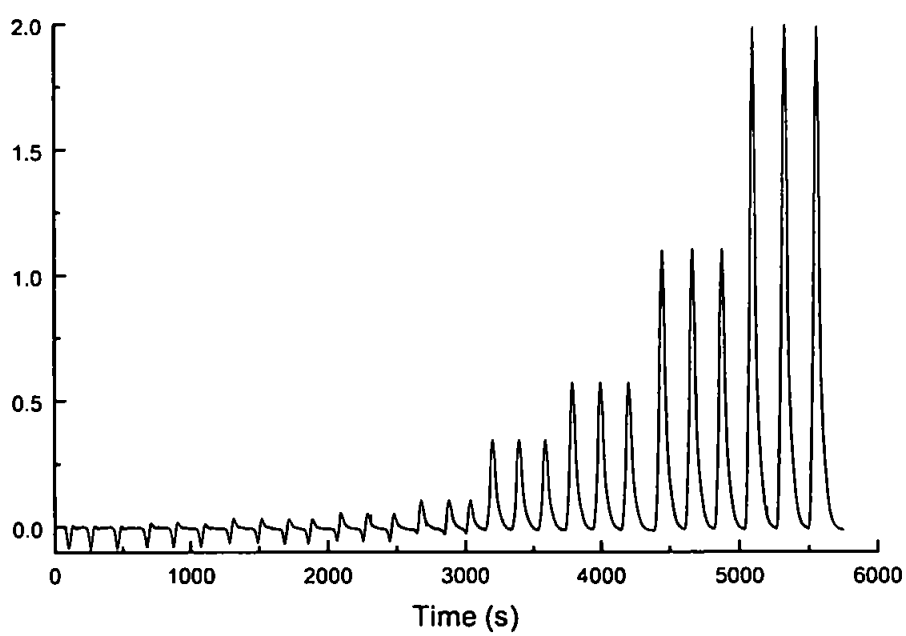

Figure 4.16 **Calibration data obtained using optimised manifold (Figure 4.15) for 0.01, 0.03, 0.05, 0.1, 0.5, 1.0 and 2.0 mg l^{-1} NO_3-N standards, monitored at 540 – 425 nm.**

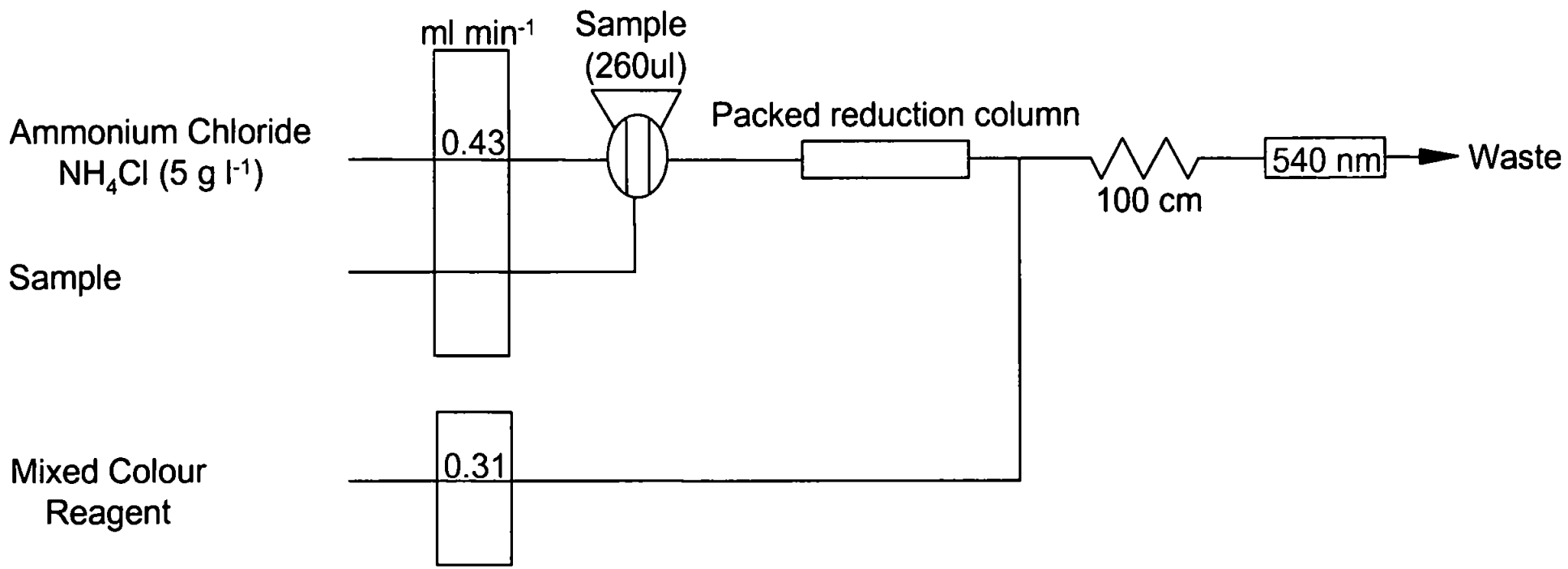

Figure 4.15 **Final nitrate manifold configuration.**

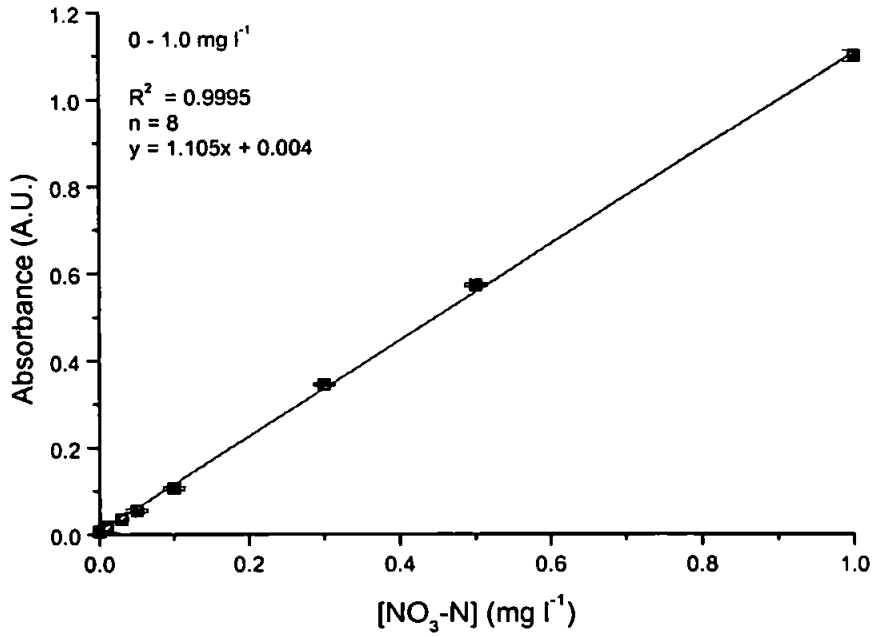

Figure 4.17 Calibration graph for 0 – 1 mg l^{-1} NO_3-N for optimised manifold (Figure 4.15).

4.3.9 DETERMINATION OF NITRITE USING THE SLAVE CHANNEL

With the full spectrum acquisition advantage of the Ocean Optics PSD – 1000 spectrometer the possibility of a multi-analyte FI system arises. This could be used in single channel mode with spectral deconvolution to determination e.g. TON and ammonia simultaneously. However problems may arise due to e.g. interactions between the different reagents or large differences in concentrations of the two analytes. An alternative approach with the Ocean Optics PSD – 1000 is to utilise its dual channel capability, e.g. to use the Master channel to determine TON (as in section 4.3.8) and the slave channel to determine nitrite. This section shows the feasibility of this approach. The slave channel (section 2.2.2) can be used over the spectral range 500 nm – 1000 nm. The baseline reference wavelength of 425 nm used in the determination of nitrate was not visible within the spectral range of the slave channel (500 nm – 1000 nm). Therefore an alternative baseline reference was taken at 650 nm, and subsequently used to correct the analytical wavelength as described previously in section 4.3.3.

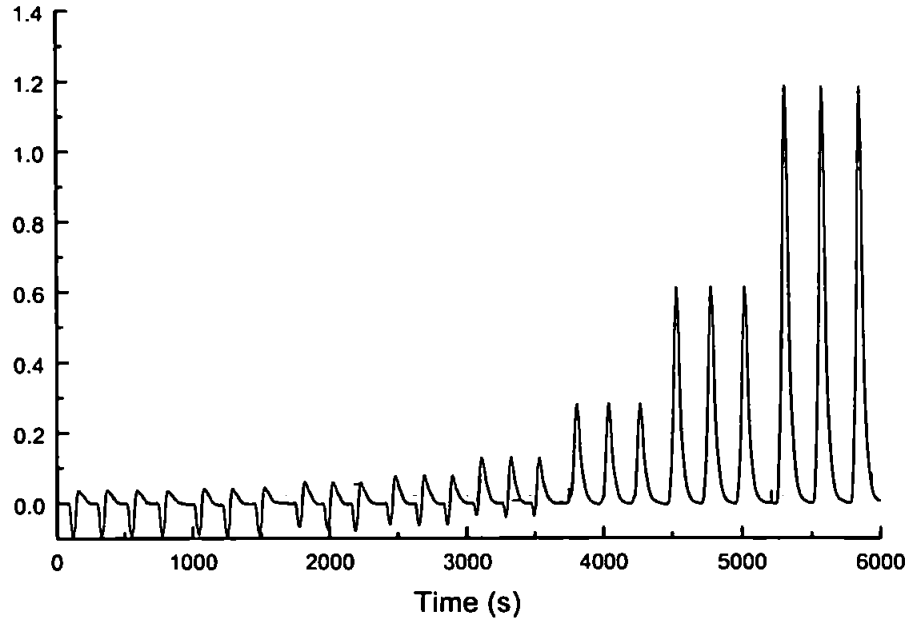

Figure 4.18 **Calibration data obtained using optimised manifold (Figure 4.15) for 0.01, 0.03, 0.05, 0.1, 0.3, 0.5 and 1.0 mg l^{-1} NO_2-N standards, monitored at 540 – 650 nm.**

Figure 4.18 shows a NO_2-N calibration performed using the slave channel for the concentration range 0 – 1 mg l^{-1} NO_2-N. Manifold parameters were identical to those shown in Figure 4.15, with the exception of manual three-way key valves which enabled by-passing of the cadmium reduction column.

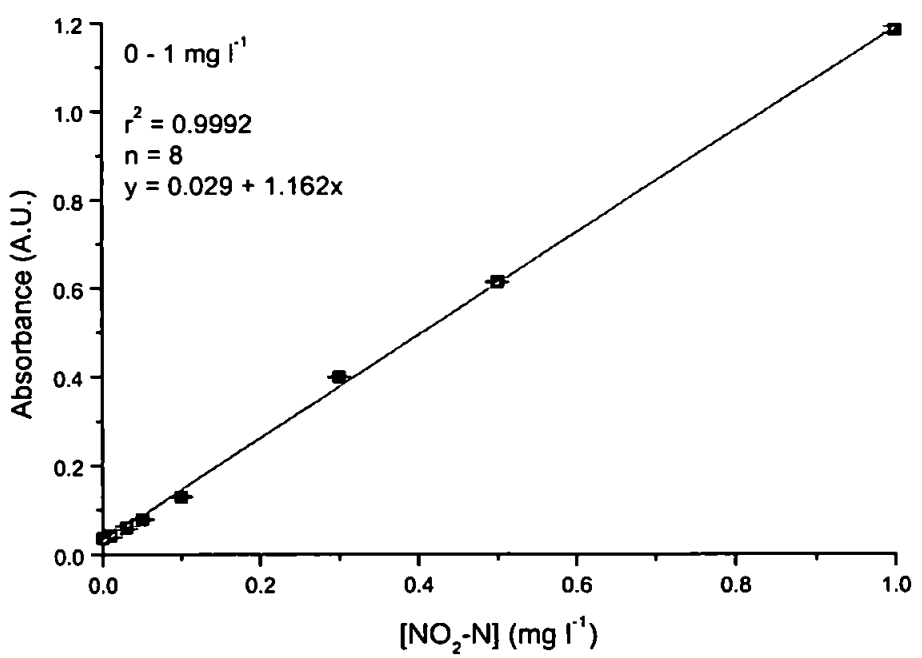

Figure 4.19 **Calibration graph for 0 – 1 mg l^{-1} NO_2-N for optimised manifold (Figure 4.15).**

The analytical performance of the manifold was linear for the concentration range used 0 – 1 mg l^{-1} NO_2-N (r^2 = 0.9992, n = 8) and achieved a limit of detection of 8 μg l^{-1} NO_2-N. Reproducibility was also good with R.S.D.s typically less than 1.5 % (n = 3).

4.4 CONCLUSIONS

The following specific conclusions can be drawn from the research reported in this chapter:

1. The refractive index (Schlieren) problems associated with mixing zones of significantly different ionic strengths, e.g. a 10 g l^{-1} ammonium chloride stream and a natural (freshwater) sample, are more severe when using the Ocean Optics PSD – 1000 spectrometer and associated fibre optics than with a conventional single beam spectrophotometer with conventional optics.

2. The spectral acquisition capability of the Ocean Optics PSD – 1000 spectrometer can be used for dual wavelength measurements to automatically compensate for refractive index changes in the reagent / sample stream. For the determination of nitrate the recommended wavelengths are 540 nm for the analytical signal (λ_{max}) and 425 nm for the reference (background) signal.

3. Physical methods of improved sample mixing, i.e., a packed mixing column, a knitted coil mixer and a reed mixer were not as effective as the dual wavelength method in compensating for the refractive index changes associated with the Ocean Optics PSD – 1000 spectrometer and its associated optical fibres.

4. An ammonium chloride concentration of 5 g l^{-1} provides the best compromise between long cadmium column lifetime and reduced refractive index problems.

5. Using the Master channel (540 nm – 425 nm) nitrate (strictly TON) could be determined with a detection limit (3σ) of 6 μg l^{-1}, a linear range of 0 – 1 mg l^{-1} (r^2 = 0.9995, n = 9) and a R.S.D. of < 2 % (n = 3) over the entire range.

6. Using the Slave channel (540 nm – 650 nm) nitrite could be determined with a detection limit (3σ) of 8 μg l^{-1}, a linear range of 0 – 1 mg l^{-1} NO_2-N (r^2 = 0.9992, n = 8).

Chapter Five

Design and Field Deployment of a Portable Flow Injection Based Nitrate Monitor

"The great thing in this world is not so much where we are,

but in what direction we are moving"

- Oliver Wendell Holmes -

5.1 INTRODUCTION

This chapter describes the miniaturisation and automation of the nitrate manifold described in Chapter Four using micro-solenoid pumps and micro-electronic switching valves. Control of all FI manifold parameters and spectrometer data acquisition were simultaneously achieved using an in-house designed graphical user interface programmed in National Instruments LabView™. Control over spectral acquisition enabled the adaptation of the system to perform nitrate determination at low (0 – 1 mg l^{-1} NO_3-N) and high (0 – 9 mg l^{-1} NO_3-N) concentration ranges. Field deployment and evaluation of the monitor was conducted during a six-week expedition to Lesotho, South Africa and a 48 h sampling campaign on the River Frome at the Institute of Freshwater Ecology, Dorset, U.K.

5.2 EXPERIMENTAL

5.2.1 REAGENTS & STANDARDS

All nitrate manifold reagents, ammonium chloride, N1NED and sulphanilamide were prepared as described in section 4.2.1. All working standards were prepared from a 100 mg l^{-1} stock nitrate (NO_3-N) solution (section 4.2.1) in clean glass volumetric flasks. All glassware and HDPE storage containers were soaked in Nutricon detergent (nutrient free) (Merck Ltd.) for 24 h before rinsing with Milli-Q and were then transferred to a 10 % HCl acid bath for a further 24 h, prior to a final Milli-Q rinse, repeated three times. Reagents and standards for the Lesotho field trial were prepared prior to the expedition as above and then transferred to clean collapsible medical plasma bags which were stored in the dark until required.

5.2.2 INSTRUMENTATION

(a) MANIFOLD DESIGN & CONSTRUCTION

The FI manifold used was as described in Chapter 4 (Figure 4.15), this was incorporated within the automated monitor as shown in Figure 5.1. Peristaltic pumps were replaced by three solenoid operated self priming micro pumps (BIO-CHEM VALVE ™ series 120SP12 – 25, (PD Marketing, Chichester, U.K.), for the sample, carrier and reagent streams. All electronic switching valves were solenoid operated Teflon® isolation valves (BIO-CHEM VALVE ™ series, 075T12-32, (PD Marketing)

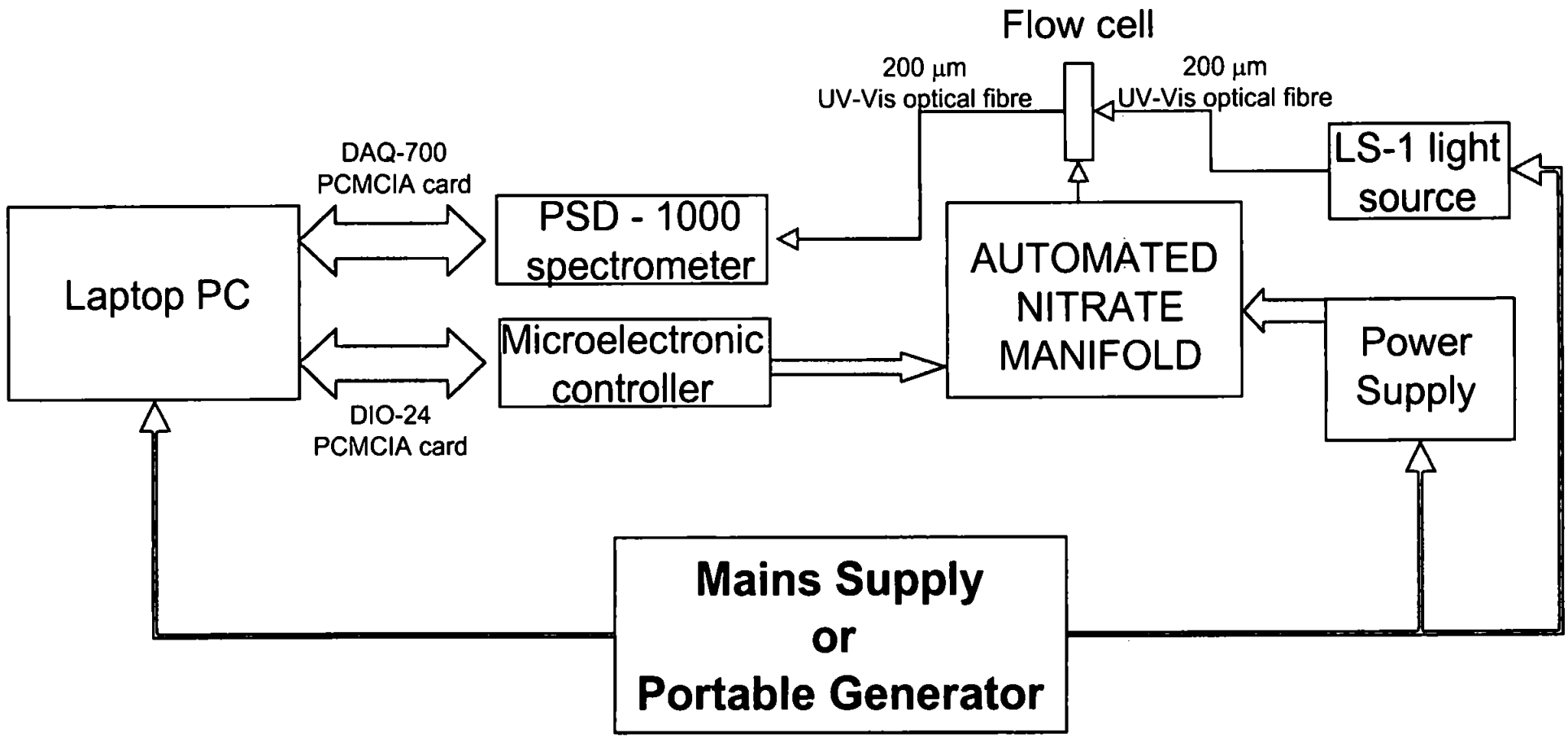

Figure 5.1 **Block diagram of instrumentation used for automated nitrate monitor.**

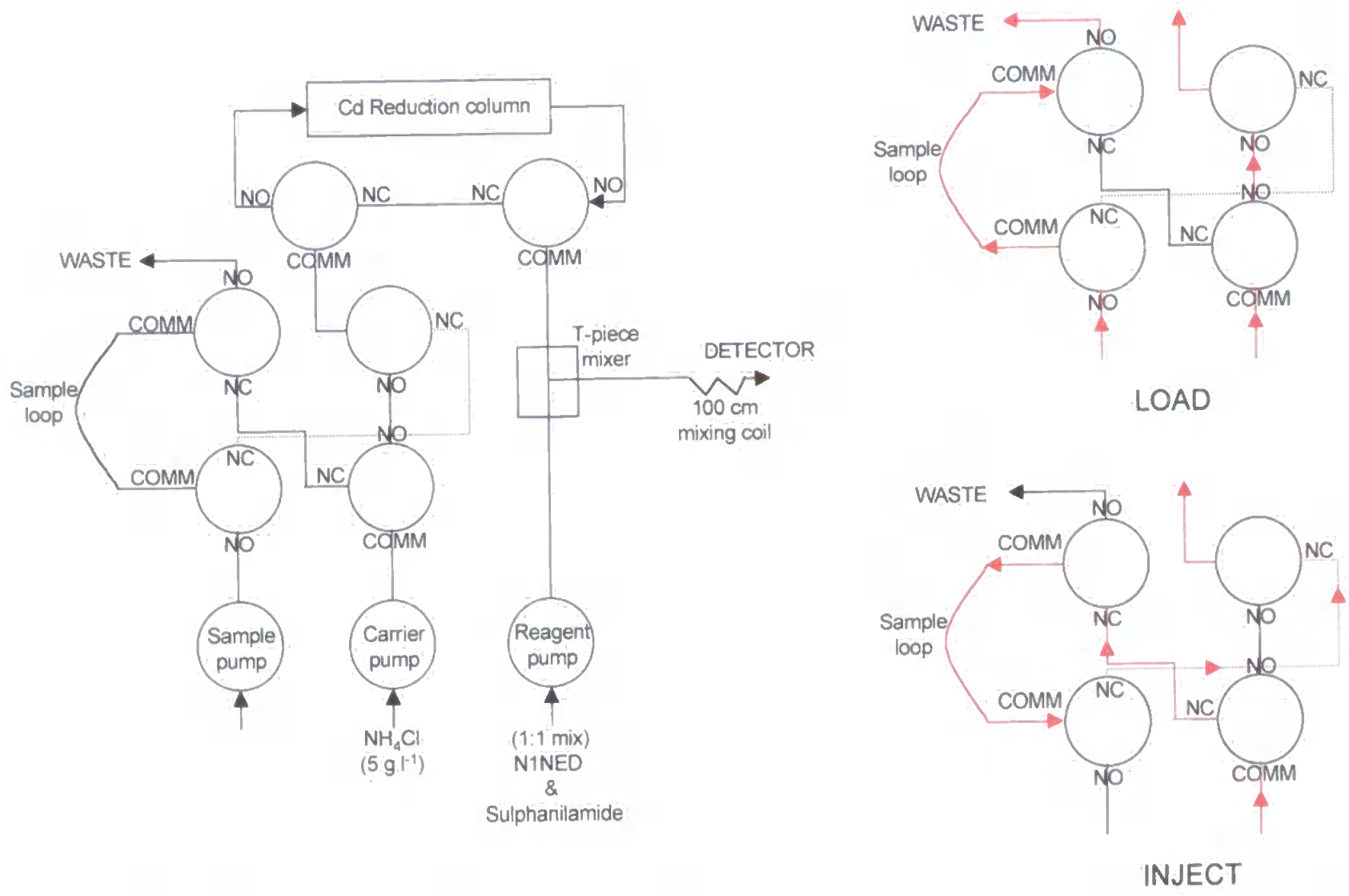

Figure 5.2 **Layout of Automated nitrate manifold : LOAD and INJECT configurations shown, red line indicates active flow channel with flow direction shown by red arrows.**

Switching valves were default set to normally open – common (NO / COMM) when de-energised and when power was supplied the valves switched to the normally closed – common (NC / COMM) position. Figure 5.2 shows the layout of the automated nitrate manifold, expanded views illustrate the switching configurations for load and inject positions of the sample injection system. All micro-pumps and switches were operated by 12 V DC supplied from a portable power supply (Altai regulated DC power supply (13.8 V, 3 – 5 A), Ruthern Instruments Ltd., Bodmin, U.K.). The automated manifold was mounted on an aluminium sub-chassis and housed in a shock resistant polystyrene (IP 65 rated) hinged lid enclosure (l x w x h, 210 mm x 185 mm x 100mm) (R.S. Components, Corby, Northants, U.K.). Microelectronic design and construction was conducted in consultation with Mr John Wood (Ruthern Instruments Ltd., Bodmin, U.K.) and housed in a shock resistant polystyrene PCB mounting enclosure (200 mm x 110 mm x 50 mm). Communication between the microelectronic controller and the automated manifold used a multipole circular connector and chassis mounted plug (IP 67 rated, Binder 723 series, R.S. Components, U.K.). Power supply was achieved using either domestic mains supply or a portable generator (Honda EX500B, Mike Phillips Honda Centre, Truro, Cornwall, U.K.), for which the technical specifications are given in Table 5.1.

Table 5.1 Technical specifications of Honda EX500B portable generator.

PARAMETER	PERFORMANCE
Rated AC output	200 - 450 W
Max. output	500 W
AC frequency	50 Hz
Engine type	2 stroke air cooled
Fuel tank capacity	0.8 litre
Continuous operating hours	2.5 @ 200 W
Without re-fueling	1.5 @ 500 W
Certified sound level (7 meters)	50dB(A) @ 200 W
	58dB(A) @ 500 W
Dimensions (l x w x h)	365mm x 195mm x 305mm
Dry Weight	8.8 kg

Full technical specifications of the spectrometer, data acquisition, optical fibre and flow cell parameters were as described in section 2.2.2. Data communication to and from the microelectronic controller was performed using a type II PCMCIA DAQ-DIO-24 card (National Instruments Corp., Newbury, Berks, U.K). The controlling notebook PC was a Toshiba Satellite 4030CDS (Pentium 300 MHz, 64 MB RAM) (Toshiba Information Systems Ltd, Weybridge, Surrey, U.K).

All automation of manifold parameters and data acquisition were performed by a program written in LabView™ version 5.0 (National Instruments Corp.) in conjunction with Mr John Wood (Ruthern Instruments Ltd.). Figure 5.3 shows a block diagram of the designed automated injection sequence and how it related to the switching of the micro-pumps and electronic switches of the FI manifold (Figure 5.2).

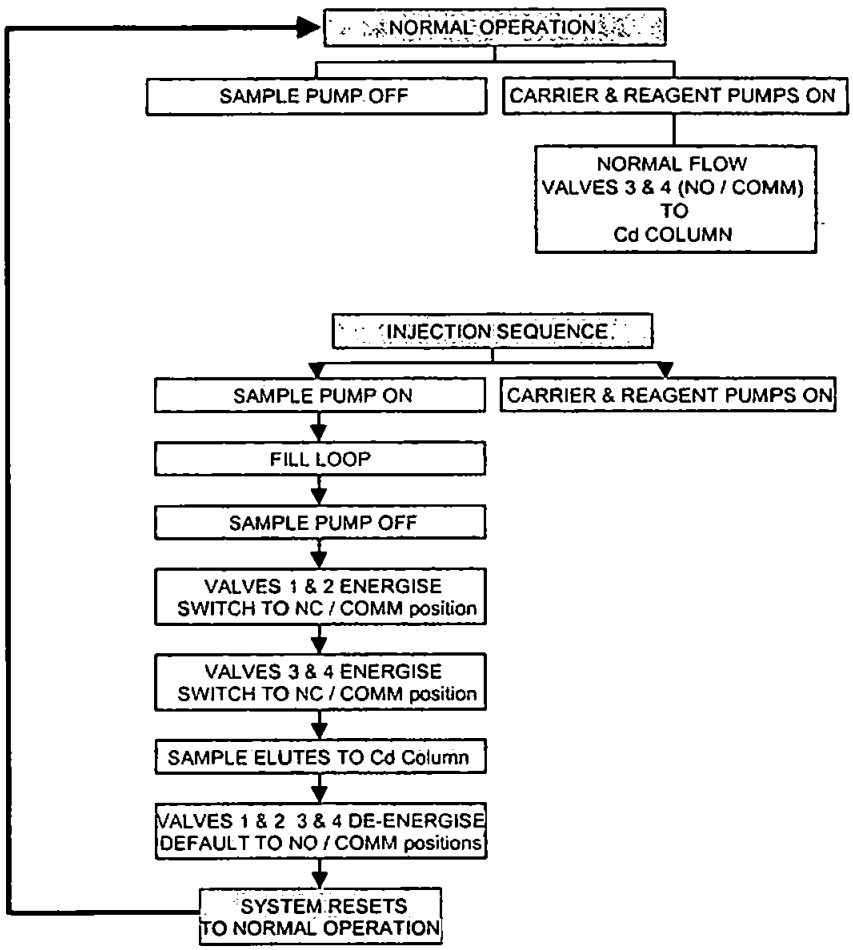

Figure 5.3 Flow diagram of valve operation during injection sequence.

5.2.3 FIELD DEPLOYMENT SITE DESCRIPTIONS

(a) LESOTHO EXPEDITION FIELD TRIAL

The expedition to Lesotho provided a unique opportunity to gather field data from a mountainous, environment in the Southern Hemisphere which receives relatively low nutrient inputs. The expedition provided a challenging environment for practical work and the opportunity to acquire a unique data set that could be used for future studies by the wider scientific community. In addition the expedition provided excellent opportunities to further develop interpersonal and team management skills and promote them in others.

The sampling trial was part of a larger 6-week B.S.E.S expedition (British Schools Exploring Society, London, U.K.), in which the author was Team Leader for a group of 17 young people (15 from U.K., 2 from Lesotho). The project was devised to fulfill personal research objectives and to promote environmental sciences to a wider community in Lesotho and the U.K. A schematic overview of the project is presented in Figure 5.4. The aims were :-

- To prove the viability of deploying the automated instrumentation in a remote location.
- Engender an inter-disciplinary scientific approach to problem solving in Environmental Sciences.
- To provide training for young people in the use of a range of chemical and physical field measurements, including sampling and data processing.
- To improve and promote interpersonal skills e.g. teamwork, project planning, decision making, communication, problem solving and analytical skills.
- Provide a baseline reference data set with regard to water quality of the only National Park in Lesotho that could subsequently be used in future studies in order to assess environmental impact on the National Park.

KINGDOM OF LESOTHO

The Kingdom of Lesotho is a mountainous landlocked African state, wholly surrounded by South Africa (Figure 5.5). It lies between latitudes 28 degrees and 31 degrees south and longitudes 27 degrees and 30 degrees east. The lowlands in the west and south of the country are 1500 to 1820 meters above sea level and the remaining highlands range from 2000 to 2730 meters above sea level. Lesotho also has two mountain ranges, the Maluti range and the more famous Drakensburg mountain range which reaches a highest point of 3465.5 meters at Thabana Ntlenyana. The capital is Maseru with an estimated population of 109 382 and a total population for the whole country is 1, 774, 000 (1993) and increasing by 2.7 % per year. Lesotho's climate can be described as continental but is affected by altitude with marked differences in daily and nightly temperatures ranging from – 7 °C to 32 °C. Rainfall averages 740 mm, which mostly falls between October and April (summer months).

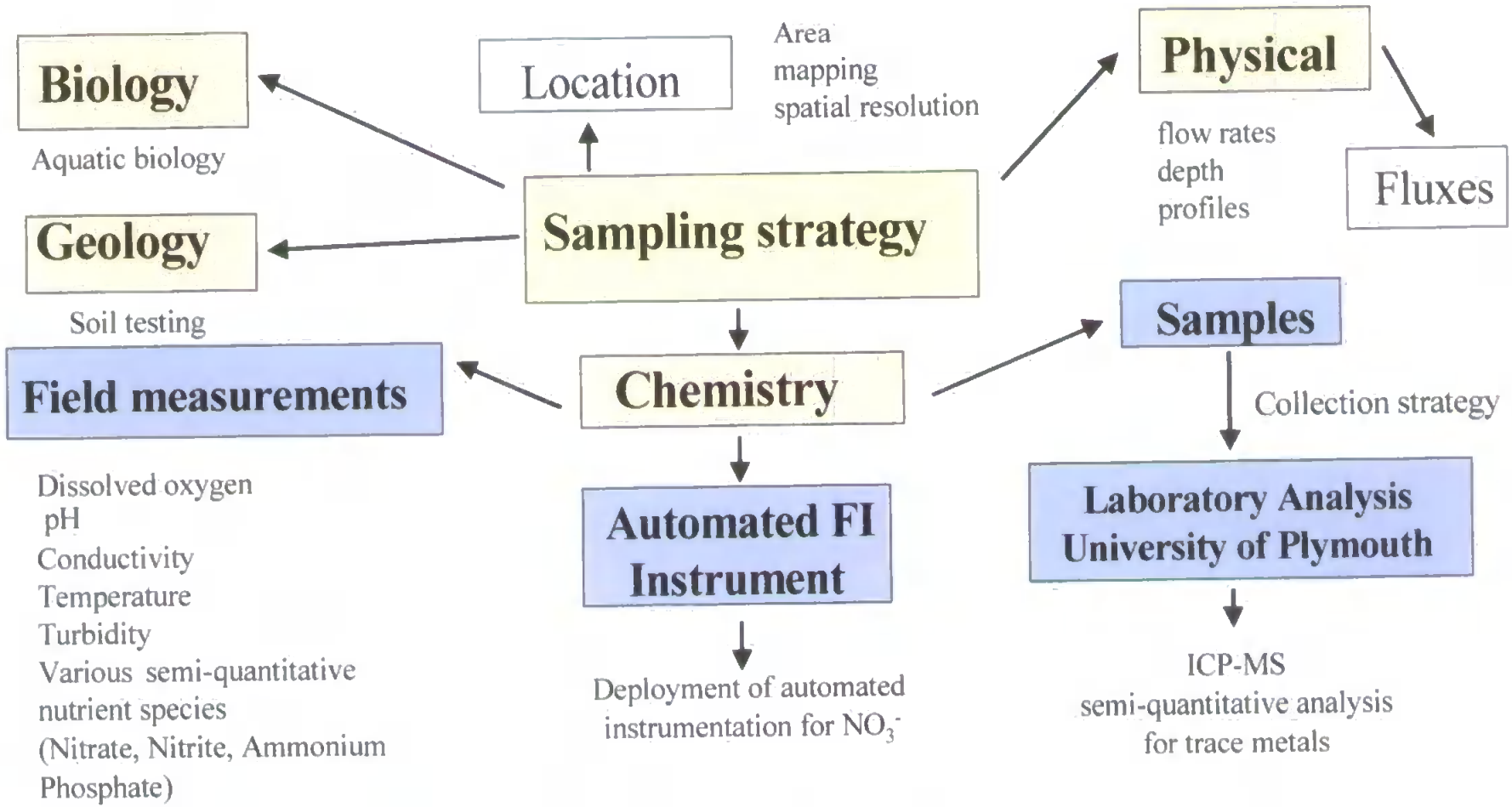

Figure 5.4 **Schematic diagram of field sampling campaign of Lesotho expedition field trail.**

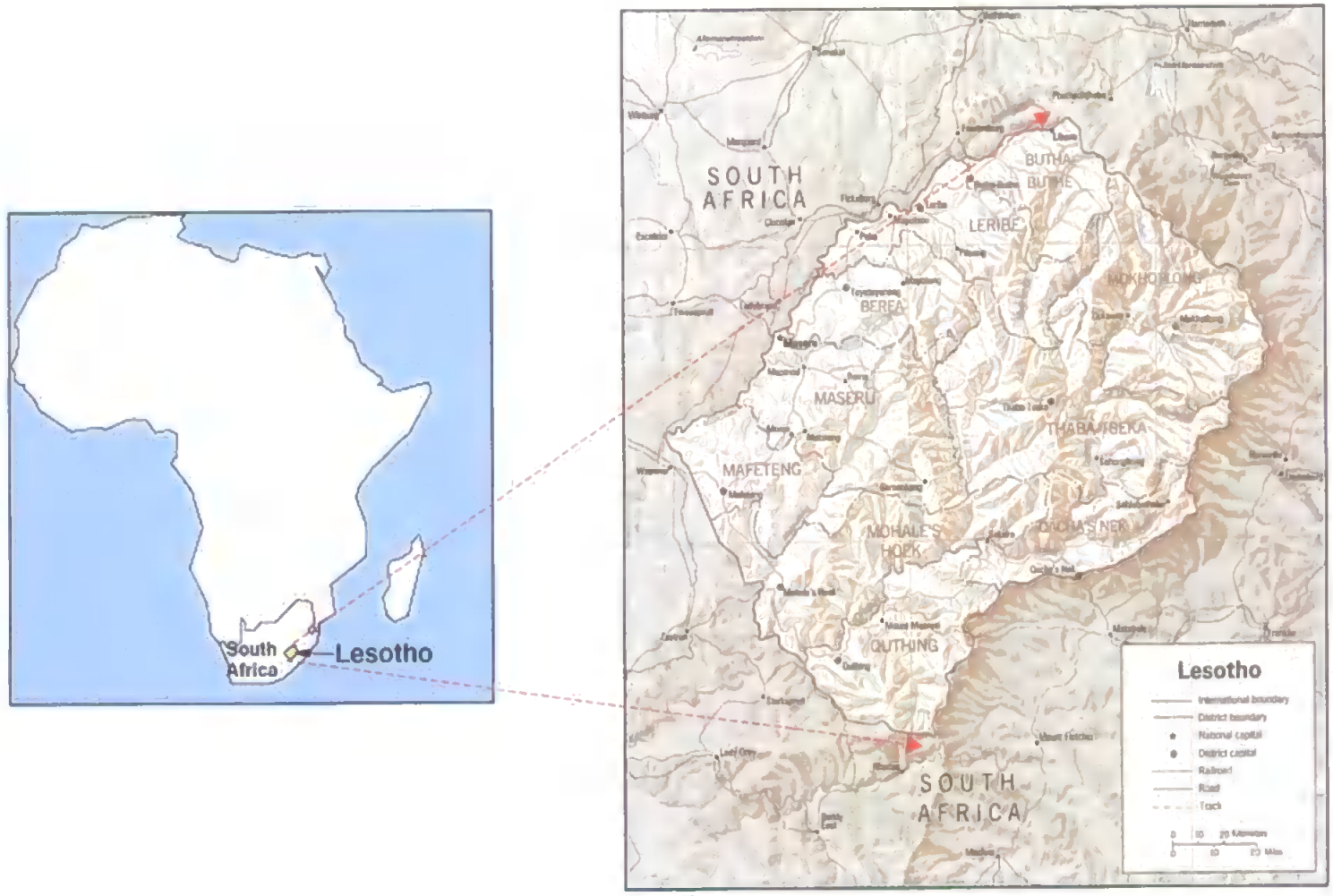

Figure 5.5 Location of Lesotho on the African continent; Sehlabathebe National Park located in far south-east of Lesotho.

SEHLABATHEBE NATIONAL PARK

Sehlabathebe National Park is located in the far southeast of Lesotho near the town of Quacha's Nek (Figure 5.5) is Lesotho's only National Park. It has an average altitude of 2400m, making this park one of the highest in Africa.

Plate 5.1 **Team camped on first night in National Park at Park Lodge (Figure 5.7) with the "Three Bushmen" mountains of the Drakensburg Escarpment in background.**

Plate 5.2 **Typical upland ground in Sehlabathebe National Park, Author in centre ferrying field instrumentation, Tsoelikane River to centre left.**

Proclaimed a National Park in 1970, this conservation area covers 7500 ha of mountains, valleys and waterfalls, and is the catchment for the trout-filled upper Tsoelike River. The park offers visitors the chance to see the rare bearded vulture (also known as the lammergeiger). In addition to the vultures it is possible to see the tiny Oreodaimonqathlambae fish, thought for decades to be extinct and only recently rediscovered in the lakes of the Drakensburg Mountains. Other game that can be seen includes black eagles, baboons, rhebok, eland and occasionally the secretive oribi. Plates 5.1 & 5.2 show the typical landscape of the Sehlabathebe National Park, high altitude sparsely covered grasslands / moorland with large rocky outcrops and mountainous hilltops.

LESOTHO SAMPLING SITE LOCATIONS

Each site had originally been identified according to its geographical location and intersection with other tributaries from a 1:250000 map (Figure 5.6) prior to arriving in Lesotho. However when studying the 1:50000 map of the Sehlabathebe area (Figures 5.7 and 5.8) in Lesotho some sites were not accessible due to topography considerations and the increased abundance of tributaries. In addition to this initial problem the fact that the sampling trial was conducted during the dry winter /spring season meant that numerous sampling sites as identified on maps were in fact dry stream beds. Therefore the sampling sites were chosen according to a number of individual factors, topography and accessibility, geographical location in relation to other tributaries and intersections of the river, travelling distance to the sampling site and the sites' suitability for field sampling by "on the ground" assessment by the Author. In total 36 sites were chosen, 22 in the National Park and 14 in the Leqooa Catchment (see below).

Geologically the whole sampling area belongs to the South Africa Karoo Supergroup. Although the majority of Lesotho's geology is dominated by the basalt lavas of the Draskensburg group, the Sehlabathebe area has a more varied geology. In particular the sampling area of the Sehlabathebe National Park is comprised of sedimentary Stormberg beds which are conformably overlain by volcanic Drakensburg lavas. Interspersed with the sedimentary beds of the National Park are numerous intrusions of dolerite dykes and the one intrusion of a diamond bearing kimberlite dyke. The Elliot and Clarens sandstones of the Stormberg group are characterised by yellow and light red fine grained sandstones which often grade into siltstones. As a consequence drainage within the Park is generally free and soils a mixture between sandy and clay loams.

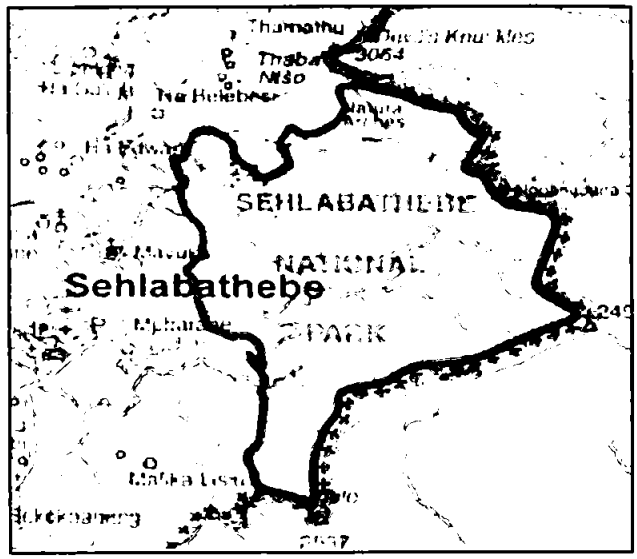

Figure 5.6 Zoomed region of 1:250 000 map of Lesotho showing Sehlabathebe National Park.

From Figure 5.6 it can be seen that all the tributaries in the Sehlabathebe National Park catchment area feed into the Tsoelikane river which links up with the larger Leqooa/Tsoelike river downstream and ultimately feeds into Lesotho's major river, the Senqu. This is a major water supply source to South Africa. To contrast data from the Sehlabathebe National Park (a protected area) a second sampling area was identified, namely the mountainous Leqooa river catchment to the N.W of the park (Figure 5.9).

(b) RIVER FROME FIELD TRIAL

Figure 5.10 (a) shows a schematic map of the River Frome & Piddle catchment. The Catchment lies entirely within the county of Dorset. The catchment is predominantly rural, with only two major settlements, Dorchester (population. 15, 104) and Wareham (population. 8, 092). The Frome originates on the North Dorset Downs near Evershot and flows in a southeasterly direction to be joined by the Wraxall Brook near Cattistock and also by the River Hooke at Maiden Newton. Two smaller streams, Sydling Water and the Cerne also join the Frome upstream from the town of Dorchester. As the river turns slowly east the South Winterbourne, Tadnoll Brook and the Win enter the Frome from the south. The Frome then meanders east and, with the River Piddle, enters Poole Harbour at Swineham Point. The rivers drain an area of 660 km^2 into the harbour. Poole Harbour itself is centrally located on the south coast of England and is one of the largest and shallowest natural harbours in the world.

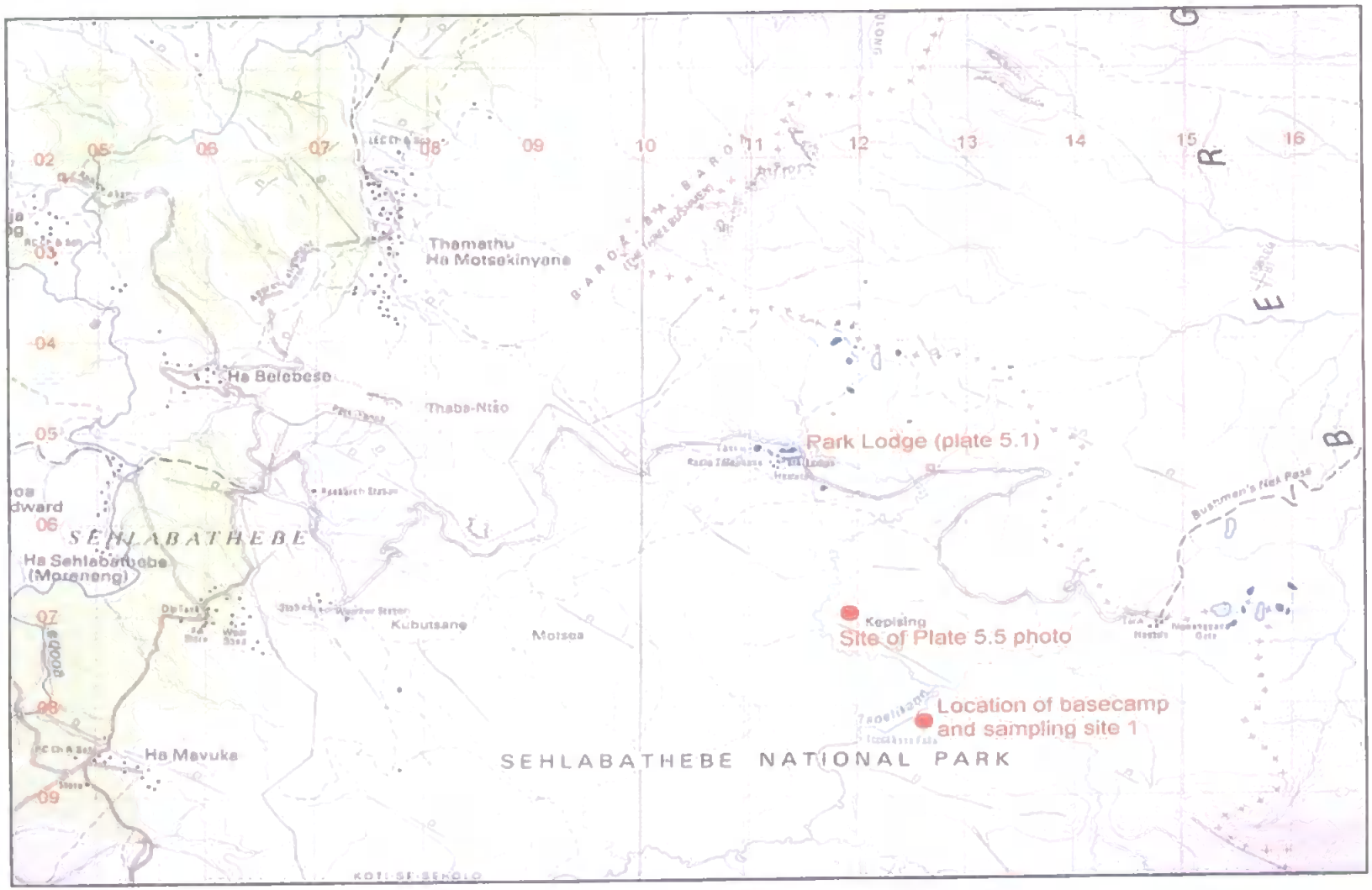

Figure 5.7 1 : 50 000 map of northern section of Sehlabathebe National Park (Series L50, no. 58, Edn. 4-D.O.S.1983)

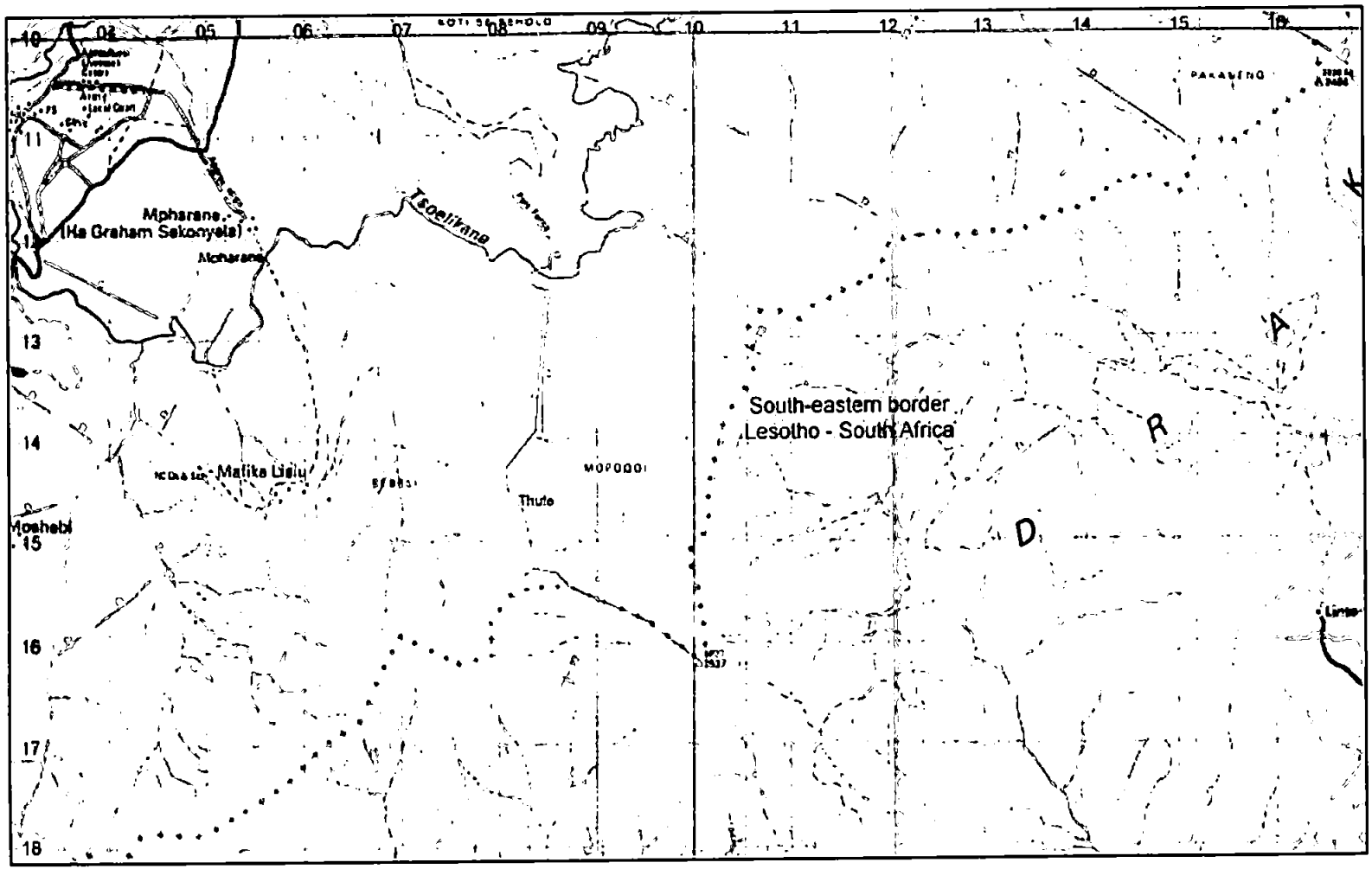

Figure 5.8 **1 : 50 000 map showing southern section of Sehlabathebe National Park (Series L50, no. 58, Edn. 4-D.O.S.1983).**

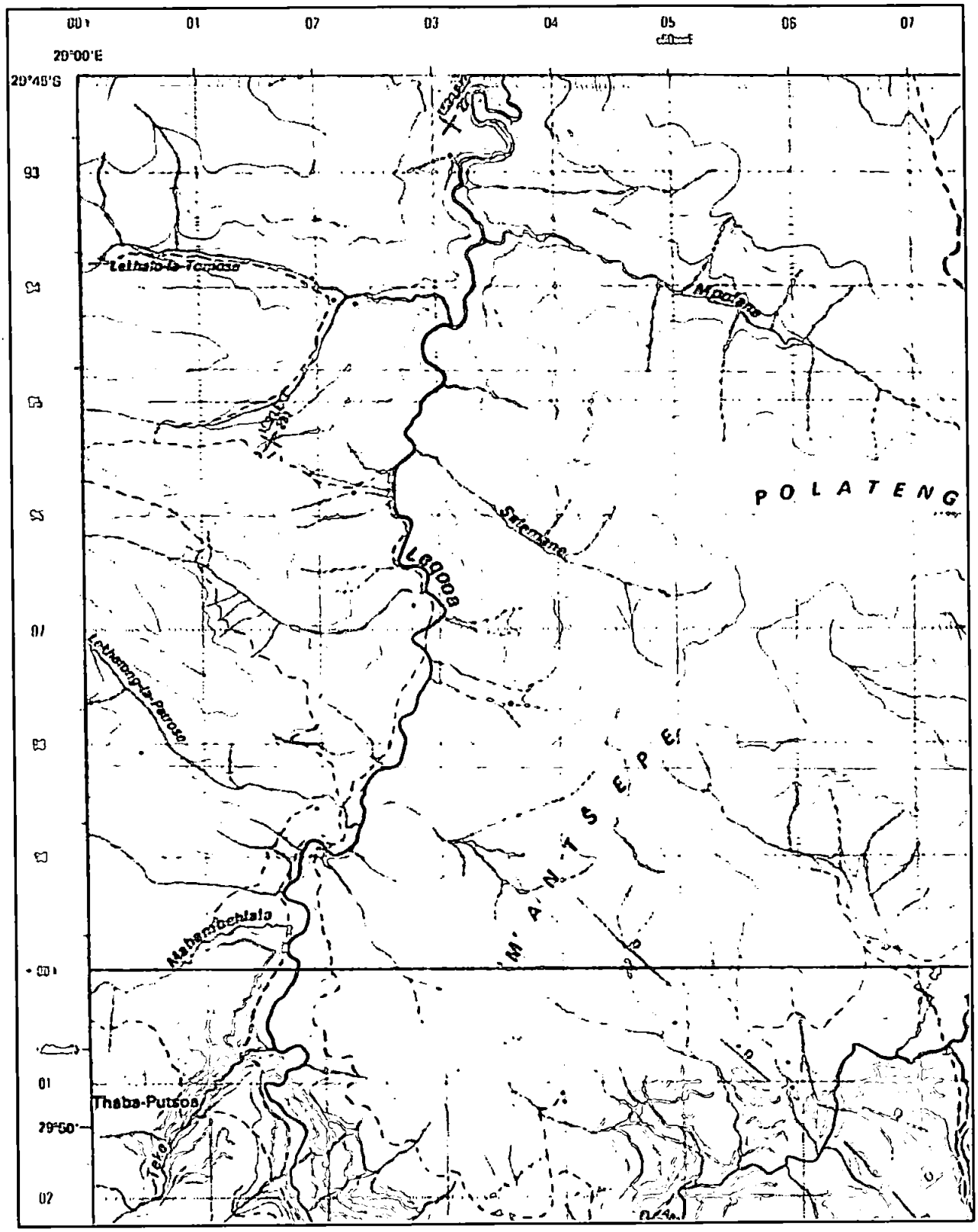

Figure 5.9 **1 : 50 000 map showing Leqooa River Mountain Catchment to north-west of Sehlabathebe National Park (Series L50, no. 58, Edn. 4-D.O.S.1983).**

The upper part of the catchment is dominated geologically by Chalk from the Cretaceous epoch (Figure 5.10 (b)), this is interspersed with complicated geological faulting and clay outcrops. The soils are characteristically shallow, well drained and chalky, although there are substantial areas of heavier, clay-influenced soils. The upper tributaries flows through typical chalk valleys, much of which is designated an Area of Outstanding Natural Beauty and is protected landscape. In lower parts of the catchment, more recent geology dominates with sands, gravels and clays, and the land being characterised by valley pastures and fields. Downstream the floodplain widens to extensive tracts of pasture, marsh and some heathland. Land use in the area is typically permanent grassland and natural wetland.

The sampling site for the evaluation of the automated nitrate monitor was located at the Natural Environment Research Council (NERC) funded Institute of Freshwater Ecology (IFE), sited on the Frome between Wool and Wareham. The River Laboratory at the IFE conducts research into River Quality Classification, Fish Ecology, Aquatic Botany and Aquatic Chemistry. The automated nitrate monitor was set up in the Institutes' Fluvarium. The Fluvarium (see Plate 5.3) is a purpose built concrete structure which the River Frome flows through. The river is split into two channels, each passing into the building and through the glass sided observation channels (Plate 5.5). The nitrate monitor (Plate 5.5) was set up below one of the observation channels and a siphon arrangement was constructed to enable sampling directly from the main river flow (see section 5.2.4 (c)).

5.2.4 PROCEDURES

(a) LABORATORY STUDIES

In order to convert the digital pump rates of the micro pumps in terms of flow rate in ml min^{-1}, calibrations were performed for each individual pump (sample, carrier and reagent). The flow of Milli-Q water was measured for a 5 min duration at digital pump rates of 10, 15, 20, 30, 40, 50. The total volume collected during the calibration period was divided by five to yield flow rate in ml min^{-1}.

Baseline stability of the automated monitor was assessed using the optimum flow rates specified in section 4.3.7, 0.43 ml min^{-1} for the NH_4Cl carrier and 0.31 ml min^{-1} for the mixed colour reagent. Response was monitored at $\lambda_{max.}$ (597 nm) minus a baseline reference wavelength at 444 nm for 1 h.

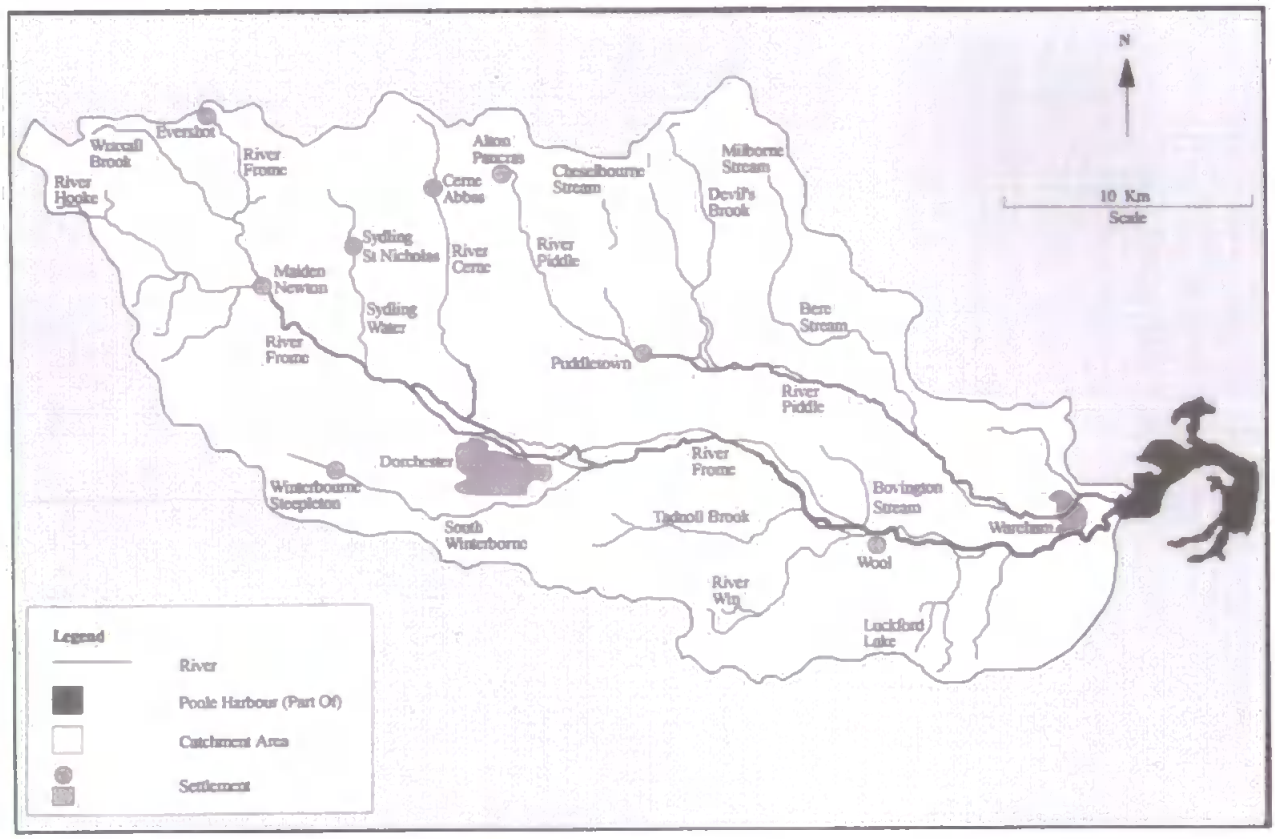

Figure 5.10 (a) Map of Frome & Piddle catchment.

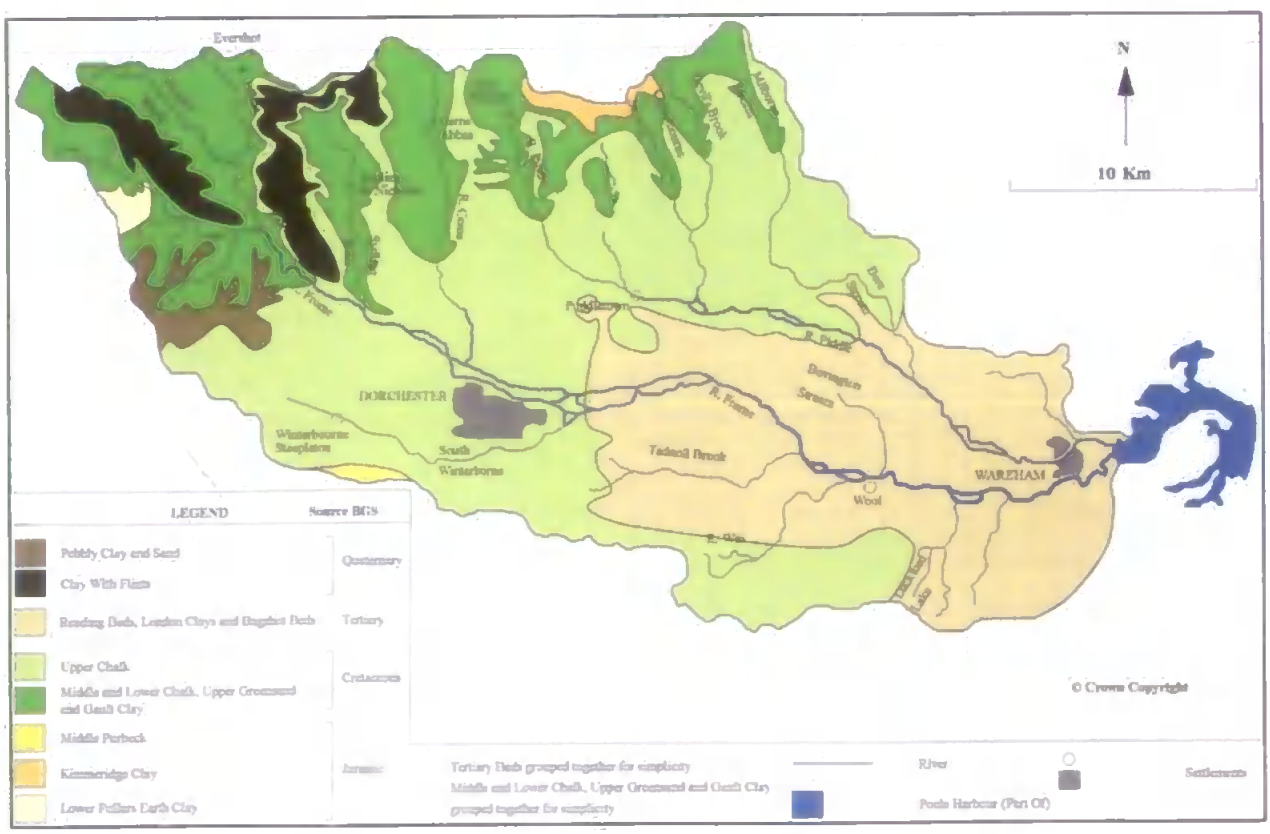

Figure 5.10 (b) Geological map of Frome & Piddle catchment.

Plate 5.3 Fluvarium at the Institute of Freshwater Ecology, Wareham, Dorset.

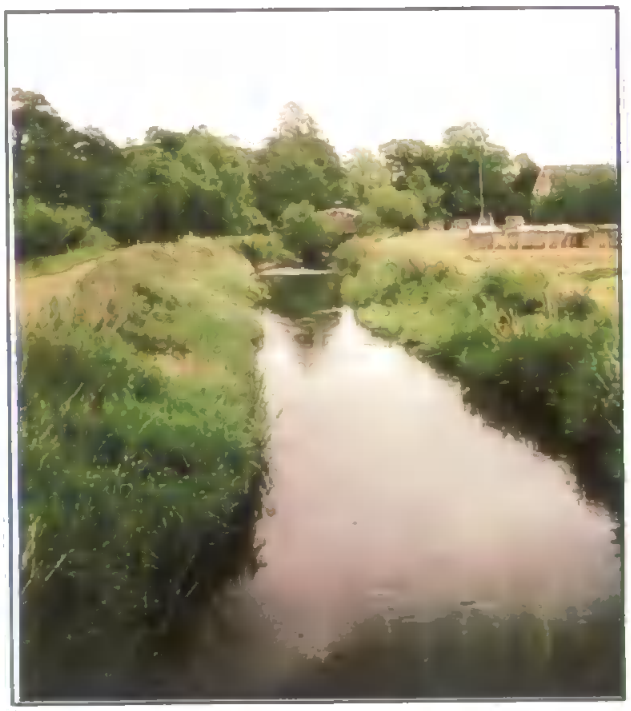

Plate 5.4 Downstream view toward Fluvarium.

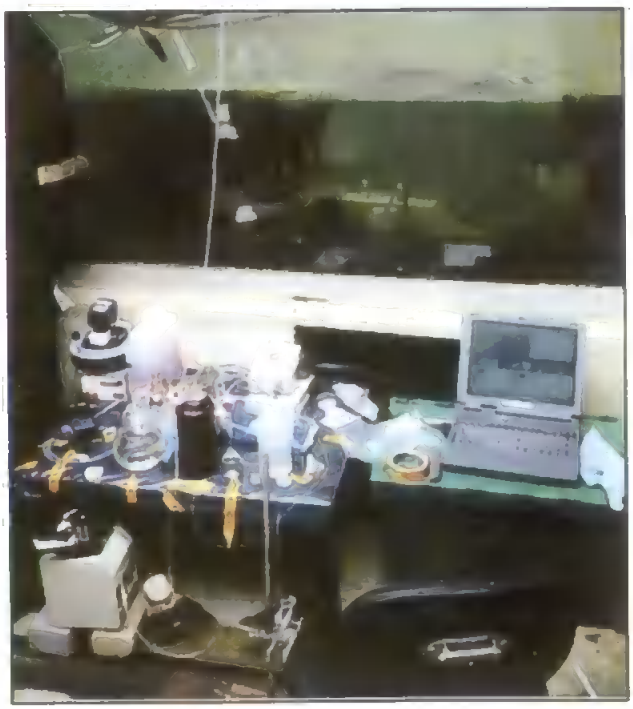

Plate 5.5 Automated nitrate monitor sampling from left hand channel of Fluvarium.

Calibration of the monitor for the concentration range 0 – 1 mg l^{-1} NO_3-N was performed using standards of 0, 0.01, 0.05, 0.1, 0.3, 0.5 and 1.0 mg l^{-1} NO_3-N, and each standard was analysed in triplicate. In order to extend the linear range of the monitor to perform NO_3-N determinations at higher levels than those already optimised for (0 – 1 NO_3-N, Chapter Four), calibrations were performed using 0, 1.0, 3.0, 5.0, 7.0 and 9.0 mg l^{-1} NO_3-N standards and a 90 µl sample loop (as opposed to 260 µl). To determine the optimum wavelength to extend the linear range of the manifold, several calibrations monitored at different wavelengths were performed.

(b) LESOTHO EXPEDITION FIELD TRIAL

A fixed sampling location was the most feasible way to evaluate the automated nitrate monitor. While in the National Park (approximately 12 days), a basecamp was established 500 m upstream from Tsoelikane Falls (Figure 5.7). The instrumentation was set up in approximately 1 h and sited next to the Tsoelikane River. The nitrate monitor was calibrated in the field using pre-prepared (University of Plymouth, 0, 0.5 and 1.0 mg l^{-1} NO_3-N standards) nitrate standards stored in medical plasma bags. Samples were introduced to the manifold via an in-line interchangeable (disposable) 0.45 µm membrane syringe filter (Merck Ltd.). Once calibrated the monitor was set to sample every 20 min.

In addition to the fixed site for the automated nitrate monitor, further field data was obtained by performing a range of sampling techniques throughout the Sehlabathebe National Park (Figures 5.7 and 5.8) and the Leqooa River mountain catchment (Figure 5.9). On arrival at each sampling site, the team was divided into separate groups to conduct different tasks. Each site had its geographical location mapped (longitude and latitude) by a hand held Garmin – 12 G.P.S (Global Positioning System) (Taunton Lesiure Co., Taunton, Somerset, U.K.). This data was supported by triangulated compass back bearings using surrounding local topography and features to provide a map grid reference. Altitude reading were also recorded from the G.P.S unit. Determination of nitrate and nitrite using the cadmium reduction method, ammonia by the salicylate method, and reactive phosphorus using the molybdate blue method, were performed in duplicate using two Hach DR – 890 pocket colourimeters (Camlab Limited, Cambridge, U.K.). Standard reagent test kits for the above methods (0 – 0.5 mg l^{-1} NO_3-N, 0 – 0.35 mg l^{-1} NO_2-N, 0 – 0.5 mg l^{-1} NH_3-N and 0 – 2.5 mg l^{-1} PO_4) were obtained from Camlab Limited and the procedures detailed in the DR – 890 handbook were

followed. pH was measured using two 9025 portable pH meters (Hanna Instruments, Patterson Scientific, Luton, Bedfordshire, U.K.), calibrated prior to use with buffers of 4.0 and 7.01 pH. Conductivity was measured using two portable microprocessor conductivity meters (Hanna Instruments) previously calibrated using 84 μS and 1413 μS standards. Dissolved oxygen (YSI – 55, YSI, Farnborough, Hampshire, U.K.) was also measured after calibration at 100 % relative humidity and corrections for altitude and salinity were made. pH, conductivity and dissolved oxygen measurements were made in triplicate. Water velocity was measured using an in-house designed impeller driven revolution counter (Geographical Sciences, University of Plymouth). A macro-invertebrate study was conducted using the standard "kick test" method. This involved using a riffle zone within the stream / sampling site and kicking sediment and water towards a fine mesh net for a duration of 2 min. The organisms caught were transferred to trays, identified and counted; this procedure was repeated 3 times. River water samples were also collected within Sehlabathebe National Park for ICP – MS semi-quantitative trace metal analysis on return to the U.K., analysis procedure and presentation of the results are given in Appendix II.

(c) RIVER FROME FIELD TRIAL

The river-water was siphoned to a 500 ml beaker at a flow rate of 375 ml min^{-1}. The sample was then drawn through a 0.45 μm (47 mm dia.) cellulose acetate membrane filter incorporated into a syringe membrane holder using a Gilson Minpuls-3 peristaltic pump into a clean 100 ml HDPE sample bottle at a flow rate of 15 ml min^{-1}. Calibration of the automated nitrate monitor was performed every evening during the field trial. Calibration standards (0, 1.0, 3.0, 5.0, 7.0 & 9.0 mg l^{-1} NO_3-N) were analysed in triplicate. The automated sampling procedure consisted of sampling from the filtered collection bottle at a flow rate of 5 ml min^{-1} for a duration of 3 min. The automated monitor then injected the sample with a sample flush time (carrier flowing through sample loop) of 1 min prior to resetting the instrument. The sampling cycle was configured to sample every 30 min to enable good resolution of nitrate concentrations within the river. During the day every sample injection was followed by a manual injection of a mid calibration range standard (5 mg l^{-1} NO_3-N). Conductivity, pH, air, reagent, and river temperature were also recorded at the time of sampling.

After the automated nitrate monitor had sampled from the bottle, it was labeled and stored in the dark at 4°C. Upon return to the laboratory (1 – 3 days, depending on when sample was collected) the

samples for intercomparison were allowed to warm to room temperature and analysed immediately using a SA 4000 Skalar Segmented Flow Analyser (Skalar Analytical B.V., Netherlands) connected to a SA 1050 random access auto sampler (Skalar Analytical B.V., Netherlands). The instruments were controlled by DOS-based software, Data acquisition module ver.62x24 (Skalar Analytical) and data processing program ver.62x23 (Skalar Analytical), operating on a Dell Dimensions V333c (Pentium 333 MHz, 64 MB RAM) personal computer (Dell Computer Corporation). The Skalar instrument was configured for the concentration range 0 – 5 mg l^{-1} NO_3-N, and the Frome river samples therefore required 1:1 dilution using Milli-Q water. Each standard was analysed once and a 2.5 mg l^{-1} NO_3-N standard was used to assess instrumental drift prior to and after the calibration. Baseline stability was assessed using a Milli-Q wash cycle. Samples were analysed in triplicate and in sets of five with every sixth sample consisting of a 2.5 mg l^{-1} NO_3-N standard. An ICP-MS analysis (semi-quantitative) of River Frome water was also performed and the results are given in Appendix II.

5.3 RESULTS & DISCUSSION

5.3.1 VIRTUAL INSTRUMENTATION GRAPHICAL PROGRAMMING

(a) LabView™ OVERVIEW

National Instruments LabView™ is a universal programming system, which utilises a graphical user interface or "Panel" and a graphical programming code or "Diagram". It was designed to facilitate scientists and engineers who may not possess an extensive programming knowledge and to enable easy programming of data acquisition, data handling and data display functions. LabView enables the integration of external measurement devices (e.g. IEEE 488 (GPIB) or RS 232 controlled and data acquisition PC cards) with a graphical user interface into a personal computer based measurement instrument and simplifies scientific computation, process monitoring and control, and test and measurement applications.

LabView 's graphical language G differs from conventional text-based software packages (e.g. C, BASIC and Pascal) in one important respect. These other packages use text-based languages to create lines of code, while G uses a graphical programming language to create programs in block diagram form. G, like C or BASIC, contains extensive libraries of functions for any programming task. The language includes libraries for data acquisition, GPIB and serial instrument control, data analysis, data presentation, and data storage.

G also includes conventional program debugging tools, such as the setting of breakpoints to view data transfer, animation of the execution of a program to observe how data passes through the program, and single-step through functions which allow the user to following every step of data operation within the program. These features allow easier program development and debugging.

Text languages also require a greater degree of specialist knowledge with extensive time being needed to learn the programming language, obtain an overview of the libraries and gain experience in using them. The graphical nature of LabView is inherently easier to understand and use, enabling the development of a graphical user interface in a relatively short space of time. The MS-windows environment also offers outstanding programming tools, a standard user-interface, near-real-time performance and significant tools to aid data processing (e.g. dynamic data exchange (DDE) and ActiveX facilities).

A program written in LabView is known as a *"Virtual Instrument"* (VI) and consists of two components, the panel window and the diagram window. The panel is where the user designs the interface and ready to use components such as switches, buttons, controls and graphical displays can be placed within the window. The connectors of the elements placed in the "control panel" appear simultaneously in the graphical "wiring diagram". This panel is the main difference between LabView G programming and other programming systems.

The connectors of the components placed on the "control panel" in the "wiring diagram" can be connected to each other or to additional functions such as mathematical operations, file management and inputs and outputs of data to and from acquisition cards simply by the use of a wiring tool. Therefore programming in LabView mainly involves wiring together data operations and functions within the diagram panel. No text input from the keyboard or editing of the source code is necessary. This exceptional functionality enables the user to quickly design a graphical user interface in considerably less time than a conventional language.

LabView also allows the formation of "subVIs" within a main VI. Instead of having a mass of graphical programming to perform a set function, the program code responsible for that function can be represented as an icon with terminals for its inputs and output appearing in the diagram of the main VI.

Thus complex programming can be condensed into smaller modular units for use in other VIs' double clicking on that icon opens the sub VI and the code can be edited. This modular approach to the layout of the program is extremely powerful and can be utilised to simplify complex programming tasks.

(b) AUTOMATION PROGRAM

Figure 5.11 shows the front panel designed for the automation program (combo6.vi). The front panel is split into two sections, as is the block diagram. One section controls all manifold parameters, e.g. pump and switch activation (ON / OFF), pump rate, sampling mode, analyte to be determined (NO_3-N or NO_2-N) and injection timing sequence. Micro-pumps are set to active by pressing the square ON / OFF buttons whilst pump rates are set by the blue indicators above the switches. Pump units are set from 0 – 255 as 8-bit numerical values, flow rates in ml min^{-1} are calculated from a previously obtained calibration. Once sample loop and carrier switches are enabled (ON) the injection sequence can take place. In the OFF position the NH_4Cl carrier bypasses the sample loop and flows normally through the manifold.

Sampling mode allows the user to enable an automatic sampling regime defined by the blue indicators (fill, flush and cycle time). Fill time defines how long the sample loop is filled for, flush time how long the sample loop is flushed for and cycle time defines how often the injection sequence takes place. Manual sampling mode allows the user to perform a single injection whose parameters are defined by fill and flush time. When pressed, the analyte button activates two electronic switching valves which allow the bypass of the cadmium reduction column for the determination of NO_2-N only. The select and update controls allow the flow rate of any pump to be changed while the program is running.

The second part of the VI concerns all the scan and display acquisition from the spectrometer. The bottom left graph (Figure 5.11) displays the raw data (intensity graph, i.e. the output spectrum of the lamp) and allows reference spectra to be saved. The bottom right graph (absorbance graph) displays the absorbance spectrum in real time and also allows the user to save absorbance spectra. This is calculated by performing a negative logarithmic function on the constantly updating intensity values (I) divided by the saved reference intensity values (I_0).

The top right graph (history graph) can be viewed as analogous to a chart recorder. It displays (Figure 5.11) the absorbance value as defined by the diode select indicator (diode 513, wavelength 520.65 nm) minus a baseline reference wavelength at 444.58nm which is defined by the cursor position. The "log data to file" button, when activated, records the history data to file with the file destination shown in the yellow / red bordered indicator.

Sections 5.3.1 (c) and 5.3.1 (d) discuss the second part of any VI, the block diagram. For simplicity this has also been split into manifold control and spectrometer scan and display sections. Each section shows the main graphical code and then highlights and discusses key components of the VI. Section 5.3.1 (e) briefly discusses the hierarchical structure of the overall program. In order to facilitate the interpretation of the graphical code, a brief glossary of the main programming structures used is given below.

VI PROGRAMMING GLOSSARY

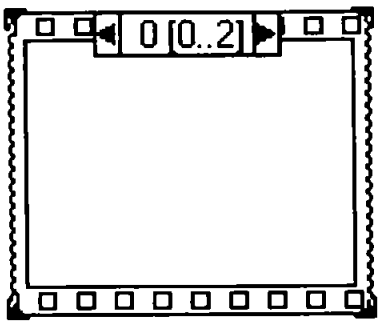

(A) – Sequence Structure.

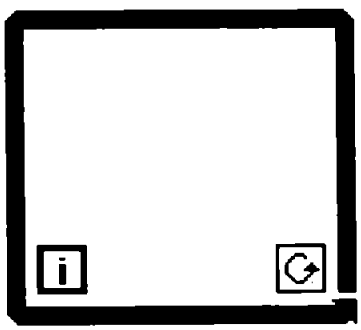

(B) – While Loop

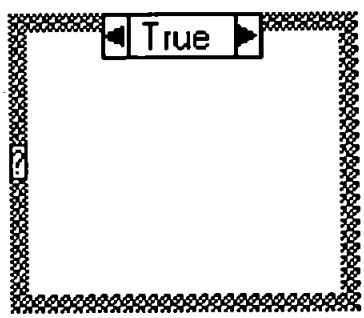

(C) - Case Structure

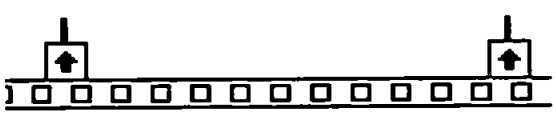

(D) – Sequence local variable

(E) – Global variable

The sequence structure, which looks like a frame of film, can have multiple subdiagrams, configured like a deck of cards, of which only one is visible at a time. Code written inside the structure is executed sequentially from frame to frame. To pass data from one frame to any subsequent frame, sequence locals are used (see VI glossary (D))

The while loop is a structure that repeats a section of code until a condition is met. The while loop executed the code within it until the Boolean value passed to the condition terminal (green circle arrow) is false. The iteration terminal (blue i) outputs the number of times the loop has executed.

The case structure has two or more subdiagrams which execute code written within it based upon an input value known as the selector (? Symbol). This structure shows a Boolean case in which a true / false input wired to the input selector will execute any code within the subdiagram selected.

A sequence local variable allows data to be passed between frames of a sequence structure. Data wired to a sequence local is only available to subsequent frames of the sequence structure and not preceding frames.

Global variables unlike local variables store data used by several VIs and can be used in any structure of a VI.

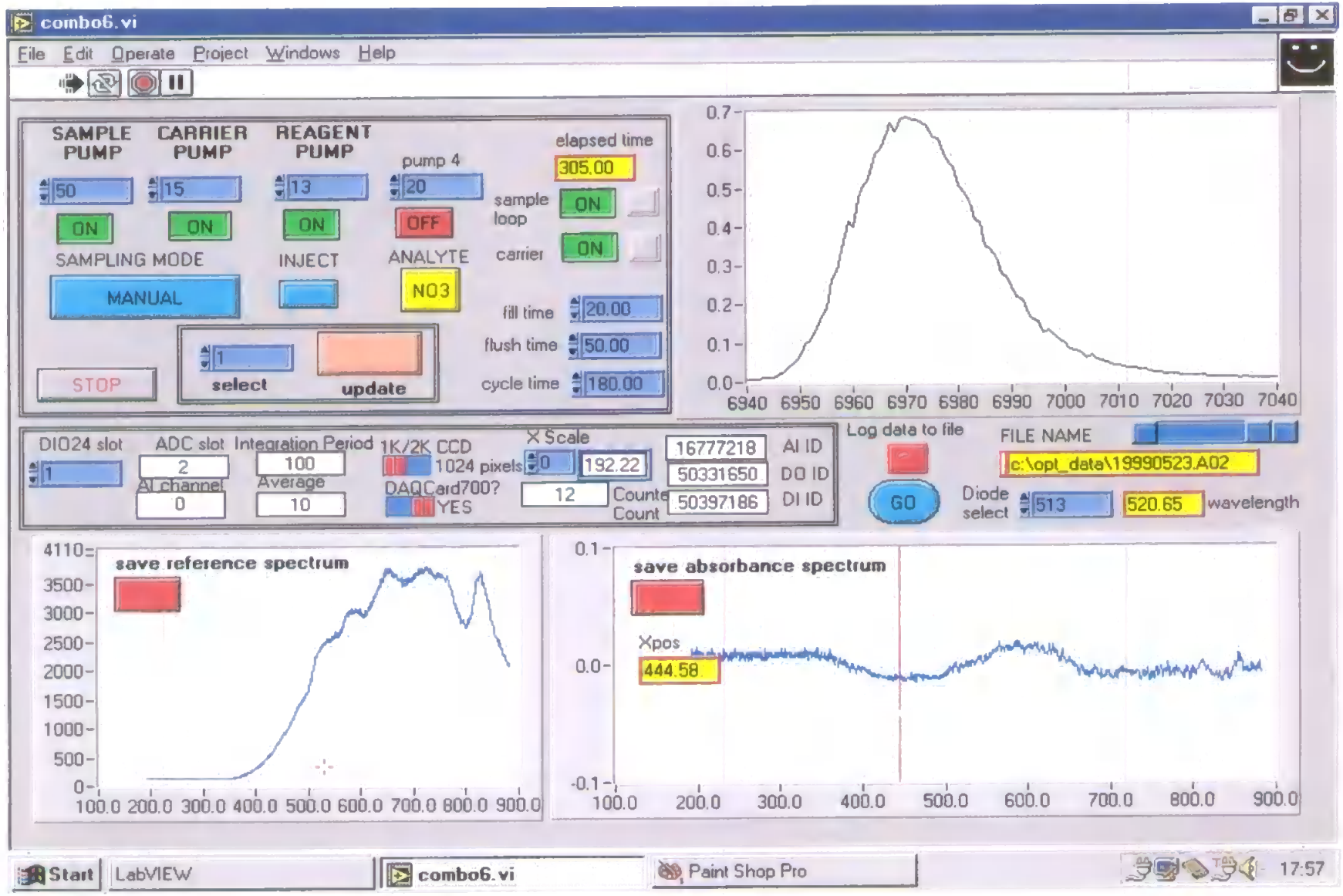

Figure 5.11 Graphical user front panel for the automated nitrate monitor; screen capture showing passage of nitrate azo dye peak.

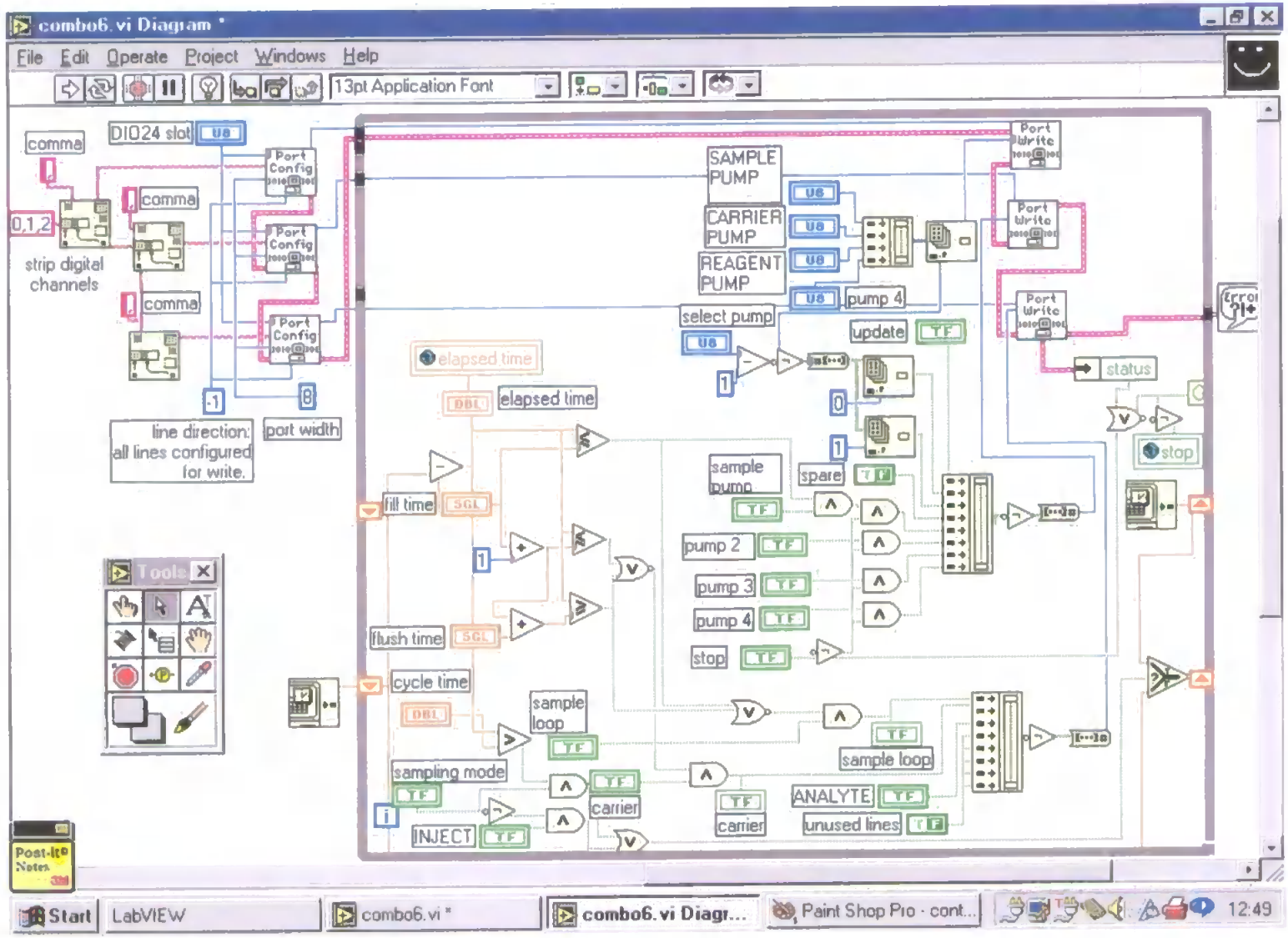

Figure 5.12 Graphical code for manifold control.

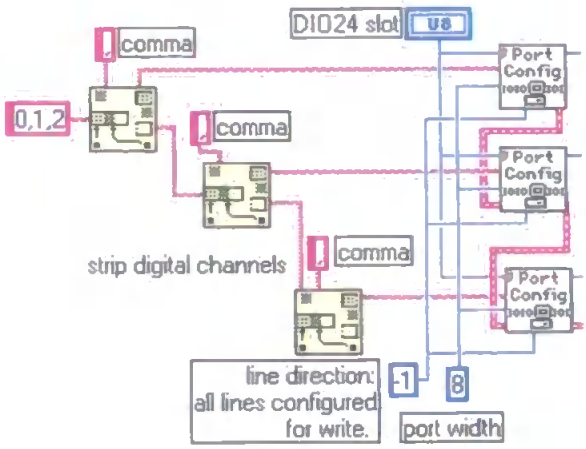

5.12 (a) Initialisation routine for digital ports.

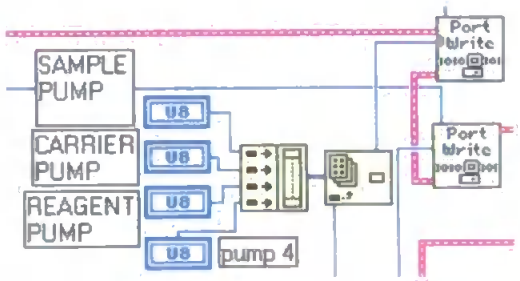

5.12 (b) Setting of pump speeds.

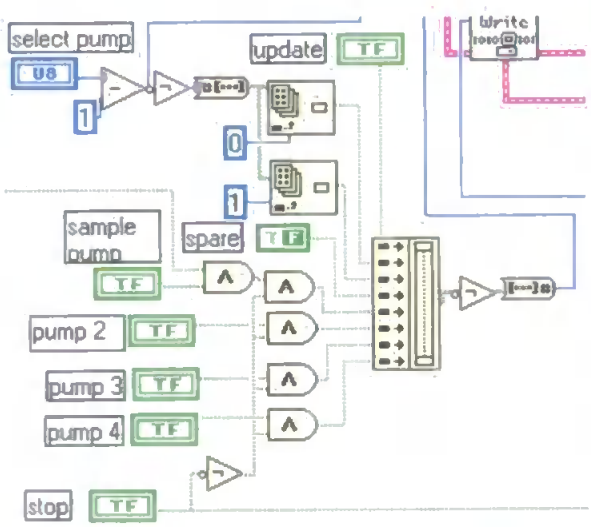

5.12 (c) Pump activation and update functions

The DIO-24 PCMCIA card provides 24 digital inputs or outputs split into three 8-bit ports (A, B & C). This portion of the main controlVI (see Figure 5.12) operates in cascade and labels each port as digital channels 0, 1, 2 with a default port width of 8 bits. The "port config" VI establishes the digital channel configuration and outputs a task ID that is used in the digital port VIs.

This code controls the pumping rates of the micro-pumps (sample, carrier and reagent). Values are entered on the user front panel (blue indicators, Figure 5.11) with the 8-bit numerical values being built into an array and written to port A (top "port write", Figure 5.12).

This section of code takes the Boolean values from the pump ON / OFF switches on the user front panel (Figure 5.11) passes them through AND logic gates (must be high to pass data) and builds them into an array of values. The outputted binary array (green line) is then converted to a decimal (blue line) form recognised by the digital port. The values are then written to port B (middle "port write", Figure 5.12). The select pump and update functions allow changes to be made to a pumps flow rate. The front panel "stop" button when pressed is connected to a global variable stop which writes to all loops and VIs in the program and stops the execution of the VI.

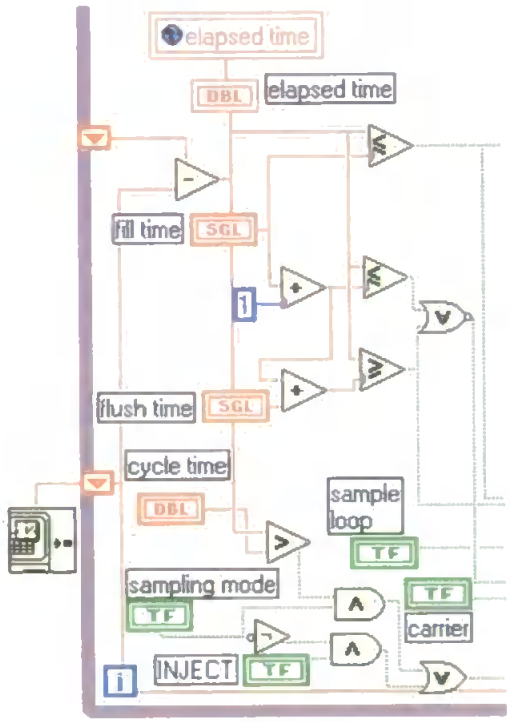

5.12 (d) Sampling mode and timing sequence.

This section of code concerns all the timing of the injection sequence and whether manual or auto sampling are activated. On first execution date and time are written to a shift register (orange arrow – shift registers are local variables that transfer or feed back values from the completion of one interation to the beginning of the next) and compared with another timer inside the loop. The global variable elapsed time gives the elapsed time since execution of the program or from when an injection is made. All thick bordered orange boxes correspond to the blue timing controls on the user front panels (fill, flush & cycle times). These are arranged within the VI to ensure correct timing of the injection sequence. Activating the sampling mode button (front panel control) to "auto" or "manual" determines whether the VI uses the old elapsed time ("manual") or takes a new reference as zero time "auto". The Boolean front panel ON / OFF switches (bold green bordered TF symbols) must be set high (ON) for the valve(s) to operate.

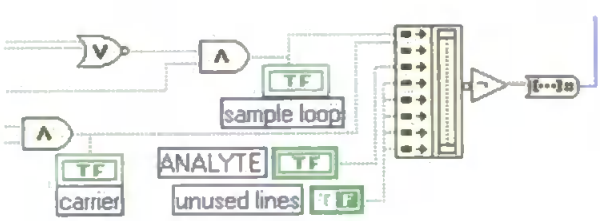

5.12 (e) Writing sampling conditions to digital port.

This last section of code takes all the injection timing sequence and builds them into an 8-bit array. The Boolean array is then converted to decimal (see e) and written to port C (bottom "port write", Figure 5.12).

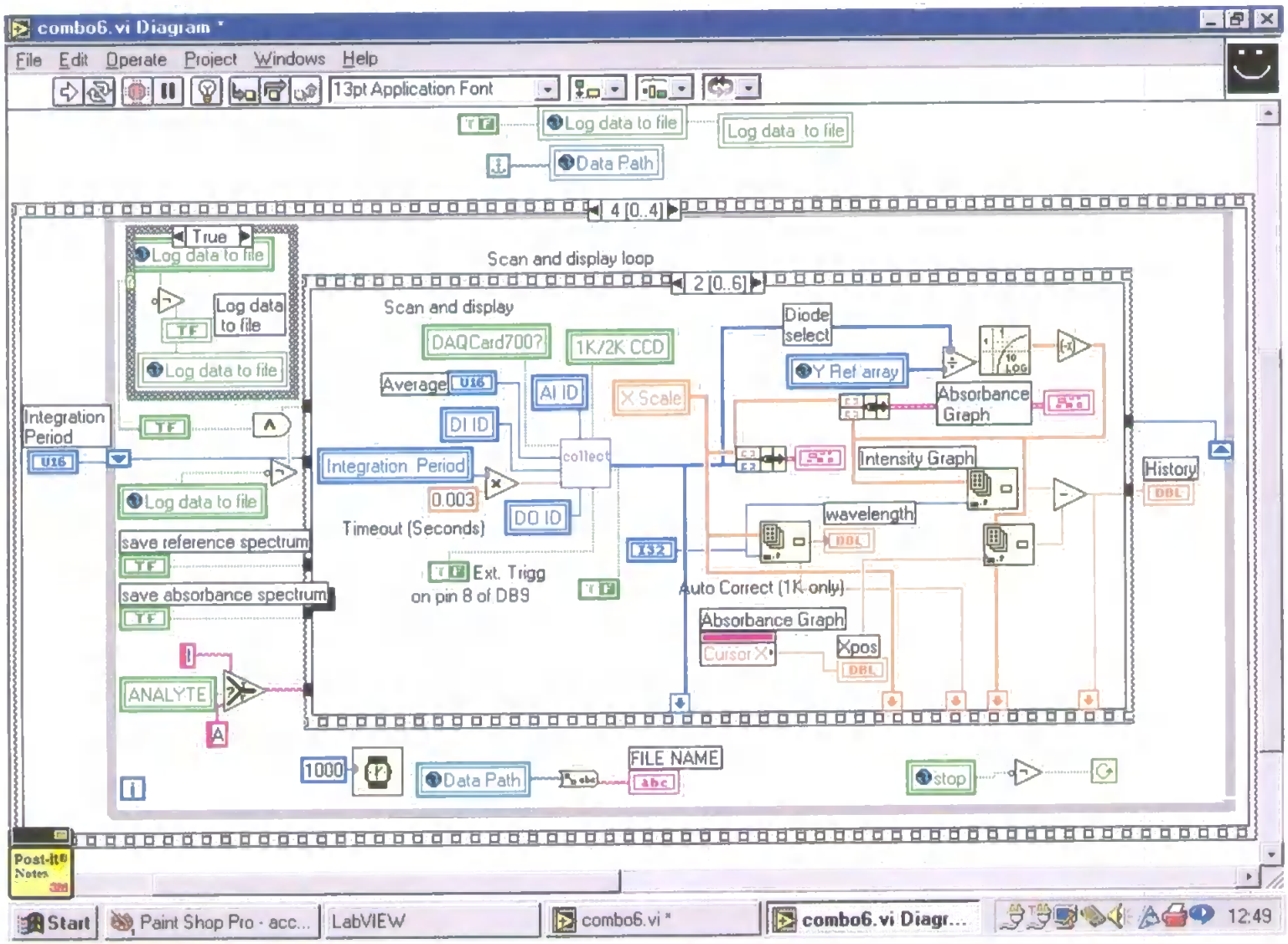

Figure 5.13 **Graphical code for spectrometer scan and display.**

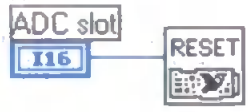

The first sequence is responsible for the resetting of the data acquisition card (DAQ – 700).

5.13 (a) Sequence 0 Board reset

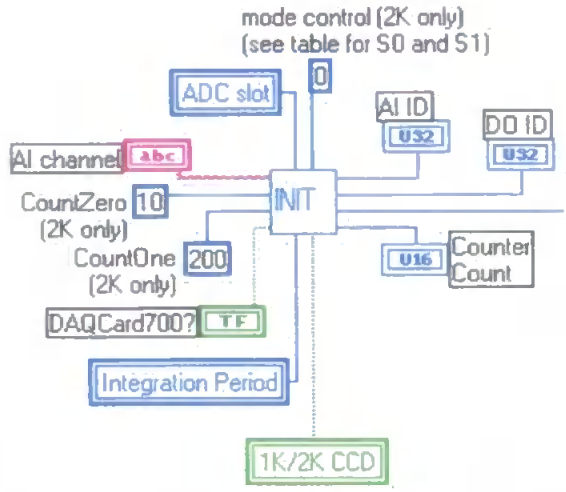

The "INIT" square icon represents a subVI (see explaination section 5.3.1 (a)). It is one of the VIs written by World Precision Instruments provided with the LabView spectrometer drivers. It is responsible for the initialisation of the A/D board and the spectrometer, allowing the selection of 1K (1024 elements, series 1000 spectrometer) or 2K (2048 elements, series 2000 spectrometer) and the selection of the integration period.

5.13 (b) Sequence 1 Initialisation of spectrometer.

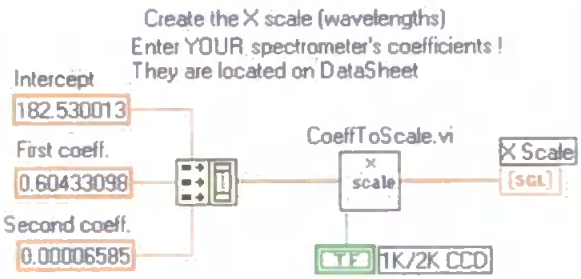

This sequence contains a VI later used as a subVI that converts an array consisting of the three second-order polynomial regression coefficients (see section 2.2.3 (a)) (factory calibrated, supplied with every Ocean Optics spectrometer) into an array of 1024 elements of wavelength values. Each wavelength corresponds to one CCD pixel.

5.13 (c) Sequence 2 Creating wavelength scale

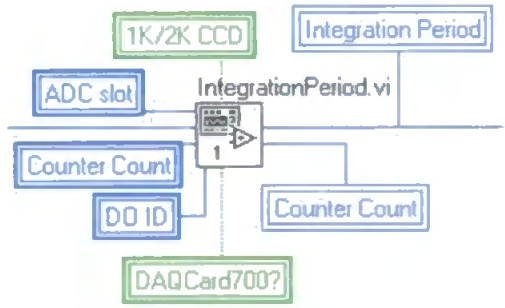

This VI uses the last counter count value to set a new integration period. The counter count consists of an internal number to keep track of the spectrometers' system clock count.

5.13 (d) Sequence 3 Change integration period

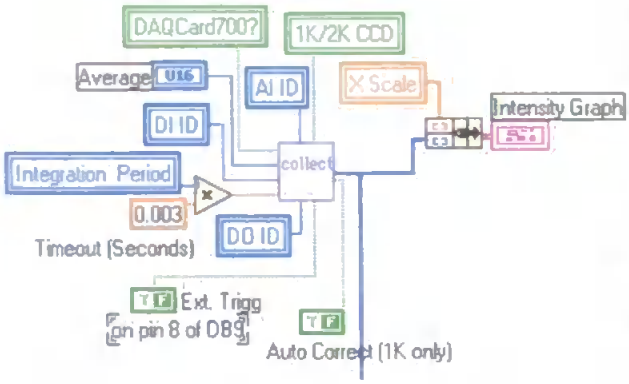

5.13 (e) Spectrometer scan and display

This section of code receives values generated from the "init" VI (5.13 (b)) and allows the setting of the number of CCD scans to be averaged for one spectrum display. The VI scans the spectrometer and constructs the intensity spectrum (user front panel) from x scale (wavelength) and y scale (raw counts) data.

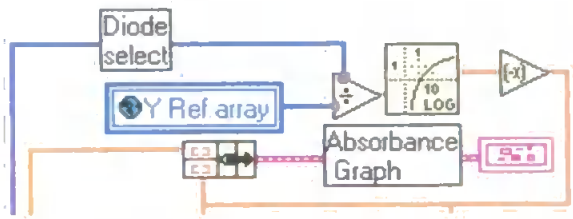

5.13 (f) Convert acquired data to Absorbance

This section of the main acquisition VI (Figure 5.13) takes the global variable "Y Ref array" (last reference spectrum) and ratios it to the y data currently being scanned from the spectrometer. The output then undergoes a negative logarithmic function to convert the output to absorbance (thick orange line). This absorbance data is then bundled with x (wavelength) data to produce the absorbance graph on the user front panel.

5.13 (g) Select baseline reference wavelength

This section of code allows the user to select wavelengths on the absorbance graph by using a cursor (see user front panel). The cursors position is then used to index the absorbance spectrum array and pick out the desired absorbance value.

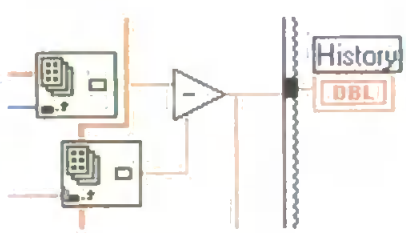

5.13 (h) Output baseline corrected data to graph

This section performs a ratio of wavelength as selected by "diode select" and the cursor position (performing baseline correction) and outputs the absorbance value to the history chart on the front panel..

Log History Data to File

Sequence structure three (Figure 5.14) of the scan and display loop basic function is to log data to file. The user specifies the wish to save data to a file by switching the front panel "log data to file switch" on. This switches the Boolean logic functions in the sequence to true. With this condition met, the sequence then takes the specified wavelength value and the absorbance values of the history graph from the sequence local variables (orange arrows on bottom of sequence). The program then builds them into an array with the global variable "elapsed time" and logs them to a spreadsheet file in CSV (comma separated variable) format. This continues until the user switches the "log data to file" button on the front panel again to stop the data logging to file. However this operation does not stop the continuous acquisition of data; only the global variable "STOP" button stops all manifold control and spectrometer scan acquisition.

Save Reference Spectrum

Sequence four (Figure 5.15) of the scan and display loop takes reference x scale (wavelength) data and y scale (raw counts) data and saves them to a spreadsheet file. When the front panel "save reference spectrum" (red button) is pressed the Boolean logic function (green TF button) is then true. The sequence then takes the two 1-D arrays of raw y data (blue sequence local) and x data (wavelength) (orange sequence local) and merges them into a 2-D array, writing x values (wavelength) against y values (raw count intensity). The "for loop" structure (resembling a stack of paper) executes this function N times, where N is the number of values in the array. The raw y data in this sequence also constitutes a global variable and forms the Y reference array, "Y Ref Array" (I_0 in the calculation of absorbance), that is used in latter sequences to convert raw y response into an absorbance response.

Save Absorbance Spectrum

Sequence five (Figure 5.16) of the scan and display loop takes x scale (wavelength) data and y scale (absorbance) data and saves them to a spreadsheet file. When the user presses the front panel "save absorbance spectrum" (red button), the Boolean condition is then set to true and the loop merges two 1-D arrays of x and y data and writes them to file. The primary difference between this sequence and sequence four (Figure 5.15) is that the "Y Ref array" (I_0) global variable created in sequence four has now undergone the negative logarithmic function ($A = - \log (I / I_0)$ to convert raw y data (I) to absorbance.

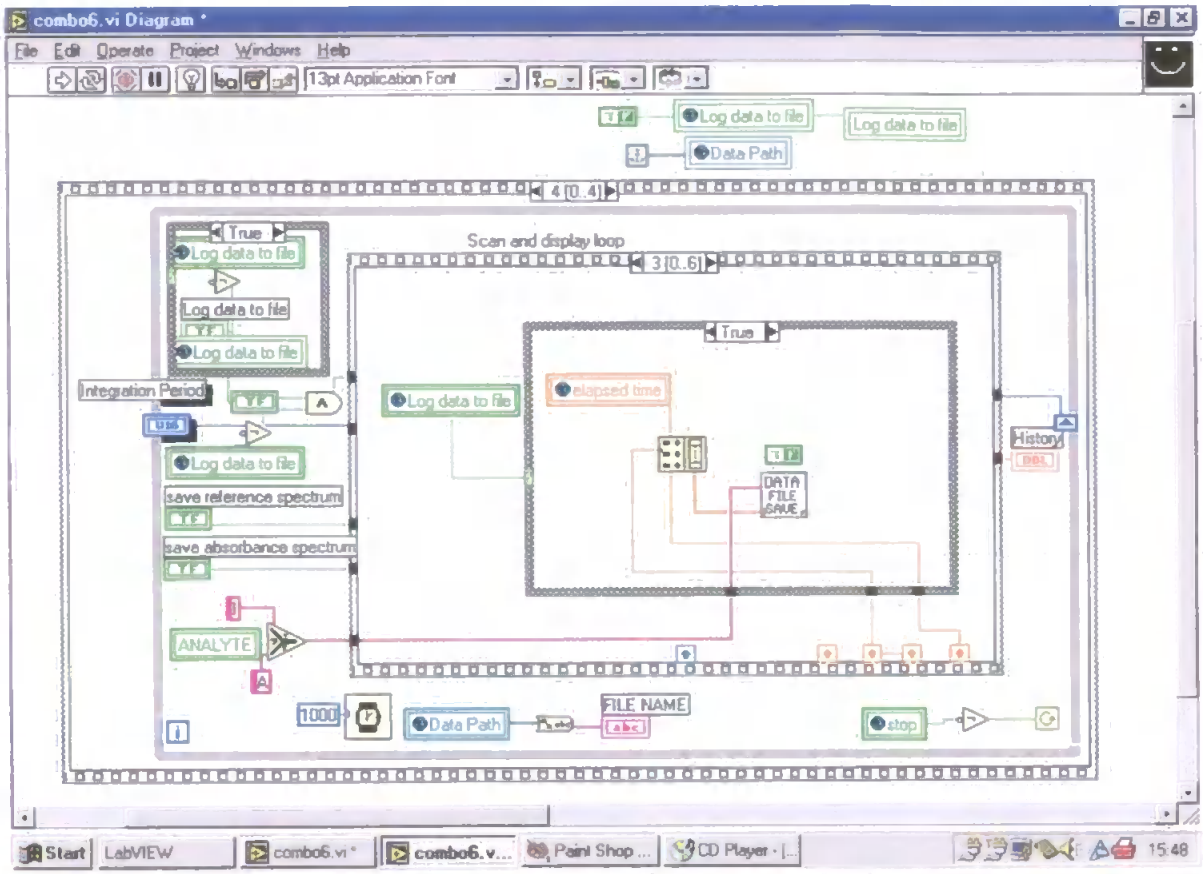

Figure 5.14 Sequence structure 3, graphical code responsible for saving history data to file.

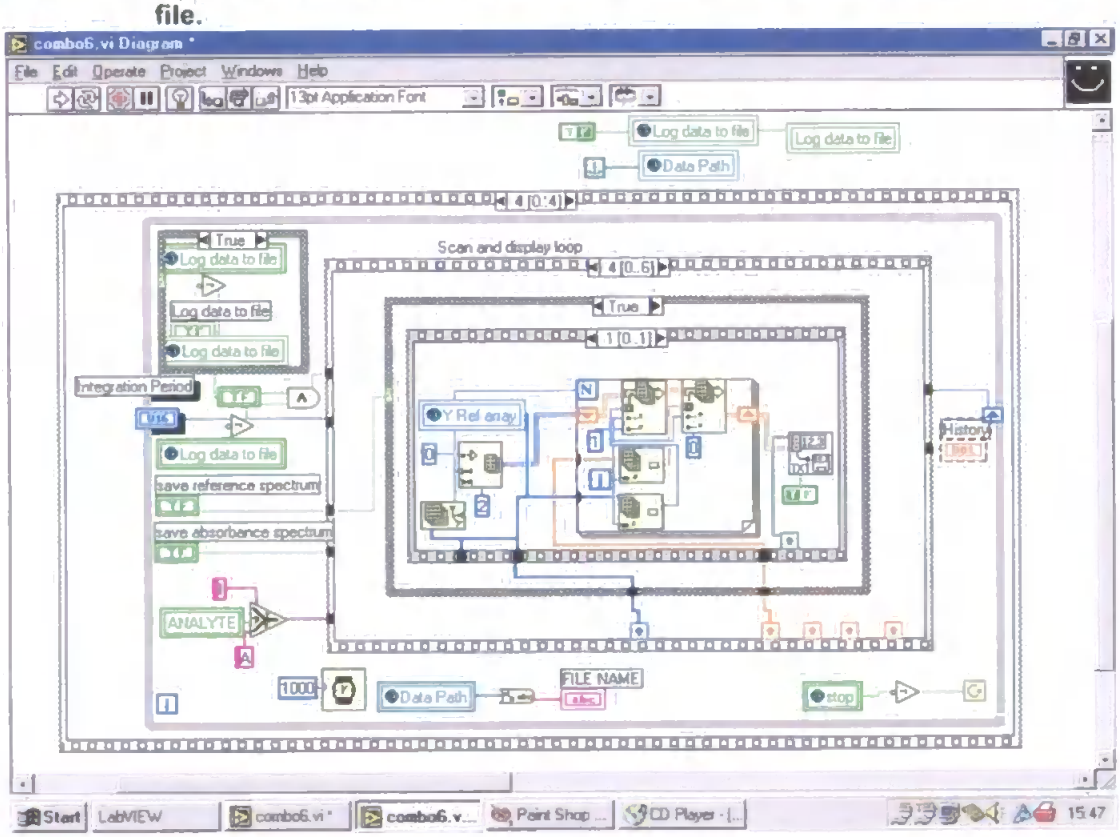

Figure 5.15 Sequence structure 4, graphical code responsible for saving reference spectrum to file.

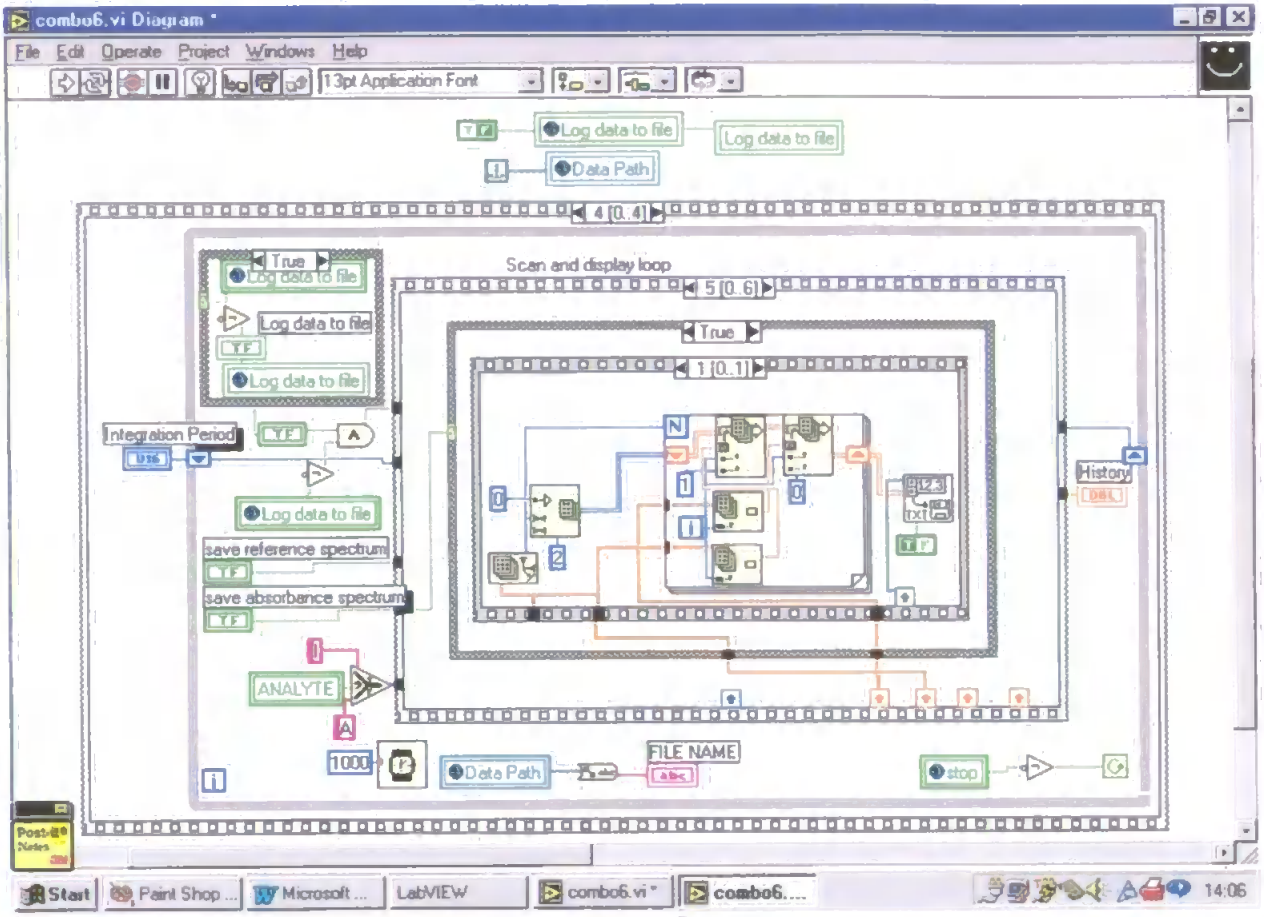

Figure 5.16 Sequence structure 5, graphical code responsible for saving absorbance spectrum to file.

(e) VI HIERACHY OF OVERALL PROGRAM

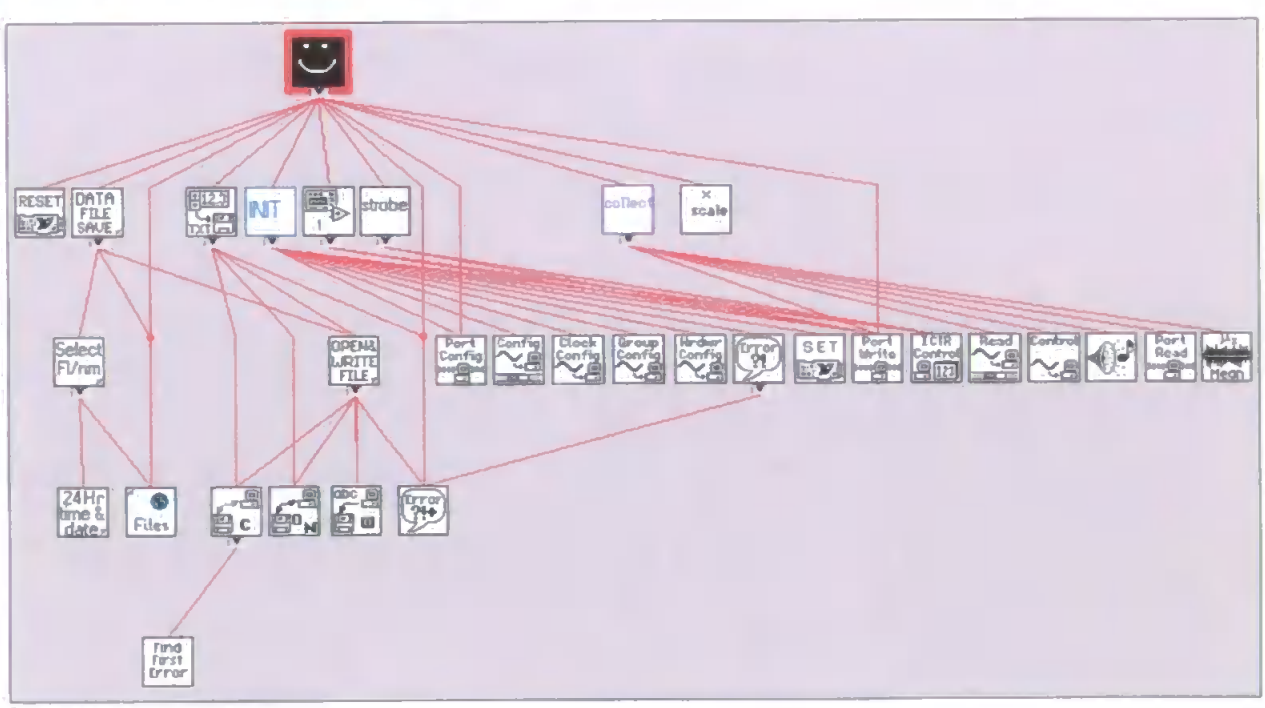

Figure 5.17 VI Hierarchy for nitrate monitor automation program.

Figure 5.17 shows the VI Hierarchy diagram for the automation program. The Hierarchy window displays a graphical representation of the order in which all VIs in memory address or call each other and displays the dependency of VIs upon other VIs. As discussed in section 5.3.1 (a) LabView allows the creation of VIs which can be used as subVIs in the block "wiring" diagram of higher level VIs. A subVI is analogous to a subroutine in a conventional text-based language. The top-level VI (main application program) calls lower level subVIs to perform the desired operations on the data as it flows through the block diagram. This modular approach makes applications easy to understand, debug and maintain. The main VI "combo6.VI" first calls on the subVIs immediately below it (e.g. reset, init, collect, x scale), these lower subVIs have their own hierarchy and call on other lower level subVIs to perform the desired operations.

5.3.2 MICRO-ELECTRONIC CONTROLLER

Figure 5.18 shows a simplified version of the microelectronic circuit that controlled the automation and timing sequences of the manifold hardware (micro-solenoid pumps and electronic switching valves). Figure 5.19 shows a block diagram representing this circuit. The primary feature of the circuit is the controlling quad digital to analogue converter (DAC). The microelectronic chip consists of four DACs but only three of these were used. 8 bit binary data from port A in the control section of the main LabView VI was written to the DAC. Addresses 0 and 1 come from port B (manifold control VI, section 5.3.1 (c)) and indicate which pumps are active.

The output from the DAC passes to voltage to frequency converters, which convert the signal into a pulse train (of the order of 2 KHz). However the pumps are unable to operate at these high frequencies, therefore the signal is then passed to a frequency divider where the signal is divided by 32 to a realistic value able to drive the solenoids of the micro-pumps. This approach was taken due to the increased reliability of running the voltage to frequency converters at high rates and then separately dividing frequency down as opposed to attempts to run the converters at lower frequencies. Switching valves (sample loop, carrier and analyte choice) are configured from port C in the manifold control section of the main LabView VI.

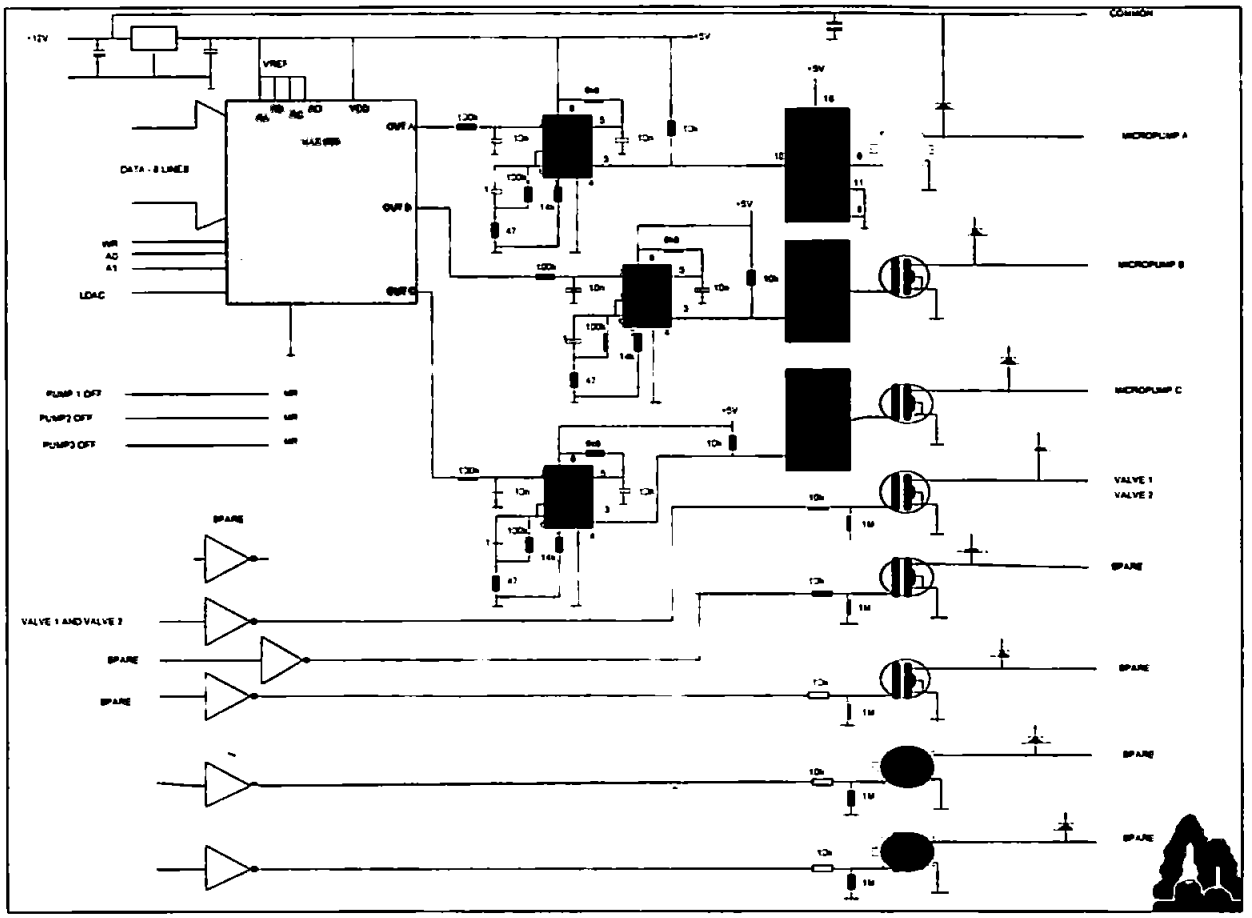

Figure 5.18 **Microelectronic controlling circuit.**

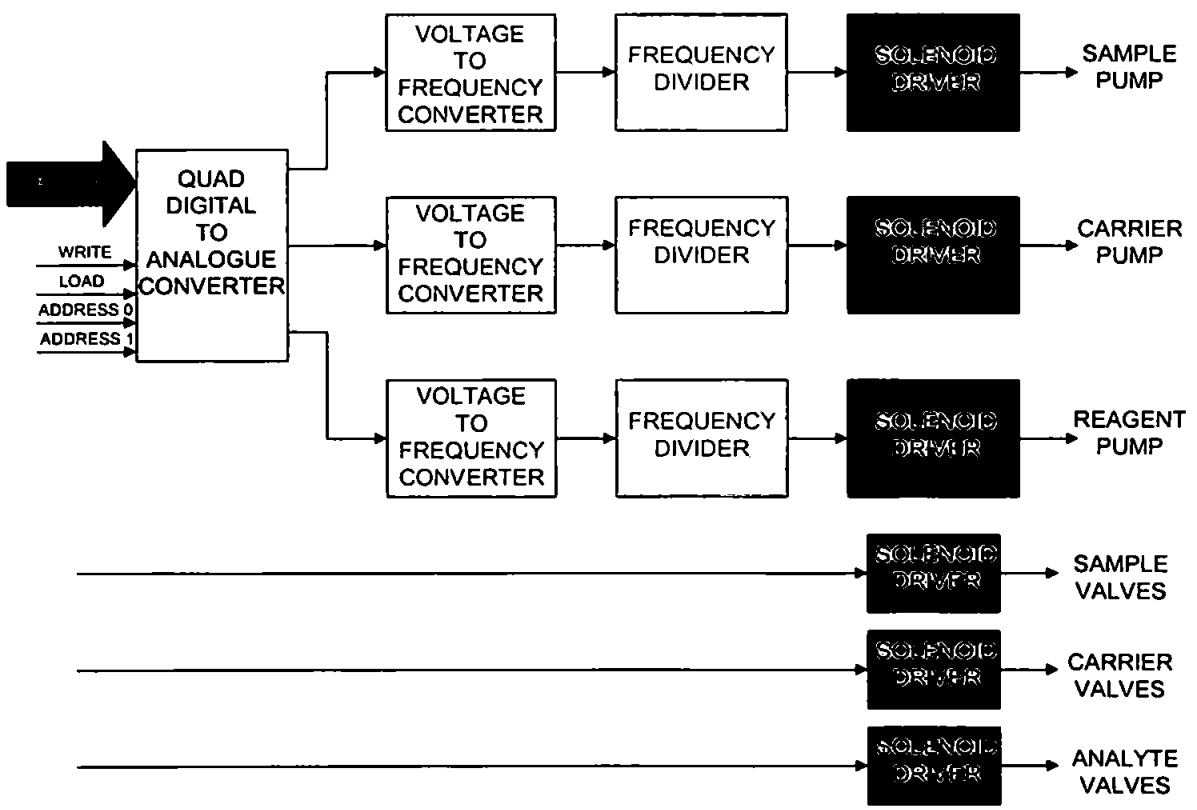

Figure 5.19 **Block diagram of microelectronic controller.**

5.3.3 LABORATORY OPTIMISATIONS

(a) MICRO-PUMP CALIBRATION

Table 5.2 shows the calibration data obtained for the sample, carrier and reagent micro solenoid pumps for the range 0 – 50 (digital units). Using the linear equations obtained, digital pump rates entered on the user front panel of the main VI can be converted to flow rates in ml min^{-1}. Therefore the flow rate range 0 – 50 digital units corresponds to flow rate ranges of 0 – 2.6 ml min^{-1}, 0 – 2.1 ml min^{-1} and 0 – 1.7 ml min^{-1} for sample, carrier and reagent micro pumps respectively. The gradients are different for each pump due to individual physical differences in the micro pumps themselves e.g. slight differences in volumes, backpressures and solenoid activation time. The flow rate for the sample pump was not important and only had to be set sufficiently high to fill the sample loop in the time specified on the front panel controls. The optimum flow rates determined in Chapter Four for the nitrate manifold were 0.43 and 0.31 ml min^{-1} for carrier and reagent respectively. Therefore substituting these values into the linear equations (Table 5.2) the digital pump rates for the carrier and reagent micro pumps were calculated as 10 and 8.

Table 5.2 Flow rate linear regression data for solenoid micro-pump calibrations (range 0 – 50 digital units).

PUMP	GRADIENT (ml min^{-1}) digital pump $unit^{-1}$	r^2
SAMPLE	0.0516	0.9990
CARRIER	0.0412	0.9987
REAGENT	0.0339	0.9985

(b) BASELINE STABILITY

Figure 5.20 shows the typical baseline stability observed while monitoring under the conditions specified in section 5.2.4 (A). Mean absorbance for a 1-hour acquisition (sampling rate every 2 s) was 0.004 A.U. ± 0.006 A.U. (3 s.d.) and illustrates the stability of the system over at least this time duration.

Error bars represent ± three standard deviations for all absorbance values obtained (n = 1800, t = 3600 s) during the 1-hour acquisition. The spikes in the baseline were attributed to power fluctuations caused by other laboratory equipment switching ON and OFF.

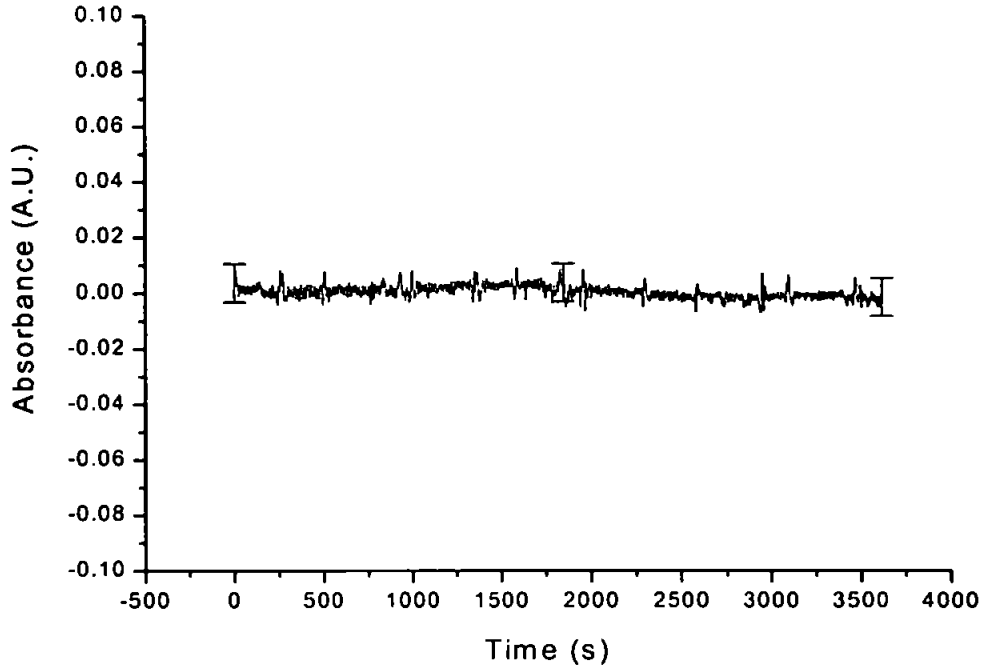

Figure 5.20 **Baseline stability of automated nitrate monitor (monitored at 597 nm – 444 nm) over a period of 1 hour, error bars showing ± 3 s of the complete data set have been added at t = 0, 1800 and 3600 s.**

(c) CALIBRATION OF THE AUTOMATED NITRATE MONITOR

Figure 5.21 shows a typical calibration of the automated nitrate monitor using the optimum manifold parameters identified in section 4.3.7. Excellent linearity (r^2 = 0.9998, n = 7) was achieved for the concentration range used. The limit of detection (calculated from the mean of the blank plus three times the standard deviation of the blank) was 0.007 mg l^{-1} NO_3-N, which compares well with the limit of detection calculated for the conventional nitrate manifold (section 4.3.8) of 0.006 mg l^{-1} NO_3-N. This suggests that the conversion of the nitrate manifold to an automated system was successful and sufficiently sensitive for the determination of nitrate in natural (unpolluted) waters.

(d) EXTENSION OF THE LINEAR RANGE

Extension of the linear range utilising the multi-wavelength capabilities of the spectrometer was discussed in Chapter 3 for the determination of ammonia. To increase the deployment potential of the automated monitor it was necessary to adapt it to determine nitrate in impacted (polluted) as well as pristine waters, thereby improving its versatility for deployment in a range of different field environments.

The River Frome, Dorset, U.K. (field trial, see section 5.2.3 (b)) experiences concentrations up to approximately 9 mg l^{-1} NO_3-N, and was identified as a potential site for field deployment. It was decided to adapt the nitrate monitor to be able to provide reliable analytical field data for this higher concentration range.

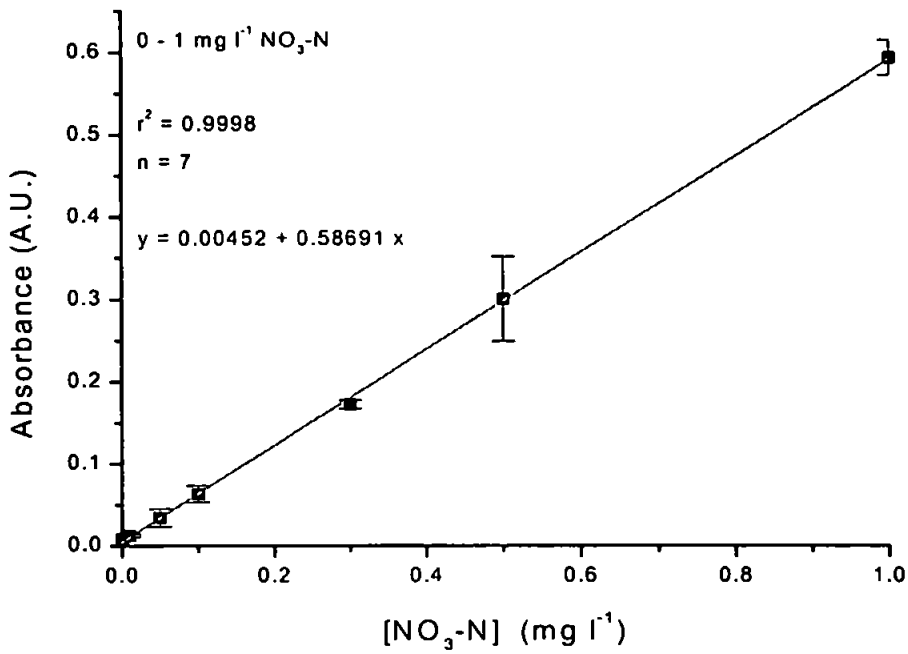

Figure 5.21 Automated nitrate monitor calibration graph (0 – 1 mg l^{-1} NO_3-N); error bars represent ± 3 standard deviations.

The simplest way to extend the linear range of a FI monitor is to reduce the sample volume that is injected into the manifold, thereby increasing dispersion. Therefore sample loop volume was reduced from 260 µl value as determined by McCormack[292] and David[293] and used in section 5.3.3 (c) for the concentration range (0 – 1 mg l^{-1} NO_3-N) to 90 µl. In addition, less sensitive wavelengths of the nitrate azo dye spectrum were monitored. Table 5.3 shows the linear regression equations obtained from calibration at 0 – 9 mg l^{-1} NO_3-N when monitoring at different wavelengths with a 90µl sample loop. Initial monitoring at $\lambda_{max.}$ (597 nm) minus a baseline reference wavelength at 444 nm, showed that linearity was lost due to the higher range standards giving absorbance values that were beyond the previously determined linear range of the instrument (section 2.3.4, photometric linearity).

Calibration at a less sensitive (1/2 peak maximum) wavelength 540 nm – 444 nm improved the range of the instrument (0 – 9 mg l^{-1} NO_3-N), but linearity was lost at the top of the concentration range (r^2 = 0.9979, n = 5, for 0 – 7 mg l^{-1} NO_3-N).

Table 5.3 Linear regression equations for 0 – 9 mg l^{-1} NO_3-N calibrations at different wavelengths

Wavelengths monitored (nm)	GRADIENT (A.U. $l \cdot mg^{-1}$)	INTERCEPT (A.U.)	r^2
597 - 444	0.2078	0.0348	0.9478
540 - 444	0.1117	0.0430	0.9909
510 - 444	0.0592	0.0015	0.9988

This was not considered sufficient for the nitrate levels expected at the River Frome deployment site. At 510 nm – 444 nm (1/4 of peak maximum), the monitors performance was linear up to 9.0 mg l^{-1} NO_3-N with good reproducibility (< 2 % R.S.D). Therefore (510 nm – 444 nm) was identified as the best measurement protocol for this particular deployment. This approach to optimising the linear range shows the power of the instrumentation for field deployment. A number of linear ranges can be predetermined in the laboratory and changed instantly in the field to suit the local environmental requirements. This would not require any prior knowledge of the local conditions. It would also be possible to build some remote decision making into the instrument so that concentration ranges could be adjusted automatically, e.g. to monitor a rainfall event after a dry period in which a sudden, short term rise in NO_3-N would be expected to occur.

5.3.4 LESOTHO EXPEDITION FIELD TRIAL

(a) AUTOMATED MONITOR RELIABILITY

Plate 5.6 shows the automated nitrate monitor sampling from the Tsoelikane river next to the basecamp location shown in Figure 5.7. Although the inherent portability of the monitor was demonstrated with field deployment in a remote location very little field data was obtained. This was due to blockages within the electronic switching valves used in the injection procedure (Figures 5.1 & 5.2) that could not be remedied with the tools available in the field. The blockage occurred in the NO / COMM position of the first switching valve after the micro sample pump. In addition the housing of the manifold was not fully ruggedised, particularly with respect to

temperature. Although temperatures during the day were in the range 0 °C – 22 °C, nightly temperatures fell to as low as – 20 °C. Reagents were stored in inner tent compartments overnight and therefore not subjected to such extreme temperatures. However the instrumentation was stored overnight in outer tent compartments (due to size restrictions) and some freezing within the switching valves occurred.

(b) NATIONAL PARK AND LEQOOA MOUNTAIN CATCHMENT FIELD DATA

In addition to the deployment of the automated nitrate monitor an intensive manual sampling and field analysis campaign was undertaken using commercially available instrumentation and chemical test kits. 36 sampling sites were tested during the four-week campaign, 22 sites within the Sehlabathebe National Park and 14 in the Leqooa mountain catchment, Plates 5.7 – 5.8 show typical sampling sites and Plate 5.9 shows a typical "roaming camp" used when travelling between sampling site areas. All physico-chemical data are presented in Tables 5.4 and 5.5. Data presented for nitrate, nitrite, ammonia and phosphorus concentrations, pH, conductivity, dissolved oxygen and flow rate, represent mean averaged values for the data collected. Site descriptions, macro-invertebrate data and cross sectional area data for all 36 sampling sites, and ICP-MS semi-quantitative analysis data for the first 20 sampling sites of the National Park, are all reported in Appendix II.

Plate 5.6 **Automated nitrate monitor sampling from Tsoelikane River adjacent to basecamp in Sehlabathebe National Park**

Plate 5.7 Biogeochemistry Team collecting field data (directly downstream from Plate 5.6)

Plate 5.8 Typical terrain and sampling site location in National Park. Main River Tsoelikane with adjoining mountain stream tributary. (Picture taken from Kepising (translated: The Cap) facing directly east (see Figure 5.7))

Table 5.4 **Physico-chemical data for Sehlabathebe National Park sampling sites 1 – 22.**

SITE NO.	GRID	POSITION.	ALT. (ft)	DATE	TIME	NO_3-N (mg l^{-1})	NO_2-N (mg l^{-1})	NH_3-N (mg l^{-1})	PO_4 (mg l^{-1})	pH	COND. (µS)	D.O. (%)	SOIL pH	SOIL TYPE	TURB. (F.A.U)	FLOW (ms^{-1})	TEMP. (°C)
1	125083	S 29 53.717 E 029 07.690	7700	26-Jul	11.00	0.05	0.042	0	1.63	7.71	51.3	79.0	5.5	-	2	0.19	
2	116071	S29 53.132 E 029 07.285	7800	26-Jul	14.15	0.03	0.008	0	0.39	7.93	52.5	82.4	6.0	SANDY LOAM	3	0.11	11.8
3	143090	S 29 54.154 E 029 08.868	7545	27-Jul	10.20	0.05	0.012	0.15	0.55	7.95	104.7	68.2	6.0	SANDY LOAM	0	N/A	11.8
4	128099	S 29 54.605 E 029 07.957	7680	27-Jul	14.30	0.06	0.011	0.04	0.30	8.15	94.3	71.9	5.5	CLAY LOAM	0	0.15	9.9
5	116085	S 29 53.901 E 029 07.351	7400	28-Jul	10.45	0.062	0.019	0.08	0.64	7.50	49.9	69.9	6.5	GRITTY LOAM	0	0.09	6.7
6	109097	S 29 54.485 E 029 06.766	7300	28-Jul	13.40	0.07	0.039	0.10	0.24	8.44	39.0	74.7	6.5	SILTY CLAY	2	0.18	8.8
7	108098	S 29 13.621 E 029 06.770	7600	29-Jul	10.05	0.06	0.003	0.05	0.23	8.06	91.5	72.4	6.5	SILTY CLAY	12	N/A	5.8
8	095092	S 29 54.156 E 029 05.904	7500	29-Jul	12.30	0.07	0.012	0.02	0.29	7.27	57.8	62.8	7.0	SILTY LOAM	4	0.11	7.3
9	133074	S 29 53.321 E 029 08.292	7758	31-Jul	09.15	0.06	0.010	0.02	0.19	6.84	32.2	52.2	5.5	SILTY LOAM	0	0.14	5.1
10	149079	S 29 53.235 E 029 09.419	7673	31-Jul	13.10	0.05	0.013	0.10	0.37	6.16	7.8	56	4.5	SILTY LOAM	2	N/A	7.2
11	115046	S 29 51.781 E 029 07.123	6700	01-Aug	10.00	0.06	0.008	0.06	0.16	6.70	7.8	76.2	6.0	SILTY CLAY	0	N/A	3.4

Table 5.4 contd. Physico-chemical data for Sehlabathebe National Park sampling sites

SITE NO.	GRID	POSITION	ALT. (ft)	DATE	TIME	NO_3-N (mg l^{-1})	NO_2-N (mg l^{-1})	NH_3-N (mg l^{-1})	PO_4 (mg l^{-1})	pH	COND. (µS)	D.O. (%)	SOIL pH	SOIL TYPE	TURB. (F.A.U)	FLOW (ms^{-1})	TEMP. (°C)
12	112043	S29 51.598 E 029 06.901	6832	01-Aug	11.50	0.07	0.019	0.06	0.21	7.36	24.0	74.8	6.0	SILTY CLAY	-	0.09	6.3
13	125056	-	-	01-Aug	14.20	0.05	0.011	0.03	0.28	7.28	30.8	78.0	6.0	SANDY CLAY	0	0.08	7.0
14	075119	S 29 54.872 E 029 05.221	7546	02-Aug	10.30	0.04	0.010	0.10	0.15	7.46	45.4	74.1	5.5	SILT	0	0.16	5.9
15	093122	S 29 55.811 E 029 05.752	7580	02-Aug	13.00	0.09	0.020	0.13	0.16	7.72	54.0	79.6	5.5	SILT	1	0.05	10.9
16	096117	S 29 55.595 E 029 05.964	7484	02-Aug	-	0.06	0.012	0.01	0.18	7.44	51.8	78.9	6.0	SILT	0	N/A	7.8
17	054106	S 29 52.189 E 029 06.732	8067	03-Aug	10.05	0.05	0.022	0.03	0.21	7.17	80.4	73.6	5.5	SILT LOAM	0	0.12	5.2
18	096055	S 29 52.346 E 029 06.240	8156	03-Aug	12.25	0.09	0.610	0.15	0.14	7.58	78.2	76.15	5.5	SILT LOAM	2	0.12	8.2
19	102056	S 29 52.356 E 029 06.408	8144	03-Aug	14.15	0.03	0.013	0.14	0.18	7.60	29.0	71.8	5.0	SILT LOAM	9	N/A	6.8
20	153104	S 29 54.853 E 29 8.198	7802	04-Aug	09.50	0.03	0.014	0.08	0.35	7.21	113.9	72.4	6.0	SILT	5	0.12	2.9
21	107078	S 29 53.489 E 029 06.666	8000	05-Aug	09.50	0.06	0.020	0.05	0.15	7.07	12.4	81.4	5.0	LOAMY SAND	2	N/A	4.2
22	102078	S 29 53.310 E 029 06.325	8107	05-Aug	12.30	0.12	0.043	0.10	0.23	7.06	24.8	69.4	6.0	SANDY LOAM	2	N/A	7.3

Table 5.5 Physico-chemical data for Leqooa Mountain Catchment sampling sites 23 – 36

SITE NO.	GRID	POSITION	ALT. (ft)	DATE	TIME	NO_3-N (mg l^{-1})	NO_2-N (mg l^{-1})	NH_3-N (mg l^{-1})	PO_4 (mg l^{-1})	pH	COND. (µS)	D.O. (%)	SOIL pH	SOIL TYPE	TURB. (F.A.U)	FLOW (ms^{-1})	TEMP. (°C)
23	016996	S 29 49 076 E 029 00.999	7850	10-Aug	08.45	0.11	0.033	0.06	0.06	7.74	65.9	77.2	6.0	SANDY LOAM	2	0.12	5.5
24	029955	S 29 46.813 E 029 01.736	8487	10-Aug	13.20	0.27	0.010	0.04	0.79	8.19	71.2	73.0	6.5	LOAM	3	0.04	7.4
25	035925	S 29 45 317 E 029 02.241	8530	12-Aug	8.40	0.47	0.013	0.03	0.18	7.83	77.8	68.5	6.0	SANDY LOAM	0	0.40	4.6
26	035936	S 29 45.810 E 029 02.110	8500	12-Aug	11.15	0.54	0.060	0.05	0.14	7.85	119.6	60.9	5.5	SANDY LOAM	0	0.04	11.7
27	029941	S 29 46.071 E 029 01.884	8500	12-Aug	14.05	0.34	0.053	0.04	0.19	8.13	65.8	56.3	6.0	SANDY LOAM	0	0.15	15.1
28	027965	S 29 47.333 E 029 01.692	8338	13-Aug	09.30	0.20	0.015	0.05	0.09	8.04	72.8	72.5	5.5	SANDY LOAM	0	0.27	5.7
29	018989	S 29 48.544 E 029 01.176	7593	13-Aug	12.25	0.31	0.015	0.02	0.09	8.37	47.6	60.1	6.0	SANDY LOAM	2	0.83	10.7
30	058017	S 29 50.104 E 029 03.779	7640	15-Aug	10.00	0.07	0.027	0.13	0.22	8.31	58.4	42.3	6.0	SANDY LOAM	4	0.27	3.5
31	042023	S 29 50.608	7600	15-Aug	12.15	0.59	0.020	0.12	0.25	7.11	76.8	29.9	6.0	LOAM	-	-	-
32	049035	S 29 51.170	7320	15-Aug	14.30	0.23	0.022	0.10	0.19	7.10	71.0	70.1	6.0	SANDY LOAM	0	0.31	7.5
33	032031	S 29 51.165	7500	16-Aug	09.05	0.44	0.034	0.02	0.17	8.28	3.2	34.4	6.0	SANDY LOAM	0	0.25	1.6
34	025029	S 29 50.802	7649	16-Aug	11.30	0.49	0.023	0.14	0.30	7.92	23.6	31.3	6.0	SANDY LOAM	1	0.08	9.6
35	019022	S 29 50.387	7654	16-Aug	13.25	0.40	0.036	0.03	0.20	8.65	117.2	31.5	6.0	SANDY	1	0.44	12.2
36	008013	S 29 50.011	7640	17-Aug	08.30	0.49	0.026	0.07	0.07	8.33	146.4	31.9	6.0	SANDY	0	0.09	3.3

Plate 5.9 **Roaming sampling camp in Leqooa mountain catchment. Altitude approximately 10 000 ft with main Drakenburg Escarpement to the north (background)**

Figure 5.22 shows nutrient data for the 36 sampling sites studied during the course of the expedition. To the left of the dotted line are sites 1 – 22, surveyed in Sehlabathebe National Park, and to the right of the line are sites 23 – 36, corresponding to the Leqooa mountain catchment. Concentrations are presented in μM to provide direct comparison of N. The nutrient data are also presented as a box and whisker plot (Figure 5.23) for the Sehlabathebe National Park and the Leqooa river mountain catchment. Each box contains the complete data set recorded for the study area. The bottom symbol (x) represents the minimum values within that data set, the *" 0^{th} percentile"*. The bottom whisker (vertical line from main box) marks the *"5^{th} percentile"*. The bottom of the box marks the *"25^{th} percentile"* with the median value, *"50^{th} percentile"* being represented by the horizontal line. The top edge of the box marks the *"75^{th} percentile"* and the top whisker the *"95^{th} percentile"*. The square symbol in the box marks the position of the arithmetic mean. The symbol above the top whisker marks the *"100^{th}"* (maximum value in data set) percentile.

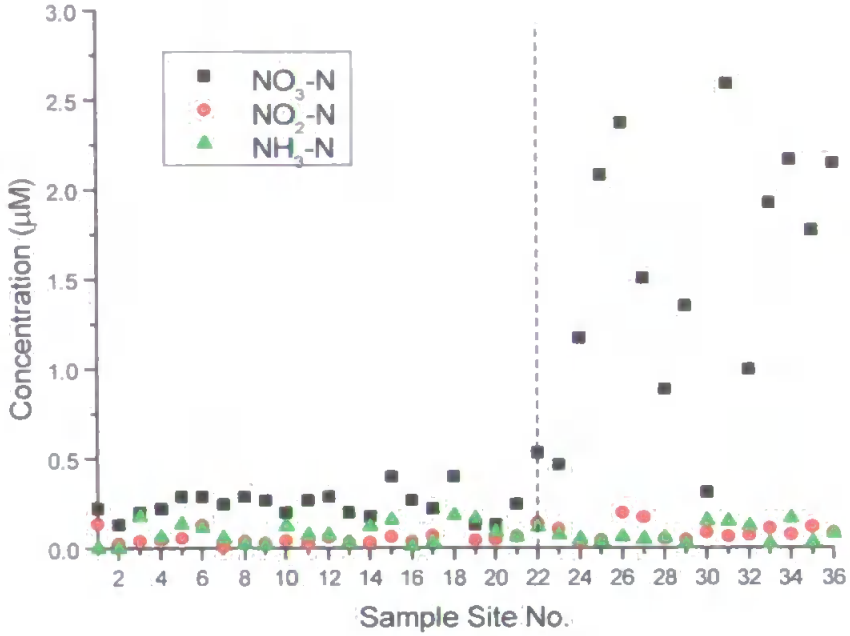

Figure 5.22 **Plot of mean nitrate, nitrite and ammonia concentrations (µM) for sampling sites 1 – 36.**

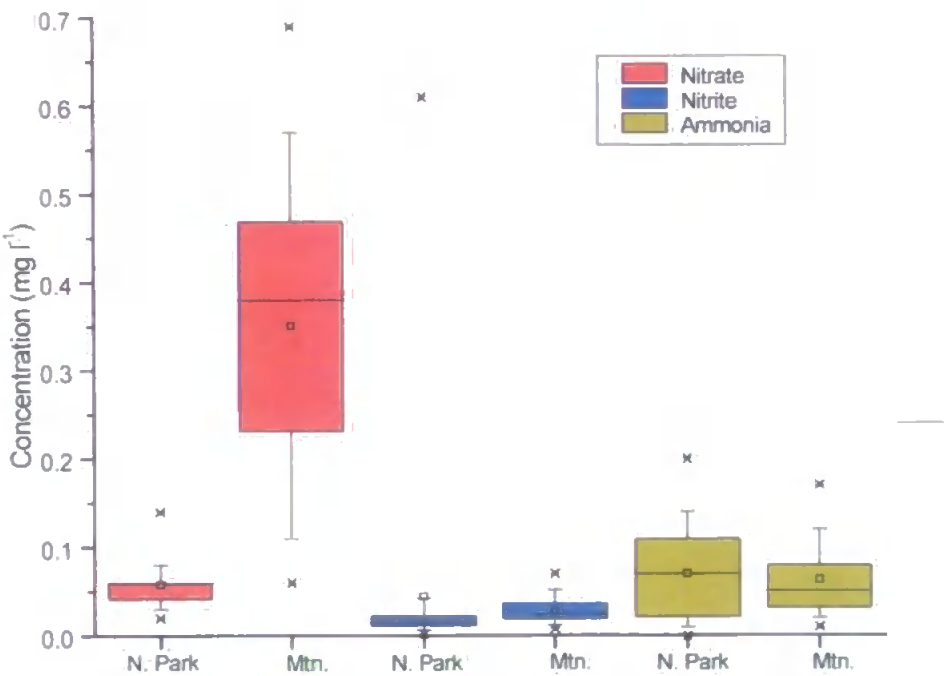

Figure 5.23 **Box and Whisker plot of nutrient data for Sehlabathebe National Park and Leqooa River Mountain Catchment.**

The nitrogen results for the National Park sites show consistently low concentrations for all three parameters (nitrate, nitrite, and ammonia). Given the semi-quantitative nature of the test kits the main

conclusions that can be drawn are that the water was of high quality (e.g. concentrations were significantly lower than the guideline levels for drinking water in the EU). Comparison of the National Park mean concentration of 0.054 mg l^{-1} NO_3-N with UK nitrate data for selected rivers is shown in Appendix II. The mean concentration for the River Teith (0.2 mg l^{-1} NO_3-N) which drains from pristine upland moor, indicates that the National Park has very little impaction from traditional sources (atmospheric deposition, diffuse input from agriculture and point sources) and can be classified as pristine. In contrast, the nitrate data from the Leqooa mountain catchment showed higher nitrate levels at certain sites. Those at 31, 33 and 34 correlate with centres of populations, (31 – Ha Soloja Lipelong village, 33 and 34 – Ha Sephelane village; agricultural villages) and the elevated levels are probably derived from domestic sewage inputs and agricultural run-off. Elevated levels at sites 35 and 36 are most likely to have arisen from the grazing of cattle in the local vicinity. The elevated levels at sites 24 – 28 are in the mountainous region of the catchment and are likely to be associated with atmospheric deposition of particulate matter carrying adsorbed NO_x from the highly industrial regions of Johannesburg (approximately 300 miles NNW from the National Park) and Durban (approximately 150 miles East from the National Park) (dependent on wind direction). Although nitrate concentrations in the Leqooa mountain catchment are elevated in comparison with those of the National Park, comparison of the mean concentration (0.35 mg l^{-1} NO_3-N) with those in Appendix II still indicate that concentrations are low and the river water is of pristine quality.

When considering an environmental interpretation of the data it is important to note that the campaign was undertaken in the dry season, with negligible rainfall, and that the chemical data was obtained with semi-quantitative dry reagent kits. There was also very little opportunity to re-analyse or re-sample due to the intensive nature of the fieldwork. Nonetheless the results provide a unique dataset from an inaccessible but generally pristine environment. This will allow the environmental impact of any future development, e.g. the proposed building of a road through the National Park and with it an increased population and vehicular traffic, to be assessed.

5.3.5 RIVER FROME FIELD TRIAL

(a) FIELD CALIBRATIONS

Field calibrations were performed each evening prior to setting the monitor to full automated mode to run continuously through the night. Figure 5.24 shows a typical calibration graph for the calibration

standards used (0 – 9 mg l^{-1}, NO_3-N). Both baseline stability (see section 5.3.3 (b)) and reproducibility were found to be excellent with typical R.S.D.s (n = 3) of less than 2 %.

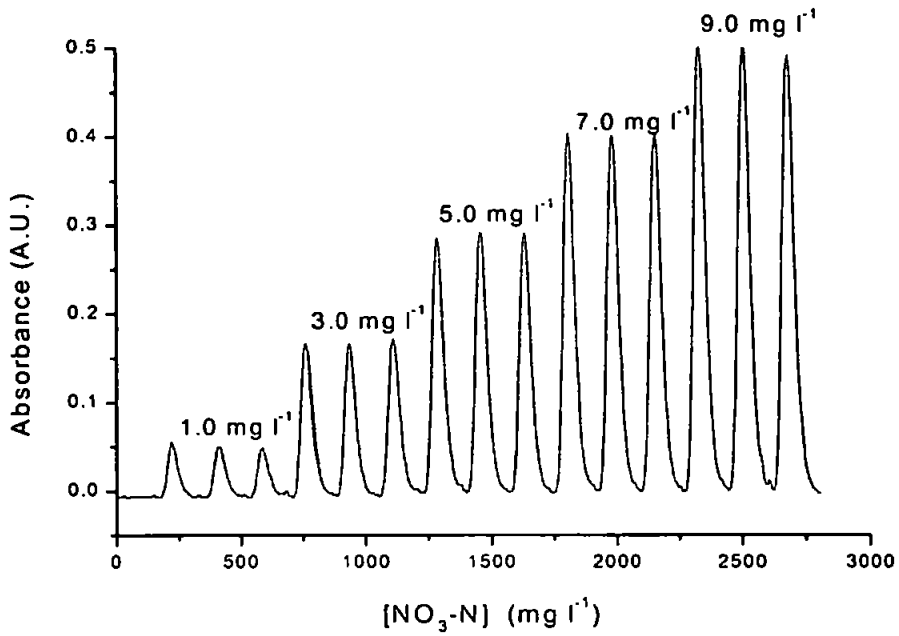

Figure 5.24 Typical field calibration data (River Frome) (0 – 9 mg l^{-1}, NO_3-N); monitored at 597 nm – 444 nm.

Table 5.6 compares the statistical data from each daily calibration. With the exception of the results obtained for the 3 and 9 mg l^{-1} NO_3-N standards on day 2 and the 1 mg l^{-1} NO_3-N standard on day 3, reproducibility between replicate injections was excellent, typically less than 2 % RSD (n = 3), with pooled (all three calibrations) R.S.Ds of less than 4 % (n = 9). Linear regression coefficients for all calibrations were good (pooled result : r^2 = 0.9998, n = 6) and the sensitivity of the system did not change during the 48 h sampling campaign. When monitoring at a less sensitive wavelength (e.g. 510 – 444 nm) (section 5.3.3 (d)) and using a smaller sample loop (90µl) no signal was observed for a blank Milli-Q water injection.

The sensitivity remained stable over the 48 h sampling period (24/06/99 – 27/06/99) but a noticeable degradation of the cadmium reductor column was observed, with a considerable reduction in packed volume from the beginning of the sampling campaign to the end. This was attributed to the higher concentrations of nitrate found in the River Frome in comparison with the lower concentrations (0 – 1 NO_3-N) that the system was originally designed for.

Table 5.6 **Comparison of field calibration data for the River Frome field trial from 24th June 99 to 27th June 99.**

[NO3-N]	Day 1		Day 2		Day 3		Pooled data	
	mean	R.S.D	mean	R.S.D	mean	R.S.D	mean	R.S.D
(mg l^{-1})	(A.U.)	(%)	(A.U.)	(%)	(A.U.)	(%)	(A.U.)	(%)
0	N/R	N/R	N/R	N/R	N/R	N/R	N/R	N/R
1	0.053	1.1	0.051	1.1	0.052	6.9	0.052	3.0
3	0.177	1.2	0.155	7.2	0.169	1.7	0.167	3.4
5	0.302	0.8	0.257	0.7	0.290	1.4	0.283	1.0
7	0.421	2.0	0.369	2.7	0.402	0.3	0.397	1.7
9	0.511	2.1	0.507	8.5	0.500	1.2	0.506	3.9
r^2	0.9988		0.9974		0.9990		0.9998	
gradient	0.058		0.055		0.056		0.056	
intercept	0.0015		-0.0071		0.0002		-0.0019	

Therefore it is recommended that for longer term deployments in high nitrate concentration environments a larger cadmium reductor column be used as opposed to the original column (dimensions specified in section 4.2.1). On-line dilution procedures incorporated into the manifold and even smaller injection volumes could also be used in conjunction with a larger cadmium column to ensure long term monitor performance at higher nitrate concentrations.

(b) AUTOMATED MONITOR RELIABILITY

Table 5.7 and Figure 5.25 show the results obtained from the monitor (running continuously) during the 48 h sampling campaign at the IFE. Abbreviations DT and CAL refer to instrument downtime and instrument calibration respectively.

Approximately 4 h was spent finding a suitable location within the Fluvarium in which the monitor could successfully sample from a flow channel. Attempts at sampling from directly above the flow channels proved unsuccessful due to the sample micro-pump being unable to pump the river water sample vertically upwards (1.5 m) to the manifold.

Table 5.7 Concentration data obtained over the 48 hour sampling campaign (DT = downtime, CAL = calibration, Sam = sample collected).

	real-time	Conc. (mg l^{-1})
Night1	22:10	6.4
24/05/99	22:40	6.6
	23:10	4.7
	23:40	3.2
25/05/99	00:10	2.8
	00:40	2.0
	01:10	2.0
	01:40	2.1
	02:10	1.8
	02:40	1.6
	03:10	1.6
	03:40	0.0
	04:10	2.0
	04:40	2.2
	05:10	2.2
	05:40	2.5
	06:10	2.4
	06:40	2.4
	07:10	2.3
	07:40	2.1
	08:10	2.0
DT	08:40	N/R
DT	09:10	N/R
DT	09:40	N/R
DT	10:10	N/R
DT	10:40	N/R
DT	11:10	N/R
Day1 / Sam1	12:00	5.8
Sam2	12:30	5.9
Sam3	13:00	5.7
Sam4	13:30	6.1
Sam5	14:00	6.3
Sam6	14:30	6.3
Sam7	15:00	5.6
Sam8	15:30	6.1
Sam9	16:00	5.9
Sam10	16:30	5.9
Sam11	17:00	5.8
CAL	17:30	CAL
CAL	18:00	CAL
CAL	18:30	CAL
Sam12	19:00	5.4

	real-time	Conc. (mg l^{-1})
night2	19:30	5.6
25/05/99	20:00	5.4
	20:30	5.6
	21:00	6.3
	21:30	6.3
	22:00	6.3
	22:30	5.5
	23:00	6.5
	23:30	6.5
26/05/99	00:00	6.5
	00:30	6.3
	01:00	0.0
	01:30	0.0
	02:00	5.8
	02:30	6.8
	03:00	6.7
	03:30	6.6
	04:00	6.7
	04:30	7.0
	05:00	7.1
	05:30	8.4
	06:00	8.1
	06:30	7.7
	07:00	7.7
	07:30	7.8
	08:00	7.7
day2 / sam13	08:30	6.8
DT	09:00	N/R
sam14	09:20	5.2
sam15	09:50	5.5
sam16	10:20	5.9
sam17	10:50	5.9
sam18	11:20	5.7
sam19	11:50	5.3
sam20	12:20	5.6
sam21	12:50	5.9
sam22	13:20	5.7
sam23	13:50	5.5
sam24	14:20	5.5
sam25	14:50	5.3
sam26	15:20	5.5
sam27	15:50	5.4
sam28	16:20	5.1
sam29	16:50	5.6
sam30	17:20	5.6
CAL	17:50	CAL
CAL	18:20	CAL
CAL	18:50	CAL
sam31	19:20	5.2
sam32	20:50	5.4

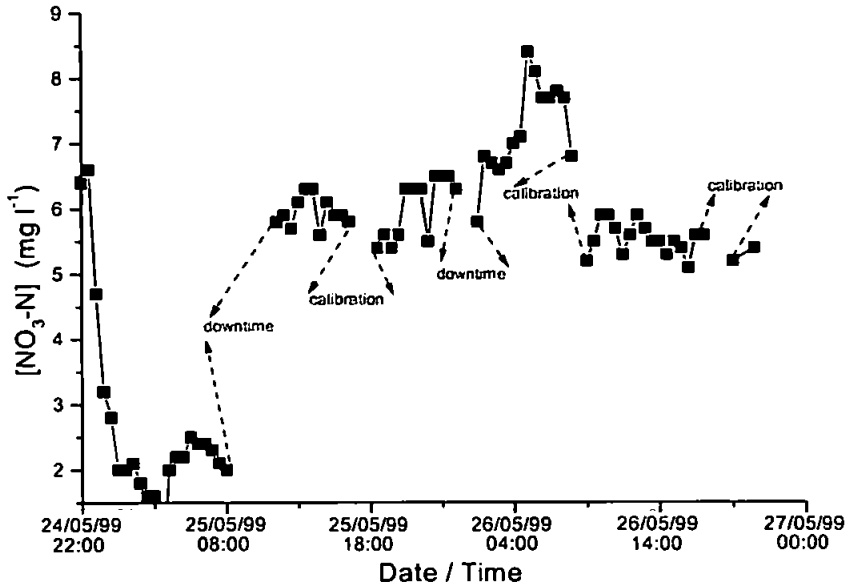

Figure 5.25 Concentration data obtained over the 48 hour sampling campaign.

The most successful sample introduction method was found to be a siphon arrangement (section 5.2.4 (c)) with the monitor sited below the flow channel (Plate 5.5). Installation of the monitor then took approximately 1 h. With exclusion of the setup and installation time but including calibration time the monitor ran for 3 days and acquired data over 48 hours with sampling occurring every 30 min. Two periods of instrumental downtime occurred during the field trial, the most severe after the first over-night run. Figure 5.25 shows the decline in monitor performance during the first over-night run with reported concentration values dropping to approximately 2 mg l^{-1} NO_3-N. The cause of the problem was traced to very small blockages occurring over time in the first electronic switching valve of the manifold (NO / COMM position, Figure 5.2). Although improvements in the sample collection protocol were made with the use of siphon configurations and larger filtration arrangements, the problems that occurred were identical to those experienced in the Lesotho field trial (5.3.4 (a)). The problem was overcome by the introduction of a rapid switching cycle (20 s) between the sample and carrier pumps (running at high flow rates of 100 digital pump units). The FI connector (COMM position, first sample switching valve, Figure 5.2) was disconnected from the manifold to reduced backpressure and air bubbles were introduced to the sample stream. Using this approach blockages were cleared from the switching valve quickly (< 30 min) and downtime was reduced. In general the monitor performed well and obtained field data for at least 48 h with a 30 min analysis frequency.

(c) DAYTIME OPERATION OF MONITOR.

There were large variations in air temperature in the Fluvarium, particularly the contrast between night / early morning operation and late afternoon / early evening operation. Due to the possibility of ambient air and water temperatures having an effect on the reaction kinetics, air, reagent and river temperatures (and river pH and conductivity) were recorded at each sample analysis time. Table 5.8 presents the data obtained during the daytime operation of the monitor. River pH varied slightly with a mean value of 8.22 and a range of ± 0.7 pH. This relatively large range was attributed to the fact that the pH meter needed re-calibrating every half-day and drifted considerably if a strict calibration routine was not applied. Conductivity readings (Table 5.8) were consistent and gave a mean conductivity of 633 μS with a range of ± 27 μS.

Figures 5.26 and 5.27 show plots of temperature variations and NO_3-N concentration data for the automated runs conducted during the daytime. Air temperatures were highly variable and depended upon the degree of sunshine that was impinging upon the Fluvarium. The Fluvarium had a glass roof, much like a greenhouse, and during a sunny period the heat in the Fluvarium rose significantly. This was particularly noticeable in the mornings (08:00) when air temperatures were approximately 12° C, by mid-morning (11:00) temperatures rose to approximately 20° C. However once the Fluvarium had warmed up temperatures stabilised and maintained at approximately 20° C, until slowly cooling in the evening.

Reagent temperatures (red traces, top graphs, Figures 5.26 & 5.27) experienced large differences between the beginning of the day from the end. Recorded reagent temperatures ranged from a minimum of 14.2° C to a maximum of 25.4° C on day 1, and from a minimum 13.0° C to a maximum of 25.5° C on day 2. River temperatures followed the natural diurnal cycle one would expect. Small increments in river temperature were observed from the early morning throughout the day as the river and surrounding land slowly heated up. The river temperature reached its maximum in the early evening and then slowly cooled overnight.

Although the monitors performance has not been assessed fully with respect to temperature it is clear that ambient temperatures, particularly reagent temperature, will affect the performance of the monitor. In light of the numerous factors that could affect performance it was decided that during the day when the monitor could be manned that a mid calibration range standard (5.0 mg l^{-1}

NO_3-N) should be run after each automated sample analysis. Figures 5.26 & 5.27 show the benefit of normalising the raw data response to that of a 5.0 mg l^{-1} NO_3-N standard response. Error bars for the 5.0 mg l^{-1} NO_3-N standard represent three standard deviations for replicate injections (n = 3) for that standard. Statistical analysis of the results obtained during the day runs are presented in section 5.3.5 (d).

Table 5.8 Associated data collected during daytime operation of the monitor.

Sample no.	Date	Time	Air (°C)	Reagent (°C)	River (°C)	pH	Conductivity (µS)
1 st calibration run (24/05/99) (21.00)							
	25/05/99	09.15	16.0	14.2	14.2	N/R	N/R
	25/05/99	11.20	19.4	17.5	15.1	N/R	N/R
1	25/05/99	11.50	21.4	18.6	15.4	7.6	630
2	25/05/99	12.30	19.2	18.5	15.4	7.6	660
3	25/05/99	13.10	21.0	19.9	15.1	8.2	647
4	25/05/99	13.45	20.0	20.8	15.9	7.5	632
5	25/05/99	14.20	20.0	21.6	16.0	7.6	642
6	25/05/99	14.50	20.4	23.2	16.3	7.6	630
7	25/05/99	15.30	20.5	24.8	17.2	8.2	632
8	25/05/99	16.00	20.2	25.4	16.2	8.2	632
9	25/05/99	16.35	19.6	25.3	16.6	8.6	632
10	25/05/99	17.05	20.2	24.5	16.5	8.5	630
11	25/05/99	17.35	19.9	23.5	16.5	8.4	630
2 nd calibration run (18.00)							
12	25/05/99	18.50	18.4	20.4	16.1	8.3	635
	25/05/99	21.30	14.7	17.9	15.6	8.3	626
13	26/05/99	08.15	14.1	13.0	15.0	8.3	630
14	26/05/99	09.20	16.2	14.8	15.0	8.3	628
15	26/05/99	09.50	17.3	15.7	14.8	7.9	636
16	26/05/99	10.25	17.9	16.0	14.4	8.1	638
17	26/05/99	11.00	20.0	17.0	14.4	8.4	638
18	26/05/99	11.33	17.6	17.3	14.4	8.4	638
19	26/05/99	12.07	18.4	17.8	14.8	8.1	634
20	26/05/99	12.41	18.4	18.8	15.0	8.0	632
21	26/05/99	13.11	19.9	19.3	15.0	8.6	633
22	26/05/99	13.45	19.9	19.7	15.0	8.4	635
23	26/05/99	14.19	19.4	20.8	15.1	8.6	633
24	26/05/99	14.53	19.8	22.6	15.7	8.2	628
25	26/05/99	15.30	20.4	24.6	15.7	8.4	626
26	26/05/99	16.00	20.1	25.5	15.9	8.6	627
27	26/05/99	16.30	20.1	25.3	16.2	8.6	631
28	26/05/99	17.00	20.3	24.6	16.3	8.6	630
29	26/05/99	17.30	19.8	24.0	16.3	8.5	627
30	26/05/99	18.00	19.8	23.3	16.3	8.6	626
3 rd calibration run (18.20)							

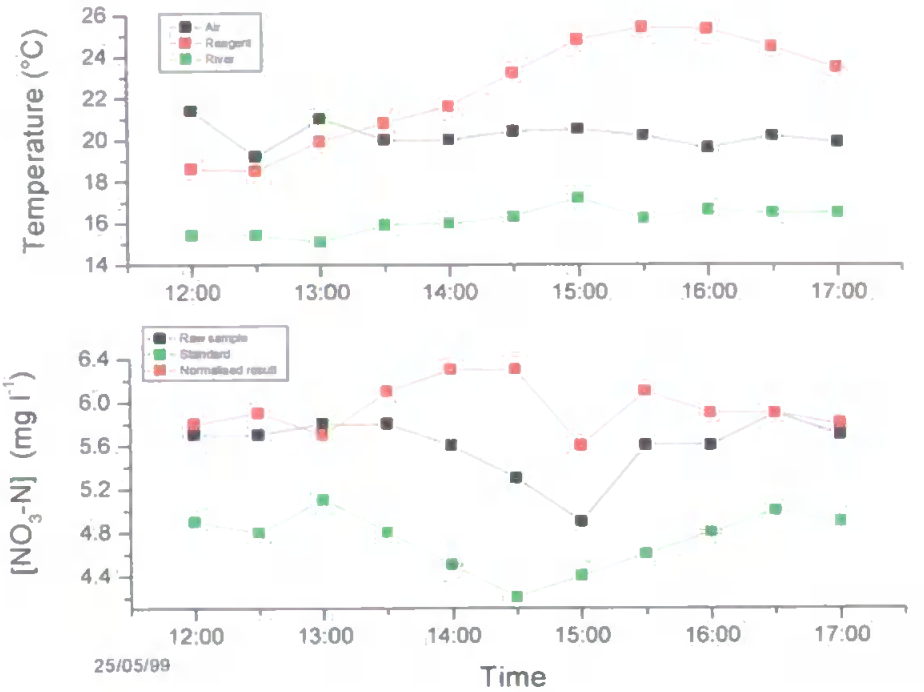

Figure 5.26 **Nitrate concentration and temperature results for DAY 1 of River Frome field trial; error bars on standard concentration data represent ± 3 s.**

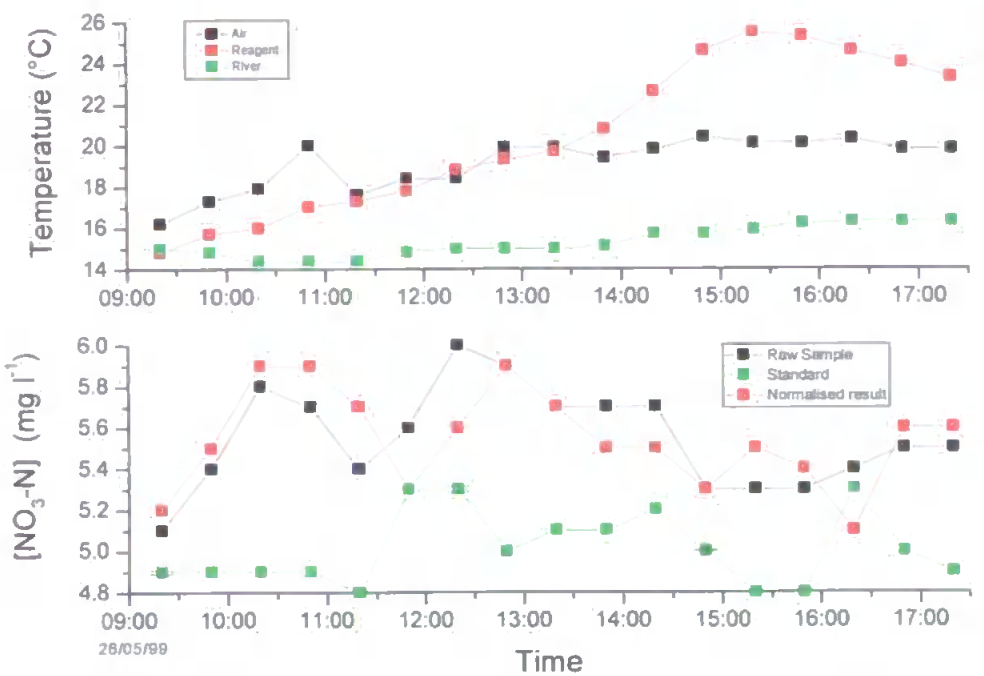

Figure 5.27 **Nitrate concentration and temperature results for DAY 2 of River Frome field trial; error bars on standard concentration data represent ± 3 s.**

(e) INTERCOMPARISON STUDY

Figures 5.28 & 5.29 show bar charts for the results obtained for the collected Frome samples. Samples were analysed in situ by the automated nitrate monitor and also collected and stored (see section 5.2.4 (c)) for analysis using an automated air segmented flow analyser (Skalar Instrument, see 5.2.4 (c)) on return to the University of Plymouth. Error bars are represented as three times the standard deviation for that sample. Excellent agreement is seen for all samples analysed by the two instruments. Nitrate monitor values ranged from 5.1 mg l^{-1} to 6.3 mg l^{-1} NO_3-N with a mean value of 5.7 mg l^{-1} NO_3-N and Skalar monitor values ranged from 5.4 mg l^{-1} to 6.4 mg l^{-1} NO_3-N with a mean value of 5.8 mg l^{-1} NO_3-N. Reproducibilities for the automated nitrate monitor were slightly better than those obtained for the Skalar with R.S.D.s in the range 0 – 3 % (n = 3) compared with 0 – 6 % (n = 3) for the Skalar monitor.

To test whether the results obtained by the two methods differed significantly from each other due to the presence of a systematic error in one of both of the systems, a paired t-test was applied to the data (Table 5.9).

$$|t| = \bar{x}_d \sqrt{n / s_d}$$

Where $|t|$ has (n – 1) degrees of freedom, $|t|$ = (t calculated from substituting experimental results into equation, calculated value without regard to sign), $\bar{x}_d$ = mean difference of paired values, n = number of samples, s_d = standard deviation of the differences between paired values. The null hypothesis assumed was that there was no statistically significant difference between the means of the results obtained from the two instruments.

Substituting values into the paired t-test equation;

$$|t| = -0.1 \sqrt{28} / 0.3467, \text{ therefore } |t| = 0.90.$$

The critical value of $|t|$ at the 95 % confidence level is 2.01. Since the calculated value of $|t|$ is less than the critical value the null hypothesis is retained. Therefore the two instrumental methods do not give significantly different values for the nitrate concentration for the River Frome samples at the 95 % confidence level.

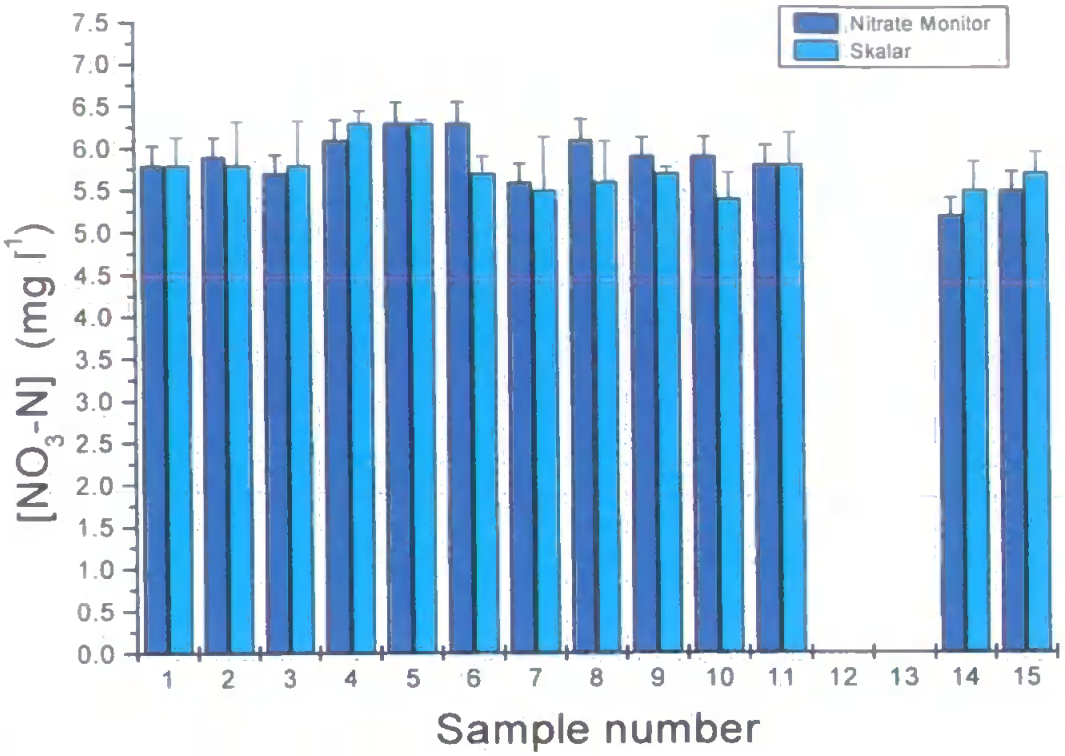

Figure 5.28 **Intercomparison of nitrate results obtained from River Frome Field Trial (samples 1 – 15)**

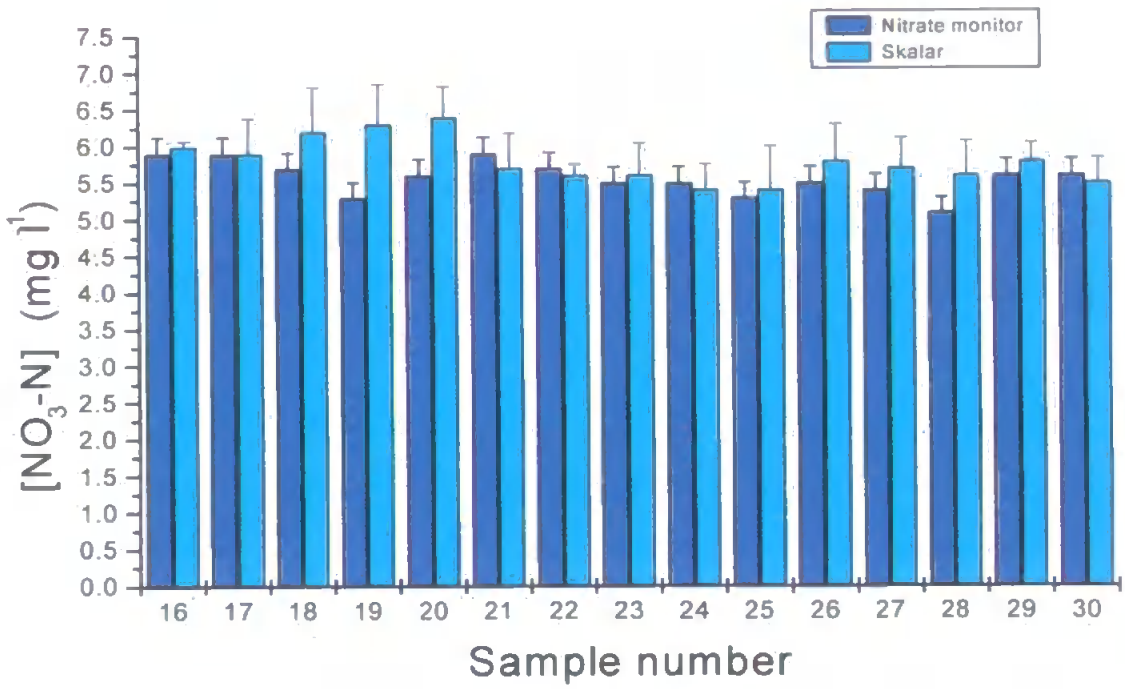

Figure 5.29 **Intercomparison of nitrate results obtained from River Frome Field Trial (samples 16 - 30)**

Table 5.9 **Paired t-test of Frome field trial results.**

Sample no.	Nitrate monitor (mg l^{-1})	Skalar (mg l^{-1})	Monitor-Skalar
1	5.8	5.8	0.0
2	5.9	5.8	0.1
3	5.7	5.8	-0.1
4	6.1	6.3	-0.2
5	6.3	6.3	-0.1
6	6.3	5.7	0.5
7	5.6	5.5	0.1
8	6.1	5.6	0.5
9	5.9	5.7	0.2
10	5.9	5.4	0.5
11	5.8	5.8	0.0
14	5.2	5.5	-0.4
15	5.5	5.7	-0.2
16	5.9	6.0	-0.1
17	5.9	5.9	0.0
18	5.7	6.2	-0.5
19	5.3	6.3	-1.0
20	5.6	6.4	-0.8
21	5.9	5.7	0.2
22	5.7	5.6	0.0
23	5.5	5.6	-0.1
24	5.5	5.4	0.1
25	5.3	5.4	-0.2
26	5.5	5.8	-0.3
27	5.4	5.7	-0.2
28	5.1	5.6	-0.5
29	5.6	5.8	-0.2
30	5.6	5.5	0.1
mean	**5.7**	**5.8**	**-0.1**
Std dev	**0.3022**	**0.2859**	**0.3467**
Variance	**0.0913**	**0.0817**	**0.1202**
n	**28**	**28**	**28**

(e) ENVIRONMENTAL INTERPRETATION OF FROME DATA

The provision of high quality analytical data for nutrient concentrations is of prime importance to water regulating bodies such as the U.K. Environment Agency (formally the National Rivers Authority, N.R.A.) to ensure compliance with the standards laid down in European Community (EC) directives. Table 5.10 gives the current classification system for river water quality, known as the River Ecosystem Use Classes. The classes are applied to every stretch of classified river and are based on the chemical water quality requirements of different types of ecosystem and the type of fisheries they are capable of supporting. The Frome and Piddle Catchment consists of waters of high quality which meet the water quality objectives defined in Table 5.10 to be classified as either RE1 or RE2.

Table 5.10 **Standards for the five River Ecosystem (RE) use classes.**

Use Class	DO (% sat) 10%ile	BOD (ATU) ($mg\ l^{-1}$) 90%ile	Total Ammonia ($mgN\ l^{-1}$) 95%ile	Un-ionised Ammonia ($mgN\ l^{-1}$) 95%ile	pH 5%ile & 95%ile	Hardness ($mg\ l^{-1}$) CaCo3	Dissolved Copper ($\mu g\ l^{-1}$) 95%ile	Total Zinc ($\mu g\ l^{-1}$) 95%ile	Class Description
1	80	2.5	0.25	0.021	6.0 - 9.0	≤10 >10 & ≤50 >50 & ≤100 >100	5 22 40 112	30 200 300 500	Water of very good quality suitable for all fish species
2	70	4	0.6	0.021	6.0 - 9.0	≤10 >10 & ≤50 >50 & ≤100 >100	5 22 40 112	30 200 300 500	Water of good quality suitable for all fish species
3	60	6	1.3	0.021	6.0 - 9.0	≤10 >10 & ≤50 >50 & ≤100 >100	5 22 40 112	300 700 1000 2000	Water of fair quality suitable for high class coarse fish populations
4	50	8	2.5		6.0 - 9.0	≤10 >10 & ≤50 >50 & ≤100 >100	5 22 40 112	300 700 1000 2000	Water of fair quality suitable for coarse fish populations
5	20	15	9						Water of poor quality which is likely to limit coarse fish populations

The river stretch at the Institute of Freshwater Ecology, East Stoke, is currently classified as RE 1. Of the 82 classified stretches in the Frome and Piddle catchment, only 3 significantly failed (95 % confidence) and 6 marginally failed (50 % confidence) to meet their objectives in 1995[294]. Water quality at the site of the field trial is therefore very good and supports a thriving salmon fishing activity. However there have been concerns expressed by the local Environment Agency and English Nature about the impact of nutrients. Anthropogenic nutrient inputs to the catchment are numerous and arise from diffuse and point sources which are briefly discussed below.

Point source nutrient inputs to the Frome catchment arise from some of the 206 abstraction licenses in the catchment, 72 % of which are classed as non-consumptive (water used is returned to the catchment). There are 11 public sewage treatment works (STW) (50 in total including private sewage works in the whole Frome and Piddle catchment) that discharge to the River Frome. Three of the largest STWs (> 500 m^3 d^{-1}) discharge upstream of the River Laboratory at East Stoke, two of which (1 at Dorchester and 1 at Wool) also receive substantial trade effluents. The importance of investigating the nutrient status of waters in the catchment was given particular importance in the Frome & Piddle Catchment Management Plan[295] in which the Frome downstream from the Dorchester STW was a proposed Eutrophic Sensitive Area under the EC Urban Waste Water Directive. In 1993 there were also 70 (un-specified in nature) substantiated pollution incidents within the catchment. Other substantial points sources in the catchment arise from commercial aquaculture operations, production of watercress and fish farming.

Five cress farms operate on the River Frome, where activities such as bed cleaning, disinfection, fertiliser application and pest control (treatment with zinc to control crook root fungus and watercress yellow spot) can cause pollution problems if discharges are untreated. Changes in the biology of the Frome watercourse have been detected immediately downstream from cress farm discharges[295]. Control of cress farm discharges are given high priority in the Frome Catchment Management Plan[295] and current measures, include discharge consent levels, settlement tanks, research and development projects and zinc monitoring. Considerable point sources of nutrients, particularly nitrogenous compounds, arise from the seven fish farms adjacent to the River Frome. Organic wastes, ammonia and therapeutics from the large populations of fish can contaminate the effluent discharges from the fish farms.

As a result of large discharges of effluent, considerable loads of these substances can be discharged into the river. Several marginal and significant failures to comply with designated RE Use Class have occurred in the Frome in sections containing fish farms.

Diffuse inputs primarily result from the pollution of surface and groundwaters from agricultural activities and falls into the legislation of the EC Nitrates Directive which concerns the protection of water against pollution caused by nitrates from agricultural sources. It requires Member States to identify water affected by pollution from nitrates or which could be affected if protective measures are not taken. Land draining to these areas are designated as Nitrate Vulnerable Zones (NVZ) and action plans must be established to reduce existing nitrate pollution and prevent further pollution. Currently there are no designated zones within the Frome and Piddle catchment.

In the upland areas of the catchment pesticides and fertilisers are widely used for arable crops, while sheep and pig farming are becoming increasing more popular. Dairy farming activities tend to be more dominant in the lower part of the catchment with some arable farming also taking place. In some parts of the upper Frome catchment, clay soils can create the potential for run-off problems, while the permeable nature of other parts of the catchment mean that groundwater contamination is also a possibility.

The combination of nutrient inputs from point sources discharges and diffuse inputs means that the Frome and Piddle catchment may be undergoing eutrophication and its current trophic status is unknown. Recent years have seen a rise in complaints concerning water quality and the lack of clarity of the water in the lower Frome in the spring and early summer months. Algal blooms, such as those seen during the field trial, result from eutrophication and are likely to cause these clarity problems. Therefore it is of considerable importance to monitor nutrient levels on a frequent basis. Owing to this need, a weekly manual sampling and laboratory analysis programme has been in operation at the IFE River Laboratory[298] since 1965. The River Laboratory has also been the site for short term[296] and long term (9 – months) field trials of an automated spectrophotometric nitrate monitor[298]. Casey et al.[296] showed that nitrate concentrations in the River Frome have been rising steadily from 1965 - 1987. Mean nitrate concentration for the year 1965 was 2.04 mg l^{-1} NO_3-N, 3.38 mg l^{-1} NO_3-N for 1975, and 4.41 mg l^{-1} NO_3-N in 1987 with a maximum concentration of 5.60 mg l^{-1} NO_3-N. Mean nitrate concentration for the samples collected during the field trail was 5.7

mg l^{-1} NO_3-N and this is clearly in line with the trend of increasing nitrate concentration. The nitrate / nutrient supply to the River Frome are inherently controlled by the physical characteristics and the use of its catchment, and evidence shows nitrate inputs are clearly on the increase.

As mentioned in section 5.2.3 (b), the dominant geology of the catchment is chalk. The underlying chalk is the major aquifer or reservoir of underground water in the catchment and allows the transmission of large quantities of water through cracks and fissures. The upper tributaries are predominately spring-fed and although levels fall in the summer months the majority of the flow remains stable, with any rainfall being absorbed by soils. Only in winter months when soils are saturated and the aquifer recharged flows are the flows more variable due to direct surface run-off. Typical summer (July) flows at the East Stoke site (effectively the flow-out of the Frome catchment) are 2 – 3 m^3 s^{-1} (cumecs), rising to 10 m^3 s^{-1} in January. Flow exceeded for 95 % of the time (Q_{95}) was 2.14 m^3 s^{-1}. Flow rates measured during the field trail gave a mean of 0.68 ms^{-1}, corresponding to 1.5 m^3 s^{-1} (2.5 % R.S.D, n = 9).

In summary, the increasing impaction of the Frome catchment by nitrogen over many years means that regular and frequent monitoring is required. Nitrate data with a high temporal resolution would help to refine models of nutrient cycling in the Frome and in conjunction with hydrographic data, e.g. flow rates, rainfall, identify the major inputs of nitrate to the Frome catchment. The type of monitor described in this chapter has been shown to be suitable for acquiring nitrate data reliably with the required sampling frequency.

5.4 CONCLUSIONS

The following specific conclusions can be drawn from the research reported in this chapter:

1. LabView™ has been shown to be an effective tool for automating the control and operation of a FI manifold incorporating an Ocean Optics PSD – 1000 array detector. Data acquisition and processing can also be controlled. The software is relatively easy to program and provides an interactive graphical display for the user.

2. The micro-solenoid pumps are easy to control with variable flow rates in the range (0 – 10 ml min^{-1}), however they give a pulsed flow and are sensitive to particulate matter in the sample stream. The negative effect of the pulsations can be removed using the multi-wavelength capabilities of the Ocean Optics PSD – 1000 spectrometer.

3. The dynamic range of the instrument can automatically be adjusted in the field, to suit local environmental conditions, by changing the wavelength at which the analytical signal is measured.

4. The automated FI monitor did not work well in Lesotho due to problems encountered with blockage of the pumps due to particulate matter and sub – zero temperatures. However it was possible to obtain a unique dataset from a pristine upland environment using simple field instrumentation and dry reagent test kits.

5. The automated FI monitor operated successfully for 48 h at a field site on the River Frome, East Stoke, Dorset, for the determination of TON in river water. Results were obtained at 30 min intervals during this period and the data were in good agreement with the results from a laboratory based air-segmented analyser. The monitor had a linear range of 0 – 9 mg l^{-1} NO_3-N (r^2 = 0.9998, n = 6) and R.S.Ds were < 4 % (n = 9).

Chapter Six

Determination of Selected Major Anions &Cations In Precipitation by Ion Chromatography

"Perseverance will prevail where all others will fail"

- Anonymous -

6.1 INTRODUCTION

Previous chapters have reported FI methods for the determination of ammonia and nitrate in natural waters. Although very versatile and ideally suited to in situ and on-line monitoring, FI methods are usually limited to single analyte determinations for each manifold. Alternative analytical approaches for the determination of ammonia and nitrate have been discussed in sections 1.5 and 1.6, and one of the more commonly used methods is ion chromatography[65;68;96;103]. This technique has the advantage of being able to perform multi-analyte determinations with high sensitivity (typical detection limits 10 – 100 μg l^{-1}) and good reproducibility. This chapter describes two sections of work involving the ion chromatographic analysis of dissolved major anions and cations in precipitation. The first section presents data generated over a four month sampling campaign conducted at the University of Plymouth and examines the influence of the aerosol source on the chemical composition of precipitation. The second section describes the ion chromatographic analysis of dissolved major ions in precipitation as part of the Austrian precipitation network, and discusses the distribution of wet deposition loads of ammonium, nitrate and sulphate over Austria for the year 1993. The potential merits of applying multivariate data analysis techniques to these large environmental datasets is also discussed.

6.2 EXPERIMENTAL

6.2.1 REAGENTS

(a) PLYMOUTH SAMPLING CAMPAIGN

The anion chromatographic system used a 25 mmol l^{-1} sodium hydroxide solution as the eluant. This was prepared by dissolving 1.0 g of NaOH in 1 l of Milli-Q water. Regenerant used for the micro-membrane suppressor was prepared by dissolving 2.8 ml of concentrated sulphuric acid (H_2SO_4) to 5 l with Milli-Q. All anion standards (sulphate (SO_4^{2-}), nitrite (NO_2^-), nitrate (NO_3^-) and chloride (Cl^-)) were prepared from serial dilution of 1000 mg l^{-1} stock solutions (0.1371 g Na_2SO_4, 0.150 g $NaNO_2$, 0.163 g KNO_3, 0.1649 g NaCl) (Aristar grade, Merck Ltd.) made up to 100 ml with Milli-Q water. Mixed anion calibration standards were prepared by serial dilution of a 1 mg l^{-1} multi-anion stock solution.

Cation analyses were performed using various analytical techniques. Calcium (Ca^{2+}) and magnesium (Mg^{2+}) were analysed by flame atomic absorption spectroscopy (FAAS). Sodium (Na^+) and potassium (K^+) were analysed by flame photometry. All standards were prepared from 1000 mg l^{-1} Spectrasol grade stock standards (Merck).

Ammonia determination utilised the indophenol-blue method and UV – Vis spectroscopic detection. A 1000 mg l^{-1} (NH_3-N) stock solution was prepared by dissolving 3.819 g of ammonium chloride (previously dried at 105°C) in 1 l of Milli-Q water. An ammonia solution of 100 mg l^{-1} was prepared by dilution of the stock solution to 1 l with water. A 0.05 mol l^{-1} EDTA solution was prepared by dissolving 18.6 g of ethylenediaminetetra-acetic acid disodium salt in 1 l of Milli-Q water. Sodium phenate solution was prepared by dissolving 12.5 g of phenol in 3.7 ml of acetone and 20 ml of ethanol. This solution was then mixed with 20 ml of ethanol and 20 ml of 270 g l^{-1} NaOH solution and diluted to 100 ml with Milli-Q water. Stock sodium hypochlorite solution was prepared by diluting 25 ml of sodium hypochlorite solution (GPR grade, Merck). Standards of 0.02, 0.05, 0.1, 0.3, 0.5 and 1.0 mg l^{-1} NH_3-N were prepared by serial dilution of the 100 mg l^{-1} stock solution.

(b) AUSTRIAN SAMPLING CAMPAIGN

The cation chromatographic system used a 17 mM methane sulphonic acid (MSA) solution as eluant. This was prepared by diluting 5.5 ml of MSA (Fluka, Chemika, purity >99%) with 5 litres of Milli-Q water. The elution of the anion system used an eluant of 1.8 mM sodium carbonate and 1.7 mM sodium hydrogen carbonate. All solutions that required dilutions were prepared using deionised water purified by a Milli-Q plus 185 (Millipore Waters, Bedford, Massachusetts 01730,USA) analytical reagent grade water purification system (18.2 MΩ cm^{-1} at 25°C). All glassware and flask stoppers used were pre-rinsed six times with deionised water prior to use. All standards were prepared by dissolving the appropriate amount of analytical grade solid to a volumetric flask. Working standards were prepared by serial dilution of the stock solutions.

6.2.2 INSTRUMENTATION

(a) PLYMOUTH SAMPLING CAMPAIGN

Precipitation pH was measured using a portable pH meter (Hanna Instruments) which was calibrated prior to use using buffers of 4.0 and 7.01 pH. Conductivity measurements were performed using a portable microprocessor conductivity meter (Hanna Instruments). A Varian Star 9012 HPLC pump (Varian Ltd, Walton-on-Thames, Surrey, U.K.) was used in conjunction with the anion chromatographic parameters given in Table 6.1. Detection was performed using a Waters 431 conductivity detector. Integration of results and data storage was performed on an Amstrad 1640 HD20 desktop PC running a DOS based chromatography software program. Results were plotted to an Epson LX – 800 dot matrix printer.

Table 6.1 Anion chromatographic parameters

PARAMETER	ANION
Analytical column	Dionex Ion Pac AS4S
Precolumn	None
Eluent	Optimised value : 25mM NaOH Range : 20 – 35 mM
Flow rate	Optimised value : 0.8 ml min^{-1} Range : 0.7 – 1.2 ml min^{-1}
Suppressor	Dionex AMMS-II (micromembrane)
Regenerant	25 – 50 mM H_2SO_4
Regenerant flow rate	7.0 – 10.0 ml min^{-1}
Sample loop	100 µl
Detection	Conductivity

A Varian Spectra AA – 400 Plus FAAS instrument was used for the determination of Ca^{2+} and Mg^{2+} using the manufacturers recommended instrumental parameters. Determination of Na^+ and K^+ was performed using a Corning 400 Flame Photometer and standard manufacturers conditions. Ammonium determination was performed using a Hewlett Packard 8453 UV-Vis spectrometer (see section 2.2.2). Principal Components Analysis (PCA) was performed using The Unscrambler version 6.1 multivariate analysis software package (Camo AS, Trondheim, Norway).

(b) AUSTRIAN SAMPLING CAMPAIGN

The pH measurements conducted on all rain samples were performed using a internally referenced Type Flushtrode P/N 238'060 electrode (Fa. Hamilton) connected to a Type pH523 meter (WTW). Conductivity measurements were performed using a glass electrode PW 9510/00 (cell constant of 0.5-0.8/cm, range 10 µS/cm to 30 mS/cm, temperature range 0-50°C) connected to a Philips PW 9505 conductivity meter operated at a constant temperature of 25°C. The ion chromatographic analysis was performed solely with Dionex equipment; the parameters for both anionic and cationic analyses are given in Table 6.2 below.

Table 6.2 Parameters of the IC-systems.

PARAMETER	CATION	ANION
System	Dionex-Qic Analyser	Dionex GPM-2, CD-20
Analytical column	Dionex Ion Pac CS12	Dionex Ion Pac AS4A-SC
Precolumn	Dionex Ion Pac CG12	Dionex Ion Pac AG4A-SC
Eluent	17mM MSA	1.8 mM Na_2CO_3 + 1.7 mM $NaHCO_3$
Flow rate	1 ml/min	1 ml/min
Suppressor	Dionex CSRS 1 - 4mm (Electrochemical)	Dionex ASRS 1 - 4mm (Electrochemical)
Regenerant	Eluent in circle	Eluent in circle
Sample loop	10 µl	30µl
Detection	Conductivity	Conductivity
Sensitivity range	10µS	5-30µS

6.2.3 SAMPLING METHODS

(a) PLYMOUTH BULK COLLECTOR

Sample collection at the Plymouth urban site utilised a simple "bulk" type manual precipitation collector. The collector was constructed with a metal frame-work base with a wooden top-plate into which 4 HDPE plastic tubes were secured in a square arrangement. The whole structure (approx. height 2m) was coated in a durable epoxy based paint to prevent contamination of the samples from the collector support. Sample collection (described in section 6.2.4.1 (a)) was performed using pre-cleaned polythene collection funnels (cone diameter 16 cm) secured in place by plastic clips attached to elasticated cord. The funnels drained into pre-cleaned 500 ml HDPE sample bottles placed within the plastic tubes attached to the top plate of the collector. The sample site was situated on the roof (20 m above ground level)) of the Fitzroy Building at the University of Plymouth (see section 6.2.5 (a)). An automated meteorological station was also sited on the roof and recorded wind speed, wind direction, rainfall amount, temperature and pressure at intervals of 10 min.

(b) WET & DRY ONLY PRECIPITATION SAMPLER (WADOS)

The Austrian precipitation sampling network was equipped with the WADOS ("Wet and dry only precipitation sampler")[299]. The WADOS unit consisted of two containers symmetrically placed on a cross-arm. A common lid moved by a driving mechanism, controlled by an electronic device, covered either one or the other collecting funnel. A precipitation detector sensed rain or snow and communicated with the electronically controlled driving mechanism.

The detector was set to sense the beginning and end of a precipitation event by measuring the resistance of a copper grid. The sensor was in the form of a cone, hence enabling sensing of precipitation from all directions. As a safeguard against heavy wind and fouling from birds, a protection tube surrounded the rain sensing cone. In addition a ring was situated on the top of the sensing cone to catch ice events such as hail and ice-pellets and to aid their melting. The electronic device of the detector had a heating unit to maintain a constant surface temperature of 20°C. When a precipitation event was "sensed" the temperature rose to 50°C. This aided the melting of ice samples and evaporated residual drops after the event had finished. To prevent excessive "back and forth" movement of the lid at extremely light precipitation, a time delay for the return of the cover was incorporated into the control circuit.

Upon sensing a precipitation event, the lid, which had protected the wet-only container, shifted to the dry-only container in which the dust fall-out was collected. The collection funnel of the wet-only section was then open and the water was gathered and funnelled into a sample bottle, to prevent the collection of leaves and debris a filter was situated over the bottle. The detachable bottle was housed in the upper part of the tube which blocked out heavy light that may have lead to degradation of the sample. Normally the sample was small enough to be poured into a small bottle, ready for storage.

The wet-only part of the WADOS was designed with a heating unit which melted snow and ice precipitation. The heating device was situated in the base of the collecting funnel and therefore the snow would not melt immediately. It would only melt when the lid was returned back to its default position, thus minimising losses through evaporation. The heater was controlled by a thermostat and the temperature was held between 8 and 10°C. Normally the water would freeze again when it was drained into the sample bottle. Local observers carried out the daily control of the samples, usually in the morning, between 07:00 and 08:00 Central European Time. The samples were stored in polyethylene bottles at 0-4°C and transported in biweekly intervals to the central laboratories and analysed, generally within 1-4 weeks of receipt.

6.2.4 PROCEDURES

6.2.4.1 PLYMOUTH SAMPLING CAMPAIGN

(a) SAMPLE COLLECTION, TREATMENT & STORAGE

All analytical and sample handling procedures were carried out using disposable gloves to avoid contamination. All sample collection bottles and funnels were thoroughly cleaned with Milli-Q water. Using ion chromatographic analysis of the resultant washes, optimum wash volumes were 200 ml Milli-Q for the 500 ml HDPE sample bottles and 500 ml Milli-Q for the sample collection funnels. All cleaned equipment was stored in resealable plastic bags to avoid external contamination. Figures 6.1 and 6.2 show the protocol devised for sample collection and analysis. Samples were collected after a 24 h exposure (excluding weekends due to access problems) if a rain event had occurred during that period. If no rain had occurred after 48 h from first deployment then samples were collected to study dry deposition.

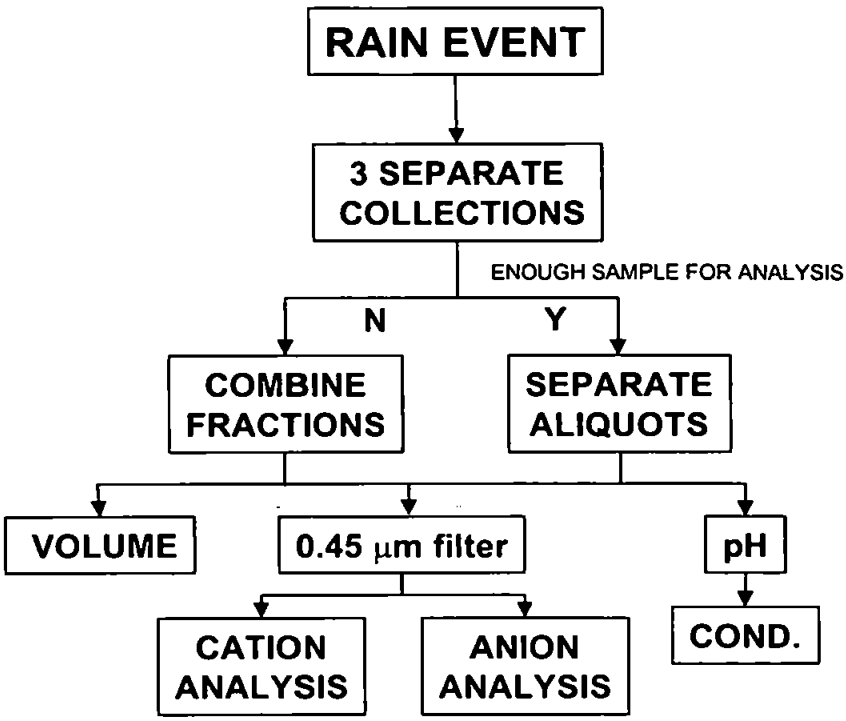

Figure 6.1 **Schematic diagram of sample collection protocol – rain event occurred.**

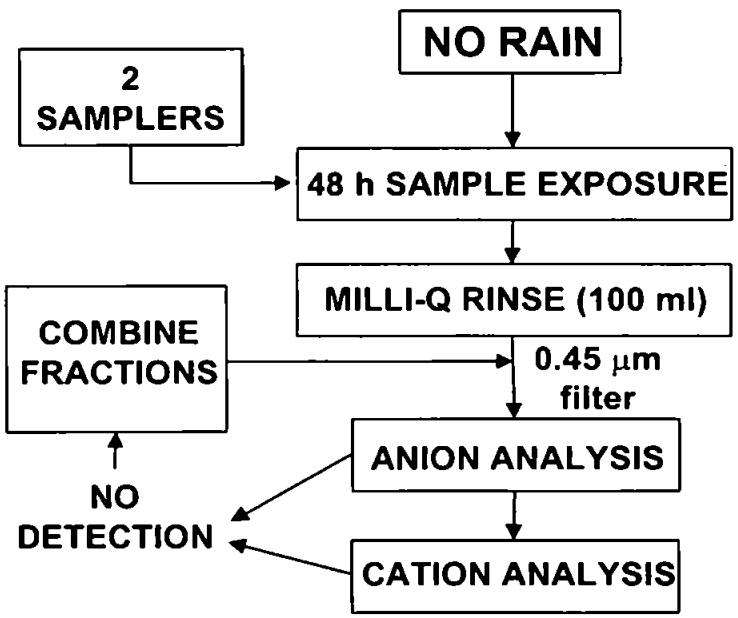

Figure 6.2 **Schematic diagram of sample collection protocol – no rain event.**

All samples were filtered through a 0.45μm cellulose acetate membrane filter. All filtration equipment were cleaned with Milli-Q prior to use (1500 ml each). Ideally collected samples were analysed immediately but filtered samples which could not be analysed immediately were stored at 4°C in a laboratory refrigerator.

(b) SAMPLE ANALYSIS

100 µl of mixed anion (SO_4^{2-}, NO_3^-, Cl^-) standards of concentrations (0.03, 0.05, 0.1, 0.2 and 0.4 mg l^{-1}) were injected to the analytical column. All injections were repeated three times, and calibrations were performed using area integrations of the resultant chromatographic peaks. pH and conductivity were measured on the day of collection on the raw unfiltered samples. Ion chromatographic analysis of the samples involved 100 µl of filtered sample being injected onto the analytical column. Samples were analysed in duplicate and samples yielding concentrations above the calibration range were diluted with Milli-Q water to bring them into range.

Calibration standards for calcium were 1.0, 2.0, 3.0, 4.0, 5.0 and 7.0 mg l^{-1}, and standards used for the magnesium analysis were 0.1, 0.25, 0.5, 0.75 mg l^{-1}. All filtered samples and calibration standards were analysed in triplicate. All sodium standards (5.0, 10.0, 20.0, 30.0 and 40.0 mg l^{-1}), potassium standards (0.5, 1.0, 2.0, 3.0 and 5.0 mg l^{-1}) and collected samples were analysed in triplicate.

Ammonia determinations were performed using the indophenol blue spectrophotometric method. A series of 50 ml volumetric flasks were used, one for reagent blank, one for each sample and six for calibration standards. To each sample flask 15 ml of well mixed sample was added. Calibration standards of 0.02, 0.05, 0.1, 0.3, 0.5 and 1.0 mg l^{-1} NH_3-N were prepared by serial dilution of the 100 mg l^{-1} NH_3-N stock solution. To all flasks 1.0 ml of 0.05 mol l^{-1} EDTA, approximately 20 ml of Milli-Q water and 8 ml of sodium phenate was added. Having mixed the contents of each flask, 6.0 ml of freshly prepared sodium hypochlorite was added, the flasks were then made up to volume with Milli-Q water and allowed to stand for 30 min for full colour development to occur. The solutions were then measured at 630 nm in a 1 cm glass cuvette, using the reagent blank as a reference.

6.2.4.2 AUSTRIAN SAMPLING CAMPAIGN

(a) SAMPLE ANALYSIS

Samples that had been refrigerated were allowed to reach room temperature over a minimum of 4 hours (especially important for conductivity measurements). 1000µl of sample was then transferred to an Eppendorf container via a pipette. This procedure was repeated in quadruplicate, one for the cation analysis, one for the anion analysis, and two for potential repeats. Samples were

analysed immediately or stored in a refrigerator at 4°C to await analysis. These samples were loaded into an autosampler with sample identity and autosampler loading position recorded. Quantitative analysis was performed via a series of external standards, the concentrations of which are given in Tables 6.3 and 6.4 below.

Table 6.3 Cation calibration standards.

	Na^+ (mg l^{-1})	NH_4^+ (mg l^{-1})	K^+ (mg l^{-1})	Mg^{2+} (mg l^{-1})	Ca^{2+} (mg l^{-1})
Standard 1	0.5	0.5	1.0	1.0	1.0
Standard 2	1.0	3.0	3.0	3.0	3.0
Standard 3	5.0	5.0	5.0	5.0	5.0

Table 6.4 Anion calibration standards.

	Cl^- (mg l^{-1})	NO_3^- (mg l^{-1})	SO_4^{2-} (mg l^{-1})
Standard 1	0.5	2.0	2.0
Standard 2	2.0	7.0	7.0
Standard 3	3.0	13.0	13.0

Calibration was performed at the start of an analysis with the first three analyses being of the calibration standards. Precipitation samples were then loaded to the autosampler with every sixth position being occupied by a calibration standard. This was to perform a check on any instrumental drift that may have occurred during analysis. A full set of calibration standard was also analysed at the end of an analysis run. Samples with analyte concentrations above the calibration range were subsequently diluted and re-analysed.

After ion chromatographic analysis, the conductivity of the sample was measured. Calibration of the meter prior to use was performed using a 0.001M KCl solution prepared fresh from a 0.1M stock solution. Calibration and analysis were performed at 25°C. The conductivity probe was washed thoroughly in de-ionised water before placing in the calibration solution, the metered reading was adjusted if necessary to 147 $\mu S\ cm^{-1}$ (25°C). A portion of the sample was poured into a small beaker and the conductivity measured; the probe and beaker were washed between each stage of the analysis.

pH was the final parameter measured due to the fact that KCl diffuses from the probe into the solution during measurement which would affect the ionic concentration of K and the measurement of conductivity. The pH meter was calibrated with buffers at pH 4 and 7 at 25°C prior to use; this calibration was stable for at least a day.

(b) DATA COLLECTION

Upon collection of a sample, sampling station operators recorded the weather conditions e.g. storm, fog. Any additional useful comments were recorded such as the possibility of sample contamination, the deposition type (rain or snow) and the total volume of a collected sample. This information was entered onto a master recording sheet upon receipt of the sample at the laboratory. The analytical information was then recorded, along with station number, conductivity, pH, analytical comments and ionic concentrations.

Sample contamination occurred with approximately 5% of samples, either during collection, transport or analysis. Contamination was either clearly visible (e.g debris) or became apparent during chemical analysis. These contaminated samples were excluded from subsequent data processing and interpretations. Gaps in the datasets also occurred due to instrumental downtime.

6.2.5 SAMPLING SITE DESCRIPTIONS

(a) PLYMOUTH URBAN ENVIRONMENT

The Plymouth urban precipitation site was located on the roof of the Fitzroy building at the main campus of the University of Plymouth. This site was chosen because the atmosphere is influenced by contrasting aerosol sources, which potentially lead to strong gradients in the detected precipitation chemistry of the major ions. By considering changes in the precipitation chemistry the influence of different aerosol sources and meteorological parameters may be defined.

(b) AUSTRIAN PRECIPITATION NETWORK

In 1982 a framework for a national precipitation sampling network was established in Austria and the sampling network consists at present of 33 stations. Three of the stations are also part of the EMEP-network (Co-operative programme for monitoring and evaluation of the long range transmission of air pollutants in Europe). Figure 6.3 shows a map of the Austrian sampling sites together with the EMEP stations, each site is allocated a code which is referred to in Table 6.5.

The stations are operated by the environmental authorities of the local governments of the nine counties of Austria, the exceptions being the EMEP sites in Austria which are operated by the Federal Environmental Authority. The number of sampling sites can be justified by the considerable variation in terrain within Austria. Altitudes range from only 155 m.a.s.l (metres above sea level) to 3106 m.a.s.l in the central Alps, with annual precipitation amounts ranging from 260mm to over 2100mm.

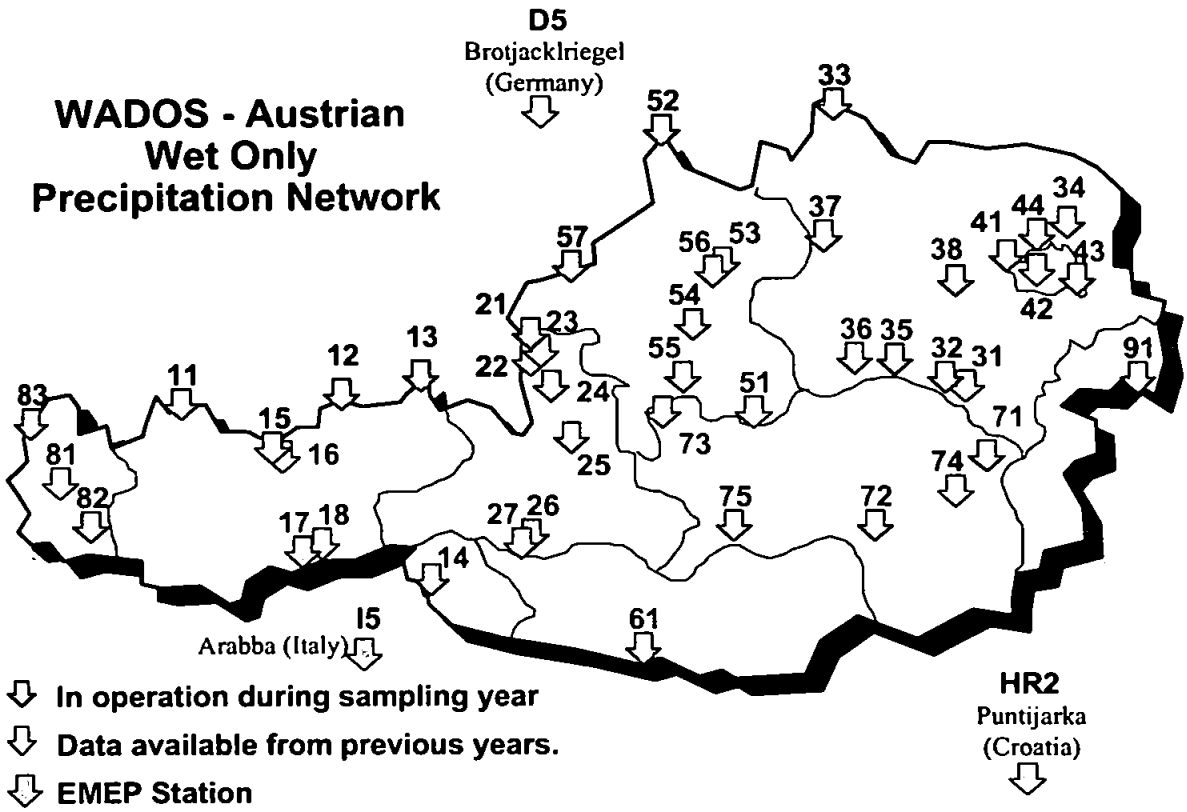

Figure 6.3 Austrian precipitation network, location of sampling sites.

The function of the network is to estimate the wet deposition loads of major ions and to enable the determination of trends in the composition of wet deposition in Austria. The data set, which is updated annually, is used to estimate the development of soil conditions by studying critical loads and levels[300], investigating mechanistic processes in the atmosphere[301] and validating of air chemistry models[302]. The data also forms the basis for future pollution risk assessments and forward planning for the next monitoring programme for acid deposition.

The measurements are designed to investigate both temporal and spatial trends and fluxes of sulphur and nitrogen compounds, free acids and neutralising cations. The sampling and analysis of wet deposition complies with the regulations "Emission monitoring of wet deposition and atmospheric dust" as specified by the Austrian Ministry of Health and Environment (BMGU)[303]. The applied methods also ensure both national and international comparability of data.

Table 6.5 Description of sampling sites in Austrian Precipitation Network.

Region	Site Code	Station	Longitude	Latitude	Height (m.a.s.l)	Period (MM/JJ)	Analysis Laboratory
Tirol	11	Reutte	10.40.54	47.29.11	930	11/83-	IAC, TU-Wien
	12	Achenkirch	11.38.25	47.34.55	840	11/83-	Ministry for Environment
	13	Kufstein	12.13.38	47.39.47	680	11/83-	IAC, TU-Wien
	14	Innervillgraten	12.21.10	46.49.06	1730	8/84-	IAC, TU-Wien
	15	IBK-Seegrube	11.22.48	47.18.24	1960	10/86-3/88	IAC, TU-Wien
	17	IBK-Reichenau	11.25.05	47.16.36	570	10/86-3/88	IAC, TU-Wien
	18	Noblach	11.28.20	47.03.22	1420	10/84-9/85	IAC, TU-Wien
	19	Innerschmirin	11.36.18	47.06.34	1570	10/85-2/88	IAC, TU-Wien
Salzburg	21	Haunsberg	13.01.00	47.57.23	520	10/83-	IAC, TU-Wien
	22	Szbg Flughafen	12.55.53	47.47.36	433	10/83-9/86	IAC, TU-Wien
	23	Gaisberg	13.06.53	47.47.45	1010	10/89-11/90	IAC, TU-Wien
	24	St. Koloman	13.14.00	47.39.03	1020	10/83-	Ministry for Environment
	25	Werfenweng	13.15.12	47.25.18	940	10/83-	IAC, TU-Wien
	26	Kolm Saigum	12.59.04	47.04.05	1600	10/89-4/95	IAC, TU-Wien
	27	Sonnblick	12.57.32	47.03.15	3106	10/87-	IAC, TU-Wien
Niederosterreich	31	Hirschwang	15.48.28	47.42.33	500	4/86-3/88	IAC, TU-Wien
	32	Nasswald	15.42.26	47.46.04	600	5/88-	IAC, TU-Wien
	33	Litschau	15.02.20	48.57.20	560	10/89-	IAC, TU-Wien
	34	Wolkersdorf	16.31.22	48.23.02	180	10/89-	IAC, TU-Wien
	35	Josefberg	15.18.56	47.50.42	1010	11/89-	IAC, TU-Wien
	36	Lunz	15.04.07	47.51.18	618	4/90-	IAC, TU-Wien
	37	Ostrong	15.05.02	48.13.15	575	4/91-	IAC, TU-Wien
	38	Kl.-Leopoldsdf	15.59.56	48.05.20	400	7/91-	IAC, TU-Wien
Wien	41	Lainz	16.14.07	48.12.07	230	4/86-	IAC, TU-Wien
	42	Laaer Berg	16.23.39	48.09.41	250	4/86-3/90	IAC, TU-Wien
	43	Lobau	16.30.51	48.11.15	155	4/86-	IAC, TU-Wien
	44	Bisamberg	16.22.59	48.18.49	310	4/90-	IAC, TU-Wien
Oberosterreich	51	Wurzeralm	14.16.30	47.38.48	1400	1/84-7/89	County Laboratory
	52	Schoneben	13.57.02	48.42.43	920	1/84-	County Laboratory
	53	Steyregg	14.21.16	48.17.23	335	1/84-	County Laboratory
	54	Kremsmunster	14.07.49	48.03.21	384	1/86-	County Laboratory
	55	Grunau	13.57.22	47.46.22	591	1/87-	County Laboratory
	56	Linz-ORF	14.18.09	48.17.52	263	5/90-	County Laboratory
	57	Aspach	13.17.51	48.11.07	430	2/94-	County Laboratory
Karten	61	Nassfeld	13.16.33	46.33.37	1530	11/89-	IAC, TU-Wien
Steiermark	71	Masenberg	15.52.56	47.20.53	1137	3/90-	LR STMK , Division 1a
	72	Hochgosnitz	15.01.00	47.03.33	900	3/90-	LR STMK , Division 1a
	73	Grundlsee	13.47.48	47.37.50	954	3/90-	LR STMK , Division 1a
	74	Weiz	15.37.49	47.13.03	456	4/90-9/92	LR STMK , Division 1a
	75	Stolzalpe	14.12.10	47.07.50	1302	12/91-	LR STMK , Division 1a
Vorarlberg	81	Thuringerberg	09.47.05	47.13.05	960	4/90-3/92	IAC, TU-Wien
	82	Gaschurn	10.01.30	46.59.30	960	4/92-3/94	IAC, TU-Wien
	83	Hard	09.41.17	47.30.08	400	5/94-	IAC, TU-Wien
Burgenland	91	Illmitz	16.46.12	47.46.12	117	8/83-	Ministry for Environment

6.3 RESULTS & DISCUSSION

6.3.1 PLYMOUTH SAMPLING CAMPAIGN

Tables 6.6 and 6.7 show the linear regression equations for typical anion and cation calibrations. Limits of detection were calculated from the mean of the blank signal plus three times the standard deviation of the blank. Calibrations were accepted if the regression coefficient (r^2) was equal to or greater than 0.995. Below this limit, calibrations were considered unacceptable and therefore repeated.

Table 6.6 Summary of calibration statistics for anion analysis by ion chromatography

	Sulphate (SO_4^{2-})	Nitrate (NO_3^-)	Chloride (Cl^-)
Analysis method	IC	IC	IC
Sensitivity (Area / mg l^{-1})	20889	15433	26167
Intercept	26.40	0.02	191.70
r^2	0.9994	0.9996	0.9992
LOD (mg l^{-1})	0.006	0.001	0.001

Table 6.7 Summary of calibration statistics for cation analysis, (FAAS = Flame Atomic Absorption Spectroscopy, FP = Flame Photometry, UV-Vis = UV-Vis Spectroscopy)

	Calcium (Ca^{2+})	Magnesium (Mg^{2+})	Sodium (Na^+)	Potassium (K^+)	Ammonium (NH_4^+)
Analysis method	FAAS	FAAS	FP	FP	UV – Vis
Sensitivity (Absorbance / mg l^{-1})	0.020	0.901	9.204	20.043	0.132
Intercept	0.003	0.012	0.523	0.057	0.002
r^2	0.9970	0.9994	0.9998	0.9999	0.9996
LOD (mg l^{-1})	0.010	0.017	0.037	0.070	0.004

Excluding weekends or periods when access to the bulk precipitation collector was restricted, samples were collected from 27/01/98 – 11/05/98. Concentration (μequ l^{-1}) data for chloride, nitrate, sulphate, ammonium, sodium, potassium, calcium and magnesium are contained in Appendix III. Meteorological conditions (rainfall volume, wind speed, wind direction, air temperature, humidity and atmospheric pressure) for all samples are also listed in Appendix III.

Table 6.8 Overview of concentration data for samples collected between 27/01/98 – 11/05/98 (concentrations in μeq l^{-1}).

Analyte	Mean	Std. Dev.	Median	Geomean	Min value	Max value
Chloride (Cl^-)	384	423	206	191	13.2	1563
Nitrate (NO_3^-)	77	124	23	28	1.9	458
Sulphate (SO_4^{2-})	120	115	88	72	5.2	467
Ammonium (NH_4^+)	65	66	49	37	2.8	231
Sodium (Na^+)	386	451	242	118	3.5	1731
Potassium (K^+)	8.0	7.0	4.9	4.7	0.5	25
Calcium (Ca^{2+})	109	123	60	64	10.0	507
Magnesium (Mg^{2+})	97	101	60	55	6.6	398

Rainwater concentrations were presented as volume weighted means, as well as in geometric and arithmetric means (Table 6.8), to give a more representative value of the major ion concentrations over the sampling period. The volume weighted mean takes into account extreme concentrations owing to either intense or weak rainfall events. The volume weighted mean is calculated according to the equation:

$$C_{vw} = \Sigma C^* V_{rw} / \Sigma V_{rw}$$

Where C_{vw} = volume weighted mean, C = concentration of analyte in individual rainwater sample, V_{rw} = volume of rainwater in individual sample

Table 6.9 presents volume weighted mean concentrations for the Plymouth urban site data collated over the period 27/01/98 – 11/05/98. Table 6.9 also presents a range of data reporting typical precipitations collected in different environments and highlights some similarity with the Plymouth results. Maritime dominated environments such as those at Corsica[305] and Aberdeen[306] show the highest chloride and sodium concentrations. As the Plymouth atmosphere is also strongly influenced by sea-salt injection concentrations of Na and Cl show good agreement with those reported for the Corsican data. However concentrations for nitrate, sulphate and ammonium for the Plymouth data also show similarities with urban classified sites such as the one located at Leeds,U.K. This suggests that the Plymouth precipitation major ion concentration may be classified as being influenced by both maritime and urban sources.

Table 6.9 Precipitation chemical composition (μeq l^{-1}) for different environments.

	Cl^-	NO_3^-	SO_4^{2-}	NH_4^+	Na^+	K^+	Ca^{2+}	Mg^{2+}
Strasbourg (France)[304] URBAN	71	68	128	70	36	2	101	19
Sewen (France)[304] RURAL	17	26	30	38	15	4	5	3
Corsica (Italy)[305] MARITIME	357	28	42	25	261	9	33	36
Aberdeen (Scotland)[306] MARITIME	2655	54	151	18	2232	60	90	263
Mt. Sonnblick (Austria)[307] HIGH ALT. RURAL	4	8	13	3	4	1	11	2
Leeds (U.K.)[18] URBAN	126	46	121	30	94	9	62	29
Plymouth urban site	370	42	88	32	358	7.3	62	92

To evaluate whether the measured cation and anions represented the majority of the major ions in the collected rainwater, an ionic balance was calculated. The results of the calculations are presented in Figure 6.4.

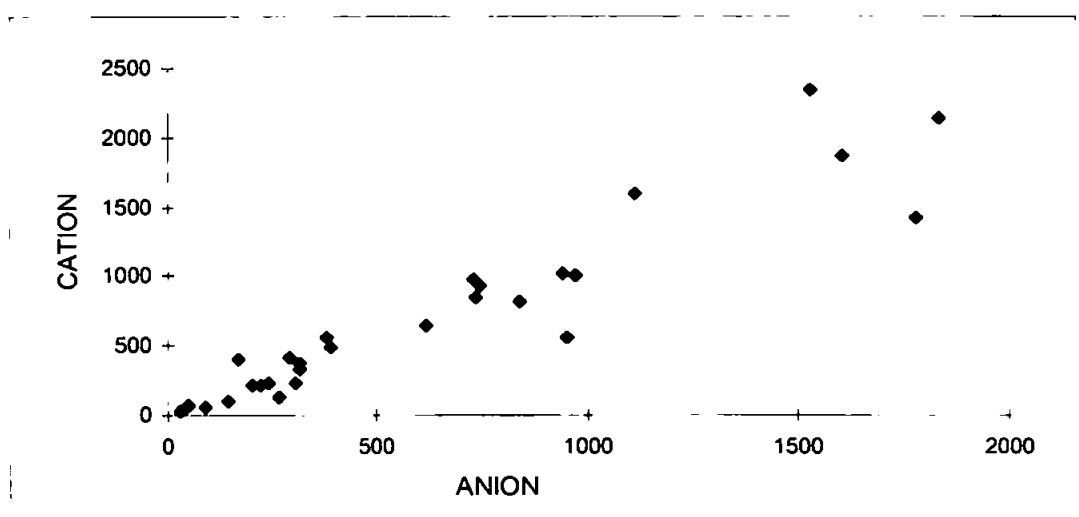

Figure 6.4 Ionic balance for precipitation data collected between 27/01/98 – 11/05/98 (concentrations in μeq l^{-1}), $r^2 = 0.8962$.

The correlation coefficient of 0.8962 indicates a deviation from perfect equivalence of less than 11%. It has been estimated that a quantitative balance is achieved if this deviation varies between 0% and 15% from perfect equivalence[308,309]. Since 11 % deviation lies within this range, it can be suggested that all of the major ions have been analysed.

However it must be noted that the majority of the samples present an anion deficit. This was probably due to the lack of bicarbonate and carbonate and short chain organic acids (e.g. acetate, formate, pyruvate) quantification in the analysis.

Potential influences on the chemical composition of precipitation are (1) source type and emission intensity of scavenged aerosol material (2) intensity of rain events and (3) removal processes during aerosol transport from the source to the sampling location. For the current study the impact of aerosol source on the rainwater composition will be highlighted. The Plymouth urban site aerosol population may be influenced by a number of source categories, these are;

- *Sea-salt generation*: The generation of sea-salt aerosols in a maritime dominated environment such as Plymouth is a major contribution to precipitation chemistries. Contributions to Plymouth precipitations from sea-salt aerosols are controlled primarily by wind speed (higher wind speeds, greater sea-salt generation) and wind direction (SW / S / NW, across the sea to Plymouth).
- *Long range pollutants and local anthropogenic materials*: Easterly winds transport air masses from the U.K and Western and Eastern Europe which may have higher loadings of nitrogen compounds such as nitrate and ammonia in addition to sulphates.
- *Crustal materials*: The influx of crustal materials such as calcium (Ca^{2+}) and magnesium (Mg^{2+}) being controlled by the surrounding geological characteristics.

Of these factors, sea-salt aerosols are likely to be the predominant factor contributing to Plymouth precipitation chemistry. Bubble-bursting processes occurring in the whitecaps of ocean seas inject large quantities of seawater into the atmosphere as microscopic droplets. The flux of bubbles to the surface has been estimated at around 2×10^6 m^{-2} s^{-1} with production rates increasing with wind strength[310]. Although a large proportion of sea-salt aerosols generated return to the oceans, a considerable amount can reach land in coastal regions, particularly during storms. This marine influence on precipitation composition in coastal regions can be so dominant that coastal precipitation composition is often thought of in terms of how it deviates from seawater composition. Sodium chloride dominates the composition of maritime precipitation, with concentrations decreasing exponentially with distance from the coast[305;306;311]. Therefore in coastal regions contributions to precipitation composition of species such as SO_4^{2-} and Ca^{2+} can be derived from

marine and terrigenic sources. However distinction can be made between the two due to the composition of major ions in seawater being relatively constant. Therefore compensation of "excess sulphate" or "non-marine sulphate" can be calculated using a sea-salt tracer element. Sodium is generally considered as the tracer of marine source and assuming all sodium originates from the marine source*, the marine contribution of an element X can be calculated by its [X] / [Na^+] ratio. For seawater the ratio of SO_4^{2-} / Na^+ is 0.12 (expressed in μeq l^{-1})[312] and for calcium it is 0.434. Therefore non-marine sulphate and calcium concentrations were calculated as follows.

$$nm\,[X] = [X] - [\text{marine } Na^+] \times ([X] / [Na^+])_{seawater}$$

To investigate the potential influence of different sources of aerosol material to the Plymouth precipitation chemistry, the individual rainwater major ion concentrations were separated into wind sector classifications (NE – SE, SE – SW, SW – NW) and respective volume weighted mean concentrations were calculated. The results are presented Table 6.10, and a number of trends can be highlighted.

Table 6.10 Volume weighted mean concentrations (μeq l^{-1}) for each wind sector.

Wind Sector	pH	Cl^-	NO_3^-	SO_4^{2-}	$nmSO_4^{2-}$	NH_4^+	Na^+	K^+	Ca^{2+}	$NmCa^{2+}$	Mg^{2+}
NE-SE	5.15	371	209	255	251	133	338	8	183	169	73
SE-SW	5.34	268	49	90	84	35	264	6	76	67	73
SW-NW	5.33	661	13	72	64	11	609	11	27	16	142

Mean wind speeds calculated for the wind sectors during the sampling campaign are shown below;

NE-SE	SE-SW	SW-NW
2.63 ms^{-1}	3.42 ms^{-1}	4.47 ms^{-1}

Air masses arising from the Atlantic (SW-NW) and English Channel (SE-SW) directions recorded the highest mean wind speeds producing, favourable conditions for the generation of sea-salt aerosols.

* Using a tracer of purely terrigenic origin (aluminium) a maximum contribution of 2 μeq l^{-1} from crustal sources has been evaluted.[310]

The marine influence is particularly strong in the dominant air mass which reaches Plymouth from a SW-NW direction and these samples had the highest concentrations of sodium and chloride. The dominant maritime sector (SW-NW), and to a lesser degree (SE-SW), also have the lowest concentrations of sulphate, nitrate and ammonium, with the proportion of sulphate derived from non-marine sources increasing as the air masses approached from the east. Minor contributions of sulphate, nitrate and ammonium to the composition of Plymouth precipitation will arise from short range local anthropogenic sources e.g. domestic heating and vehicle emissions. However the large increase in concentrations in the easterly dominated air masses (i.e. NE-SE) indicated long range transport of these pollutants from the rest of the U.K, Western and Eastern Europe. The highest concentrations of nitrate and sulphate also have a marked influence on the mean pH value which decreases due to increased formation of acidic aerosols.

6.3.2 AUSTRIAN SAMPLING CAMPAIGN

(a) ANNUAL PRECIPITATION DATA

Annual precipitation data obtained from the Austrian precipitation network was supplied by the Technical University of Vienna and was recorded in several different formats. These included the precipitation weighted mean concentrations in mg l^{-1} in monthly, quarterly and yearly form and the wet deposition loads in g/m^2 and kg/ha, also in monthly, quarterly and yearly format. This data was recorded along with site identification codes as listed in Table 6.5. Data can then be averaged for specific areas such as counties, geographical position (e.g. east , west) or total aerial deposition over the whole of Austria. The data is updated yearly, with trends and observations highlighted by yearly reports[313]. Table 6.11 shows the yearly averages (mg/l) for wet deposition recorded at the Mount Sonnblick Mountain Observatory for 1987 – 1995.

Table 6.11 Yearly averages (1987-1995) for wet deposition at the Sonnblick Mountain Observatory.

Season	Total vol.	PH	H^+	NH_4^+-N	Na^+	K^+	Ca^{2+}	Mg^{2+}	Cl^-	NO_3-N	SO_4^{2-}-S
	Mm						mg l^{-1}				
1987/88	1375.2	4.8	0.016	0.33	0.14	0.09	0.37	0.04	0.28	0.24	0.53
1988/89	1431.0	4.8	0.015	0.28	0.15	0.08	0.47	0.05	0.31	0.20	0.48
1989/90	1029.4	4.9	0.013	0.29	0.11	0.06	0.41	0.04	0.46	0.20	0.40
1990/91	1533.1	4.8	0.017	0.34	0.13	0.07	0.53	0.04	0.45	0.27	0.44
1991/92	1474.3	5.2	0.006	0.28	0.10	0.04	0.62	0.05	0.38	0.21	0.37
1992/93	1674.6	4.9	0.013	0.32	0.10	0.04	0.39	0.04	0.26	0.21	0.36
1993/94	1658.0	5.0	0.010	0.18	0.07	0.02	0.24	0.02	0.16	0.15	0.26
1994/95	1674.3	4.9	0.012	0.21	0.08	0.04	0.30	0.03	0.195	0.17	0.29

The majority of the concentrations for all of the analytes remained relatively stable over the duration of the sampling sites programme. However the sulphate plot showed a general decrease in concentration over the whole time period, whereas the calcium and chloride plots showed considerable variation in yearly concentration. In addition to individual elemental variations, there were also some variations that occurred from year to year, e.g. the year 1990 showed a general increase in concentrations for all analytes in contrast to 1993 which showed a general decline in concentrations.

(b) SPATIAL TRENDS IN AUSTRIAN PRECIPITATION FOR 1993

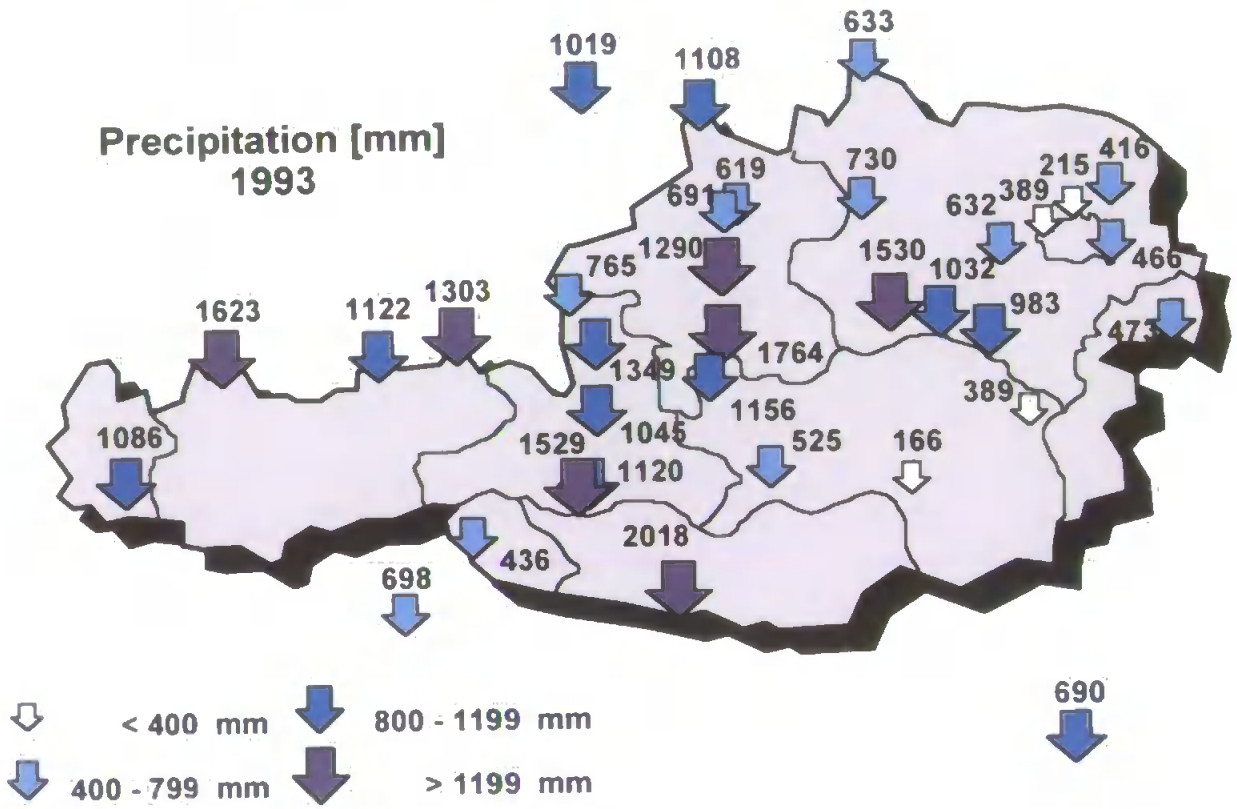

Figure 6.5 Total precipitation over Austria for 1993.

Wet deposition loads are not only influenced by the ionic concentrations in precipitation but also by the precipitation volume. With the complex and varying terrain in Austria, precipitation volume at the sampling sites showed large variations (between 166 mm and 2018 mm) for the year 1993. With the appreciably higher precipitation at highly elevated sites and the observed ionic concentrations found in those regions, can lead to high wet depositions loads[301]. This can be observed by comparing the two high altitude sites, Sonnblick Observatory (3106 m.a.s.l) (site code 27, Table 6.5) and Kolm Saigurn (1600 m.a.s.l) (site code 26, Table 6.5). Kolm Saigurn is located on the same mountain ridge below Sonnblick, lying in a northeastly position from the observatory.

From Figures 6.6-6.8 the concentrations of the components have comparable values, whereas the wet deposition loads are higher at the Mount Sonnblick site. This increase can be explained in terms of the higher precipitation at the higher altitude site of Sonnblick, 1529mm compared to 1120mm. This effect is important when considering critical loads in sensitive ecosystems[300]. In contrast, sampling sites which showed some of the highest concentrations for SO_4^{2-}-S, NO_3^--N and NH_4^+-N, namely the stations around Vienna, had considerably lower wet deposition values due to the low precipitation in the north east of Austria (215mm-632mm) (Figure 6.5).

(c) SPATIAL TRENDS IN AUSTRIAN NITRATE, AMMONIUM & SULPHATE DEPOSITION FOR 1993

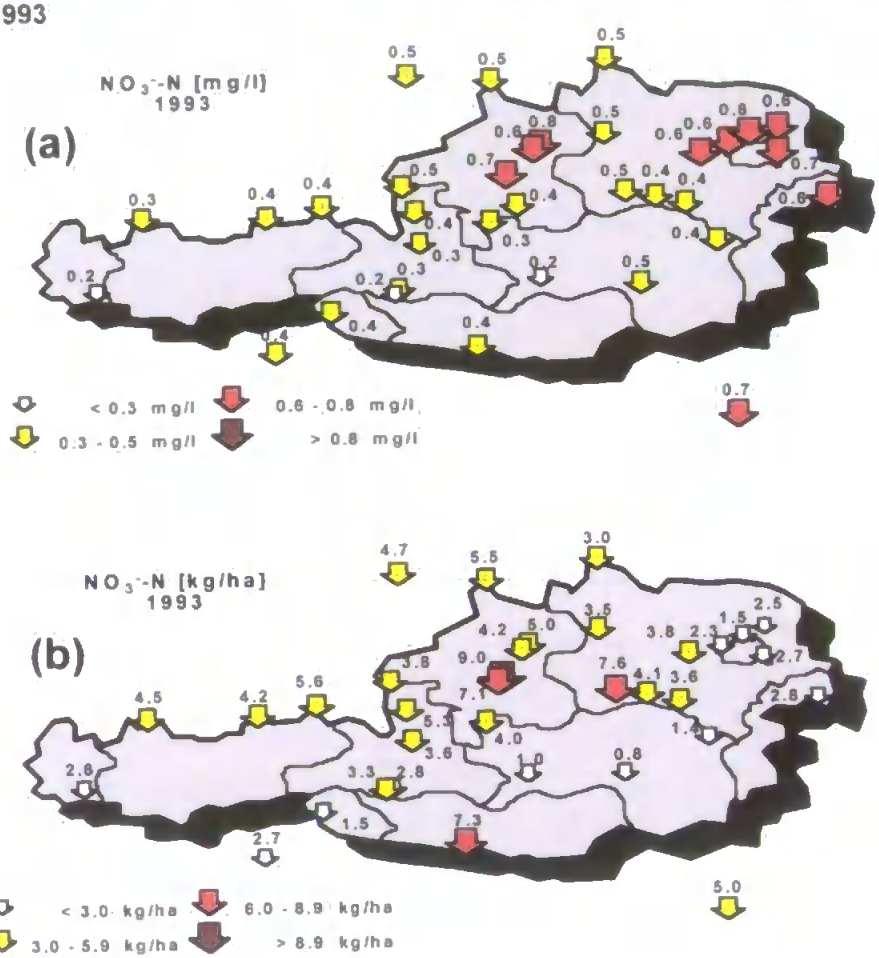

Figures 6.6a and 6.6b Spatial distributions of NO_3^--N over Austria for 1993, (a) ionic concentrations, (b) wet depositions loads.

Figures 6.6a and 6.6b for NO_3^--N show the same general spatial trends as discussed below for SO_4^{2-}-S. There is an increasing concentration gradient from the west of Austria to the east, and a decrease in concentrations from the north to the south of the country. These trends were first identified in an earlier study[301] using data from 1987-1989. The effect of precipitation on the wet deposition values is particularly prominent for NO_3^--N; low ionic concentrations for the mountain

sampling sites (26 & 27) with high precipitation volumes gave rise to wet deposition loads of 3.3 and 2.8 units respectively. Conversely, sampling sites located around the capital Vienna have much higher ionic concentrations (approximately twice that of the mountain sites), but when combined with the lower precipitation amounts gave rise to lower wet deposition values. A large influence on ionic composition (particularly nitrate, ammonium and sulphate) arises from domestic and foreign (former Eastern European countries) industrial activities with up to 3-fold differences in concentrations between the West and the East (see below).

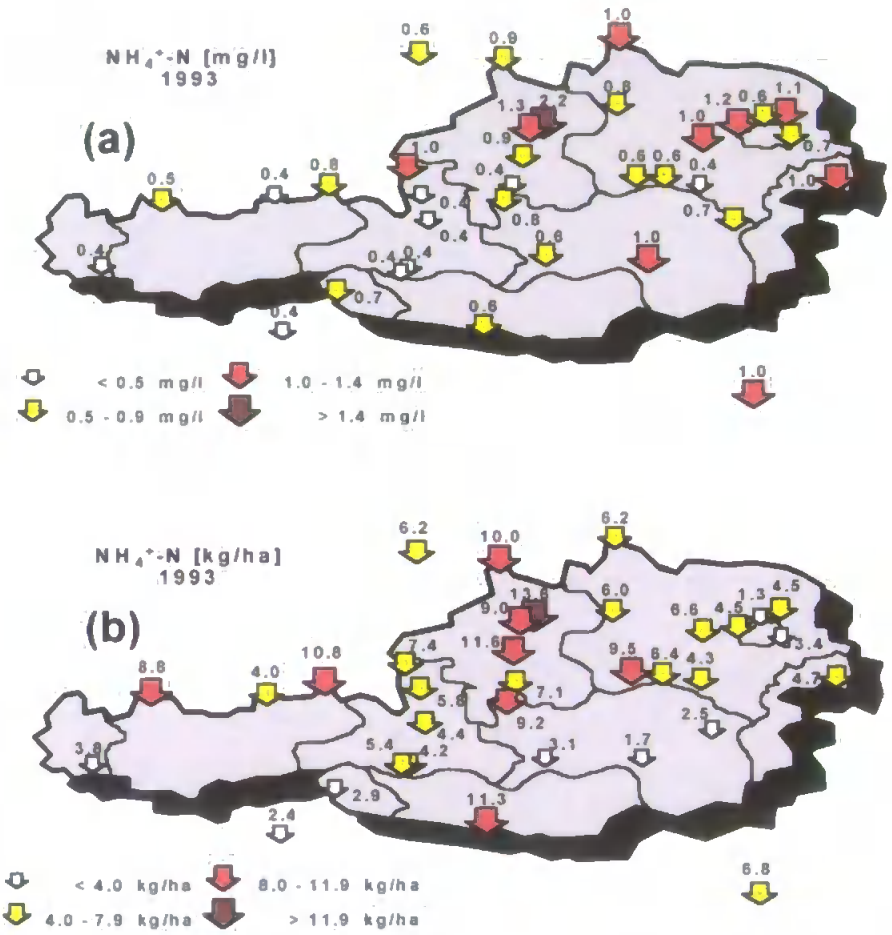

Figures 6.7a & 6.7b Spatial distributions of NH_4^+-N over Austria for 1993, (a) ionic concentrations, (b) wet depositions loads.

For all the Figures 6.6 – 6.8 the city sampling sites at Linz and Steyregg (56 & 53, respectively) showed concentrations around three times those of the surrounding areas, which directly reflected the high amount of industry in that area. Due to these abnormally high values the data set from these sites was excluded when calculation involving the deposition rates over the whole country were made. The increasing concentration gradients from West to East and North to South are also present in the ammonia deposition data.

Due to Austria's relatively small size (83900 km^2) the major proportion of SO_2 depositions is imported and this has been estimated to be up to 90%[314]. From Figure 6.8a the effect of the former Eastern European countries on the sulphate gradient can clearly be seen by comparing concentrations in the west e.g. sites 82 (Gaschum) and 11 (Reutte) (0.4 mg l^{-1} SO_4^{2-}-S) with the concentrations in Vienna which show increased concentrations 1.2mg l^{-1} SO_4^{2-}-S)

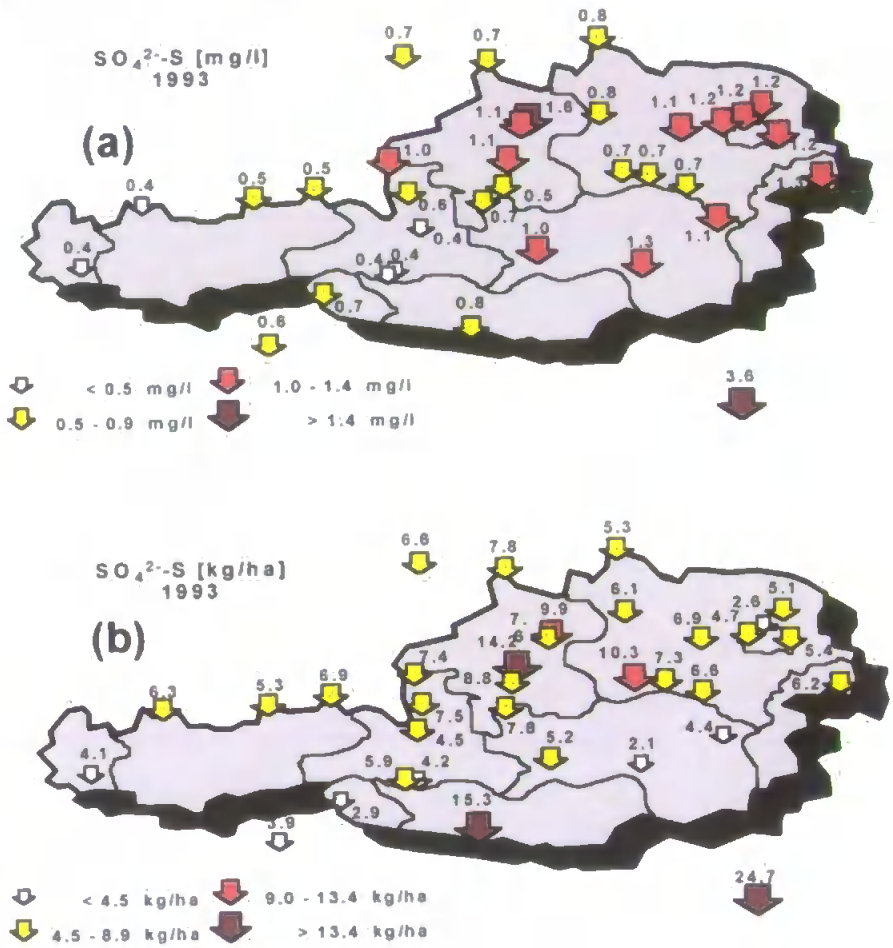

Figures 6.8a & 6.8b **Spatial distributions of SO_4^{2-}-S over Austria for 1993, (a) ionic concentrations, (b) wet depositions loads.**

6.6.3 CHEMOMETRIC ANALYSIS OF PRECIPITATION DATA.

An understanding of common environmental influences on the variability of major ions in rainwater (e.g. aerosol source, source emission strength, etc.) may be achieved by the application of statistical and mathematical methods to the data set. This section describes the effectiveness of a multivariate *"chemometric"* analysis on the precipitation datasets generated at both the Plymouth and Austrian sampling sites.

Brown et al.[315] have defined chemometrics as the 'discipline concerned with the application of statistical and mathematical methods, as well as those methods based on mathematical logic, to chemistry'. The three main aims of chemometrics, as defined by Haswell[316], are:

- the calibration, validation and significance of analytical measurement.
- the optimisation of chemical measurement and experimental procedures.
- the extraction of the maximum chemical information from analytical data.

Chemometric techniques can be viewed as analytical and interpretative tools, that help to find meaningful information, if any, in complex data sets. Multivariate modelling and analysis has proved to be a most active research area with the realisation that a holistic view of the data set facilitates overall judgement and evaluation of an observed system more effectively then examining one variable at a time[317]. The purpose of exploratory data analysis is to attain the best possible picture of the structure of the raw data matrix[318]. This can be achieved using traditional descriptive statistics such as the cross correlation matrix which is commonly used for this type of analysis, but in cases where there are many response variables, methods such as principal components analysis (PCA) are preferred[319].

PCA is a projection method which compresses the most salient information in the response variables into a much smaller number of principal components (PCs). A PC (also known as a factor or a loading vector) is defined as any linear combination of the response variables. Therefore, PCA can be visualised as a method for finding 'lines and planes of closest fit to systems of points in space'[320]. With a three dimensional cloud of data points, a system of three vectors, one in each dimension, would describe the variance in the three response variables. The same is true of higher dimensional spaces. By projecting the original variables onto these vectors one can obtain PCs that describe the original data set. A traditional method of data analysis to show trends or correlations between variables is the cross correlation matrix. The cross correlation matrix for the Plymouth data set (ion concentrations and meteorological data) is presented in Table 6.12.

Correlations were considered very good if $r > 0.8$, good if $0.6 \leq r \leq 0.8$ and marginal if $0.4 < r < 0.6$ at a confidence interval of 95 %[321]. Correlations between sodium, chloride and magnesium were very good (0.96), indicative of the common ion source, i.e. sea-salt generation.

This was confirmed from wind sector analysis as discussed in section 6.3.1. Very good correlations were also detected between calcium with sulphate and ammonium. This common variability is unlikely to be due to common sources, as calcium will be derived from terrestrial crustal material whereas sulphate and ammonium will be anthropogenic in origin. The good correlation may reflect the common continental source location or in the case of calcium and sulphate the interaction and formation of calcium sulphate at the aerosol surface during evaporation / condensation reactions during the aerosol atmospheric transport from source to rainfall washout at the sampling location. Similarly ammonium in the atmosphere is known to significantly contribute to the neutralisation of acid aerosols, consequently ammonium sulphate and ammonium nitrate are important compound in the atmosphere[322;323], confirmed by their respective correlation coefficients of 0.79 (NH_4^+ / SO_4^{2-}) and 0.63 (NH_4^+ / NO_3^-).

The use of Principal Component Analysis (PCA) to investigate correlations in the data will not only support traditional methods but, due to the holistic nature of PCA, any hidden information contained within the dataset may also be revealed. One of the advantages of chemometric techniques over the more traditional statistical data treatments (as in Table 6.12) is that of processing time. For example, all of the data for all the Austrian precipitation network sites over the whole of their operational lifetime (thirteen years in some cases) can be processed in approximately 5 min but the equivalent analysis using a more traditional method such as a correlation matrix would take several days or weeks to calculate. The monthly averaged concentration data from Austria was arranged in a data matrix form as shown below in Figure 6.9 and the Plymouth data set was arranged in a similar matrix containing both ionic concentrations and meteorological conditions data.

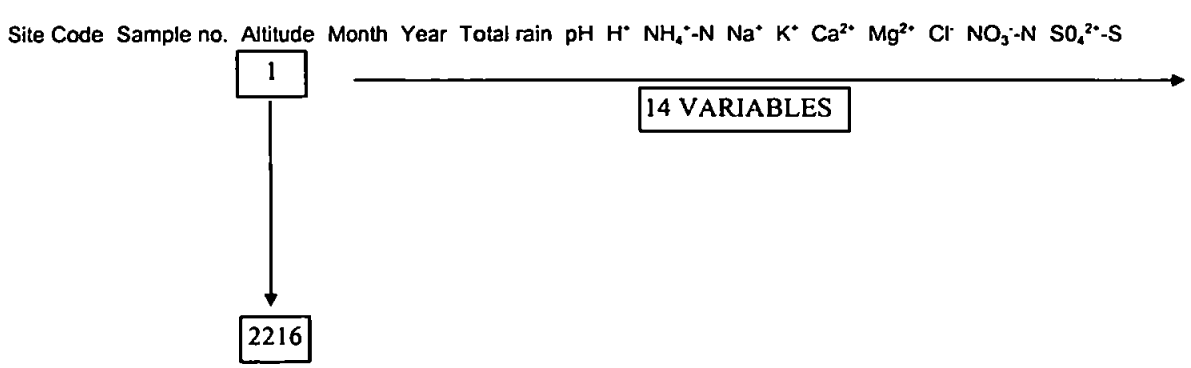

Figure 6.9 **Arrangement of data matrix for chemometric analysis of Austrian precipitation data.**

Table 6.12 Cross correlation matrix for Plymouth precipitation data set.

Red = very good correlation, Blue = good correlation

Concentrations = μequ l^{-1}, RAIN = mm W.S. = wind speed (ms^{-1}), W.D. = wind direction (degrees), PRESS = atmospheric pressure (Hpa).

	Cl^-	NO_3^-	SO_4^{2-}	NH_4^+	Na^+	K^+	Ca^{2+}	Mg^{2+}	RAIN	W.S.	W.D.	PRESS
Cl^-												
NO_3^-	-0.01											
SO_4^{2-}	0.40	0.59										
NH_4^+	-0.03	0.63	0.79									
Na^+	0.96	-0.02	0.44	0.01								
K^+	0.78	0.18	0.69	0.36	0.84							
Ca^{2+}	0.26	0.49	0.90	0.81	0.30	0.65						
Mg^{2+}	0.96	-0.06	0.43	0.04	0.96	0.82	0.38					
RAIN	-0.18	-0.3	-0.58	-0.56	-0.24	-0.32	-0.57	-0.28				
W.S.	0.10	-0.54	-0.52	-0.58	0.12	-0.01	-0.44	0.07	0.67			
W.D.	0.31	-0.43	-0.45	-0.44	0.27	0.03	-0.43	0.27	0.33	0.40		
PRES.	0.02	0.13	0.22	0.41	-0.02	0.07	0.25	0.06	-0.46	-0.52	0.3	

The raw experimental data may have a distribution that is not optimal for analysis, and data pre-processing may be necessary. Data pre-processing techniques can reduce the noise (non-analytical information) from such effects and lead to enhanced information recovery. There are many data pre-processing techniques available but the most applicable to the Austrian data set is weighting the raw experimental data.. The most common options are weights of 1.0 or the inverse of the standard deviation of the response variables (sd^{-1}). A weighting of 1.0 represents the raw data. Applying weights of sd^{-1} (autoscaling or standardisation) by dividing each response variable by its standard deviation results in all responses having a variance of 1. This is useful when the magnitude of responses for selected variables is not comparable as in this case e.g. altitudes compared with concentrations. Therefore in this work the raw data matrix was autoscaled by applying weights of sd^{-1} prior to PCA.

(a) PLYMOUTH SAMPING CAMPAIGN

PCA residual calibration variance revealed little reduction of the dataset, due to the high degree of variability in the dataset, with no dominant factors. The first three PC'S, PC1, PC2 and PC3, normally account for around 85-99 % of variability in a data set, but only contributed 36, 27 and 11 % for the Plymouth rain data, giving a total of 74 % of variability described.

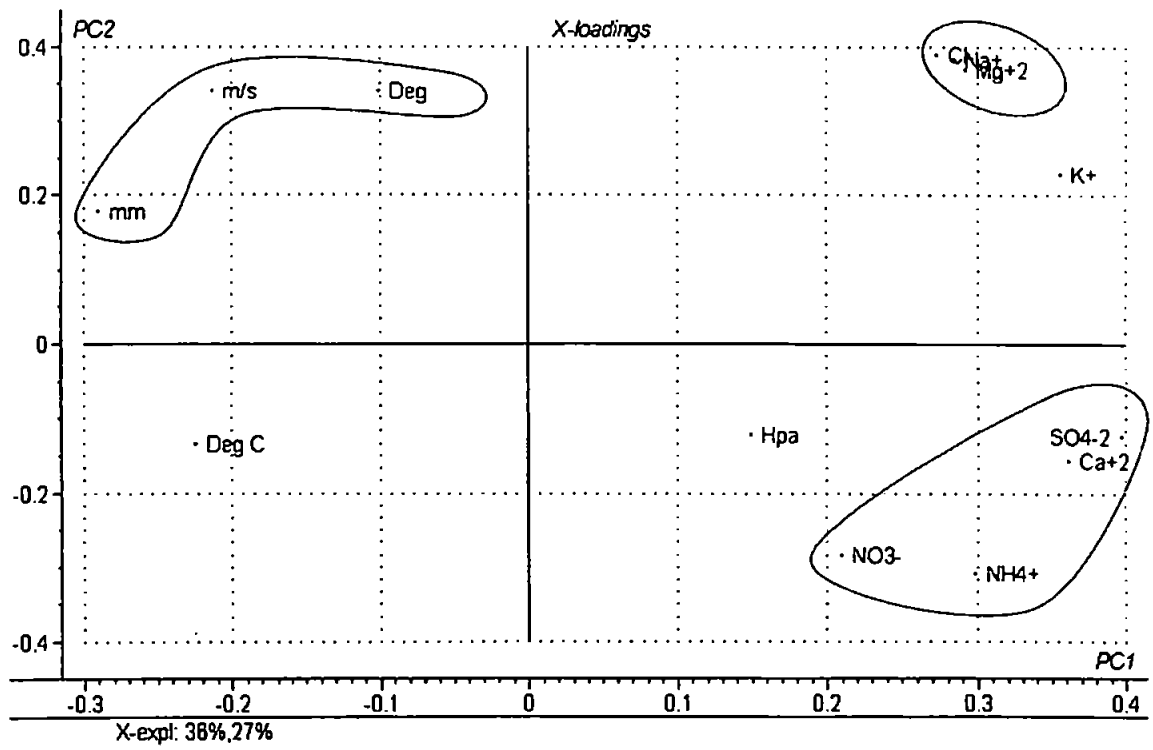

Figure 6.10 2D loadings plot for PC1 versus PC2 for Plymouth precipitation (27/01/98-11/05/98).

Figure 6.10 shows the importance of the different variables for the principle components 1 and 2 which represent the largest variations in the dataset, 36 % and 27 % respectively. The major cluster within the dataset showed a strong, tightly grouped positive co-variance of Cl^-, Na^+ and Mg^{2+}, which supports the hypothesis of a common marine ion source for the Plymouth precipitation samples (refer to sections 6.3.1 and 6.3.3). The plot also showed other tentative (less tightly grouped) correlations between SO_4^{2-}, Ca^{2+}, NH_4^+ and NO_3^-, highlighting the neutralisation of acid aerosols by NH_4^+ and Ca^{2+} during evaporation / condensation at the aerosol surface during atmospheric transport. The Ca^{2+}/SO_4^{2-} cluster supports the hypothesis that Ca^{2+} is the main constituent for the neutralisation of SO_4^{2-} in precipitation. The meteorological data however showed no significant trends. This is most likely due to the lack of data points or highlights the complexity and variation of the factors controlling precipitation chemistry.

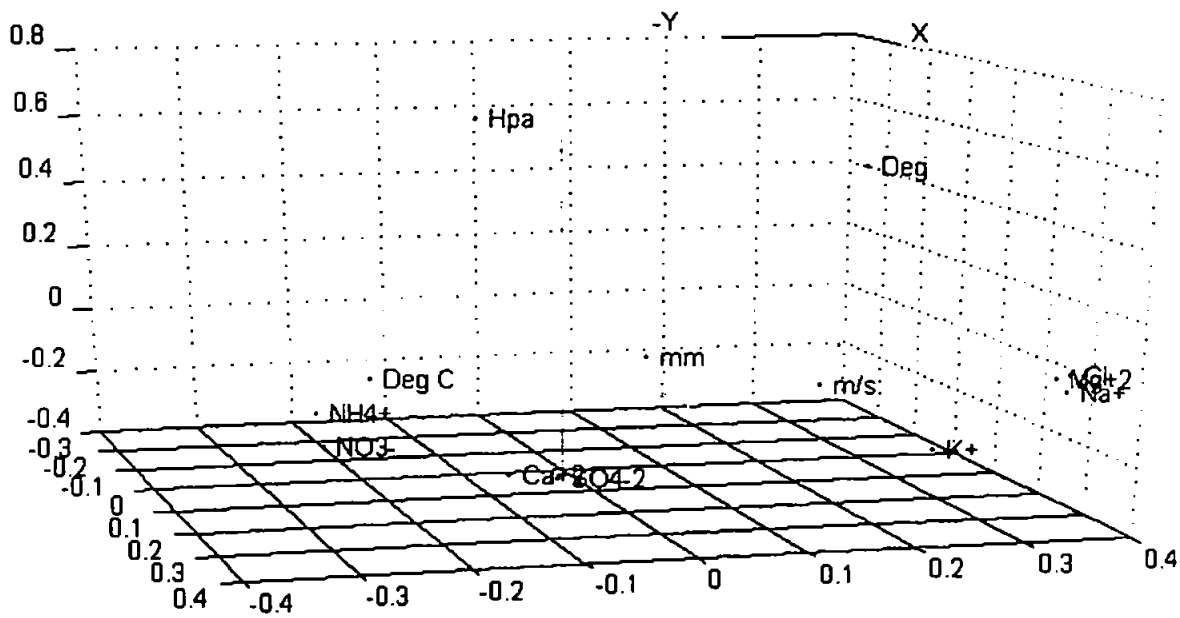

Figure 6.11 3D loadings plot of Plymouth precipitation data (27/01/98-11/05/98).

Figure 6.11 shows the 3D loadings plot for principle components 1, 2 and 3. Using this plot it is possible to identify whether the clusters observed in the 2D loadings plot (Figure 6.10) are in fact clusters or a function of the graphical representation itself. It shows the tight grouping of Na^+, Cl^- and Mg^{2+}, confirming their strong marine origin, and also the Ca^{2+}/SO_4^{2-} neutralisation relationship. Figure 6.12 shows the projection of the dataset onto the planes of PC1 and PC2, and is known as a scores plot.

The plot gives information on the relationships between samples and how samples are positioned in multivariate space. Most of the samples are found near the origin and this shows similarities between samples with respect to PC1 and PC2. This cluster is not very tightly grouped and is most likely due to the small number of samples which were used for this work. It is expected that if the dataset had been larger, this cluster would have contained the majority of samples.

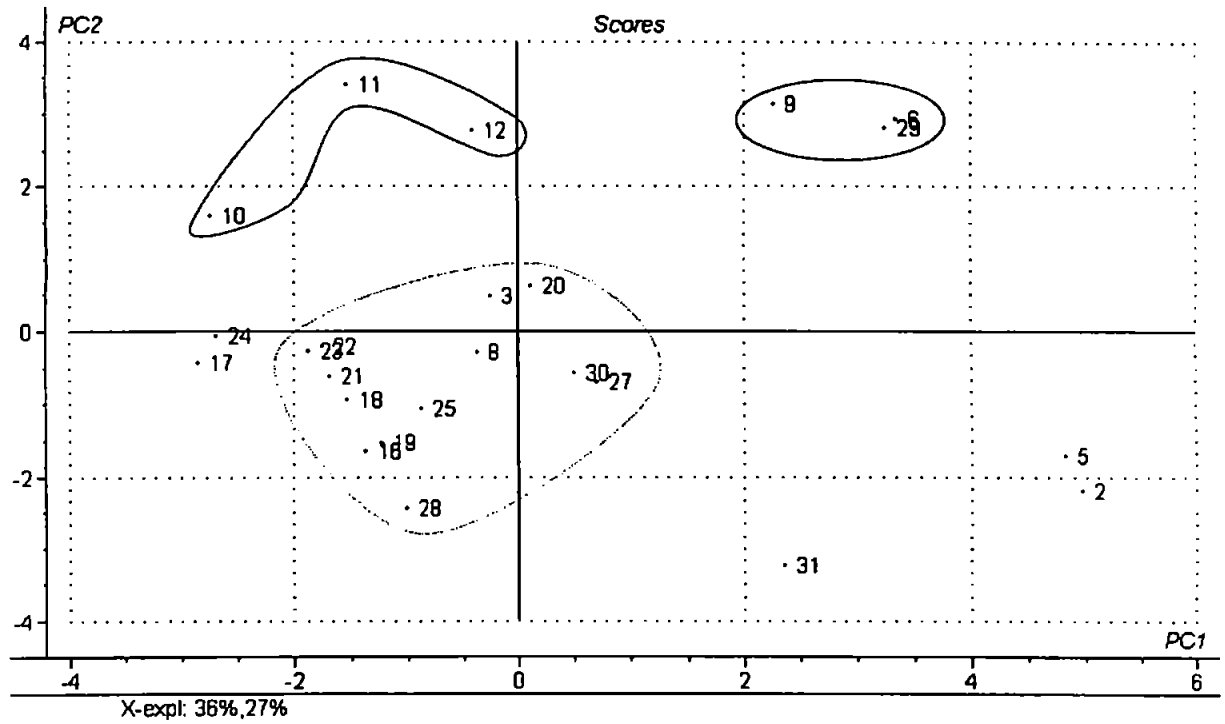

Figure 6.12 Scores plot for the Plymouth precipitation data (27/01/98-11/05/98).

The scores plot can be used together with its corresponding loadings plot (Figure 6.10 - same principle components), to determine which variables were responsible for the differences between samples. For example, samples with high scores along the first component usually have a large value for variables with high loadings along the first component. The score plot is also useful for the detection of outliers in the data set. In Figure 6.12, the two most distinctive sets of samples (excluding origin cluster) are the small cluster in the upper left quadrant of the plot and the cluster in the upper right quadrant. Examination of the corresponding loading plots revealed that the samples from the upper right cluster had abnormally high Cl^-, Na^+ and Mg^{2+} concentrations (strong marine salt influence), and the samples from the upper left quadrant were sampled under abnormal meteorological conditions.

Samples 5 and 2 were investigated due to their isolation within the dataset (Figure 6.12). By comparing this with the corresponding loadings plot (Figure 6.10), these samples were found to have the highest concentrations of sulphate. Comparison of Figures 6.10 and 6.12 highlights the inverse correlation between concentration and rainfall amount. Samples lying on the right hand side of PC1 had the highest concentrations and lowest rainfall amounts, and samples on the left of PC1 had the lowest concentrations and highest amount of rainfall.

(b) AUSTRIAN SAMPLING CAMPAIGN

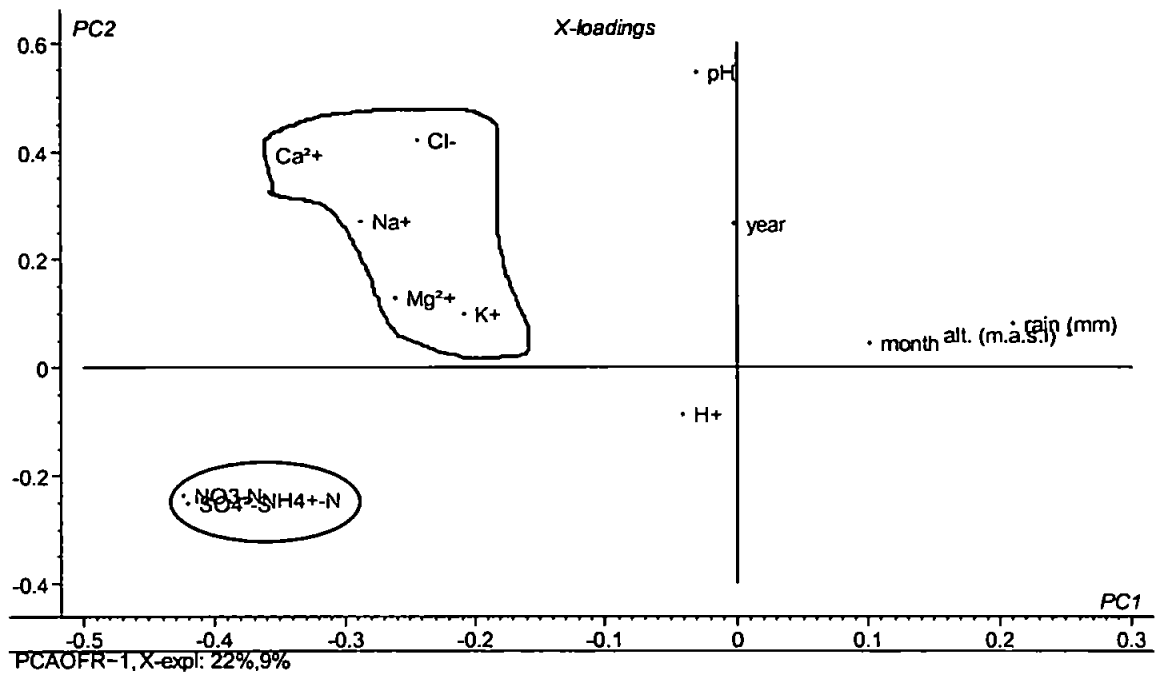

Figure 6.13 2D loadings plot of PC1 versus PC2 for Austrian precipitation (1987-1993)

The PCA residual calibration variance showed only a small reduction in the variance of the Austrian precipitation dataset. Principle components 1, 2 and 3 only accounted for 22, 9 and 5 % respectively (39 % total) of the variability in the datset. Figure 6.13 shows the 2D loadings plot of PC1 versus PC2. The major cluster highlighted showed a strong positive co-variance of SO_4^{2-}-S, NO_3^--N and NH_4^+-N, and compared well with data obtained for the Plymouth sampling campaign. This supports the conclusion that NH_4^+ is the main constituent for the neutralisation of acid aerosols[322;323]. Figure 6.15 also highlights the expected strong positive correlation between altitude and rainfall. The other highlighted section of the plot showed a weaker correlation between calcium, chloride, sodium, magnesium and potassium. The cluster is also less pronounced than that observed for the Plymouth rainwater dataset. This may be explained by the lower marine influence on the aerosol population at the land locked Austrian sampling sites.

Figure 6.14 shows the scores plot of the Austrian precipitation for PC1 & PC2. The main bulk of the samples were concentrated around the origin and this showed that there were high similarities between samples with respect to PC1 and PC2.

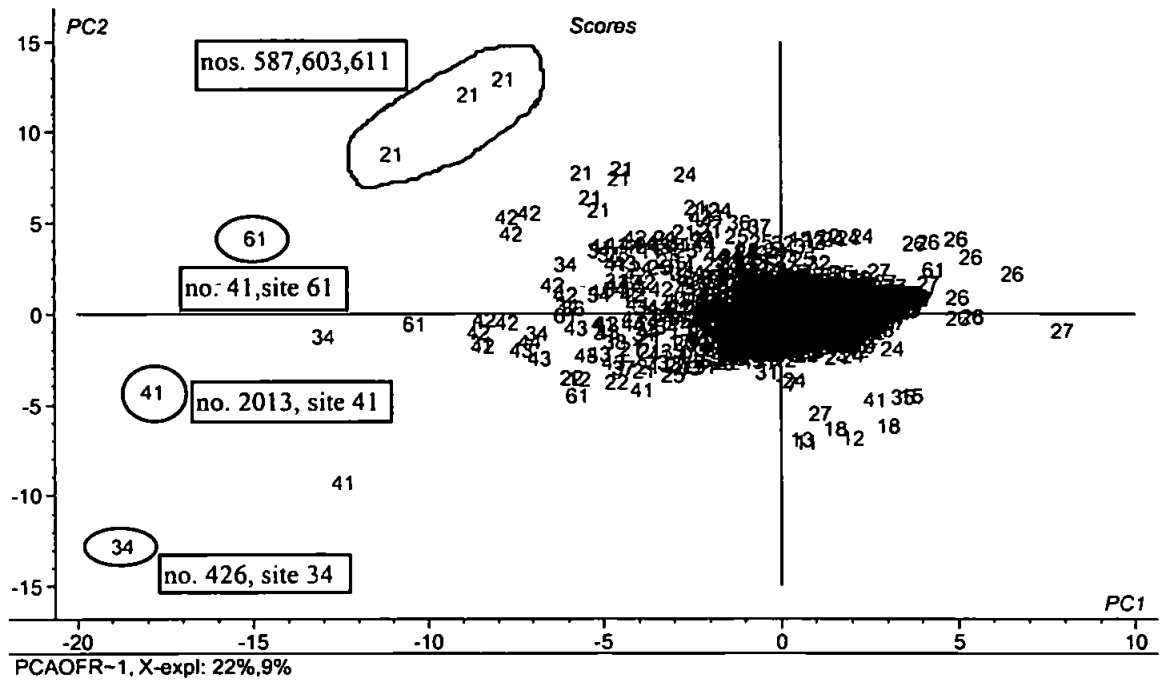

Figure 6.14 Scores plot of Austrian precipitation data.

The most distinctive "different" set of samples was the small cluster in the top left quadrant of the plot, i.e. those samples belonging to site 21. With examination of the corresponding loadings plot (Figure 6.13) it follows that these samples may have different calcium and/or chloride concentrations in comparison with the bulk dataset. This can be confirmed directly using the Unscrambler package. By highlighting an individual sample using a cursor, the corresponding position in the raw data matrix is given. The three outlier samples had calcium and chloride values an order of magnitude higher than the other samples. Other outliers investigated are also highlighted in Figure 6.16. Highlighted sample 41 (site 61) revealed that no H^+ calculation had been made for this sample. Examination of sample no. 2013 (site 41) found that the sample had a lower pH value and generally higher concentrations of analytes than other samples. Sample 426 (site 34) was found to have a very low precipitation volume (0.3 mm), possibly indicating a loss during collection, transport or analysis. This sample also reported high NH_4^+-N, SO_4^{2-}-S, NO_3^--N and Ca^{2+} concentrations.

6.4 CONCLUSIONS

The following specific conclusions can be drawn from the research reported in this chapter:

1. It is important to maintain rigorous cleaning protocols for all sampling containers and accessories in order to minimise contamination and maximise the reliability of the data set. Extensive rinsing with Milli-Q water and storage in zip lock bags is the most effective cleaning protocol.

2. Ion chromatography with conductimetric detection is an excellent laboratory technique, with suitable detection limits, for rapidly quantifying several anions (chloride (LOD, 1 $\mu g\ l^{-1}$), nitrate (LOD, 1 $\mu g\ l^{-1}$) and sulphate (LOD, 6 $\mu g\ l^{-1}$)) and cations (ammonium (LOD, 4 $\mu g\ l^{-1}$), sodium (LOD, 37 $\mu g\ l^{-1}$), potassium (LOD, 70 $\mu g\ l^{-1}$), calcium (LOD, 10 $\mu g\ l^{-1}$) and magnesium (LOD, 17 $\mu g\ l^{-1}$)) in precipitation samples.

3. The chemical composition of Plymouth precipitation is strongly influenced by the marine environment shown by the strong correlations between marine generated sea-salt ions (Cl^- Na^+ and Mg^{2+}) which was confirmed by PCA. The importance of the marine source for these components was highlighted by high concentrations in rain waters associated with air masses from the west. PCA also showed a weaker correlation between the anthropogenically derived chemical components (NO_3^-, NH_4^+) which can be explained by chemical transformations and removal processes during transport of these components from distant European sources.

4. The Austrian data was characterised by strong correlations between the anthropogenic components, NH_4^+, NO_3^- and SO_4^{2-} , and weaker correlations between Cl^-, Na^+ and Mg^{2+}. These observations are explained by the close proximity of Eastern European / industrial sources and the lower impact of the sea-salt contribution to the Austrian aerosol population.

5. Chemometric techniques (autoscaling and PCA) provide a much more rapid means of investigating large environmental data sets than the traditionally used correlation matrix. They also have the potential to determine more complex, multi-parameter interactions in the data set.

Chapter Seven

Conclusions & Future Work

"A doctorate is one percent inspiration and ninety-nine percent perspiration"

- Adaptation from Thomas Eddison –

7 CONCLUSIONS AND FUTURE WORK

7.1 GENERAL CONCLUSIONS

In addition to the specific conclusions reported at the end of each experimental chapter, the following general conclusions can be drawn from the work described in this thesis;

Ocean Optics PSD – 1000 Spectrometer.

The Ocean Optics PSD – 1000 spectrometer is relatively low cost in comparison with a conventional spectrophotometer, inherently portable and of rugged construction, which makes it ideally suited for in situ and process deployments. Its size, optical components (e.g. optical fibres), rapid spectral acquisition and flexible software make it compatible with FI technologies for monitoring transient signals. The wavelength repeatability, photometric linearity, instrumental noise and drift of the Ocean Optics PSD – 1000 are sufficiently good for environmental monitoring. The spectrometer's components are susceptible to temperature effects and any application involving significant temperature fluctuations would need a thermostatted housing.

FI Chemistries.

The results reported in this thesis confirm literature data in terms of optimum FI manifold parameters for nitrate and ammonia. On-line chemical (e.g. solid phase cadmium reduction column) and physical (e.g. gas diffusion) sample treatment can be incorporated within the manifold and remotely deployed, making FI a powerful technique for environmental monitoring. The Ocean Optics PSD – 1000 spectrometer and associated optical fibres can be effectively incorporated within the FI system to provide enhanced information content compared with conventional single beam detectors.

Automation & Fieldwork.

Micro-solenoid pumps and switching valves are now widely commercially available as an alternative to conventional peristaltic pumps and are compatible with miniaturised FI systems. Their size, weight and power consumption are ideally suited to incorporation in field deployed FI systems. The pumps are of low maintenance (no pump tubing) and capable of long periods of unattended operation. Sample presentation is important and on – line filtration or cross – flow filtration is recommended to

avoid particulate matter blocking the small apertures within the pumps. National Instruments LabView™ is an extremely flexible and powerful programming tool that is well suited to the development of user interactive, windows based, control and data acquisition software for the automation of FI systems. The software is capable of adjusting the linear range by using different wavelengths for calibration, which makes it sufficiently flexible for deployment throughout the UK river network at any time of year.

Precipitation Sampling, Analysis & Interpretation.

Ion chromatography is well suited to the laboratory analysis of precipitation samples, providing high quality analytical data for environmental interpretation. However care must be taken at all sample collection, pre – treatment and analysis stages to avoid contamination of the samples. The collected environmental datasets highlighted the strong influence of aerosol source on the chemical composition of precipitation samples. Principal Components Analysis (PCA) was shown to complement traditional statistical analysis techniques (e.g. cross correlation matrix), with the added advantage of being able to rapidly process multi – parameter environmental datasets.

7.2 SUGGESTIONS FOR FUTURE WORK

Possible directions for future work arising from this research can be divided into four separate areas;

FI Instrumentation.

Design modifications to the automated monitor and ruggedisation would improve its versatility, reliability and analytical performance. These include;

- The use of custom designed fibre optics and flow cell configurations.
- Improvements to / or replacement of the micro – solenoid pumps to provide smoother flows within the FI manifold.
- Thermostatted temperature control of the monitor housing.
- Incorporation of the FI manifold, reagents, micro – electronic controller, spectrometer and optical components in a custom built, environmental proof (water, dust and shock) housing.
- The incorporation of on – board standards, with associated programming to enable full user control and automated calibration routines (the current manifold already incorporates the associated hardware for this modification to be made).
- The flexibility of LabView™ and the dual wavelength capability of the Ocean Optics PSD – 1000 spectrometer are suited to the development of simultaneous multi – analyte determinations e.g. NH_3 / NO_3^-, NO_3^- / PO_4^- by the incorporation of the appropriate FI manifolds.
- The versatility of LabView™ also enables the possibility of incorporating on board "intelligence" or decision making routines. These could be used to automatically adjust monitor acquisition parameters to respond to real – time environmental changes (e.g. transient increases in concentration in a river due to a pollution event).
- LabView™ remote communications to and from the monitor could be incorporated through an internal computer modem linked to an external communications device e.g. mobile / satellite phone.

FI Chemistries.

The ammonia gas diffusion manifold could be modified to reduce the ambient level of ammonia within the carrier stream and thereby lower the blank level and improve the detection limit. This could be

achieved with an on – line scrubbing system, by passing the carrier stream through a porous PTFE membrane tube immersed in an acidic solution (e.g H_2SO_4). The laminar flow system was not completely successful in this work, and ruggedisation of the optical components would improve the reliability of this approach.

Further development of the nitrate / nitrite manifold to incorporate LabView™ controlled switching routines would facilitate the determination of nitrate and nitrite, either sequentially using a single spectrometer channel (e.g. Master) or simultaneously using both channels (Master and Slave) of the Ocean Optics PSD – 1000 spectrometer. Replacement of the toxic copperised cadmium reduction column by e.g. on – line photo – oxidation of nitrate to nitrite would minimise waste and reduce environmental impact. This will become an increasingly important factor as the availability and use of cadmium becomes increasingly restricted.

Field Deployment.

Longer field deployments (e.g. at the River Frome site) of the automated monitor could be used to further the investigation into its long term performance and provide seasonal nitrate concentration trends. The incorporation of on – line filtration or sample pre-treatment would improve its reliability for deployments in rivers with high suspended particulate matter. Further field deployments at a variety of river locations, including more remote sites, would not only prove the inherent portability of the monitor (no mains supply required) but also provide unique data sets to aid in the understanding of nutrient biogeochemical cycling. The issue of biofouling for long term, unattended deployments would also need to be considered.

Precipitation Studies.

A large database for Plymouth precipitation, facilitated by on-going collection and analysis of precipitation, would enable improved modeling of seasonal trends and interpretation of aerosol sources. PCA applied to other environmental databases would enable comparisons to be made with the Plymouth and Austrian data sets and further assess the validity of the PCA approach. An improvement of the quality of the Plymouth precipitation data could be achieved with the use of a "wet and dry" precipitation sampler, thereby eliminating dry deposition contamination of wet samples.

References

1. Antai, N. J.; Harrison, P. J.; Oliveira, L.; *Phycologia* **1991**, *30*, 1.

2. Robards, K.; McKelvie, I. D.; Benson, R. L.; Worsfold, P. J.; Blundell, N. J.; Casey, H.; *Analytica Chimica Acta* **1994**, *287*, 147.

3. Royal Society; *The Nitrogen Cycle of the United Kingdom*. London, The Royal Society. **1983**.

4. Torrey, M. S.; Lee, G. F.; *Limnology.Oceanography* **1976**, *21*, 365.

5. Stewart, W. D. P.; Sinada, F.; Christofi, N.; Daft, M. J.; *Symposium of the Society of Applied Micro-Biology* **1977**, *6*, 31.

6. Coleman, N.; Stewart, W. D. P.; *British Phycology Journal* **1979**, *14*, 21.

7. Stewart, W. D. P.; Preston, T.; Peterson, H. G.; Christofi, N.; *Philosophical Transaction of the Royal Society London* **1982**, *B296*, 491.

8. Heathwaite, A. L.; O'Sullivan, P. E.; *Hydrobiologia* **1991**, *214*, 125.

9. Preston, T.; Stewart, W. D. P.; Reynold, C. S.; *Nature* **1980**, *288*, 365.

10. Jones, J. G.; Simon, B. M.; Horsley, R. W. *J.; Genetic Microbiology* **1982**, *128*, 2823.

11. Burt, T. P.; Heathwaite, A. L.; Trudgill, S. T.; *Nitrate - Processes, Patterns and Management*; John Wiley & Sons: Chichester, England, **1993**.

12. Wild, H. E.; Sawyer, C. N.; McManon, J. C.; *J.Water Pollution Control Federation* **1971**, *43*, 1845.

13. Ellis, K. V.; *Surface Water Pollution and its Control*; Macmillan: **1989**.

14. Jones, J. G.; Downes, M. T.; Talling, I. B.; *Freshwater Biology* **1980**, *10*, 341.

15. Royal Commission on Environmental Pollution:; *Pollution in some British Estuaries and Coastal Waters. Royal Commission on Environmental Pollution*. Third. London, H.M.S.O. **1972**.

16. Moss, B., Balls, H., Booker, I., Manson, K., and Timms, M.; *Problems in the construction of a nutrient budget prior to restoration of the R. Bure and its Boards, Norfolk, from eutrophication*. University of East Anglia. **1999**.

17. Gostick, K. G.; *Philosophical Transaction of the Royal Society London* **1982**, *B296*, 329.

18. Clarke, A. G.; Lambert, D. R.; Willison, M. J.; *Atmospheric Environment* **1990**, *24B*, 159.

19. Golding, K. W. T.; *Soil Use & Management* **1990**, *6*, 61.

20. Addiscott, T. M.; Whitmore, A. P.; Powlson, D. S.; *Farming, Fertilisers and the Nitrate Problem*; CAB International: Wallington, **1991**.

21. Barrett, C. F.; *Acid Deposition in the United Kingdom*; Crown Copyright: Stevenage, U.K., **1987**.

22. Dollard, G. J.; Atkins, D. H. F.; Davies, T. J.; Healy, C.; *Nature* **1987**, *326*, 481.

23. Casey, H.; Clarke, R. T.; Smith, S. M.; *Chemistry Ecology* **1993**, *8*, 105.

24. Burns, I. G.; Greenwood, D. J. *Agriculture and Environment* **1982**, *7*, 35.

25. Foster, S. S. P.; Cripps, A. C.; Smith-Carrington, A.; *Philosophical Transaction of the Royal Society London* **1982**, *B296*, 341.

26. Smith, R. M.; Martell, A. E.; *Critical Stability Constants: Volume 2*; Plenum Press: New York, **1975**.

27. Russo, R. C.; Thurston, R. V.; *Toxicity of ammonia, nitrite and nitrate to fishes. Aquaculture and water quality in: Advances in world aquaculture.*; WAS Publishers: **1991**.

28. Hargreaves, J. A.; *Aquaculture* **1998**, *166*, 181.

29. PersonLeRuyet, J.; Chartois, H.; Quemener, L.; *Aquaculture* **1995**, *136*, 181.

30. Wilson, R. W.; Taylor, E. W.; *J.Experimental Biology* **1992**, *166*, 95.

31. Handy, R. D.; Poxton, M. G.; *Fish Biology* **1993**, *3*, 205.

32. Environment Protection Agency; Office of Research and Development.; *Water quality criteria for the protection of aquatic life and its uses: Ammonia*. 189pp. Duluth, Environmental Research Laboratory. **1983**.

33. Ruffier, P. J.; Boyle, W. C.; Kleinschmidt, J. K.; *Journal WPCF.Water Pollution Contz.Fed.* **1981**, *53*, 367.

34. Arillo, A.; Margiocco, C.; Melodia, F.; Mensi, P.; Schemone, G.; *Ecotoxicology Environmental Safety* **1981**, *5*, 316.

35. PersonLeRuyet, J.; Boeuf, G.; *Bulletin Francais de la Peche et de la Pisciculture* **1998**, 393.

36. PersonLeRuyet, J.; Boeuf, G.; Infante, J. Z.; Helgason, S.; LeRoux, A.; *Comparative Biochemistry and Physiology A-Molecular and Integrative Physiology* **1998**, *119*, 511.

37. Magee, P. N. *Philosophical Transaction of the Royal Society London* **1982**, *B296*, 543-550.

38. Jaffe, E. R.; *Clinical Hematology* **1981**, *10*, 99.

39. Preussman, R. and Stewart, B. W.; *N-nitroso carcinogens, Chemical Carcinogens*, A.C.S. Monographs 182. 643-828. Washington DC, American Chemical Society. **1984**.

40. Hartmann, P. E.; *Environmental Mutagensis* **1983**, *5*, 111.

41. Armijo, R.; Coulson, A. H.; *International J.of Epidemiology* **1975**, *4*, 301.

42. Al-Dabbagh, S.; Forman, D.; Bryson, D.; *British Journal of Industrial Medicine* **1986**, *43*, 507.

43. Forman, D.; *Cancer Surveys* **1989**, *8*, 443.

44. Hayes, C. R.; Greene, L. A.; *Water Pollution Control* **1984**, *83*, 42.

45. Henderson-Sellars, B.; Markland, H.; *Decaying Lakes: origins and control of eutrophication.*; Wilrey & Sons: Chichester, U.K., **1987**.

46. Collingwood, R. W.; *A Survey of Eutrophication in Britain and its Effects on Water Supplies* - Water Research Centre Technical Report TR40. **1977**.

47. Johnson, D., Farley, M. R., Youngman, R. E., Yadav, N. P., and West, J. T.; *Removal of algae by various unit processes* - Water Research Centre Technical Report TR45. **1977**.

48. Robbins, J.; *New Civil Engineer* **1990**, *31 May*, 5.

49. Van Vlymen, C. D.; *PhD Thesis - The water balance, physio-chemical environment, and phytoplankton studies of Slapton Ley, Devon*, University of Exeter **1980**.

50. Meybeck, M.; *American Journal of Science.* **1982**, *282*, 401.

51. Meybeck, M., Chapman, D., and Helman, P.; *Global Freshwater Quality: a first assessment.* Global Environmental Monitoring System/ UNEP/ WHO. **1989**.

52. Office for Official Publications of the European Communities; *European Community Environmental Legislation*; Luxembourg, **1996**.

53. Ministry of Agriculture, Fisheries and Food; *Code of Good Agricultural Practice for the Protection of Water.* **1991**.

54. US Environmental Protection Agency; Criteria and Standards Division. *Ambient water quality critieria for ammonia* - 1984, EPA - 440/5-85-001. Washington, DC. **1984**.

55. Environment Canada; *Inland Water Directorate*. Canadian Water Quality Guidelines. **1991**.

56. Lloyd, R.; *Pollution and Freshwater Fish*; Fishing News Books - Blackwell Scientific Publications Ltd: London, **1991**.

57. Heathwaite, A. L.; Burt, T. P.; *IAHS Publication* **1991**, *203*, 209.

58. Akse, J. R.; Thompson, J. O.; Sauer, R. L.; Atwater, J. E.; *Microchemical Journal* **1998**, *59*, 372.

59. Defaria, L. C.; Pasquini, C.; *Analytica Chimica Acta* **1991**, *245*, 183.

60. Shen, H. D.; Cardwell, T. J.; Cattrall, R. W.; *Analyst* **1997**, *122*, 89.

61. Nakamoto, Y.; Tomiyama, T.; Kumamaru, T.; *Analytical Sciences* **1997**, *13*, 379.

62. Kerouel, R.; Aminot, A. *Marine Chemistry* **1997**, *57*, 265.

63. Liu, R. M.; Sun, B. T.; Liu, D. J.; Sun, A. L.; *Talanta* **1996**, *43*, 1049.

64. Gibb, S. W.; Mantoura, R. F. C.; Liss, P. S.; *Analytica Chimica Acta* **1995**, *316*, 291.

65. Fujinari, E. M.; Courthaudon, L. O.; *J.of Chromatography, A.* **1992**, *592*, 209.

66. Isildak, I.; Asan, A.; *Talanta* **1999**, *48*, 967.

67. Trinkel, M.; Trettnak, W.; Reininger, F.; Benes, R.; OLeary, P.; Wolfbeis, O. S.; *International Journal of Environmental Analytical Chemistry* **1997**, *67*, 237.

68. Mizobuchi, M.; Tamase, K.; Kitada, Y.; Sasaki, M.; Tanigawa, K.; *Analytical Chemistry.* **1984**, *56*, 603.

69. Shen, H.; Cardwell, T. J.; Cattrall, R. W.; *Analyst* **1998**, *123*, 2181.

70. Herrmann, S.; Vonau, W.; Gerlach, F.; Kaden, H.; *Fresenius' Journal of Analytical Chemistry* **1998**, *362*, 215.

71. Hara, H.; Matsumoto, S.; *Analyst* **1994**, *119*, 1839.

72. Narayanaswamy, R.; *Science of the Total Environment* **1993**, *135*, 103.

73. Niessner, R.; *Trends In Analytical Chemistry* **1991**, *10*, 310.

74. Wolfbeis, O. S.; *Journal of Molecular Structure* **1993**, *292*, 133.

75. Reichert, J.; *GIT Fachzeitschrift fuer das Laboratorium* **1995**, *39*, 216.

76. Lobnik, A.; Wolfbeis, O. S.; *Sensors and Actuators, B* **1998**, *B51*, 203.

77. Water Research Council; *Methods for the Examination of Waters and Associated Materials, Ammonia in Waters.* **1981**.

78. Water Research Council.; *Analyst* **1982**, *107*, 680.

79. Ruzicka, J.; Hansen, E. H.; *Analytica Chimica Acta.* **1975**, *78*, 145.

80. Andrew, K. N.; Worsfold, P. J.; Comber, M.; *Analytica Chimica Acta* **1995**, *314*, 33.

81. VanStaden, J. F.; Taljaard, R. E.; *Analytica Chimica Acta* **1997**, *344*, 281.

82. Liu, R. M.; Wang, H. S.; Sun, A. L.; Liu, D. J.; *Talanta* **1997**, *45*, 405.

83. Desor, M.; *LaborPraxis* **1997**, *21*, 72, 75.

84. Oms, M. T.; Cerda, A.; Cladera, A.; Cerda, V.; Forteza, R.; *Analytica Chimica Acta* **1996**, *318*, 251.

85. Clinch, J. R.; Worsfold, P. J.; Sweeting, F. W.; *Analytica Chimica Acta* **1988**, *214*, 401.

86. MenezesSantos, M.; FreiredosReis, B.; Bergamin, H.; Baccan, N.; *Analytica Chimica Acta* **1992**, *261*, 339.

87. Bloxham, M. J.; Depledge, M. H.; Worsfold, P. J.; *Laboratory Robotics And Automation* **1997**, *9*, 175.

88. Cerda, A.; Oms, M. T.; Forteza, R.; Cerda, V.; *Analytica Chimica Acta* **1995**, *311*, 165.

89. Willason, S. W.; Johnson, K. S.; *Marine Biology* **1986**, *91*, 285.

90. Funazo, K.; Kusano, K.; Tanaka, M.; Shono, T.; *Analyst* **1982**, *107*, 82.

91. Christensen, S.; Tiedje, J. M.; *Applied Environmental Microbiology* **1988**, *54*, 1409.

92. Dunphy, M. J.; Goble, D. D.; Smith, D. J.; *Analytical Biochemistry* **1990**, *184*, 381.

93. Jain, A.; Smith, R. M.; Verma, K. K.; *Journal Of Chromatography A* **1997**, *760*, 319.

94. Yang, Y. T.; Liu, F. J.; Kang, J. W.; Ou, Q. Y.; *Journal of Chromatography, A* **1999**, *834*, 393.

95. Padarauskas, A.; Olsauskaite, V.; Paliulionyte, V.; *Journal of Chromatography, A* **1998**, *829*, 359.

96. Han, S. H.; Park, Y. S.; Park, S. D.; Joe, K. S.; Eom, T. Y.; *Analytical Science & Technology* **1999**, *12*, 99.

97. Yang, J. N.; Hong, M.; Cai, C.; X. *Sepu* **1998**, *16*, 62.

98. Sakai, H.; Fujiwara, T.; Kumamaru, T.; *Analytica Chimica Acta* **1996**, *331*, 239.

99. Carrozzino, S.; Righini, F.; *Journal of Chromatography, A* **1995**, *706*, 277.

100. Breitkopf, K.; *LaborPraxis* **1994**, *18*, 64.

101. Briski, F.; CerjanStefanovic, S.; Sipos, L.; *International Journal of Environmental Analytical Chemistry* **1993**, *52*, 137.

102. Stanley, M.A.; Maxwell, J.; Forrestal, M.; Doherty, A.P.; MacCraith, B.D.; Diamond, D.; Vos, J.G.; *Analytical Chimica Acta* **1994**, 299, 81.

103. Tabatabai, M. A.; Dick, W. A.; *Journal Of Environmental Quality* **1983**, *12*, 209.

104. Burke, E. M.; Suarez, F. X.; Hillman, D. C.; Heithmar, E. M.; *Water Research* **1989**, *23*, 519.

105. Mahr, A.; Turk, T.; Dobrowolski, A.; Horn, R.; *Zeitschrift fur Pflanzenernahrung and Bodenkunde* **1991**, *154*, 369.

106. Braman, R. S.; Hendrix, S. A.; *Analytical Chemistry* **1989**, *61*, 2715.

107. Aoki, T.; Wakabayashi, M.; *Analytica Chimica Acta* **1995**, *308*, 308.

108. Aoki, T.; Kado, N.; Nakaoa, Y.; Mukai, H.; *Journal of Flow Injection Analysis* **1997**, *14*, 47.

109. Liu, D. J.; Liu, R. M.; Sun, A. L.; Liu, G. H.; *Fenxi Huaxue* **1995**, *23*, 321.

110. Renmin, L.; Daojie, L.; Ailing, S.; Guihua, L.; *Talanta* **1995**, *42*, 437.

111. Koschay, U. E.; *LaborPraxis* **1998**, *22*, 100.

112. Lapa, R. A. S.; Lima, J. L. F. C.; Barrado, E.; Vela, H.; *International Journal of Environmental Analytical Chemistry* **1997**, *66*, 71.

113. Sun, B.; Fitch, P. G.; *Electroanalysis* **1997**, *9*, 494.

114. Doherty, A. P.; Stanley, M. A.; Leech, D.; Vos, J. G.; *Analytica Chimica Acta* **1996**, *319*, 111.

115. Miles, D. L.; Espejoi, C.; *Analyst* **1977**, *102*, 104.

116. Cawse, P. A.; *Analyst* **1967**, *92*, 311.

117. Rennie, P. J.; Sumner, A. M.; Basketter, F. B.; *Analyst* **1979**, *104*, 837.

118. Holm, T. R.; Kelly, W. R.; Sievers, L. F.; Webb, D. L.; *Spectroscopy* **1997**, *12*, 38.

119. Bachmann, R. W.; Canfield, D. E.; *Hydrobiologia* **1996**, *323*, 1.

120. Zheng, C. L.; *Lihua Jianyan, Huaxue Fence* **1997**, *33*, 556.

121. Jenkins, D.; Medsker, L. L.; *Analytical Chemistry* **1964**, *36*, 610.

122. Snell, F. D.; *Photometric and Fluorometric Methods of Analysis, Nonmetals*; Wiley Interscience: New York, **1981**; pp. 544.

123. Ciesielski, H.; Sorgnet, G.; Catone, M.; Vancayzeele, P.; *Analusis* **1978**, *6*, 38.

124. Viriot, M. L.; Mahieuxe, B.; Carre, M. C.; Andre, J. C.; *Analusis* **1995**, *23*, 312.

125. Hilton, J.; Rigg, E.; *Analyst* **1983**, *108*, 1026.

126. Kempers, A. J.; Luft, A. G.; *Analyst* **1988**, *113*, 1117.

127. Defaria, L. C.; Pasquini, C.; *Analytica Chimica Acta* **1991**, *245*, 183.

128. Su, X. L.; Chen, P.; Qu, X. G.; Wei, W. Z.; Yao, S. Z.; *Microchemical Journal* **1998**, *59*, 341.

129. Bajic, S. J.; Jaselskis, B.; *Talanta* **1985**, *32*, 115.

130. Margeson, J. H.; Suggs, J. C.; Midgett, M. R.; *Analytica Chimica Acta* **1982**, *142*, 119.

131. Gaugush, R. F.; Heath, R. T.; *Water Research* **1984**, *18*, 449.

132. Cerda, A.; Oms, M. T.; Forteza, R.; Cerda, V.; *Analytica Chimica Acta* **1998**, *371*, 63.

133. Danet, A. F.; David, V.; *Analytical Letters* **1998**, *31*, 751.

134. Blundell, N. J.; Hopkins, A.; Worsfold, P. J.; Casey, H.; *Journal of Automatic Chemistry* **1993**, *15*, 159.

135. Nydahl, F. *Talanta* **1976**, *23*, 349.

136. Nakashima, S.; Yagi, M.; Zenki, M.; Takahashi, A.; Toei, K.; *Fresenius Zeitschrift Fur Analytische Chemie* **1984**, *319*, 506.

137. Baveja, A. K.; Nair, J.; Gupta, V. K.; *Analyst* **1981**, *106*, 955.

138. Tarafder, P. K.; Pathmore, D. P. S.; *Analyst* **1988**, *113*, 1073.

139. Horita, K.; Wang, G. F.; Satake, M.; *Analyst* **1997**, *122*, 1569.

140. Puri, S.; Satake, M.; Wang, G.; *Annali di Chimica* **1998**, *88* , 685.

141. Chen, D.; De Castro, M. D. L.; Valcarcel, M.; *Analyst* **1991**, *116*, 1095.

142. Benson, R. L.; Worsfold, P. J.; Sweeting, F. W.; *Analytical Proceedings* **1989**, *26*, 385.

143. MacLaurin, P.; Andrew, K. N.; Worsfold, P. J.; *in Process Analytical Chemistry*; Chapman & Hall: London, **1995**.

144. Andrew, K. N.; Blundell, N. J.; Price, D.; Worsfold, P. J.; *Analytical Chemistry* **1994**, *66*, A916.

145. Trojanowicz, M.; Benson, R. L.; Worsfold, P. J.; *Trends In Analytical Chemistry* **1991**, *10*, 11.

146. Motomizu, S.; Oshima, M.; Ma, L.; *Analytical Sciences* **1997**, *13*, 401.

147. David, A. R. J.; McCormack, T.; Worsfold, P. J.; *Journal of Automated Methods & Management in Chemistry* **1999**, *21*, 1.

148. Blundell, N. J.; Worsfold, P. J.; Casey, H.; Smith, S.; *Environment International* **1995**, *21*, 205.

149. Ma, L.; Oshima, M.; Motomizu, S.; Hattori, T.; *Bunseki Kagaku* **1998**, *47*, 375.

150. Wang, Y. L.; Gao, J. Z.; *Fenxi Huaxue* **1998**, *26*, 1384.

151. Nikonorov, V. V.; Moskvin, L. N.; *Zhurnal Analiticheskoi Khimii* **1996**, *51*, 737.

152. Shanthi, K.; Balasubramanian, N.; *Journal of AOAC International* **1994**, *77*, 1639.

153. Manzoori, J. L.; Sorouraddin, M. H.; HajiShabani, A. M.; *Talanta* **1998**, *46*, 1379.

154. ZhiQi, Z.; LouJun, G.; HanYing, Z.; QianGuang, L.; *Analytica Chimica Acta* **1998**, *370*, 59.

155. Motomizu, S.; Sanada, M.; *Analytica Chimica Acta* **1995**, *308*, 406.

156. Sun, A. L.; Wang, H. S.; Liu, D. J.; *Fenxi Huaxue* **1997**, *25*, 1334.

157. Takeda, K.; Fujiwara, K.; *Analytica Chimica Acta* **1993**, *276*, 25.

158. Olsthoorn, C. M.; Fong, N. K.; *Nutrient Cycling In Agroecosystems* **1998**, *52*, 269.

159. Haber, C.; VanSaun, R. J.; Jones, W. R.; *Analytical Chemistry* **1998**, *70*, 2261.

160. Motomizu, S.; Mikasa, H.; Toei, K.; *Analytica Chimica Acta* **1987**, *193*, 343.

161. PerezRuiz, T.; MartinezLozano, C.; Tomas, V. *Analytica Chimica Acta* **1992**, *265*, 103.

162. Sasaki, S.; Ando, Y.; Dejima, M.; Arikawa, Y.; Karube, I.; *Analytical Letters* **1998**, *31*, 555.

163. Stanley, M. A.; Maxwell, J.; Forrestal, M.; Doherty, A. P.; MacCraith, B. D.; Diamond, D.; Vos, J. G.; *Analytica Chimica Acta* **1994**, *299*, 81.

164. Torro, I. G.; Mateo, J. V. G.; Calatayud, J. M.; *Analytica Chimica Acta* **1998**, *366*, 241.

165. Markusova, K.; *Analytica Chimica Acta* **1989**, *221*, 131.

166. Markusova, K.; Kohutova, L.; Dzurov, J.; *Electroanalysis* **1996**, *8*, 582.

167. Silva, S. M.; Alves, C. R.; Machado, S. A. S.; Mazo, L. H.; Avaca, L. A.; *Electroanalysis* **1996**, *8*, 1055.

168. Defaria, L. C.; Pasquini, C.; *Analytica Chimica Acta* **1991**, *245*, 183.

169. Mikuska, P.; Vecera, Z.; Zdrahal, Z.; *Analytica Chimica Acta* **1995**, *316*, 261.

170. Aoki, T.; Fukuda, S.; Hosoi, Y.; Mukai, H.; *Analytica Chimica Acta* **1997**, *349*, 11.

171. Liu, R. M.; Liu, D. J.; Sun, A. L.; Liu, G. H.; *Talanta* **1995**, *42*, 437.

172. Chaurasia, A.; Verma, K. K.; *Talanta* **1994**, *41*, 1275.

173. Nikonorov, V. V.; Moskvin, L. N.; *Journal Of Analytical Chemistry* **1996**, *51*, 679.

174. Horita, K.; Wang, G.; Satake, M.; *Analytica Chimica Acta* **1997**, *350*, 295.

175. Zhang, Z. Q.; Gao, L. J.; Zhan, H. Y.; Liu, Q. G.; *Analytica Chimica Acta* **1998**, *370*, 59.

176. Guerrero, R. S.; Benito, C. G.; Calatayud, J. M.; *Talanta* **1996**, *43*, 239.

177. Cerda, A.; Oms, M. T.; Forteza, R.; Cerda, V.; *Analytica Chimica Acta* **1997**, *351*, 273-279.

178. Daniel, A.; Birot, D.; Lehaitre, M.; Poncin, J.; *Analytica Chimica Acta* **1995**, *308*, 413.

179. Cerda, A.; Oms, M. T.; Forteza, R.; Cerda, V.; *Analytica Chimica Acta* **1998**, *371*, 63.

180. Ruzicka, J.; Hansen, E. H.; *Analytica Chimica Acta* **1978**, *99*, 37.

181. Li, Y.; Ma, H.; *Talanta* **1995**, *42*, 2033.

182. Ruzicka, J.; Hansen, E. H.; *Flow Injection Analysis*; Wiley - Interscience: New York, **1988**.

183. Ruzicka, J.; Hansen, E. H.; *Analytica Chimica Acta* **1984**, *161*, 456.

184. Selvaka, C. M.; Jiao, K. S.; Krull, I. S.; *Analytical Chemistry* **1987**, *59*, 2221.

185. Benson, R. L.; Worsfold, P. J.; Sweeting, F. W.; *Analytica Chimica Acta* **1993**, *238*, 177.

186. Benson, R. L.; Worsfold, P. J.; *Science of the Total Environment* **1993**, *135*, 17.

187. Clinch, J. R.; Worsfold, P. J.; Sweeting, F. W.; *Analytica Chimica Acta* **1988**, *214*, 401.

188. Clinch, J. R.; Worsfold, P. J.; Casey, H.; Smith, S. M.; *Analytical Proceedings.* **1988**, *25*, 71.

189. Flaschka, H.; McKeithan, C.; Barnes, R. M.; *Analytical Letters* **1975**, *6*, 585.

190. Dasgupta, P. K.; Bellamy, H. S.; Liu, H.; Lopez, J. L.; Loree, E. L.; Morris, K.; Petersen, K.; Mir, K. A.; *Talanta* **1993**, *40*, 53.

191. Hauser, P. C.; Chiang, D. W. L.; *Talanta* **1993**, *40*, 1193.

192. Trojanowicz, M.; Worsfold, P. J.; Clinch, J. R.; *Trends In Analytical Chemistry* **1988**, *7*, 301.

193. Hauser, P. C.; Rupasinghe, T. W. T.; Cates, N. E.; *Talanta* **1995**, *42*, 605.

194. Liu, H.; Dasgupta, P. K.; *Analytica Chimica Acta* **1994**, *289*, 347.

195. Blanco, M.; Gene, J.; Iturriaga, H.; Maspoch, S.; Riba, J.; *Analytica Chimica Acta* **1987**, *34*, 987.

196. Lazaro, F.; Rios, A.; De Castro, M. D. L.; Valcarcel, M.; *Analytica Chimica Acta* **1986**, *179*, 279.

197. Owen A.J *The diode-array advantage in UV/Visible Spectroscopy*; Hewlett Packard Co.: **1988**.

198. Skoog D.A., Leary J. J. *Principles of Instrumental Analysis*; Saunders College Publishing: **1992**.

199. Epperson, P. M.; Sweedler, J. V.; Bilhorn, R. B.; Sims, G. R.; Denton, M. B.; *Analytical Chemistry* **1988**, *60*, 327A.

200. DenHartog, D. J.; Holly, D. J.; *Review Of Scientific Instruments* **1997**, *68*, 1036.

201. Pace, E.; Tommasi, L.; *Review Of Scientific Instruments* **1998**, *69*, 1622.

202. Berger, R.; Gerber, C.; Lang, H. P.; Gimzewski, J. K.; *Microelectronic Engineering* **1997**, *35*, 373.

203. Müller, C.; Mohr, J.; *Interdisciplinary Science Reviews* **1993**, *18*, 273.

204. Siebert, P.; Petzold, G.; Hellenbart, A.; Muller, J.; *Applied Physics A-Materials Science & Processing* **1998**, *67*, 155.

205. Zavracky, P. M.; Hennenberg, E.; Denis, K.; Xi, H. K.; *Mechatronics* **1998**, *8*, 485.

206. Internet Web Page http://www.oceanoptics.com/.

207. Muller, C.; Mohr, J.: *Interdisciplinary Science Review* **1993**, *18*, 273.

208. Mohr, J.; Ehrfeld, W.; Munchmeyer, D.; *J.Vac.Sci.Technol.B* **1988**, *6*, 2264.

209. Berger, R.; Gerber, C.; Lang, H. P.; Gimzewski, J. K.; *Microelectronic Engineering* **1997**, *35*, 373.

210. Zavracky, P. M.; Hennenberg, E.; Denis, K.; Xi, H. K.; *Mechatronics* **1998**, *8*, 485.

211. Goldsten, J. O.; McNutt, R. L.; Gold, R. E.; Gary, S. A.; Fiore, E.; Schneider, S. E.; Hayes, J. R.; Trombka, J. I.; Floyd, S. R.; Boynton, W. V.; Bailey, S.; Bruckner, J.; Squyres, S. W.; Evans, L. G.; Clark, P. E.; Starr, R.; *Space Science Reviews* **1997**, *82*, 169.

212. Siebert, P.; Petzold, G.; Hellenbart, A.; Muller, J.; *Applied Physics A-Materials Science & Processing* **1998**, *67*, 155.

213. Yee, G. M.; Maluf, N. I.; Hing, P. A.; Albin, M.; Kovacs, G. T. A.; *Sensors And Actuators A-Physical* **1997**, *58*, 61.

214. Batchelor, J. D.; Thomas, S. E.; Jones, B. T.; *Applied Spectroscopy* **1998**, *52*, 1086.

215. Osterloh, D.; *Laborpraxis* **1998**, 20,122.

216. Sembiring, H.; Raun, W. R.; Johnson, G. V.; Stone, M. L.; Solie, J. B.; Phillips, S. B.; *Journal Of Plant Nutrition* **1998**, *21*, 1189.

217. Internet Web Page http://robotics.jpl.nasa.gov/

218. Mazel, C. H.; *Optical Engineering* **1997**, *36*, 2612.

219. Belz, M.; Boyle, W. J. O.; Klein, K. F.; Grattan, K. T. V.; *Sensors And Actuators B-Chemical* **1997**, *39*, 380.

220. Hewlett Packard GmbH Germany; *HP 8453 UV-Visible Spectrophotometer - Reference Manual*; **1995**.

221. Scopatz S., Neel G.; Romesburg E.; Zivitz M.; Proc. SPIE. 1055, 306. **1989**.

222. CRC Press Inc.; *CRC Handbook of Chemistry and Physics*; 1995; pp. 10-57.

223. Internet Web Page http://www.oceanoptics.com/specifications/Optical_Resolution.asp

224. Burgess C., K. A. (ed.); *Standards in Absorption Spectrometry - UV Spectrometry Group*; **1981**.

225. Thomas M.; *Ultraviolet and Visible Spectroscopy - Analytical Chemsitry by Open Learning*; John Wiley & Sons.: **1996**.

226. Crouch, S. R. and Ingle, J. D. Jr.; Analytical Chemistry 44, 1375. **1972**.

227. Rothman L.D., Crouch S. R. Ingle J. D. Jr.; Analytical Chemistry 47, 1226. **1975**.

228. Ljunggren, E.; Karlberg, B.; *Journal of Automatic Chemistry* **1995**, *17*, 105.

229. DecnopWeever, L. G.; Kraak, J. C.; *Analytica Chimica Acta* **1997**, *337* , 125.

230. Schulze, G.; Liu, C. Y.; Brodowski, M.; Elsholz, O.; Frenzel, W.; Moller, J.; *Analytica Chimica Acta* **1988**, *214*, 121.

231. Aminot, A.; Kirkwood, D. S.; Kerouel, R.; *Marine Chemistry* **1997**, *56* , 59.

232. Aminot.A and Kirkwood.D.; *ICES Cooperative Research Report, No. 213, Report on the Results of the Fifth ICES Intercomparison Exercise for Nutrients in Sea Water.* **1995**.

233. Grasshoff, K.; *Results of the Baltic Intercalibration Workshop*, Kiel, **1977**. ICE 1977/C:4.

234. Hara, H.; Motoike, A.; Okazaki, S.; *Analyst* **1988**, *113*, 113.

235. Chen, D. L.; Chalk, P. M.; *Analytica Chimica Acta* **1991**, *245*, 49.

236. Richardson, G. T.; Davies, J. A.; Edwards, J. G.; *Fresenius Journal Of Analytical Chemistry* **1991**, *340*, 392.

237. Frenzel, W.; Grimm, E.; Gruetzmacher, G.; *Fresenius Journal Of Analytical Chemistry* **1995**, *351*, 19.

238. Aminot, A.; Kerouel, R.; *Marine Chemistry* **1995**, *49*, 221.

239. Aminot, A.; Kerouel, R.; *Marine Chemistry* **1996**, *52*, 173.

240. Water Research Council; *Methods for the Examination of Waters and Associated Materials, Ammonia in Waters.* **1981**.

241. Fresenius, W.; Quetin, K.E.; *Water Analysis – A Practical Guide to Physico-Chemical, Chemical and Microbiological Water Examination and Quality Assurance*, Heidelberg, Springer-Verlag Berlin, **1988**.

242. Spendly, W.; Hext, G. R.; Himsworth, F. R.; *Technometrics* **1962**, *4*, 441.

243. Miller, J. C.; Miller, J. N.; *Statistics for Analytical Chemistry*, Ellis Horwood Limited: Chichester, U.K., **1993**.

244. Morgan S.L.; Deming, S. N.; *Analytical Chemistry* **1974**, *46*, 1170.

245. Nelder, J. A.; Mead, R.; *Computer Journal* **1965**, *4*, 308.

246. Routh, M. W.; Swartz, P. A.; Denton, M. B.; *Analytical Chemistry* **1977**, *49*, 1422.

247. Ryan, P. B.; Barr, P. L.; Todd, H. D.; *Analytical Chemistry* **1980**, *52*, 1460.

248. Hilligsoe, B.; Hansen, E. H.; *Fresenius Journal Of Analytical Chemistry* **1997**, *358*, 775.

249. AlvaresRibeiro, L. C.; Machado, A. C.; *Analyst* **1998**, *123*, 653.

250. Deviteri, F. S.; Diamond, D.; *Analyst* **1994**, *119*, 749.

251. Stalikas, C. D.; Karayannis, M. I.; Tzouwarakarayanni, S.; *Talanta* **1994**, *41*, 1561.

252. Sultan, S. M.; Suliman, F. O.; *Analytical Sciences* **1992**, *8*, 841.

253. Sultan, S. S.; Suliman, F. O.; Duffuaa, S. O.; Abuabdoun, I. I.; *Analyst* **1992**, *117*, 1179.

254. Gine, M. F.; Tuon, R. L.; Cesta, A. A.; Packer, A. P.; Reis, B. F.; *Analytica Chimica Acta* **1998**, *366*, 313.

255. Irons.G.; *BSc Final Year Project*, University of Hull **1990**.

256. Sellien, W.; Czolk, R.; Reichert, J.; Ache, H. J.; *Analytica Chimica Acta* **1992**, *269*, 83.

257. Werner, T.; Klimant, I.; Wolfbeis, O. S.; *Analyst* **1995**, *120*, 1627.

258. McCormack, T.; David, A. R. J.; Worsfold, P. J.; Howland, R.; *Analytical Proceedings* **1994**, *31*, 81.

259. Zagatto, E. A. G.; Arruda, M. A. Z.; Jacintho, A. O.; Mattos, I. L.; *Analytica Chimica Acta* **1990**, *234*, 153.

260. Jacintho, A. O.; Rufini, I. A.; Antonio, R. F.; *Quimica Nova* **1989**, *12*, 5.

261. Bergamin F.H.; Reis, B. F.; Zagatto, E. A. G.; *Analytica Chimica Acta* **1978**, *97*, 427.

262. Betteridge, D.; Dagless, E. L.; Fields, B.; Graves, N. F.; *Analyst* **1978**, *103*, 897.

263. Thomsen, J.; Johnson, K. S.; Petty, R. L.; *Analytical Chemistry.* **1983**, *55*, 2378.

264. Zagatto, E. A. G.; Reis, B. F.; Martinelli, M.; Krug, F. J.; Bergamin F.H.; Gine, M. F.; *Analytica Chimica Acta* **1987**, *198*, 153.

265. Ham, G.; *Analytical Proceedings* **1981**, *18*, 69.

266. McKelvie, I. D.; Peat, D. M. W.; Matthews, G. P.; Worsfold, P. J.; *Analytica Chimica Acta* **1997**, *351*, 265.

267. Krug, F. J.; Bergamin F.H.; Zagatto, E. A. G.; Jorgensen, S. S.; *Analyst* **1977**, *102*, 503.

268. Johnson, K. S., Petty, R. L., and Thomsen, J.; *Mapping Strategies in Chemical Oceanography: Proc. 185th Annual Meeting of the American Chemical Society*. Seattle, WA. **1983**.

269. Daniel, A.; Birot, D.; Lehaitre, M.; Poncin, J.; *Analytica Chimica Acta.* **1995**, *308*, 413.

270. Yamane, T.; Saito, M. ;*Talanta* **1992**, *39*, 215.

271. Snyder, L. R.; Kirkland, J. J.; *Introduction to Modern Liquid Chromatography*; Wiley: New York, **1979**.

272. Chung, S.; Wen, X.; Vilholm, K.; De Bang, M.; Christian, G. D.; Ruzicka, J.; *Analytica Chimica Acta* **1991**, *249*, 77.

273. Tijssen, R.; *Analytica Chimica Acta* **1980**, *114*, 71.

274. Korenaga, T.; Ikastu, H.; *Analytica Chimica Acta* **1982**, *141*, 301.

275. McGowan, K. A.; Pacey, G. E.; *Analytica Chimica Acta* **1988**, *214*, 391.

276. Engelhardt, H.; Neue, U.; *Chromatographia* **1982**, *15*, 403.

277. Reijn, J. M.; van der Linden, W. E.; Poppe, H.; *Analytical Chemistry* **1981**, *126*, 1.

278. Reijn, J. M.; van der Linden, W. E.; Poppe, H.; *Analytical Chemistry* **1981**, *123*, 229.

279. Reijn, J. M.; Poppe, H.; *Analytical Chemistry* **1984**, *56*, 943.

280. Valcarcel, M.; Luque de Castro, M. D.; *Flow Injection Analysis - Principles and Applications.*; Ellis Horwood Ltd.: Chichester, U.K., **1987**.

281. Jordan, J. M.; Pardue, H. L.; *Analytica Chimica Acta* **1992**, *270*, 204.

282. Tyson, J. F.; *Analyst* **1987**, *112*, 523.

283. Berger, R. L.; Baka, B.; Chapman, H.; *Reviews of Scientific Instrumentation* **1968**, *39*, 493.

284. Berger, R. L.; *Biophysical Journal* **1978**, *24*, 2.

285. Spinks, T. L.; Pacey, G. E.; Fabian, L.; Lee, S.; Bubnis, B. P.; *Talanta* **1992**, *39*, 293.

286. Arnold, D. P.; Peachy, R. M.; Petty, J. D.; Sweatman, D. R.; *Analytical Chemistry* **1989**, *61*, 2109.

287. Petty, J. D., Peachy, R. M., and Sweatman, D. R.; PH 3289. Australia. **1985**.

288. Petty, J. D., Peachy, R. M., and Sweatman, D. R. [5, 080, 866]. United States. **1992**.

289. Cardwell, T. J.; Cattrall, R. W.; Cross, G. J.; Oconnell, G. R.; Petty, J. D.; Scollary, G. R.; *Analyst* **1991**, *116*, 1051.

290. Cardwell, T. J.; Cattrall, R. W.; O'Connell, G. R.; Petty, J. D.; Scollary, G. R.; *Electroanalysis* **1992**, *4*, 805.

291. Cross, G. J.; *PhD Thesis - Computer Applications in FIA*, La Trobe University, Bundoora, Vic 3083, Australia **1998**.

292. McCormack, T.; *PhD Thesis - Flow Injection Chemistries for the In Situ Monitoring of Nutrients in Sea Water.*, University of Plymouth, Plymouth, Devon, U.K. **1996**.

293. David, A. R. J.; *PhD Thesis - Flow Injection Instrumentation for the In Situ Monitoring of Nutrients in Sea Water.*, University of Plymouth, Plymouth, Devon, U.K. **1997**.

294. National Rivers Authority. - S.Western Division. *The Frome and Piddle Management Plan - Consultant Report.* **1995**.

295. Environment Agency. - *Frome & Piddle and Poole Harbour & Purbeck Catchment Management Plan - Second Annual Review.* **1998**.

296. Casey, H.; Clarke, R. T.; *Freshwater Biology* **1979**, *9*, 91.

297. Clinch, J. R.; Worsfold, P. J.; Casey, H.; *Analytica Chimica Acta* **1987**, *200* , 523.

298. Casey, H.; Clarke, R. T.; Smith, S. M.; Clinch, J. R.; Worsfold, P. J.; *Analytica Chimica Acta* **1989** , *227*, 379.

299. Winkler, P., Jobst, S., and Harder, C.; *BPT-Bericht, GSF Munich.* 5-5-**1995**.

300. Schulze, E. D.; de Vries, W.; Hauhs, M.; Rosen, K.; Rasmussen, L.; Tamm, C. O.; Nilsson, J.; *Water, Air and Soil Pollution* **1990**, *48*, 451.

301. Puxbaum, H., Vitovec, W., and Kalina, M.; *NATO ASI Series. Vol. G28*, Heidelberg, Verlag Springer Berlin. **1991**.

302. Sandnes, H.; *EMEP report 1/93.* Norway, MSC-W. **1993**.

303. Bunderministerium fur Gesundheit und Umweltschutz, Vienna Austria.; BMGU **1984**.

304. Sanusi, A.; Wortham, H.; Millet, M.; Mirabel, P.; *Atmospheric Environment* **1996**, *30*, 59.

305. Losno, R.; Bergametti, G.; Carlier, P.; Mouvier, G.; *Atmospheric Environment* **1991**, *25A*, 763.

306. Balls, P. W.; *Atmospheric Environment* **1989**, *23*, 2751.

307. Brantner, B.; Fierlinger, H.; Puxbaum, H.; *Water, Air and Soil Pollution* **1993**, *74*, 2495.

308. Melack, J. M.; Stoodard, J. L.; Ochs, C. A.; *Water Resources Research* **1985**, *21*, 27.

309. Joos, F.; Baltensperger, U.; *Atmospheric Environment* **1991**, *2*, 217.

310. Brimblecombe, P.; *Air Composition & Chemistry*; Cambridge University Press: **1986**.

311. McDowell, W. H.; Sanchez, C. G.; Asbury, C. E.; Ramos Perez, C. R.; *Atmospheric Environment* **1990**, *24A*, 2813.

312. Jacob, D. J.; Waldman, J. M.; Muncer, J. W.; Hoffmann, M. R.; *Environmental Science and Technology* **1985**, *8*, 730.

313. Kalina, M. and Puxbaum, H.; *Verteilung der nassen Deposition von Niederschlagsinhaltsstoffen in Osterreich.* Vienna, Institute for Analytical Chemistry - Technical University of Vienna. **1993**.

314. Teil, A.; *State of the Environment in Austria.* Umweltbundesamt, Wien. **1993**.

315. Brown, S. D.; Blank, T. B.; Sum, S. T.; Weyer, L. G.; *Analytical Chemistry.* **1994**, *66*, 315R.

316. Haswell, S. J.; *Practical Guide to Chemometrics*; Marcel Dekker: New York, **1992**.

317. Wold, S.; *Journal Of Pharmaceutical And Biomedical Analysis* **1991**, *9*, 589.

318. Massart, D. L.; Kaufman, L.; *The Interpretation of Analytical Chemical Data by the use of Cluster Analysis*; John Wiley & Sons: Chichester, **1983**.

319. Wold, S.; Esbensen, K.; Geladi, P.; *Chemometrics and Intelligent Laboratory Systems* **1987**, *2* , 37.

320. Anderson, T. W.; *An Introduction to Multivariate Statistical Analysis*; John Wiley & Sons: New York, **1958**.

321. Tuncel, S. G.; Ungor, S.; *Atmospheric Environment* **1996**, *30*, 2721.

322. Saxena, A.; *Atmospheric Environment* **1996**, *30*, 3405.

323. Sequeira, R.; *Atmospheric Environment* **1982**, *16*, 329.

Appendices

Appendix I

Degree of Corrosion Strength

316 Stainless Steel.

DEGREE OF CORROSION STRENGTH

No.	Corrosive Agent	Concentration %	Temperature °C	Martensitic	Ferritic	Austenitic	
				S 403 S 410 S 420 ABC S 616 S 440 C	S 430 S 430 F	S 302 S 303 S 304 S 305 S 321 S 347	S 316 S 316 L S 316 T
67	Aluminium Chloride	25		P	P	P	M
68	Ammonium Chloride	10	Boiling	P	P	P	M
69	Barium Chloride	10		M	G	G	G
70	Calcium Chloride			W	G	G	G
71	Ferric Chloride	40		P	P	P	P
72	Ferrous Chloride	20		P	P	P	P
73	Magnesium Chloride	10		M	G	G	G
74	Mercuric Chloride	10		P	P	P	P
75	Nickel Chloride	30		P	P	P	W
76	Potassium Chloride	10		G	G	G	G
77	Copper Chloride	10		P	P	P	P
78	Sodium Chloride	5		M	M	G	G
79	Zinc Chloride	10		W	W	M	G
80	Sulphur Chloride	100		P	M	M	M
81	Coke (Pure Syrup)			W	G	G	G
82	Glue			G	G	G	G
83	Ether	100		M	M	G	G
84	Fluorine (Gas)	100		P	G	G	G
85	Aluminium Flouride	5		P	P	P	P
86	Formaldehyde	40		G	G	G	G
		100		M	M	G	G
87	Sodium Phosphate	Up to 100		M	M	M	M
88	Furfural			G	G	G	W
89	Chlorine Gas	90		P	P	P	W
90	Coke-Oven Gas			G	G	G	G
91	Diesel Oil	Containing H_2S		M	M	G	G
		Refined		G	G	G	G
92	Gelatine			G	G	G	G
93	Glycerine	100		M	M	M	M
94	Ethylene Glycol	100		M	M	M	M
95	Glucose			G	G	G	G
96	Shellac			G	G	G	G
97	Ammonium Hydroxide			W	G	G	G
98	Calcium Hydroxide	10		M	M	M	M
99	Magnesium Hydroxide	100		M	M	M	M
100	Potassium Hydroxide	5		W	G	G	G
101	Sodium Hydroxide	10	100	G	G	G	G
		20	Boiling	W	W	G	G
102	Calcium Hypochlorite	100		P	P	P	W
103	Sodium Hypochlorite	100		P	P	P	W
104	Milk (Fresh or Sour)			M	G	G	G
105	Yeast			W	W	G	G
106	Mayonnaise			W	W	G	G
107	Molasses			G	G	G	G
108	Mustard			W	P	G	G

CODE: G - Good M - Medium P - Poor W - Not Measured Value

(CR/CJW/F32

Appendix II

Additional Field Data.

ICP-MS ANALYSIS (SEMI – QUANTITATIVE).

At each sampling site within Sehlabathebe National Park, river water samples were collected for ICP-MS analysis on return to the U.K. Duplicate samples were collected in clean (10 % HCl acid washed, Milli – Q rinsed) 150 ml H.D.P.E bottles. Acid stabilisation of the samples was not performed due to the logistic difficulties of flying concentrated acids. Once collected samples were stored in a cool, dark environment. On return to the U.K. (approx. 3 – 5 weeks) samples were analysed immediately by ICP-MS. Samples were transferred to clean 100 ml volumetric flasks with the addition of 1 ml of a 10 mg l^{-1} indium (^{115}In) internal standard, therefore resultant internal standard concentration being 100 μg l^{-1}. Using a semi-quantitative standard containing beryllium, magnesium, manganese, indium, barium, lead and uranium a semi-quantitative calibration was performed.

PQ2+ Turbo ICP-MS operating conditions.

PARAMETER	CONDITIONS
Operating Power	1400 W
Reflected Power	2 - 3 W
Plasma Gas Flow Rate (Ar)	15 l min^{-1}
Auxiliary Gas Flow Rate (Ar)	1.0 l min^{-1}
Nebuliser Gas Flow Rate (Ar)	0.8 l min^{-1}
Sample Flow Rate	3 ml min^{-1}
Torch Type	Standard one piece quartz
Nebuliser Type	Meinhard concentric glass
Spray Chamber	Scott-type double pass
Integration Time	30 s
Optimisation	ion lenses optimised for ^{115}In typical counts 1 x 10^6 per mg l^{-1}

Semi-quantitative ICP-MS data for River Frome, East Stoke, Dorset, U.K.

Element	Concentration (μg l^{-1})
Magnesium	3253
Vanadium	4.4054
Chromium	17.69
Manganese	20.668
Nickel	14.676
Zinc	141.14
Copper	22.166
Strontium	320.41
Molybdenum	158.85
Barium	23.904

Semi-quantitative ICP-MS data for Sehlabathebe National Park sampling sites (1 – 20), concentrations in μg l^{-1}.

	Sampling Site No.									
Element	1	2	3	4	5	6	7	8	9	10
Magnesium	1195.0	1140.1	1098.3	1196.9	1127.7	1080.6	616.8	859.7	912.1	214.1
Vanadium	0.5	0.8	1.7	0.9	0.6	0.8	1.4	0.9	0.6	0.2
Chromium	1.8	2.2	3.8	3.0	2.4	2.3	3.7	2.9	2.2	1.0
Manganese	4.7	12.3	3.5	4.1	3.7	8.7	7.2	4.5	10.3	7.2
Nickel	2.6	2.6	2.8	2.7	2.8	2.7	2.4	2.4	2.3	2.4
Zinc	8.0	6.2	6.0	4.7	8.7	6.2	4.2	3.2	3.0	5.8
Copper	0.7	0.6	0.6	0.6	0.5	0.6	0.8	0.6	0.5	0.3
Strontium	26.5	24.9	128.9	70.9	29.7	28.2	62.4	41.4	35.7	3.6
Molybdenum	122.7	52.3	52.7	44.4	39.7	33.1	24.4	21.8	19.6	19.5
Barium	9.5	4.6	46.7	35.0	9.5	10.8	23.6	10.6	28.6	8.7

	Sampling Site No.									
Element	11	12	13	14	15	16	17	18	19	20
Magnesium	536.0	1160.7	1107.1	977.3	852.0	1128.1	968.2	889.7	974.2	1161.5
Vanadium	0.4	0.9	1.1	1.2	0.9	1.3	1.5	1.7	0.7	1.2
Chromium	1.4	3.0	2.7	3.7	3.2	3.8	3.5	3.9	2.3	3.8
Manganese	2.4	1.7	3.4	2.7	39.8	17.2	2.5	2.3	7.8	8.5
Nickel	2.3	2.6	2.6	2.7	3.0	2.7	2.4	2.4	2.4	2.4
Zinc	5.5	2.8	4.5	2.9	4.2	4.4	6.0	2.9	3.6	2.6
Copper	0.4	0.3	0.4	0.6	0.8	0.6	0.8	0.4	0.4	0.5
Strontium	16.6	19.2	23.1	47.1	61.7	61.7	19.4	16.9	34.8	76.4
Molybdenum	16.0	15.2	12.7	12.4	12.3	11.2	10.1	14.1	8.9	8.0
Barium	4.6	2.0	3.3	15.3	36.5	13.2	2.1	0.8	6.0	39.7

Sehlabathebe National Park - sampling site descriptions and additional comments.

SITE NO.	SITE DESCRIPTION & COMMENTS
1	Basecamp site flowing river, grass banks, drain satis.
2	free flowing river, long grass banks, drain satis.
3	slow flow almost stagnant
4	v.slow flow,stagnant, small algae growth
5	v.v slow flow clear, coarse grass drainage free, profile drainage liable to river floods
6	gently flowing, profile draqinage free, veg-long coarse grass, drainage free
7	stagnant system, profile drainage free, drainage satisfactory, veg-stony coarse grass
8	profile drainage free, drainage satifactory, veg coarse long grass
9	prof drain free, drainage satisfactory, veg long coarse grass, short yellow grass
10	prof. drain. free, drain seasonal wetness, veg-coarse long grass bare rock
11	prof. drain free, drain. satisfactory, veg-coarse grass, high mtn stream v.little water, v. little flow
12	high mtn stream small flow stubbly burnt coarse grass step sided gully, prof drain free, drainage satisfactory
13	prof drain free, drainage satisfactory, burnt coarse grass
14	prof. drain free, drainage liable to river floods, veg. long coarse marram type grass
15	prof. drainage excessive, drain. satifactory, veg. long coarse grass
16	prof. drain excessive, drain satifactory, veg, coarse grass
17	prof. drain free, drain.satisfactory, veg thick marram grass
18	prof. drain free, drain satis. veg. marram type grass with dense gravel bed
19	prof. drain free, drain satis., veg thick marram grass
20	prof. drain free, drain satis. veg. burnt with thick layer of ash
21	prof. drain free, drain satis., veg burnt reed like plants, small running stream
22	prof. drain free, drain satis. veg. burnt grass and reed like plants

Leqooa river mountain catchment – site descriptions and additional comments.

SITE NO.	SITE DESCRIPTION & COMMENTS
23	prof. drain free, drain satis.
24	prof. drain free, drain satis. veg, clumpy marram grass, peppermint veg.
25	prof. drain free, drain satis. veg, clumpy marram grass, peppermint veg.
26	prof. drain free, drain satis. veg. dense herby bushes, rocky outcrops, marram hussocks
27	prof. drain free, drain satis. veg. burnt, veg, rocks mixed marshlike ground
28	prof. drain free, drain satis. veg. coarse grass and woody bushes
29	prof. drain free, drain satis. veg. dry dense flat grassland
30	prof. drain free, drain satis.veg. grass
32	prof. drain free, drain satis.
33	prof. drain free, drain satis.
34	prof. drain free, drain satis, veg. grass dry bushes
35	prof. drain free, drain satis. veg. bare trees, coarse grass

Nitrate data for contrasting environmental locations in the U.K.

River	Location	Nitrate - N mg l^{-1}		
		Min.	Max.	Mean
Teith	upland moor			
	Central region Scotland	0.1	0.3	0.2
Tay	Perth, Scotland	0.1	1.0	0.7
Cuckmere	(Sussex)	0.8	3.0	2.0
Stour	(Kent)	4.0	9.0	6.0
Great Eau	(Lincs.)	5.4	12.6	8.5

Adapted from *Freshwater Quality*, 16 th Report by the Royal Commission on Environmental Pollution, HMSO, London, (1992)

Cross-sectional area data for Sehalbathebe National Park (1 – 22) and Leqooa river mountain catchment (23 – 36)

SITE NO.	WIDTH (m)	DEPTH (cm)												WETTED PERIMETER (m)
		1	2	3	4	5	6	7	8	9	10	11	12	
1	5.25	0	2	0	0	1	0	4	4	4	4	2	0	5.34
2	5.3	0	2	10	2	5	10	15	4	0	3	5	0	5.43
3	1.46	36	38	45	31	29	36	37	39	38	37	35	27	2.34
4	1.5	0	10	15	21	25	16	13	10	8	8	8	0	1.64
5	5.08	0	17	29	33	44	50	61	68	66	5	2	0	5.64
6	5.4	0	14	13	11	13	21	34	35	33	26	20	14	5.58
7	2.69	0	10	19	28	26	27	29	14	16	10	6	0	2.8
8	3.83	0	4	9	11	12	7	12	18	22	16	10	0	4.13
9	0.94	6	5	9	5	8	30	45	14	16	17	16	0	1.4
10	0.29	0	5	6	7	7	7	8	8	7	6	5	0	0.41
11	0.98	0	5	6	5	5	6	6	5	5	4	3	0	1.07
12	0.96	0	2	2	2	2	2	2	2	1	1	1	0	1.08
13	1.57	0	2	3	7	9	10	7	5	19	22	16	17	1.89
14	5.44	98	101	23	44	53	24	49	50	32	2	5	0	6.8
14B	1.52	0	3	16	21	24	29	26	24	22	18	12	0	1.6
15	1.52	0	15	34	39	38	28	24	8	7	5	3	0	1.94
16	1.53	17	10	7	6	7	10	13	14	13	14	15	0	1.72
17	1.75	0	1	2	6	9	20	18	15	13	11	7	0	2.08
18	1.61	0	0	12	12	13	12	11	12	12	11	10	5	1.72
19	0.68	0	6	8	11	12	10	10	8	7	6	5	0	0.8
20	1.12	0	9	14	18	21	20	18	16	15	9	6	0	1.26
21	1.38	0	22	28	30	28	31	27	25	29	16	8	0	1.9
22	1.3	0	0	8	9	10	15	15	19	27	29	28	0	1.62
23	1.1	0	0	0	4	3	5	6	7	6	14	10	0	1.3
24	1.6	0	4	18	15	12	16	19	1	11	7	3	0	1.67
25	4.52	0	12	1	4	4	6	6	15	17	2	0	0	5
26	1.76	0	10	23	19	15	16	13	9	6	7	3	0	1.8
27	3	0	0	0	9	3	5	7	11	0	0	0	0	2.2
28	4.32	0	6	12	18	28	2	7	13	24	4	3	0	4.7
29	9.4	0	0	2	4	0	0	6	0	1	2	0	0	9.23
30	5.3	0	7	9	5	10	8	15	12	13	4	3	0	5.6
31	7.5	0	5	3	3	15	14	14	16	8	9	6	0	7.62
32	17	0	5	15	7	12	20	28	19	13	14	3	0	17.5
33	6.92	0	9	14	20	3	18	22	24	12	0	9	0	6.28
34	1.17	0	11	19	22	22	23	25	27	30	29	22	0	1.36
35	1.85	0	1	10	20	29	29	27	15	3	3	5	0	2.08
36	2.93	0	2	4	0	6	3	2	0	0	1	3	0	3.05

Macro – invertebrate data for Sehlabathebe National Park sampling sites (1 – 6).

	SAMPLING SITE NUMBER																							
	1				2				3				4				5				6			
Macro-invertebrate species	**RUN**			**Mean**	**RUN**			**Mean**	**RUN**			**Mean**	**RUN**			**Mean**	**RUN**			**Mean**	**RUN**			**Mean**
	1	2	3		1	2	3		1	2	3		1	2	3		1	2	3		1	2	3	
Mayfly Nymph	30	28	15	**24**	25	45	80	**50**	70	36	45	**50**	32	28	15	**25**	90	42	32	**55**	43	47	22	**37**
Stonefly Nymph	10	13	7	**10**	15	15	0	**15**	27	12	15	**18**	10	10	9	**10**	40	15	12	**22**	16	11	11	**13**
Freshwater Worm	10	5	12	**9**	0	2	3	**3**	6	3	2	**4**	3	2	2	**2**	5	0	0	**2**	3	2	0	**2**
Ghost Lavae	3	0	1	**1**																				
Midge Larvae	5	0	0	**2**																				
Lesser Water Boatman	2	0	4	**2**	2	0	0	**1**																
Dragonfly Nymph	0	1	0	**0**	0	1	2	**1**	0	0	1	**0**												
Water Mite	0	2	0	**1**	1		2	**2**	2	1	0	**1**	0	0	1	**0**					0	1	2	**1**
Water Beetle	0	1	0	**0**																				
Flatworm					2	4	0	**2**																
Small Freshwater Crab					0	1	1	**1**									7	3	7	**6**	2	0	0	**1**
Great Diving Beetle					0	10	8	**6**					0	3	1	**1**								
Frog									0	0	1	**0**												
Caddisfly Larvae									1	0	0	**0**												
Caddisfly																	3	2	1	**2**	4	3	3	**3**
Red Worm																								
Leech																								
Unknown					0	1	1	**1**					2	3	0	**2**	0	0	1	**0**				

Macro – invertebrate data for Sehlabathebe National Park sampling sites (7 – 12).

	SAMPLING SITE NUMBER																							
	7				8				9				10				11				12			
Macro-invertebrate species	RUN			Mean	RUN			Mean	RUN			Mean	RUN			Mean	RUN			Mean	RUN			Mean
	1	2	3		1	2	3		1	2	3		1	2	3		1	2	3		1	2	3	
Mayfly Nymph	13	9	21	14	3	23	15	14	4	42	38	28	0	2	3	2	26	18	10	18	12	15	9	12
Stonefly Nymph	0	3	9	4	0	0	6	2	2	11	6	6					5	9	2	5	2	4	3	3
Freshwater Worm	5	3	2	3	64	5	4	24	5	4	4	4	5	3	0	3	2	3	0	2	1	3	1	2
Ghost Lavae																								
Midge Larvae																								
Lesser Water Boatman					0	7	2	3	0	5	0	2					0	0	1	0				
Dragonfly Nymph																								
Water Mite	2	0	1	1									2	1	0	1	0	0	1	0	2	0	1	1
Water Beetle					15	0	5	7																
Flatworm																								
Small Freshwater Crab					0	2	1	1	0	0	3	1	0	2	0	1								
Great Diving Beetle																								
Frog									0	0	2	1									0	0	2	1
Caddisfly Larvae																								
Caddisfly									0	2	0	1									0	1	0	0
Red Worm																								
Leech					0	0	24	8																
Unknown													1	0	0	0								

Macro – invertebrate data for Sehlabathebe National Park sampling sites (13 – 18).

	SAMPLING SITE NUMBER																							
	13				14				15				16				17				18			
Macro-invertebrate species	RUN			Mean	RUN			Mean	RUN			Mean	RUN			Mean	RUN			Mean	RUN			Mean
	1	2	3		1	2	3		1	2	3		1	2	3		1	2	3		1	2	3	
Mayfly Nymph	81	76	71	**76**	53	17	24	**31**	39	43	34	**39**	58	5	71	**45**	10	31	27	**23**	16	22	28	**22**
Stonefly Nymph	22	14	19	**18**	22	4	11	**12**	5	0	0	**2**	7	16	13	**12**	3	11	6	**7**	3	7	10	**7**
Freshwater Worm	0	6	4	**3**	36	8	19	**21**									4	0	2	**2**	5	0	9	**5**
Ghost Lavae																								
Midge Larvae																								
Lesser Water Boatman													0	9	12	**7**								
Dragonfly Nymph													0	1	0	**0**								
Water Mite	0	2	0	**1**																	0	0	2	**1**
Water Beetle																								
Flatworm																								
Small Freshwater Crab	0	2	1	**1**													0	2	3	**2**	0	1	0	**0**
Great Diving Beetle																								
Frog	4	3	2	**3**																				
Caddisfly Larvae																								
Caddisfly													3	0	0	**1**								
Red Worm																	2	2	0	**1**	0	1	0	**0**
Leech																								
Unknown	1	1	0	**1**																				

Macro – invertebrate data for Sehlabathebe National Park sampling sites (19 – 22), Leqooa river mountain catchment sampling sites .

	SAMPLING SITE NUMBER																							
	19				20				21				22				23				24			
Macro-invertebrate species	RUN			Mean	RUN			Mean	RUN			Mean	RUN			Mean	RUN			Mean	RUN			Mean
	1	2	3		1	2	3		1	2	3		1	2	3		1	2	3		1	2	3	
Mayfly Nymph	15	48	41	**35**	38	32	39	**36**	23	11	16	**17**					8	56	28	**31**	38	3	7	**16**
Stonefly Nymph	8	30	18	**19**	16	9	11	**12**	5	1	2	**3**					2	39	11	**17**	13	9	13	**12**
Freshwater Worm	2	0	0	**1**	0	1	0	**0**									0	5	2	**2**	2	0	6	**3**
Ghost Lavae																	0	0	1	**0**				
Midge Larvae																								
Lesser Water Boatman																								
Dragonfly Nymph					0	1	0	**0**	2	1	0	**1**												
Water Mite																								
Water Beetle																								
Flatworm																								
Small Freshwater Crab	2	3	4	**3**																				
Great Diving Beetle																	0	4	0	**1**	1	2	0	**1**
Frog																								
Caddisfly Larvae																								
Caddisfly																								
Red Worm																								
Leech	1	0	0	**0**																				
Unknown	0	2	0	**1**					2	0	1	**1**					0	0	1	**0**				

Macro – invertebrate data for Leqooa river mountain catchment sampling sites (25 – 30).

	SAMPLING SITE NUMBER																							
	25				26				27				28				29				30			
Macro-invertebrate species	RUN			Mean	RUN			Mean	RUN			Mean	RUN			Mean	RUN			Mean	RUN			Mean
	1	2	3		1	2	3		1	2	3		1	2	3		1	2	3		1	2	3	
Mayfly Nymph	8	11	2	**7**	7	4	18	**10**	0	2	3	**2**	3	1	4	**3**	5	6	8	**6**	23	24	42	**30**
Stonefly Nymph	7	5	1	**4**	4	6	7	**6**	6	21	32	**20**	3	1	6	**3**	9	8	3	**7**	19	27	25	**24**
Freshwater Worm									5	6	4	**5**	3	5	1	**3**	4	9	9	**7**	13	19	16	**16**
Ghost Lavae													0	1	0	**0**	0	0	1	**0**				
Midge Larvae					0	0	1	**0**													1	4	7	**4**
Lesser Water Boatman																								
Dragonfly Nymph					1	0	1	**1**	0	0	1	**0**									0	1	0	**0**
Water Mite					1	0	1	**1**					1	0	0	**0**	8	2	3	**4**				
Water Beetle																								
Flatworm																								
Small Freshwater Crab	2	6	1	**3**	0	1	0	**1**													1	8	5	**5**
Great Diving Beetle	1	0	0	**0**																				
Frog	0	5	1	**2**					3	0	0	**1**												
Caddisfly Larvae																								
Caddisfly													0	2	0	**1**								
Red Worm																								
Leech									1	0	1	**1**	1	0	0	**0**								
Unknown	1	2	0	**1**					0	1	1	**1**									2	8	3	**4**

Macro – invertebrate data for Leqooa river mountain catchment sampling sites (31 – 36).

	SAMPLING SITE NUMBER																							
	31				32				33				34				35				36			
Macro-invertebrate species	RUN			Mean	RUN			Mean	RUN			Mean	RUN			Mean	RUN			Mean	RUN			Mean
	1	2	3		1	2	3		1	2	3		1	2	3		1	2	3		1	2	3	
Mayfly Nymph	29	21	10	**20**	4	8	7	**6**	0	5	3	**3**	12	34	23	**23**	5	0	3	**3**	3	2	6	**4**
Stonefly Nymph	17	13	9	**13**	1	5	3	**3**	4	2	12	**6**	10	5	7	**7**	0	2	1	**1**	11	7	13	**10**
Freshwater Worm	19	23	12	**18**	9	13	17	**13**	21	11	19	**17**	12	4	7	**8**	19	21	11	**17**	6	5	2	**4**
Ghost Lavae																								
Midge Larvae	3	0	0	**1**									1	0	3	**1**					1	0	1	**1**
Lesser Water Boatman																								
Dragonfly Nymph																					0	0	1	**0**
Water Mite					4	11	5	**7**	5	3	4	**4**												
Water Beetle																								
Flatworm	0	0	3	**1**	1	3	5	**3**	5	2	4	**5**	1	0	1	**1**	4	0	1	**2**	1	0	0	**0**
Small Freshwater Crab																								
Great Diving Beetle																								
Frog																								
Caddisfly Larvae																								
Caddisfly																								
Red Worm																								
Leech	56	58	24	**46**	14	9	4	**9**	4	6	7	**6**	1	0	3	**1**	4	6	7	**6**	2	0	3	**2**
Unknown																								

Appendix III

Plymouth Sampling Campaign

Precipitation & Meteorological Data.

Plymouth sampling campaign – Concentration data (μequ l^{-1}) for precipitation samples 1 – 31, (27/01/98 – 11/05/98)

SAMPLE NO.	Chloride (Cl^-)	Nitrate (NO_3^-)	Sulphate (SO_4^{2-})	Ammonium (NH_4^+)	Sodium (Na^+)	Potassium (K^+)	Calcium (Ca^{2+})	Magnesium (Mg^{2+})
1	13.2	10.3	5.2	0.0	4.8	0.5	20.0	6.6
2	864.8	447.7	467.2	187.8	789.1	15.6	302.2	133.3
3	500.0	30.0	88.0	16.1	493.9	10.2	10.0	121.8
4	70.1	6.8	10.0	0.0	14.8	4.4	18.0	18.1
5	516.6	199.8	400.0	228.9	647.0	22.0	506.7	186.0
6	1563.1	56.1	211.5	57.2	1387.0	17.7	278.8	398.4
7	19.2	9.5	12.1	0.0	3.5	0.5	34.4	7.4
8	270.7	33.7	74.5	86.7	314.4	6.4	81.8	66.7
9	1380.3	13.6	211.9	53.9	1336.1	15.9	123.7	335.0
10	335.2	1.9	52.0	9.4	356.1	6.9	44.4	75.7
11	856.3	9.8	105.5	2.8	787.8	15.4	34.4	159.7
12	893.0	6.3	43.3	5.0	799.6	15.9	10.0	191.8
13	59.4	9.7	20.0	0.0	8.3	1.0	30.9	14.0
14	21.1	6.1	11.0	0.0	3.5	0.8	35.4	8.2
15	28.2	7.7	15.6	0.0	4.4	0.8	59.9	9.1
16	82.0	95.3	89.9	38.9	15.7	1.8	53.4	22.2
17	98.6	6.6	36.2	18.3	32.6	1.3	25.4	23.1
18	206.2	5.2	103.2	96.7	134.4	3.6	90.8	43.7
19	51.8	55.0	133.2	63.3	5.7	3.1	131.2	25.5
20	599.4	23.4	125.3	11.1	631.7	12.8	115.7	158.9
21	134.1	15.0	51.0	12.2	131.3	2.8	27.9	40.3
22	201.7	35.3	77.6	17.8	212.2	4.1	44.9	54.3
23	79.4	24.0	62.6	46.7	242.2	4.9	49.9	60.1
24	147.9	21.9	53.1	9.4	146.5	2.6	19.0	42.0
25	398.9	458.4	97.0	47.8	359.1	6.4	75.3	75.7
26	215.2	22.1	53.9	48.9	242.2	3.8	66.8	59.3
27	423.4	52.6	253.3	48.9	487.8	13.6	303.2	125.9
28	56.6	121.3	128.6	128.9	13.9	1.5	70.3	18.1
29	1207.0	55.2	267.9	75.6	1731.3	24.6	199.0	309.5
30	479.4	203.4	154.2	73.9	493.0	8.2	117.7	130.0
31	116.6	326.1	295.1	230.6	128.3	15.1	393.0	75.7

Plymouth sampling campaign – Meteorological data for precipitation samples 1 – 31, (27/01/98 – 11/05/98)

SAMPLE NO.	DATE DEPLOYED	TIME DEPLOYED	DATE COLLECTED	TIME COLLECTED	RAINFALL (mm)	W.SPEED (ms)	W. DIREC. Deg	AIR TEMP C	HUMIDITY % R.H.	PRESS. Hpa
1	27-Jan	14:00	28-Jan	14:00	0	0.77	64.9	0.6	4.5	0.6
2	01-Feb	14:00	04-Feb	14:00	88	0.86	132.4	2.8	87.5	1014.9
3	09-Feb	14:00	08-Feb	14:00	299	2.67	198.4	7.8	95.5	1016.9
4	16-Feb	14:15	11-Feb	14:00	0	2.32	200.6	10.2	99.1	1022.5
5	19-Feb	14:00	19-Feb	15:00	13	2.21	180.4	9.1	95.9	1028.3
6	24-Feb	15:15	22-Feb	15:30	127	3.45	212.3	9.6	93.1	1013.7
7	26-Feb	14:15	26-Feb	14:00	0	1.57	210.3	9.0	82.5	1034.3
8	27-Feb	14:00	27-Feb	14:00	46	3.29	249.1	9.9	93.1	1024.1
9	02-Mar	14:00	02-Mar	14:00	235	3.33	250.5	9.0	86.4	1013.9
10	03-Mar	14:00	03-Mar	13:30	981	6.21	205.9	12.4	100.0	1002.0
11	04-Mar	13:30	04-Mar	13:30	1012	6.28	234.8	11.4	93.6	994.9
12	13-Mar	13:30	06-Mar	13:30	432	4.96	235.7	9.3	85.8	1011.6
13	13-Mar	13:30	16-Mar	13:30	0	2.4	150.1	8.8	92.0	1030.9
14	16-Mar	14:00	18-Mar	15:00	0	1.74	226.3	10.2	89.9	1031.5
15	18-Mar	15:00	20-Mar	14:30	0	1.58	173.5	9.4	81.9	1037.9
16	24-Mar	13:30	25-Mar	13:30	199	2.31	210.4	15.2	96.6	1024.9
17	25-Mar	13:30	26-Mar	13:45	636	4.15	201.4	16.2	100.0	1014.6
18	26-Mar	13:45	27-Mar	13:45	381	3.1	215.6	17.7	100.0	1011.3
19	27-Mar	13:45	30-Mar	14:00	435	2.94	158.0	11.3	87.8	1004.6
20	01-Apr	14:00	03-Apr	14:00	380	2.72	159.4	10.2	87.7	1001.4
21	20-Apr	14:00	21-Apr	14:00	262	3.03	183.1	9.9	89.8	1008.2
22	21-Apr	14:00	22-Apr	14:00	378	4.49	162.3	11.1	94.2	1004.5
23	22-Apr	14:00	23-Apr	14:00	587	3.58	185.1	11.9	99.1	1002.9
24	23-Apr	14:00	24-Apr	14:00	529	3.62	235.2	17.7	97.3	1008.7
25	24-Apr	14:00	27-Apr	14:00	545	3.02	198.7	17.9	93.0	1003.0
26	27-Apr	14:00	28-Apr	14:00		NO DATA AVAILABLE				
27	28-Apr	14:00	29-Apr	14:00	45	3.83	128.1	17.5	93.8	994.9
28	29-Apr	14:00	30-Apr	14:15	142	3.21	128.5	14.8	90.5	1003.7
29	05-May	14:00	06-May	14:00	6	4.13	199.7	11.6	89.3	1004.7
30	06-May	14:00	08-May	14:00	22	3.48	177.3	12.1	88.1	1008.8
31	08-May	14:00	11-May	13:45	131	2.64	145.9	15.1	72.2	1011.5

Appendix IV

Cation & Anion Determination In Gaseous & Aerosol Atmospheric Samples by Ion Chromatography

A REPORT PREPARED AS PARTIAL FILFILMENT OF AN ERASMUS EXCHANGE PROGRAM BETWEEN THE UNIVERSITY OF PLYMOUTH AND THE INSTITUT FUR ANALYTISCHE CHEMIE – TECHNISCHE UNIVERSITAT WIEN

1 INTRODUCTION

Aerosols play an important role in tropospheric and stratospheric chemistry. The ambient tropospheric aerosol is a complex mixture of water, electrolytes, ionic solids, metal oxides, glasses and carbonaceous materials[1]. The influence of aerosols on global climate may be as important as that of greenhouse gases but due to their considerable spatial and temporal variation in composition and concentration aerosols are difficult to sample and analyse. Presently there is no generally applicable automated instrumentation for the composition specific measurement of aerosol concentration. Previous research has focussed on automated measurement of a specific aerosol constituent e.g. H_2SO_4 or ammonium ions[2]. Various optical methods have been used for single particle analysis[3,4] in particular spectroscopic analysis of the collected aerosol. Aerosols can be collected by various techniques, e.g. inertial classification, gravitational settling, filtration, and electrostatic and thermal precipitation. However sample collection is typically long, (several hours), labour intensive and difficult to automate. Furthermore one is unable to follow rapid changes in aerosol composition. Continuous collection and wet analysis based instrumentation has the potential to be fast, sensitive, and affordable.

The following report describes one such continuous collection system developed at the Technical University of Vienna (TU Wien), based on the work of Simon and Dasgupta[5]. The system is almost identical in configuration but with the added advantage of being able to perform simultaneous cation and anion ion chromatographic analysis.

1.1 DEPLOYMENT SITE

The intended system will be permanently deployed for continuous monitoring at the Sonnblick Observatory (SBO) located at the top of Mt. Sonnblick (3106 m a.s.l). Mt Sonnblick is situated in the main ridge of the Austrian Alps (Hohe Tauern, 12°57' E, 47°03' N). Mt Sonnblick is one of the highest peaks in the area and is exposed to air masses from all directions. The observatory is surrounded by large glacier fields to the East and the South. The Sonnblick Observatory has the ideal characteristics of a high alpine background station, due to the absence of public transport there is hardly any tourism. The observatory itself is supplied with electricity and thus is not a source for exhausts originating from fuel or heating or other potential interferents with intended analytical measurements.

Plate 1 Sonnblick Mountain Observatory (3106m)

2 SYSTEM CONFIGURATION

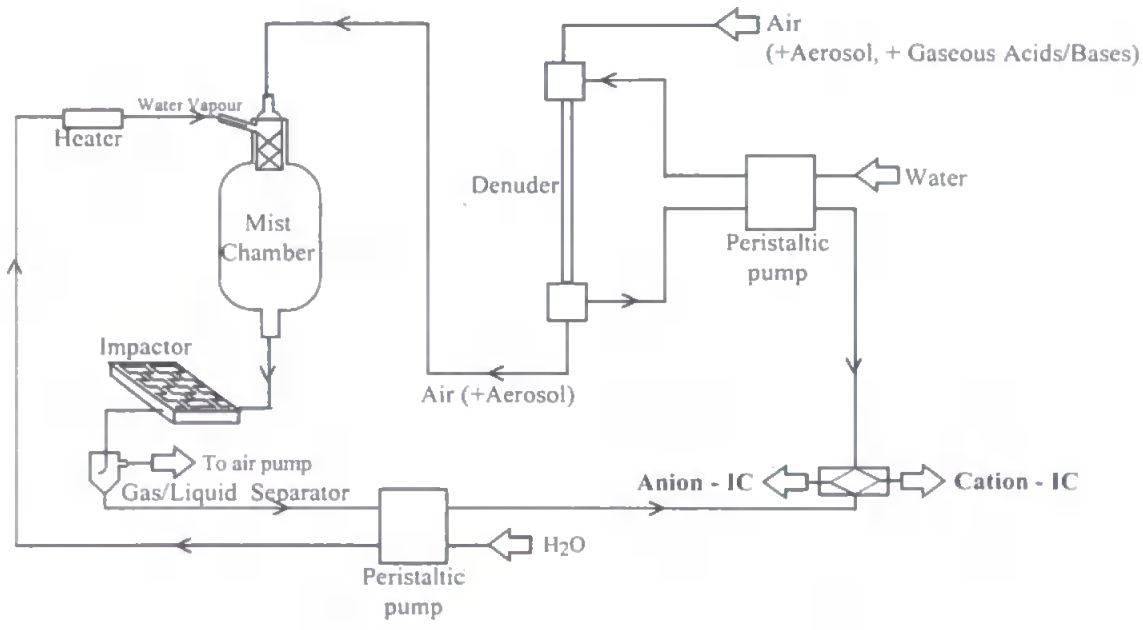

Figure 1 Schematic diagram of overall system configuration.

Air is pumped through the denuder where gaseous acids and bases (e.g. HCl, HNO_3, NaOH & KOH) are absorbed out into a flowing water stream which then passes to the mist chamber and then the impactor. Here separation of the particulate substances contained in the aerosol takes place. The resultant water flow contains the analytes of interest, which are subsequently pumped to a 4-way valve which switches alternately between the anion and cation ion chromatographic systems. The denuder is used for the separation of the dissolved gaseous air particles. For this separation a glass tube is needed in which the inner surface of the tube has a thin coating of silica gel (as described on p.34). This coated surface is necessary to enable a thin film of water to cover

the surface as homogeneously as possible. This "film" of water flows slowly down the denuder and absorbs the soluble components from the air flow. At the present stage of development both the water and the incoming air flow are in the same direction, namely down the denuder. However this is one area in which further work will be needed to investigate the effects of employing a counter-current air flow, to improve the collection efficiency.

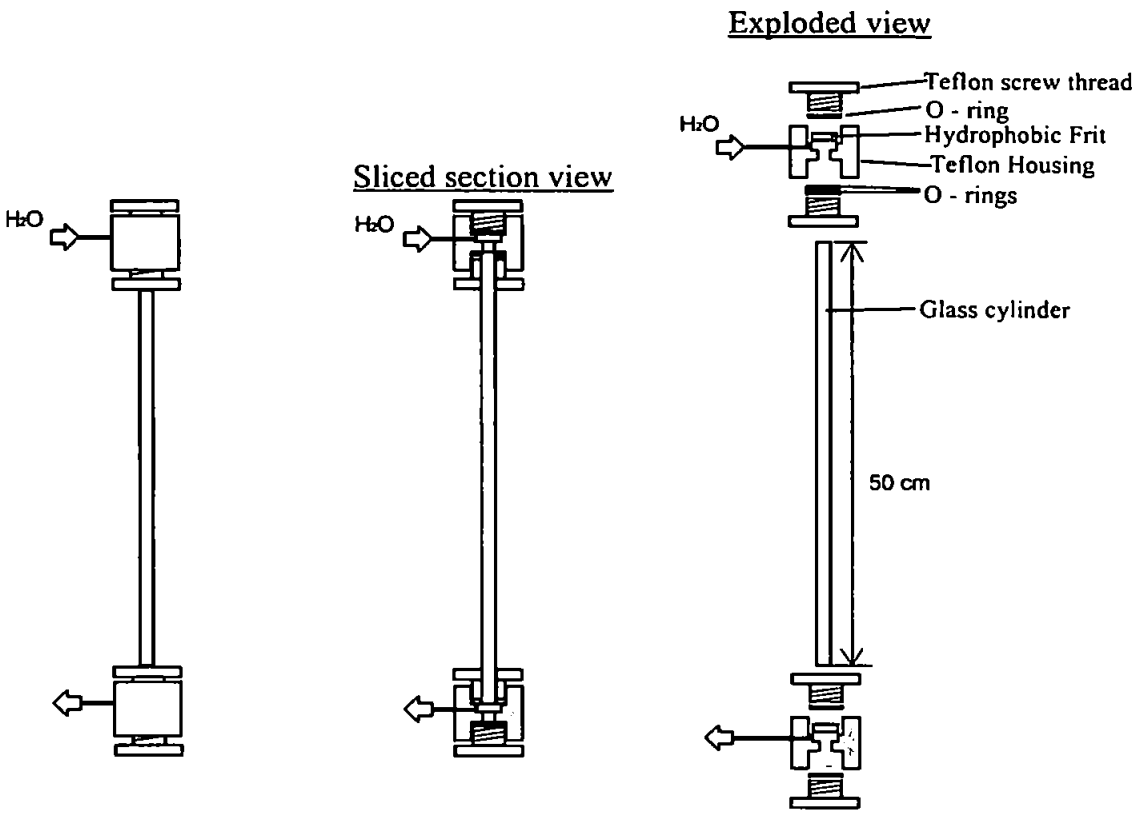

Figure 2 Schematic diagram of the denuder.

The type of denuder being used at the present is known as a "wet effluent" denuder. The incoming water flow is dispersed by the use of a hydrophobic frit into an even cylindrical "thin film" coating that slowly descends the column. As the air flows into the denuder the acidic and basic components of the air are absorbed into the water which is collected at the end by a hydrophilic frit and carried out by the action of a peristaltic pump. It is intended to improve the design of the currently used denuders to enable higher air flows to be used. These "new generation" parallel plate wet diffusion denuders have a rectangular geometry that allow higher air flows, they have already been used in the work of Simon and Dasgupta[5] with flow rates up to 10 l min^{-1}. With the current tubular design denuders (flow rates typically 3-4 l min^{-1}) subsequent measurements at higher flow rates are not representative due to the air at the centre of the flow is not fully in contact with the water film and therefore the collection efficiency decreases.

Preparation of the denuders involves the glass tube being washed with high grade acetone and 18.2MΩcm^{-1} deionised water. After drying the tube is immersed in a solution of 25g of silica gel (Aldrich, TLC high purity grade, av. particle size 5-25μm) in 5 M sodium hydroxide (Baker, 50% soln.) for a duration of two days. This process allows the inner surface of the tube to become slightly etched. Following this time the tube is rinsed again in analytical grade water and allowed to drain. The silica gel is then placed into a glass jar containing a magnetic stirrer. The jar is sealed via a bung with two air tubes passing through it. To one of these tubes the pre-etched denuder is attached, to the other a stream of nitrogen is connected. This allows the nitrogen to enter the glass jar and blow only the finest particles of silica gel out of the other tube and into the denuder, thus slowly coating the inner surface. After a sufficient coating is obtained the denuder is dried in an oven at 80°C before being transferred to an oven for 30 minutes at 630°C. In the second production of denuders this last stage was performed in a flame; here it is important to reach and slightly exceed the temperature where the glass starts to become soft, this enables the complete binding of the silica to the glass surface.

One of the primary functions of the mist chamber is to allow the aerosol to expand and grow. The air from the denuder is first warmed by a coil heater wrapped around the connecting glassware to negate the aerosol condensing too early, it is then mixed with steam at approximately 300°C, this promotes the growth of the aerosol upon entering the mist chamber. The size of the mist chamber is directly responsible for the time the aerosol can develop.

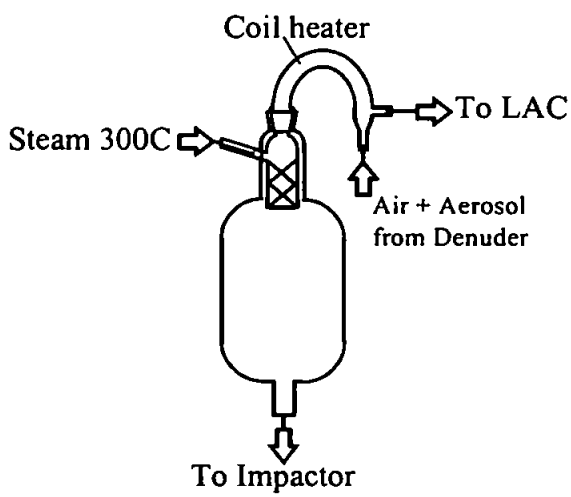

Figure 3 Schematic diagram of the mist chamber.

Before the air enters the mist chamber it is possible to examine the particle size distribution of the aerosol prior to its condensation. This is done by the introduction of a laser aerosol counter (LAC 226) as can be seen in Figure 3. With the aid a T-piece the same examination can be performed on the air passing out the gas/liquid separator and therefore a quantification of how fully the condensation has been in the mist chamber can be made. The impactor is used to cool the exiting air/aerosol to ensure complete condensation and 100% absorption of the aerosol to the water. The impactor is constructed to allow the flow to pass around many rectangular channels where, at the sharp corners, the "impaction" takes place. To cool the incoming streams four Peltier-elements are used, the temperature of these elements is set at 4°C by the use of controlling electronics. The separator (Figure 1) is used to separate the liquid or resultant water from the gas phase (air) after the impaction step. This collected analyte water is then pumped to the chromatographic systems for analysis.

2.1 ANION CHROMATOGRAPHIC SYSTEM

Table 1 and Figure 4 shows the apparatus and diagram of the anion preconcentration system used for the determination of anions in gaseous and aerosol samples.

Table 1 Anion Chromatographic Apparatus

Chromatographic Apparatus	
Analytical column	DIONEX AS-12A 4mm
Guard Column	DIONEX AG 12A 4mm
Preconcentration Column	DIONEX AG 12A 4mm
Eluents	A -Milli-Q water B -100mM NaOH
Gradient program	0 - 4.3 mins : 8%A/92% 4.3 - 6.4 mins : 17%A/83%B 6.5 - 20.0 mins : 52%A/48%B 20.1 - 30.0 mins : 8%A/92%B
Flow rate	1.2 ml/min
Suppressor	ASRS-1
Detector	DIONEX CD-20

The condensed water collected at the gas/liquid separator is pumped to the preconcentration columns which are alternatively loaded with the analyte water and then eluted as shown in Figure 5 below.

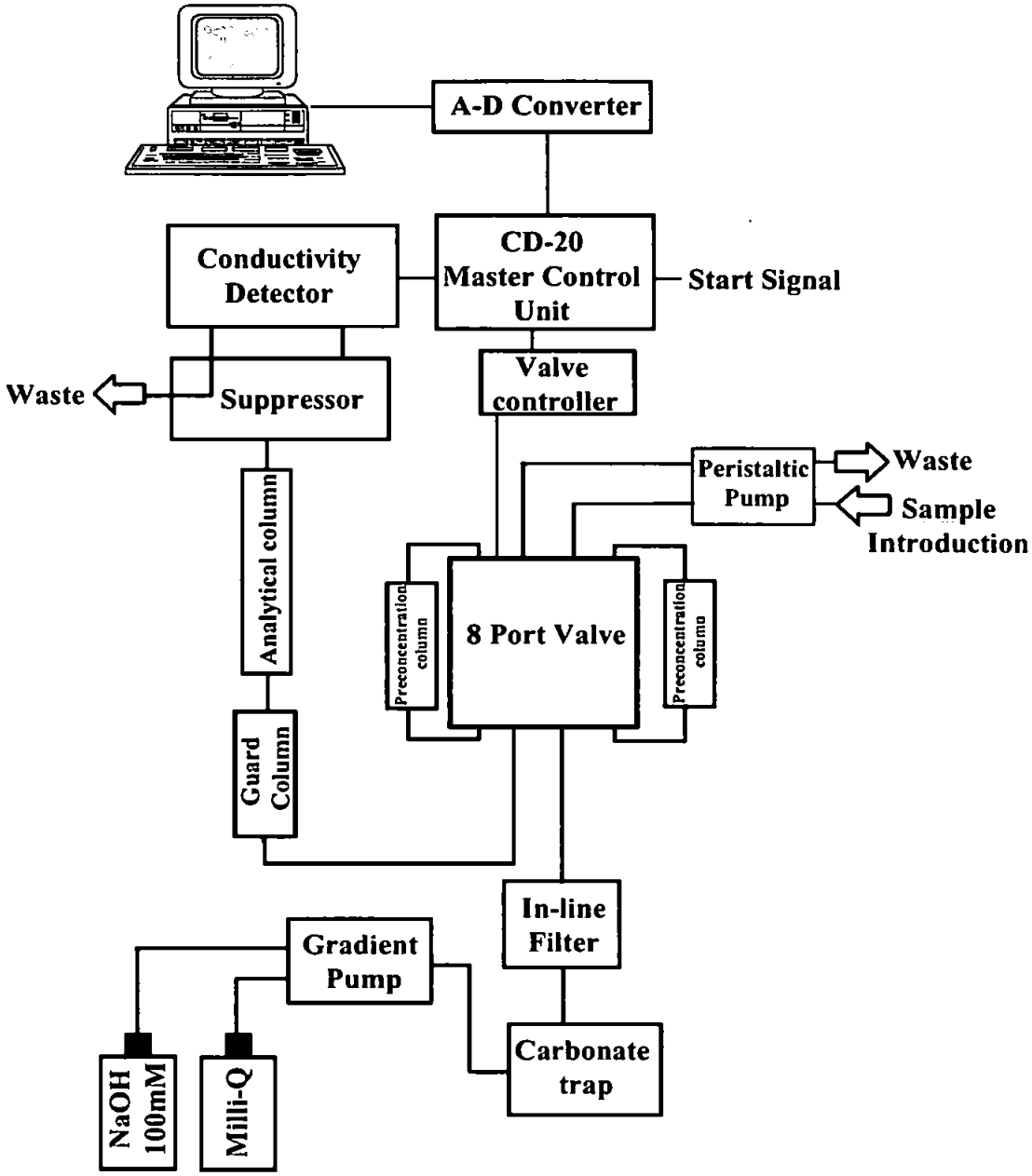

Figure 4 **Schematic diagram of the anion preconcentration system.**

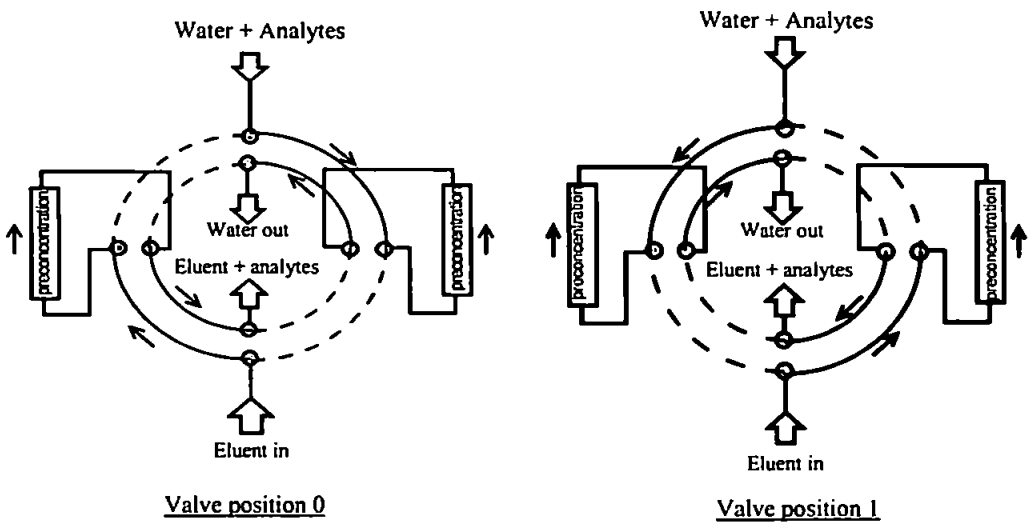

Figure 5 **Configuration of the 8 - port valves.**

The valves are pneumatic valves that operate at a pressure of approximately 70 psi (supplied by nitrogen cylinder). The switching signal for the circuit comes directly from the detector by the means of a relay signal, it is either 0 or 1, corresponding to an open or closed relay.

2.2 CATION CHROMATOGRAPHIC SYSTEM.

The cation system is principally the same as the anion system with one major difference, being that the separation of the cations can be performed with an isocratic elution. Therefore there is no need for a gradient pump or a second eluent.

Table 2 Cation Chromatographic Apparatus

Chromatographic Apparatus	
Analytical column	DIONEX CS-12A 4mm
Guard Column	DIONEX CG 12A 4mm
Preconcentration Column	DIONEX CG 12A 4mm
Eluent	17mM Methanesulphonic Acid.
Flow rate	1.2 ml/min
Suppressor	CSRS-1
Detector	DIONEX CD-20

The CD-20 detector is a programmable detector which can output or receive both RLY-relay and TTL signals. It is also possible to configure a detector to allow it to be a "master" of the whole instrumental arrangement, this is achieved by incorporating a short circuit loop which allows the detector to reset and start itself. At the start of the cation system a previously configured TTL signal simultaneously starts the anion system. Both CD-20 detectors send output signals to a recording program and the anion detector sends signals to the gradient pump to initiate the program and to reset it. After 30 minutes the 8 port valves are switched to their other position and elute to the analytical column while the other preconcentrates. After 60 minutes the cation detector resets itself (short circuit loop) and starts the process again.

2.3 AEROSOL GENERATOR

To fully characterise the sample collection system it is necessary to produce an accurately define aerosol in terms of its components and their concentration. The function of one such system is illustrated in Figure 6.

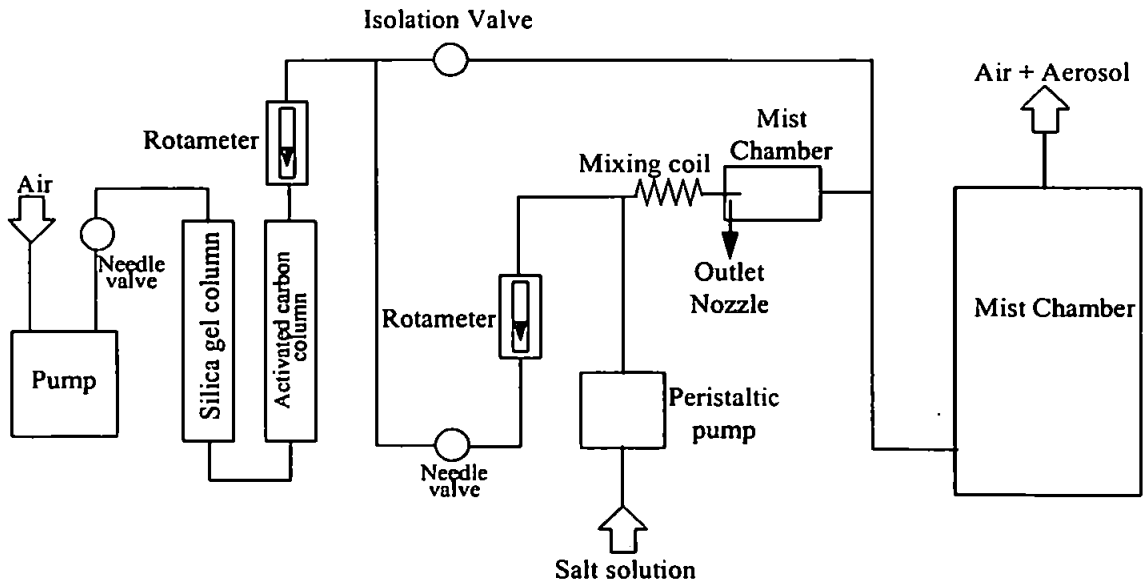

Figure 6 Schematic diagram of the aerosol generator.

Standard laboratory air is pumped through columns of silica gel and activated carbon. The resulting air should be dried and cleaned from gaseous acids and bases and particulate matter and is known as a "zero air". The zero air is then divided into two separate streams, the first is mixed with a prepared salt solution and then sprayed into the first mist chamber, after the mist chamber both flows recombine in a larger mist chamber. The underlying purpose for this configuration is that the air flow containing the aerosol is "dried" by the second flow. The salt solution is the standard for the cation and anion systems, further work in this area will evaluate the efficiency of the transport process and therefore derive the concentrations of the salt solution that will be needed to act as standards for the final system.

3 PRECONCENTRATION & CALIBRATION

Concentrator columns are short (typically 35 -50mm in length), and contain a stationary phase that is identical, or similar, to the phase in the analytical column. It is common practice for a guard column to be used as a preconcentrator column. The function of a concentrator column is to "strip" ions from a measured volume of a relatively clean aqueous sample matrix. This process "concentrates" the desired species, which leads to lower detection limits. The advantage of using concentrator columns is the ability to perform routine analysis for ions at $\mu g\ l^{-1}$ (ppb) and sub-$\mu g\ l^{-1}$ levels without extensive and laborious sample pre-treatment. With species present in aerosols commonly in this low ppb range the use of preconcentration is mandatory to enable any analysis to be performed. The following section describes the use of preconcentration for both cation and anion analysis.

3.1 CATION PRECONCENTRATION (DIONEX SYSTEM)

The first work conducted at the TU Wien was to obtain a cation calibration on the recently acquired Dionex Peaknet software system. The software allows besides normal acquisition functions the remote operation of the CD-20 detector via a DX-LAN connection. In addition the software receives a digital input and therefore previously encountered problems due to the incorrect setting of the conductivity range are no longer a concern.

3.1.1 EXPERIMENTAL

Chromatographic parameters have been detailed previously (Table 2). Working standards of 5, 7.5, 10, 20, 30 and 50 $\mu g\ l^{-1}$ were prepared by serial dilution of a 5 $mg\ l^{-1}$ stock solution (Na^+, NH_4^+, K^+, Mg^{2+} and Ca^{2+}). Each standard was analysed four times, (twice on each column), files were stored on hard disk and also exported as ASCII files for later processing in Excel 5.0 (Microsoft Corporation) and Microcal Origin v2.78 (Microcal Software, Inc). Differences in backpressure between columns results in different amounts of analytes being loaded onto the columns. Therefore it is necessary to measure the flow of analyte to the preconcentration columns in order to correct for these differences in the calibration.

3.1.2 RESULTS & DISCUSSION

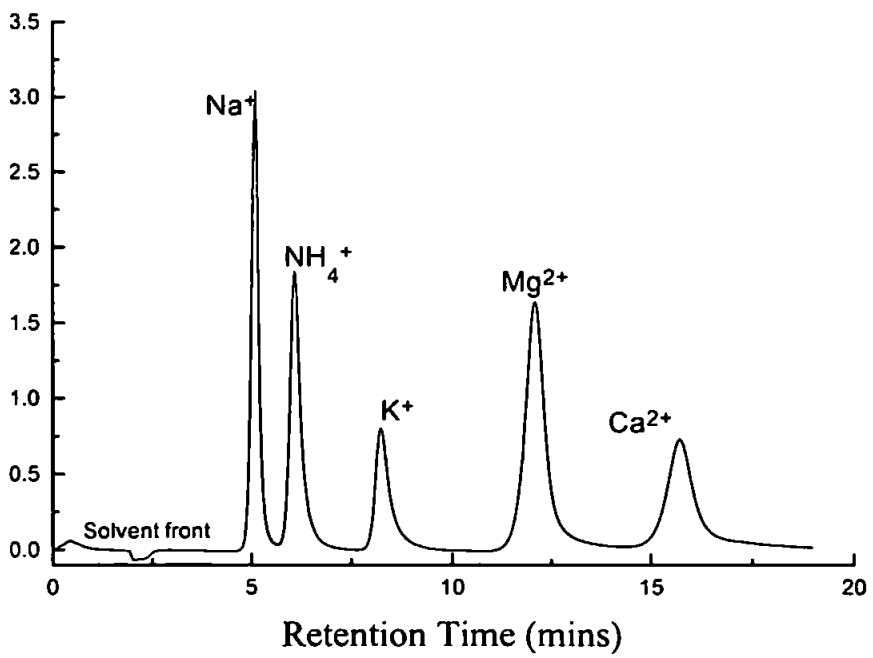

Figure 7 Typical cation chromatogram for 10 $\mu g\ l^{-1}$ mixed standard.

The solvent front elutes at approximately 2.5 min with the first analyte eluting at approximately 5 min. Flow corrected calibrations (Na^+, NH_4^+, K^+, Mg^{2+}, Ca^{2+}) for the two columns were linear ($0.9999 > r^2 > 0.9964$ for $n = 7$). The limit of detection for the method has not been calculated, however from Figure 7 it is envisaged that low $\mu g\ l^{-1}$ limits should be easily obtainable. However current developments in sensitivity are hampered by the fact that a peristaltic pump is being used to load the column. Typical backpressures from the CG-12 columns are approximately 300psi and it is clearly apparent that a peristaltic pump can not provide pressures of that magnitude, as a consequence loading flow rates are low (0.25-0.35 ml/min)(5-7ml per analysis). Different pumping configurations have also been investigated but no improvement in flow rates was found, consequently preconcentration factors are lower than could be achieved. Additionally the possibility of a combined calibration for both columns should be investigated, which would considerably reduce the time needed to calibrate the system.

3.2 ANION PRECONCENTRATION (WTS SYSTEM)

3.2.1 EXPERIMENTAL

Chromatographic parameters have been detailed previously (Table 1). A fresh stock solution was prepared by dissolving the following amounts in 1 litre of Milli-Q deionised water.

Fluoride	0.05524g	Pyruvate	0.0632g
Chloride	0.0824g	Formate	0.07552g
Acetate	0.06944g	Nitrate	0.1371g
Sulphate	0.1479g		

Resultant concentrations were 25mg l^{-1} fluoride, 50mg l^{-1} formate, acetate, pyruvate and chloride, 100mgl^{-1} nitrate and sulphate and the stock solution was stored in a refrigerator to minimise losses of the organic ions. Due to the quick deterioration of the organic ions at low concentrations, working standards of 0.25, 2.5, 5, 7.5 and 10 $\mu g\ l^{-1}$ of fluoride were prepared by serial dilution of the stock solution and analysed immediately. As for the cation calibration, each standard was analysed four times, twice on each column. In contrast to the cation system, total loaded volume was recorded as opposed to flow rate due to the changing backpressure of the system (a consequence of running a gradient elution). Optimisation of the gradient elution program was performed in order to achieve the best possible separation and resolution. The final elution program has been given previously in (Table 1). Data collection was performed on ATS WinChrom software as opposed to the Dionex Peaknet software, data was stored in hard directory and later exported as ASCII for processing in Excel 5 and Origin v2.78.

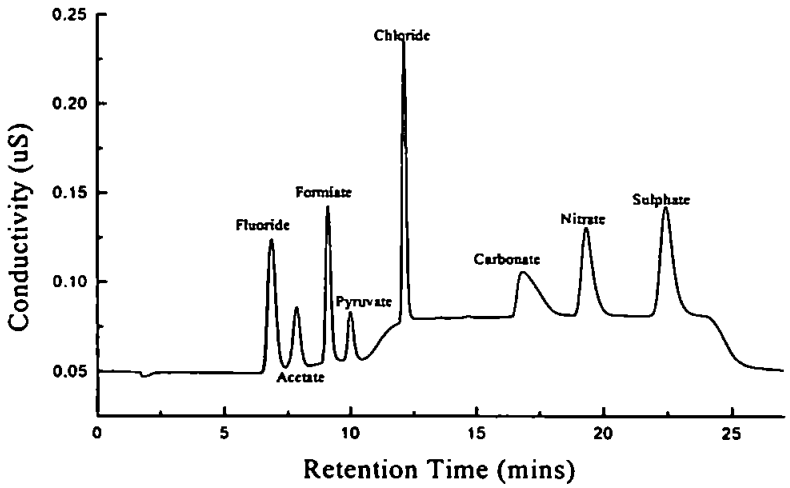

Figure 10 Typical anion chromatogram for mixed standard (5 μg l^{-1} F^-).

Combined anion calibrations (column 1 + column 2) were linear (0.9879 < r^2 < 0.9978, n = 5) and, where, possible a blank correction has been made calculated from the slight response seen for a 30 min Milli-Q blank (Figure 11). Limits of detection have been calculated from three times the standard deviation of a low concentrated standard.

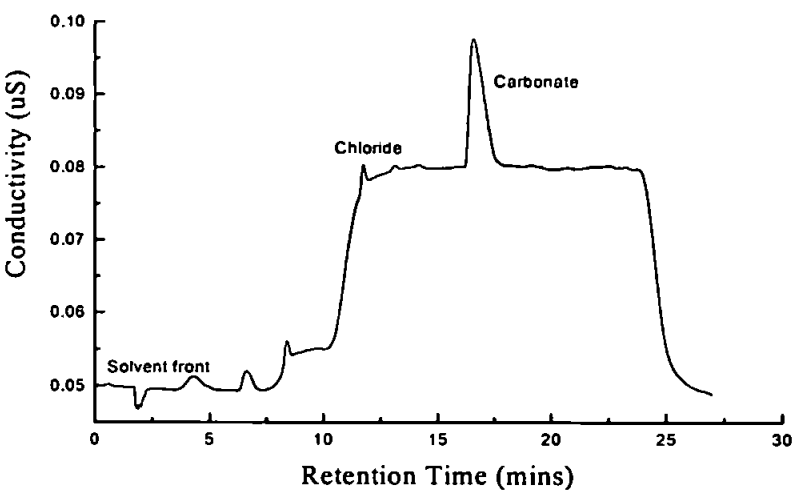

Figure 11 Typical anion chromatogram for 30 minute blank.

Correlation coefficients for the individual columns were slightly improved compared with the combined calibration results shown here. However the resulting time saving that will arise from

using a single calibration for the system upon final deployment more than counters this minimal gain in calibration stability from using individual column calibrations.

LIMITS OF DETECTION

Limits of detection have been calculated from 3 times the standard deviation (3σ) of a low concentrated standard. Firstly the standard deviation of each column was averaged to give a single value, this value was then multiplied by 3 to give the 3σ value for calculation of the detection limit. The LOD value in nanograms (ng) is then divided by the corresponding analytes molecular weight to give the LOD in nmol. However due to the fact that the system is to be utilised for gaseous sample the LOD must subsequently reflect this in its' units. With the intended use of parallel plate wet diffusion denuders a sampling rate of 10l min^{-1} ($0.01m^3min^{-1}$) will be used. Preconcentration time is 30 minutes and therefore during a single analysis the total volume sampled is given by ;

$$0.01m^3min^{-1} \times 30\ min = 0.3\ m^3.$$

The LOD in nmol can then be divided by this volume to give the LOD in $nmol/m^3$.

The LOD's given in Table 4 are the best obtainable with the system to date. It must be noted that they are calculated only from the preconcentration part of the system and are therefore not truly representative of the system as a whole. Due to the complex nature of the sampling system true limits of detection will be governed by the blanks from the whole system e.g. diffusion denuder, mist chamber, etc. Additionally the system could not be fully characterised until actual instalment at the SBO due to the differences between the laboratory and the installation site.

Table 4 Theoretical limits of detection for the anion system.

Analyte	Combined LOD (ng)	M.W	nmol	Time (mins)	Air vol. (m^3/min)	Total vol. m^3	LOD $nmol/m^3$
Acetate	8.4	59	0.142	30	0.01	0.3	0.475
Chloride	2.9	35.5	0.080	30	0.01	0.3	0.268
Fluoride	0.8	19	0.042	30	0.01	0.3	0.142
Formiate	5.7	45	0.125	30	0.01	0.3	0.419
Nitrate	8.0	62	0.129	30	0.01	0.3	0.432
Pyruvate	2.9	87	0.033	30	0.01	0.3	0.110
Sulphate	2.7	96	0.028	30	0.01	0.3	0.093

Improvements on the anion LODs are easily obtainable with the use of specific low backpressure preconcentrator columns (pressures around 70psi) as opposed to standard guard columns as used

in this study. These preconcentrator columns will facilitate increased loading of the columns and subsequently an improvement in the LOD by at least an order or two of magnitude.

3.3 CATION CALIBRATION (WTS SYSTEM)

3.1 EXPERIMENTAL

Chromatographic parameters have been detailed previously (Table 2). Working standards of 1, 2,5 and 10 μgl^{-1} were prepared by serial dilution of a 5 mgl^{-1} stock solution (Na^+, NH_4^+, K^+, Mg^{2+} and Ca^{2+}). Each standard was analysed four times, (twice on each column). Data collection was performed on ATS WinChrom software as opposed to the Dionex Peaknet software, data was stored on hard disk and later exported as ASCII files for processing in Excel 5 and Origin v2.78. The main difference between the Dionex system described above and the WTS system is that the latter does not receive a digital signal, therefore it cannot perform an auto rescale if an analyte peak is too large for the conductivity range that has been set. The following calibration was performed on a conductivity range of 10μS. Due to the flat response seen for a 20 min Milli-Q water blank (Figure 14), LOD determinations have been calculated from a 60 min preconcentration of blank water. For each column 8 blank analyses were performed, and the LODs are given as 3 times the standard deviation of the blanks and calculated in units of $nmol/m^3$.

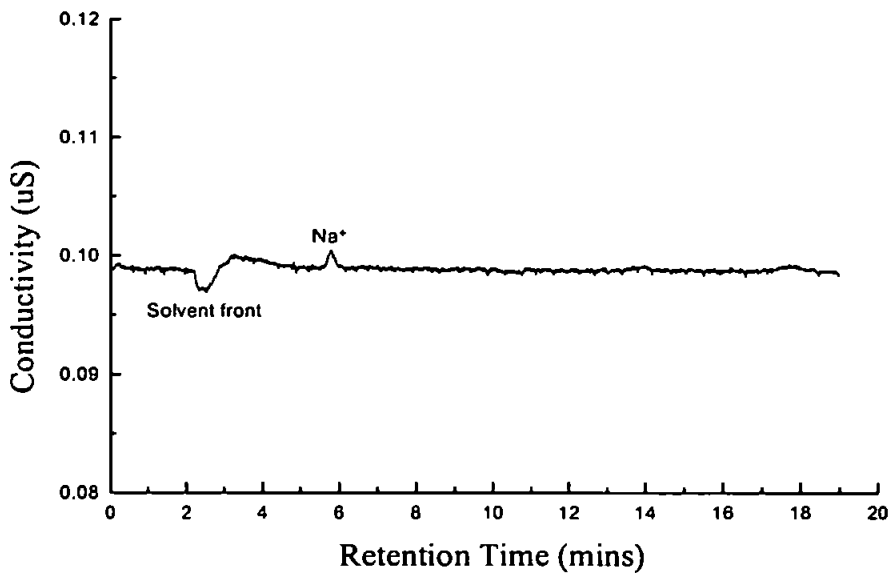

Figure 12 Typical cation chromatogram for a 20 minute blank.

3.3 2 RESULTS & DISCUSSION

The calibrations are flow corrected but due to the zero response observed for a 20min blank they do not need a blank correction. Due to a sodium contamination present in the system during calibration leading to very high observed responses the sodium data has been excluded from the calibration. Correlation coefficients of the combined calibrations for both columns for ammonium (NH_4^+ - r^2 = 0.9963, n = 5), potassium (K^+ - r^2 = 0.9963, n = 5) and magnesium (Mg^{2+} - r^2 = 0.9977, n = 5) were good, and that for calcium (Ca^{2+} - r^2 = 0.9897, n = 5) was acceptable.

Normal duration of the preconcentration run is 20 minutes, however as shown in Figure 12 no response for the analytes is observed for a Milli-Q blank. Therefore the preconcentration time was increased to 60 minutes.

Table 5 Theoretical limits of detection for the cation system.

Analyte	Combined LOD (ng)	M.W	nmole	Time (mins)	Air vol. (m^3/min)	Total vol	LOD nmol/m^3
NH4	0.23	17	0.0135	30	0.01	0.3	0.045
K	0.43	39	0.0110	30	0.01	0.3	0.037
Mg	0.59	24	0.0248	30	0.01	0.3	0.083
Ca	4.5	40	0.1125	30	0.01	0.3	0.375

The LOD's quoted can be considered as theoretical limits as they are derived just from the preconcentration system and not the sampling interface which would lead to higher values.. The LOD obtained with the aerosol system of 0.045nmol/m^3 is clearly an order of magnitude lower than the minimum value (0.2nmol/m^3) observed throughout the year. Median values, with the exception of the winter season, are generally two orders of magnitude higher than the LOD. This indicates that the system will be sufficiently sensitive for the monitoring of ammonium ions in aerosols, assuming that blank values arising from the system can be kept to a minimum.

4 CONCLUSIONS

The aerosol sampling system is still under development at the Technical University of Vienna, but this work shows that the system possesses excellent potential. With the use of low backpressure preconcentrator columns and parallel plate diffusion denuders further improvements in detection should be obtainable. In summary it is the authors opinion that the aerosol sampling system at the

Technical University of Vienna will be able to provide an automated instrument with sufficient sensitivity for the continuous monitoring of anionic and cationic constituents in tropospheric and stratospheric air samples. The system will also provide an excellent time resolution of only 30 minutes, thus enabling more accurate modelling and greater understanding of elemental fluxes over time.

5 REFERENCES

1. Stelson, A.W., *Environ. Sci. Technol.*, **1990**, 24, 1676.
2. Analuf, K.G., Fellin, P., Wiebe, H.A., Schiff, H.I., Braman, R.S., *Atmos. Environ.*, **1985**, 19, 325.
3. Bardess, D., Levin, Z., Ganor, E., *Atmos. Environ.*, **1992**, 26A, 675.
4. Appel, B.R., *In Aerosol Measurement - Principles, Techniques & Applications*, Van Nostrand Reinhold, New York, **1993**, p.233 - 259.
5. Simon, P.K. and Dasgupta, P.K., *Anal. Chem.*, **1995**, 67, 71.

Appendix V

Presentations, Conferences and Courses

PRESENTATIONS

1. *In situ monitoring by flow injection using a miniature array detector.* Poster presentation at Research and Development Topics in Analytical Chemistry, Nottingham Trent University, July 1996.

2. *On – line flow system for the determination of ammonia in freshwaters using a miniature fibre optic array detector.* Poster presentation at Research and Development Topics in Analytical Chemistry, University of Northumbria, July 1997.

3. *Flow injection with photometric detection of ammonia in effluent and natural waters.* Oral presentation at the 2nd Conference of the Process Spectroscopy Group, Astra Pharmaceuticals, Loughborough, June 1997.

4. *Field deployed flow injection instrumentation and biogeochemical field studies in the Sehlabathebe National Park, S. Africa.* Oral presentation at British Schools Exploring Society pre – Lesotho expedition meeting, Ilkley Moor, April 1998.

Regular lecture presentations at the University of Plymouth research seminars and at M Squared Technology Ltd., Totnes were also given.

CONFERENCES & COURSES ATTENDED

1. Research and Development Topics in Analytical Chemistry, University of Hull, July 1995.

2. UK Chemometrics Discussion Group – PCR, PLS and Associated Techniques, Reading University, November 1995.

3. ERASMUS exchange program, three month visit to the Institute for Analytical Chemistry, Technical University of Vienna, Austria.

4. Research and Development Topics in Analytical Chemistry, Nottingham Trent University, July 1996.

5. ERASMUS Eurocourse, Frontiers in Analytical Chemistry – Chemometrics, University of Antwerp (UIA), August 1996.

6. Analytical Science and the Environment, University of Northumbria, July 1997.

7. Research and Development Topics in Analytical Chemistry, University of Northumbria, July 1997.